From Electrical Signals to Biological Processes: Unveiling the Complexity of Electroencephalographic Epileptiform Spikes Across Sleep-Wake States

by

Darion Bryce Toutant

A Thesis submitted to the Faculty of Graduate Studies of

The University of Manitoba

in partial fulfilment of the requirements of the degree of

MASTER OF SCIENCE

Graduate Program in Biomedical Engineering

University of Manitoba

Winnipeg

Copyright © 2023 by Darion Bryce Toutant

Abstract

This thesis introduces a novel investigation into the morphological characteristics of epileptiform spikes across various sleep-wake states. A gold-standard database of spikes was created, offering insights into their variations across wakefulness, non-rapid-eye-movement (NREM) sleep stages 1-3, and particularly rapid-eye-movement (REM) sleep, and hypothesizing on the dynamics regulating its suppressive ability towards spikes.

The study employed lab-developed software to categorize sleep states and validate spikes using data from 7 epilepsy monitoring unit patients. A computational pipeline was developed to assess nine morphological spike features throughout Laplacian, Referential, and Raw montages. Due to non-normal data distribution, statistical analysis was performed using the Kruskal-Wallis test, followed by Dunn's post-hoc testing and Bonferroni correction.

Results revealed that the spike features of REM sleep are significantly different from those of other sleep-wake states. In particular, spikes during REM sleep had the shallowest ascending and descending slopes by nearly 50% of the other states, which were nearly symmetrical, blunter peaks with roughly twice the angle of other states and exhibited lower peak amplitudes less than 50% of the voltage of other states. Wakefulness was the most different state concerning duration while being, on average, 15% shorter. Finally, the spike area during REM was roughly twice as small as all other states.

This study shows significant spike feature differences throughout sleep-wake states, with REM drastically different in most features. The driving factors for changes in spike morphology throughout the sleep-wake states are unknown. However, this thesis explores the effects of ionic, neurotransmitter, astrocytic and network dynamic processes to help shed light on these changes. Notably, this thesis provides glimpses into the roles of astrocytic involvement, orexinergic systems, and network dynamics as potential contributors to the observed morphological differences within REM. Further investigations are necessary to fully understand these complex electrobiological interactions, which may be responsible for the observed anti-epileptic properties during REM sleep. This study paves the way for future work to expose and leverage the unique anti-epileptic mechanisms of REM sleep, potentially leading to the development of REM-specific therapeutic strategies for epilepsy management.

Acknowledgments

This journey of academic and personal growth would not have been possible without the support, guidance, and encouragement of several individuals whose contributions I am deeply grateful for.

First and foremost, I extend my heartfelt gratitude to my advisor Dr. Marcus Ng, whose extraordinary support, patience, and unwavering belief in my abilities have been pivotal in my journey. His expertise in neurology has not only been instrumental in the completion of this thesis but has also broadened my horizons in the realms of brain stimulation, sleep-wake states, and epilepsy. His enthusiasm to exploring and debating diverse theories, particularly in the context of why or how REM sleep's anti-epileptic effects occur, has been enlightening. Other discussions, ranging from underlying effects of HD-tDCs to the light-hearted topics ranging from sharing in science fiction shows to exotic chocolates, have added immense value to my academic and personal growth. Not to be forgotten, thank you for your countless hours in using my interface for spike validating and labelling as well as for your detailed input in editing this thesis have been invaluable. Your mentorship has been a gift for which I am profoundly grateful.

I am equally indebted to my co-advisor, Dr. Zahra Moussavi, for her unwavering support and for creating a nurturing environment in her group meetings that fostered our learning and growth. Her dedication to our success, both in coursework and providing and environment to discuss and learn other students' biomedical projects, has been a great source of motivation. Thank you, Dr. Zahra Moussavi, for your guidance and for pushing us to excel.

My heartfelt thanks to committee member, Dr. Ji Hyun Ko, whose enthusiasm and dedication to brain research have been an inspiring force in my academic journey. His tireless commitment is evident from his thorough review and insightful feedback on countless drafts of my thesis, each time providing invaluable guidance and direction. He has not only shared his expertise but also his resources, generously allowing us to utilize his EEG cap for our research. His willingness to go above and beyond, even volunteering to wear the EEG cap himself for data recording, speaks volumes about his dedication to hands-on teaching and research. His approachable nature and readiness to engage in lively discussions have added a personal and engaging dimension to my thesis work.

To Dr. Jason Morrison, who has been a pillar of support throughout not just my graduate studies but also my undergraduate journey, I extend my profound gratitude. His commitment to my project, even before officially joining the committee, exemplifies an extraordinary level of dedication and kindness. His ability to challenge my

perspectives, suggest novel approaches, and delve into thought-provoking discussions for the most part go way overtime has profoundly shaped my research journey. His involvement in my work, irrespective of his official role, has been a testament to his genuine interest in and support for my academic endeavours. His contributions, including insightful editing and always making time for discussions, have been invaluable. Thank you for your guidance and for being an integral part of my academic path. Never a dull moment building and playing with 3D-printers!

I extend my heartfelt gratitude to Sara Bettess from the charitable organization Epilepsy and Seizure Association of Manitoba (ESAM) for her invaluable support and dedication throughout my thesis journey. Her commitment to raising epilepsy awareness and advocacy for this cause has been invigorating and drove me to complete this thesis. Sara's role in partnering with MITACS provided essential financial backing and allowed me to contribute to epilepsy awareness through ESAM's social media platforms. I am deeply appreciative of her unwavering support and the significant impact she has made in helping those affected by epilepsy ultimately driving me to complete a meaningful thesis.

A special thanks to the doctors, Joseph Peedicail and Helen (Qi) Xu, for their key help in testing the spike labeling interface. Your feedback was instrumental in enhancing its functionality and efficacy.

Lastly, I am eternally grateful to my family and friends for their endless support, encouragement, and belief in me have been the bedrock of my strength. The role you've played in my life is immeasurable – I am not sure where I'd be without your unwavering presence. Thank you for being my inexhaustible support system, for cheering me on during challenging times, and for celebrating every milestone with me.

This thesis is not just a reflection of my work, but a testament to the collective support and wisdom of all these remarkable individuals. Thank you all.

Table of Contents

Abstract 1

1 Motivation 11

1.1 The Nature of Sleep: Patterns, Effects, and Relation to Epilepsy 11

1.1.1 Fundamentals of Sleep 12

1.1.2 Sleep and Epilepsy 13

1.1.3 Influence of Sleep Stages on Epileptic Spike Morphology 13

1.2 Goals and Objectives 14

1.3 Thesis Structure and Organization 15

2 Background 17

2.1 Electroencephalography (EEG) 17

2.2 Epileptiform Discharges (Spikes) 21

2.3 Foundational Neuroscience Behind Sleep-Wake States 24

2.3.1 REM, NREM, Wakefulness: Baseline EEG Patterns 24

2.3.2 Ions, Neurotransmitters, Astrocytes, and Their Role in Modulating EEG 25

2.4 The Biochemical Landscape: Neurotransmitters, Ions, Astrocytes and More 26

2.4.1 Primary Neurotransmitters 26

2.4.1.1 Glutamatergic Activity: 27

2.4.1.2 GABAergic Activity: 31

2.4.2 Secondary Neurotransmitters 34

2.4.2.1 Acetylcholine: 36

2.4.2.2 Orexin 39

2.4.3 Astrocytes: 41

2.4.4 Sleep-Wake Network Dynamics: An Overview 47

2.4.4.1 Wakefulness (Figure 3) 47
2.4.4.2 NREM (Figure 4) 49
2.4.4.3 REM (Figure 5) 52
2.5 Spike Morphology – Biological Mechanisms Derived from Scalp EEG Representation 54
2.5.1 Ascending Slope 55
2.5.2 Descending Slope 57
2.5.3 Asymmetry (Ratio of Ascending Slope over Descending Slope) 58
2.5.4 Pointiness/Spikiness 58
2.5.5 Peak height 59
2.5.6 Normalized Ascending Height 59
2.5.7 Normalized Descending Height 60
2.5.8 Duration/Length 60
2.5.9 Area of Spike 60
2.6 Problem and Solution 61
3 Methodology 64
3.1 Graphical User Interface 65
3.1.1 Functions of the Interface 67
3.1.1.1 Start 67
3.1.1.2 Read EEG Segment 69
3.1.1.3 Plotting 70
3.1.2 Tools Required for Assessing Spikes 71
3.2 Analysis results code: 73
3.2.1 Tasks Necessary for Code to Execute 73
3.2.2 Computational Pipeline for Analyzing Spikes, Including Spike Criteria 74
3.2.3 Statistical Approach: 77

3.2.4 Normality Testing 78
3.2.4.1 Normality Tests 79
3.2.4.2 Visual Representations to Distinguish Normality 80
3.2.5 Significance Testing: Kruskal-Wallis Test 82
3.2.6 Post Hoc Testing: Dunn-Sidak Test and Bonferroni Correction 83
4 Results 85
4.1 Ascending Slope (microvolts/sec) 87
4.2 Descending Slope (microvolts/sec) 90
4.3 Asymmetry (unitless ratio of Ascending slope/Descending slope) 93
4.4 Spikiness/Pointiness (degrees) 96
4.5 Peak Height (microvolts) 99
4.6 Normalized Ascending Height (microvolts) 102
4.7 Normalized Descending Height (microvolts) 105
4.8 Spike Duration (milliseconds) 108
4.9 Spike Area (microvolts * seconds) 111
5 Discussion – Spike Morphologies Throughout Sleep-Wake States 115
5.1.1 Ascending slope 118
5.1.2 Descending Slope 122
5.1.3 Asymmetry 125
5.1.4 Spikiness/Pointiness 129
5.1.5 Peak height 132
5.1.6 Normalized Ascending Height 134
5.1.7 Normalized Descending Height 136
5.1.8 Duration/Length 138
5.1.9 Area of Spike (Summary of Features) 141

5.2 Synthesis: Mechanism Describing REM Sleep's Major Morphological Differences 143
5.2.1 Astrocytic Regulation of pH and Gliotransmitters (Figure 29) 143
5.2.2 How Astrocytic Acidification can Drive Orexinergic Neuronal Firing 145
5.2.3 Why REM Spikes are Significantly Different 146
6 Limitations 149
7 Future Work 152
8 Conclusion 153
References 154
Figure References 175

List of Tables

Table 1: Demographics 86

Table 2: Ascending Slope p-values, Multiple Comparisons 89

Table 3: Descending Slope p-values, Multiple Comparisons 92

Table 4: Asymmetry p-values, Multiple Comparisons 95

Table 5: Spikiness p-values, Multiple Comparisons 98

Table 6: Peak Height p-values, Multiple Comparisons 101

Table 7: Normalized Ascending Height p-values, Multiple Comparisons 104

Table 8: Normalized Descending Height p-values, Multiple Comparisons 107

Table 9: Spike Duration p-values, Multiple Comparisons 110

Table 10: Spike Area p-values, Multiple Comparisons 113

Table 11: Colour Map of Ranked Median Spike Feature Values Across Sleep-Wake States and Montages 116

Table 12: Overview of Mechanisms and Processes to be Explored for Identifying Spike Feature Variations Across Sleep-Wake States 117

List of Figures

Figure 1: A Comprehensive Representation of the Influence of EPSPs and IPSPs on Scalp EEG 18

Figure 2: Coronal Brain Slice Elucidating the Complexities of Measuring Negative Discharges, Analogous to Epileptiform Spikes, on EEG 20

Figure 3: Neural Circuitry of Wakefulness 49

Figure 4: Neural Circuitry of NREM Sleep Regulation 51

Figure 5: Neural Circuitry of REM Sleep Regulation 54

Figure 6: Detailed Dissection of an Epileptiform Spike, Annotated to Spotlight the Multifaceted Processes Governing its Morphology 55

Figure 7: EEG Review Tool Interface 65

Figure 8: Representation of EEG Montages in the 10-20 System 76

Figure 9: Comprehensive Analysis of Data Non-Normality for the Ascending Slope Feature Using the Laplacian Montage 82

Figure 10: Illustration of the Median Epileptiform Spikes Identified Through an Aggregate Analysis of Nine Morphological Features 87

Figure 11: Visualization Showcasing the Substantial Contrast in the Ascending Slope Feature 88

Figure 12: Ascending Slope Boxplot 90

Figure 13: Visualization Showcasing the Substantial Contrast in the Descending Slope Feature 91

Figure 14: Descending Slope Boxplot 93

Figure 15: Visualization Showcasing the Substantial Contrast in the Asymmetry Feature 94

Figure 16: Asymmetry Boxplot 96

Figure 17: Visualization Showcasing the Substantial Contrast in the Spikiness Feature 97

Figure 18: Spikiness Boxplot 99

Figure 19: Visualization Showcasing the Substantial Contrast in the Peak Height Feature 100

Figure 20: Peak Height Boxplot 102

Figure 21: Visualization Showcasing the Substantial Contrast in the Normalized Ascending Height Feature 103

Figure 22: Normalized Ascending Height Boxplot 105

Figure 23: Visualization Showcasing the Substantial Contrast in the Normalized Descending Height Feature 106

Figure 24: Normalized Descending Height Boxplot 108

Figure 25: Visualization Showcasing the Substantial Contrast in the Spike Duration Feature 109

Figure 26: Spike Duration Boxplot 111

Figure 27: Visualization Showcasing the Substantial Contrast in the Spike Area Feature 112

Figure 28: Spike Area Boxplot 114

Figure 29: Illustration of Astrocytic Modulation in the Lateral Hypothalamus during Kindled REM 147

1 Motivation

Epilepsy stands as one of the most prevalent chronic neurological disorders globally, afflicting approximately 65 million individuals [1]. In Canada alone, roughly 360,000 people grapple with this condition, with half of these cases having unknown origins [2]. This disorder of the central nervous system is characterized by recurrent, unprovoked seizures stemming from interruptions in typical neuronal connections. These disruptions pave the way for abnormal electrical activities in the brain, notably epileptiform discharges (EDs).

Although medications have proven to be a viable route to mitigating EDs and consequently reducing the likelihood of seizures, their efficacy is not universal. They either exhibit limited effects or induce adverse reactions in about a third of the epileptic population [3]. While surgery is a hope for those with a discernible epileptiform zone, it is a viable option for less than 2% of individuals [3], [4]. Considering these limitations, therapies centred around diet and neuromodulation emerge as alternatives after the failure of two separate medications and when surgery is not feasible [5], [6]. However, these options generally do not parallel the effectiveness of epilepsy surgeries. Hence, researching and developing novel, safe, and reliable alternatives is paramount to enhancing the quality of life for many individuals with epilepsy. One promising and largely unexplored avenue in this research area is exploring the complex interrelations between epilepsy and sleep-wake states. Delving into the territory of morphological differences in epileptiform discharges across different sleep-wake states may pave the way for innovative theoretical perspectives, potentially fostering novel approaches for treating epilepsy.

1.1 The Nature of Sleep: Patterns, Effects, and Relation to Epilepsy

Sleep, a phenomenon characterized by distinctive and cyclical phases of brain activity, presents as a potential yet relatively untapped avenue for understanding the intricate dynamics of epilepsy. Historically, the study of epilepsy dates to the 18th century, with sleep research gaining prominence in the 19th century. However, it was only in the latter part of the 20th century that a concerted effort began to explore the intricate relationship between sleep patterns and epilepsy [7]. The interactions between diverse background electroencephalographic (EEG) waveforms observed during various sleep-wake states and the influence on modulating epileptic events hint at a promising avenue for further investigation. While the different sleep stages, marked by their unique brain activities and physiological changes, are known to influence the characteristics of epileptic activities to varying degrees, the underlying mechanisms remain largely elusive. The intricate neurophysiological processes unfolding in the different sleep-wake states may offer critical insights into the mechanisms that modulate

epileptic activity, thereby shedding light on why some stages foster or inhibit seizures and other epilepsy-related phenomena.

1.1.1 Fundamentals of Sleep

Crucially, sleep is not a singular, monolithic state but a succession of distinct stages, each with its characteristic brain activities and physiological changes. The first traditional divide is into two main categories: Rapid Eye Movement (REM) sleep and Non-Rapid Eye Movement (NREM) sleep. NREM sleep can be further divided into three stages: NREM 1 - drowsy, NREM 2 – light sleep, and NREM 3 deep sleep or slow-wave sleep [8], [9]. These states are repeated multiple times a night, inducing highly regulated events critical for various functions such as memory consolidation, learning, and brain development [10]. These functions can be related to specific sleep stages associated with explicit EEG patterns and characteristics.

During N1 sleep, often described as a transitional phase between wakefulness and sleep, the brain commences the transition from alpha (8-13 Hz) to theta (4-8 Hz) waves, accompanied by a slowing of eye movement [9]. Again, this period serves as the initial shift towards a state of sleep and generally only accounts for 10% of total sleep time.

N2 denotes the onset of established sleep primarily denoted by theta waves (4-8 Hz), during which the brain generates sleep spindles, which are rapid and rhythmic brain waves, and K-complexes, which are high-amplitude brain waves [9]. Most sleep time is typically spent in N2, accounting for approximately 50% of the total sleep time per night.

The transition from N2 to N3 is marked by the emergence of delta waves (0.5-4 Hz), high-amplitude, low-frequency waves that signify the deepest stage of sleep [9]. This stage only accounts for 10% to 20% of total sleep time, when the body performs most of its restorative processes [11], [12].

Finally, REM sleep, which often coincides with the dreaming state, manifests as rapid eye movements, significantly reduced muscle tone (near paralysis), and brain activity that resembles that of wakefulness, which is characterized by low-amplitude, mixed-frequency activity [11], [13], [14]. REM sleep exhibits numerous intricacies. Notably, it typically does not appear until approximately 90 minutes after sleep onset (falling asleep). Furthermore, REM constitutes around 20% to 25% of the total time per night, with most of REM observed during the latter half of sleep.

These sleep stages are a sophisticated, multi-staged process, each characterized by distinct brain activities and physiological changes. The variation in brain activity across sleep stages can impact various physiological

processes and conditions, including epilepsy. Understanding the interplay between these sleep stages and their associated EEG patterns is crucial to unravelling the complex relationship between sleep and epilepsy, which will be the focus of our subsequent discussion.

1.1.2 Sleep and Epilepsy

Sleep and epilepsy share a symbiotic relationship that is dynamic, multi-faceted, and complex. Only recently have clinicians considered the effects of sleep on epilepsy and its spiralling negative bi-directional relationship [15]. Poor sleep quality can exacerbate seizure frequency and severity, forming a negative feedback loop where the worsening of one condition amplifies the other [16]. An estimated 10-20% of all epilepsy cases are sleep-related, with seizures occurring exclusively at night [17]–[19].

One remarkable feature they share is the cyclical patterns in the neural networks creating distinctive changes in brain activities. These brain rhythms are crucial to the functioning of both sleep and epilepsy and, when altered, can be detrimental [16], [20]. A few of these networks where sleep can activate epilepsy are within the thalamocortical system, cholinergic arousal system and general hippocampal changes during sleep. Disruptions in these sleep networks and rhythms can precipitate sleep disorders and seizures, emphasizing the interdependency between these processes [21].

1.1.3 Influence of Sleep Stages on Epileptic Spike Morphology

The distribution of epileptiform activity across different sleep stages is not uniform. Most epileptiform discharges occur during non-rapid eye movement (NREM) sleep, while rapid eye movement (REM) sleep sees a significant reduction [22], [23]. These findings highlight the differential effects that distinct sleep stages can have on epilepsy and its manifestations. It is crucial to examine critical factors that underscore the implications between sleep stages and epileptiform activity which potentially contribute to the propagation of spikes during different sleep stages. These include but are certainly not limited to:

1. **Cortical Excitability:** The excitability of the brain's cortex changes with the different stages of sleep. During Non-Rapid Eye Movement (NREM) sleep, especially in the deep stages known as slow-wave sleep, the brain's cortex enters a highly synchronized state. This increased synchronization is thought to facilitate the generation and propagation of epileptic discharges. On the other hand, during Rapid Eye Movement (REM) sleep, cortical neurons fire asynchronously, which is generally believed to inhibit seizures [24], [25].

2. **Thalamocortical Rhythms:** The thalamus and cortex are two brain regions critically involved in sleep and epilepsy. During NREM sleep, the thalamus and cortex generate slow, rhythmic oscillations known as "sleep spindles" and "slow waves." These synchronizing rhythms are thought to generate certain types of seizures [26], [27].
3. **Neurotransmitter Systems:** Neurotransmitter systems also vary across sleep stages. For instance, GABAergic activity (which typically inhibits neuronal firing) increases during NREM sleep, while cholinergic activity (which tends to excite neurons) dominates during wakefulness and REM sleep [28], [29]. These changes in neurotransmitter activity may influence seizure generation.

The complexity of sleep extends far beyond a rudimentary comprehension of its stages. Each sleep phase is mediated by diverse pathways and systems, neurotransmitters and neuropeptides, hormones, and various other structures significantly influencing sleep-wake states, potentially affecting the manifestation and characteristics of epileptic spikes. The following section focuses on the nuances observable by scalp EEG measurements to deepen the understanding of these intricate relationships. This analysis seeks to delineate the morphological variations that dictate epileptic activity across various sleep-wake states by cortical EEG readings, providing a critical lens through which the multifaceted relationship between sleep-wake states and epileptiform activity can be examined in finer detail.

1.2 Goals and Objectives

In the pursuit of understanding the morphological changes of epileptiform discharges across different sleep-wake states, this thesis acknowledges a fundamental challenge: the vast variability and complexity inherent in defining and studying "normal sleep." The term itself, while seemingly straightforward, encompasses a range of physiological and neurological processes that are yet to be fully understood or standardized in the context of epilepsy research. The following background section in this thesis sheds light on various neurotransmitters and processes such as glutamate, gamma-aminobutyric acid (GABA), acetylcholine (ACh), orexin, serotonin, norepinephrine, astrocytes, and network dynamics essential for understanding potential changes in epileptic spikes throughout sleep-wake states. However, introducing the concept of non-normal sleep into this equation adds an overwhelming array of variables that could confound the results and obscure the understanding of epileptic activity.

The study is anchored in a literature-based understanding of normal sleep, acknowledging that this baseline might not fully represent the sleep patterns of all epilepsy patients. This grounding is crucial because it provides

a reference framework for analyzing spike morphology without the confounding influence of the myriad anomalies that non-normal sleep might introduce. The focus is on delineating the spikes observed under these controlled conditions, offering a clear baseline against which variations in epileptic patients can be compared and analysed.

The ensuing analysis ventures into the intricacies of these spikes, guided by the foundational understanding of the neurophysiological processes of sleep and the genesis of Paroxysmal Depolarizing Shifts (PDS) as observed in scalp EEG recordings. This approach will allow for a detailed exploration of the morphological changes witnessed in epileptic spikes throughout the sleep-wake states, paving the way for a deeper understanding of the relationship between sleep-wake states and epileptiform activity. This thesis primarily aims to illuminate the underlying mechanisms that govern these morphological changes by dissecting the complexities of spike morphologies across different sleep-wake states. The investigation, grounded in an established framework of normal sleep, seeks to unravel how these spike morphologies shift and what factors contribute to these changes. Through this focused analysis, the study will generate hypotheses about the biological processes influencing these morphologies, providing a platform for deeper inquiry into their potential effects on epilepsy. This exploration is anticipated to yield critical insights, particularly regarding the synchronous network dynamic effects driving the NREM morphology and potentially providing an increased prevalence of spiking during NREM sleep and a novel orexinergic-astrocytic mechanism potentially regulating the abnormal REM spike morphologies and perhaps spike breakthroughs in REM itself. Ultimately, this thesis strives to contribute not only to our understanding of spike morphology in epilepsy but also to how these changes reflect and possibly influence the broader dynamics of epileptic activity within the context of sleep-wake states.

1.3 Thesis Structure and Organization

This thesis is organized into distinct sections, each addressing a critical aspect of investigating epileptiform spike morphology across different sleep-wake states. The structure is as follows:

- **Section 2: Background**
  This section provides an essential foundation, exploring the various neurophysiological processes occurring across sleep-wake states, alongside an introduction to EEG basics. It provides a detailed analysis of how different variations in ion concentrations, neurotransmitter activities, network dynamics, and the role of astrocytes characterize sleep-wake states. Additionally, the section provides a comprehensive breakdown of the epileptic spike, categorizing it into nine distinct features. Each feature is elucidated in the context of these neurological processes, offering a deeper understanding of their

impact on spike morphology. This background is vital for understanding the potential influences on spike morphology and sets the stage for interpretation within the discussion.

- **Section 3: Methodology**

  This section introduces the custom Graphical User Interface (GUI) and the computational pipeline for spike labelling and analysis while focusing on the methodological framework. This section also delves into the methodological core of the thesis, detailing the statistical methods employed in analyzing spike morphology. It begins by assessing the non-normality of the data, which is a critical factor in selecting appropriate statistical techniques. This section details the specific methods employed, such as the Kruskal-Wallis test for determining differences across groups, followed by post hoc analyses using the Dunn-Sidak test and Bonferroni correction for multiple comparisons. This comprehensive methodological overview is crucial for determining significant differences in spike morphology across sleep-wake states and sets the stage for the empirical investigation.

- **Section 4: Results**

  This section contains the core findings, analyseincluding an analysis of 4367 spikes over nine features from seven epilepsy patients across five sleep-wake states and three EEG montages. These findings are instrumental in illustrating how the morphological features of spikes vary across sleep-wake states. It also provides the crucial empirical data necessary for the subsequent discussion, where these differences are extensively examined. The aim is to highlight the major differences in spike morphology and explore the possible underlying mechanisms influencing these changes.

- **Section 5: Discussion**

  This section integrates the empirical findings with existing literature from the background section, offering a comprehensive discussion on the alterations in spike morphologies across sleep-wake states. Particular emphasis is given to the unique characteristics of REM sleep and the impact of EEG montages on interpreting spike morphology. The section also synthesizes the interplay of neurophysiological processes in modulating spike features.

The thesis aims to thoroughly understand the morphological changes of epileptiform spikes in different sleep-wake states, contributing to the broader field of neurology and expanding the underlying knowledge of epileptic activity. Each section builds upon the previous, ensuring a cohesive narrative that effectively addresses the complex relationship between sleep physiology, epileptic activity, and EEG analysis grounded in neurological processes.

2 Background

Section 2 sets the stage for a detailed investigation into the neurophysiological underpinnings of epileptiform spike morphology across different sleep states. It begins with an essential overview of electroencephalography (EEG), epilepsy, and sleep-wake physiology, providing the necessary background to understand the nuances of epileptiform discharges. The section on sleep and epilepsy is concise, contextualizing the thesis's primary focus: the morphological attributes of epileptic spikes during various sleep stages. The section then delves into the roles of ions, neurotransmitters, network dynamics, and astrocytes, scrutinizing their contributions to EEG patterns during wakefulness, NREM and REM. This background aims to identify potential factors that could influence the morphological characteristics of epileptiform spikes. The section explains the biochemical and cellular processes that may modulate spike morphology during sleep by examining astrocytes' primary and secondary neurotransmitters, network dynamics, and function. This foundational section intends to correlate these neurophysiological changes with the observed morphological features of spikes, thereby establishing a framework for the subsequent methodological and analytical exploration.

2.1 Electroencephalography (EEG)

The field of neurophysiology, which primarily explores brain activity through chemical and electrical methods, continuously evolves to improve the resolution at which brain activity can be interpreted. One cornerstone in this discipline is electroencephalography (EEG), a non-invasive technique pioneered by the German psychiatrist Hans Berger in the 1920s [30]. The operation of EEG begins by placing electrodes on the scalp to measure the brain's electrical activity, or more specifically, the fluctuation in voltage caused by ionic current within neurons during synaptic transmission. This measurement of electrical activity is commonly referred to as a field potential, representing the aggregate electrical activity of a large population of neurons within a given volume of brain tissue [31].

At the heart of these signals are synaptic potentials, including both depolarizations and hyperpolarizations. Depolarizations, or excitatory postsynaptic potentials (EPSPs), occur when neurotransmitters like glutamate bind to postsynaptic receptors, enhancing the neuron's propensity to fire and initiate an action potential. Conversely, hyperpolarizations, or inhibitory postsynaptic potentials (IPSPs), occur when neurotransmitters such as GABA bind, reducing the neuron's likelihood of firing [32]. The cumulative effects of EPSPs and IPSPs determine whether the postsynaptic neuron's membrane potential reaches the threshold to initiate an action potential.

Figure 1 illustrates the varying outcomes observed on an EEG when EPSPs or IPSPs are activated across different cortical layers.

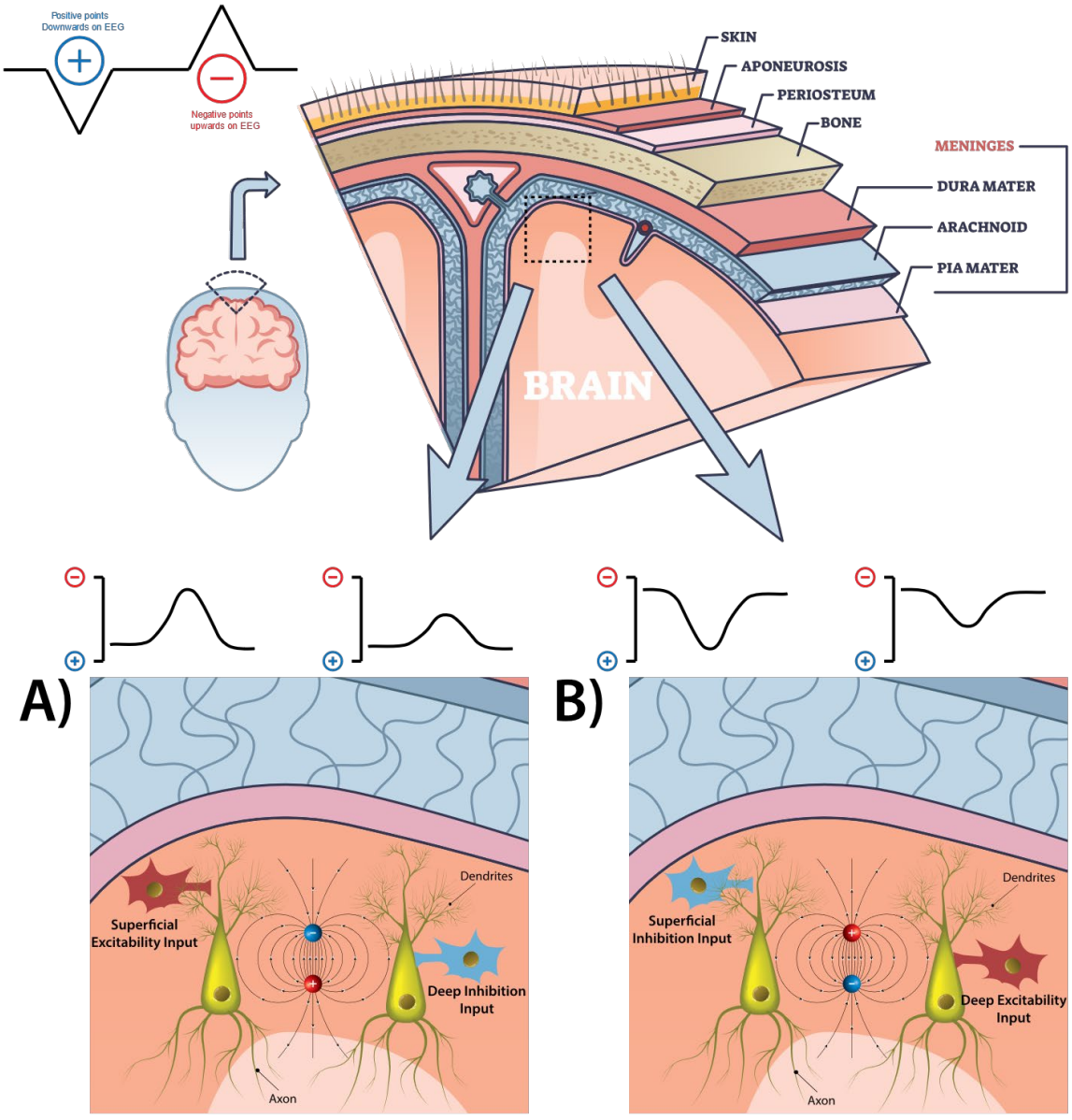


Figure 1: A comprehensive representation of the influence of EPSPs and IPSPs on scalp EEG recordings. Starting with an anatomical depiction of a human head, a sectional zoom-in reveals the stratified layers from the brain to the scalp. A subsequent focus on the cortical grey matter highlights pyramidal neurons in this region, demonstrating both superficial and deep excitability and inhibition. In Panel A, pyramidal cells exhibit negative upward dipoles, characterized by dominant superficial excitatory inputs and subdued deep inhibitory inputs. Conversely, Panel B showcases positive upward dipoles, emphasizing the reverse scenario. At the figure's summit, a legend clarifies EEG conventions: negative potentials are depicted upwards, while positive potentials point downwards. Notably, the figure underscores the significance of volume conduction, illustrating the complex

journey of the dipole through multiple media before its eventual capture at the scalp level.
Source: Figure References [1–3]

During the propagation of EPSPs, each neuron's activity contributes a small portion to the total electrical field. However, the collective, synchronous activity of many neurons, particularly those with similar spatial orientation, can generate a substantial electric field that can be detected on the scalp's surface. For the electrical signal to be captured at the scalp's surface, it must pass through various media such as cerebrospinal fluid, skull, and skin, each offering different resistive conductivities. Volume conduction is the process in which the signal traverses these media, which blurs the propagation's spatial origin, leading to an inherent limitation in EEG's spatial resolution [33].

Despite its limitations in spatial resolution, as evidenced by the need to traverse multiple media such as fluids, bone, and skin (as shown in Figure 1) and the dependency on the location of neurons relative to the electrodes (as illustrated in Figure 2), EEG excels in its temporal resolution. Based on the sampling rate, it can capture changes in brain activity in fractions of a second, making it exceptionally useful for identifying the precise timing of rapidly changing neural events, such as epileptic spikes [34]. However, the interpretation of EEG recordings is not always straightforward. For instance, a superficial EPSP can generate a negative scalp potential, while a deep EPSP generates a positive discharge due to the column-like configuration of cortical neurons [14]. Furthermore, the orientation and exact location of electrical dipoles within the brain significantly determine whether their associated activities can be detected at the scalp. Specifically, only dipoles oriented radially or perpendicular to the scalp surface can be effectively detected by EEG, while dipoles situated tangentially (parallel to the scalp surface) may be missed entirely or mislocalized [33].

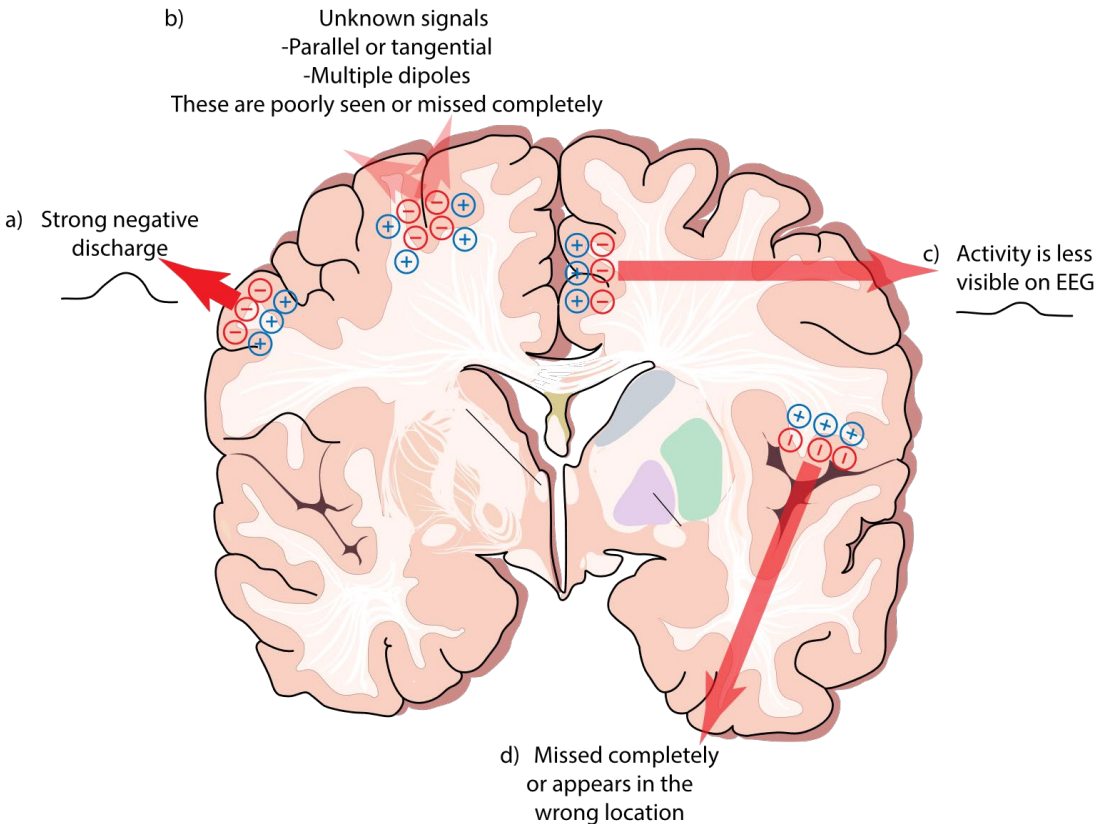


Figure 2: Coronal brain slice elucidating the complexities of measuring negative discharges, analogous to epileptiform spikes, on EEG. From left to right: a) showcases a pronounced negative polarity, driven by a dominant superficial excitatory influence, distinguishing it sharply from the more positive lower region of the cortical pyramidal neurons. b) Represents a dipole from parallel, tangential, or multiple configurations, leading to either a null EEG representation or misleading localizations due to its non-perpendicular orientation to the scalp. c) Demonstrates a more elusive EEG signal depiction, rooted deeper within the cortical grey matter, adjacent to the longitudinal cerebral fissure. This dipole, directed towards the distal side of the same hemisphere, may just as well produce EEG readings that are misleadingly and point towards the opposite hemisphere, adding layers of interpretational challenges. d) The final depiction is a silent dipole, eluding detection altogether, as its projection evades all electrodes, emphasizing the inherent challenges and limitations of EEG interpretation.
Source: Figure Reference [4]

As previously discussed, EEGs are instrumental in analyzing the complex dynamics of neuronal activity, especially in observing how groupings of neurons firing simultaneously can influence the amplitude of signals recorded on an EEG [32], [35]. Building upon this foundation, it becomes pertinent to explore the phenomenon of spikes in greater depth. Through meticulous analysis of EEG recordings coupled with insights from existing literature, we aim to unveil the underlying mechanisms that give rise to these spikes, particularly focusing on the morphological changes induced by the establishment of a Paroxysmal Depolarizing Shift (PDS) and the intricate microbiological processes at play.

2.2 Epileptiform Discharges (Spikes)

Epileptic discharges offer a fundamental interface between the worlds of EEG and epilepsy, translating the neurophysiological abnormality of the latter into the quantifiable signals of the former. Epileptiform discharges, which can indicate a predisposition to seizures, represent abnormal synchronous neuronal activities. These discharges are often recorded by EEG and provide insights into the epileptic processes but do not always confirm the presence of epilepsy.

There are several types of epileptic discharges, including spikes, sharp waves, polyspikes, spike-and-wave complexes, and many more [36]. Each represents a specific pattern of abnormal brain electrical activity, as characterized in detail by Noachtar and Rémi [37]. A spike is a transient electrical discharge unique from background activity with a duration between 20-70 milliseconds with amplitudes typically above 50 μV, while polyspikes refer to multiple occurring sequentially [36]. A sharp wave is similar to a spike but has a slightly longer duration, between 70 and 200 milliseconds (5-14 Hz), with an amplitude typically between 100-200 μV. The distinction between spikes and sharp waves, categorized by their respective durations, is not random but has a neurophysiological basis. A spike, lasting less than 70 milliseconds, is a rapid, high-amplitude discharge that indicates an abrupt, intense, and synchronous firing of a large group of neurons. This synchronous firing is a result of abnormal hyperexcitability in the neural network, which can propagate seizure activity [14]. Sharp waves, lasting between 70 and 200 milliseconds, represent a similar synchronous neuronal firing but are typically less synchronous and involve a broader region of the brain than spikes [14]. Moving forward, the term “spike” will encompass both spike and sharp waves as both epileptic discharges are examined in unison.

One commonality among these discharges is that they represent sudden, transient events of excessive and synchronous neuronal activity. Still, it is essential to understand that not all spikes or sharp waves are epileptic [38], [39]. Some of these transient electrical phenomena are perfectly normal, such as benign transients of sleep (BETS), wickets and vertex waves, often observed on EEGs of individuals without epilepsy [14], [32].

Within the context of epilepsy, the primary focus is “Interictal Epileptic Discharges” (IEDs), which are epileptiform activities that occur between seizures, otherwise known as the interictal period. These discharges can be spikes or sharp waves, with or without after-coming slow waves, and although they are not seizures, their presence is strongly associated with epilepsy [40].

At the cellular level, IEDs are fundamentally rooted in the Paroxysmal Depolarizing Shift (PDS). Characterized by a phase of sustained depolarization, a PDS features an initial burst of action potentials facilitated by AMPA and

NMDA receptor activation, which allows for the rapid influx of sodium (Na^+) and a more sustained inflow of calcium (Ca^{2+}) ions [32], [41], [42]. As the event progresses, L-type calcium channels further amplify the coupling excitatory state of the neuron [42]. As the PDS unfolds, a decline in the amplitude of the action potentials is observed. This decline is likely due to progressive inactivation or desensitization of these contributing channels during continuous depolarization [32], [43]. The termination phase is orchestrated by inhibitory $GABA_A$ and $GABA_B$ receptors that mediate a shift towards hyperpolarization by modulating chloride (Cl^-) and potassium (K^+) ion channels [32], [41]. This intricate orchestration manifests as a sharp spike (depolarization and action potential burst) followed by a slower wave (hyperpolarization), typically captured as an IED on an EEG.

Transitioning from the mechanisms underlying IEDs and their representation on EEG, it becomes apparent that the visual manifestation or the morphology of these discharges, particularly spikes, can be influenced by various factors. The distinct morphological features of these discharges serve as significant diagnostic markers and, as such, have been meticulously defined.

In this context, the International Federation of Clinical Neurophysiology (IFCN) has put forth a comprehensive set of six criteria to describe the characteristic features of an epileptiform transient, which in turn aids in their identification and differentiation from other EEG phenomena [36]. However, it is noteworthy that, despite their widespread usage, these criteria continuously evolve with the validation of the rules governing them to classify epileptic patterns. The current criteria states that for an epileptiform pattern to be recognized, it must meet at least 4 of the following six criteria [36]:

1. Waveforms have two or three distinct phases, characterized by their sharp peaks, signifying the waveform's abrupt rise and fall.
2. Wavelengths that diverge from the continuous background electrical activity either are notably shorter or extend longer, thus making them conspicuous amidst routine neural rhythms.
3. The waveform exhibits asymmetry, demonstrated by a rapid incline during the ascending phase and a slower decline during the descending phase or the reverse.
4. A slower secondary wave follows after the initial sharp wave, which is hypothesized to represent subsequent inhibitory mechanisms counteracting the initial excitatory event.
5. The regular background neural activity undergoes noticeable disturbances when these specific discharges occur, suggesting an alteration in the brain's typical operations.

6. The signal's origin within the brain is hinted at, which could be aligned radially, obliquely, or tangentially through the spatial layout of negative and positive electrical potentials on the scalp.

While these criteria are extensively utilized, a comprehensive analysis presented by Kural M.A. et al. [44] delved into the diagnostic accuracy correlating with the number of criteria required to define a spike. This pivotal study revealed that an optimal diagnostic outcome necessitates fulfilling five criteria. Moreover, it suggested that source space metrics could provide a more refined understanding of epileptiform discharges, supplementing the conventional sensor space methods.

Delving deeper into the complexities of epileptic discharges, a crucial element that demands attention is the role of thalamocortical reverberations. This system involves a sophisticated interplay between the thalamus, the brain's key relay station, and the cerebral cortex, the outer layer of the brain accountable for higher cognitive functions [45]. It involves a finely tuned balance between excitatory and inhibitory signals between the thalamus and the cortex. This process is essential for standard brain functionality, but its perturbation can also lead to the abnormal synchronization of neuronal activity that produces epileptic spikes [45]. In other words, the reverberations significantly contribute to both normal brain rhythms and pathological patterns, including the generation of epileptic spikes [45].

A compelling aspect of these reverberations is their profound influence on sleep regulation [46]. Thalamocortical interactions generate specific EEG waveforms associated with different sleep stages, including sleep spindles during stage 2 NREM (non-rapid eye movement) sleep. These sleep spindles, generated by the rhythmic activity of thalamic reticular neurons and their interaction with cortical neurons, indicate sensory processing, long-term memory consolidation, and maintaining the boundary between sleep stages, among other functions.

The intricate network of thalamocortical interactions also regulates the transition between wakefulness and sleep states. It orchestrates the irregular, low-amplitude, high-frequency activity during wakefulness and the shift to regular, high-amplitude, low-frequency activity at sleep onset [47]. Furthermore, the transition from NREM to REM (rapid eye movement) sleep involves a shift in the pattern of thalamocortical activity, paralleling wakefulness and thereby contributing to the vivid dreaming associated with REM sleep.

In summary, the pivotal role of thalamocortical reverberations not only shapes the landscape of epileptic discharges but also intricately regulates the various stages of sleep. However, our understanding of these processes still has room for significant growth. As Chapter 8 of Niedermeyer et al. [14] discloses, "Our comprehension of alpha rhythm genesis has not strikingly increased in the past several decades; it seems likely that there are corticocortical and thalamocortical systems that interact in the generation of cortical alpha

rhythms." This conclusion reflects the persistent mysteries surrounding these neural networks and their impact on the brain's functionality. Sleep and epilepsy play a pivotal role together with interactions that can provide a critical foundation for development in understanding the multifaceted nature of epilepsy and spikes.

An in-depth exploration of the fundamental neuroscience underlying these phenomena is necessary to comprehensively understand sleep-wake state-dependent spike morphological changes. Scalp EEG, while invaluable, provides only an aggregate view of brain activity due to its measurement of electrical dipoles generated by neuronal activity [14]. Therefore, it is crucial to correlate these surface-level observations to the cellular and subcellular events occurring within the brain. Such an approach can facilitate a more nuanced understanding of how individual neurons or groups of neurons modulate their firing patterns, thus influencing the morphological characteristics of EEG spikes.

2.3 Foundational Neuroscience Behind Sleep-Wake States

2.3.1 REM, NREM, Wakefulness: Baseline EEG Patterns

The neurophysiological architecture that underpins the sleep-wake cycle is complex and relies on a rich interplay of cellular and biochemical factors that translate into distinct electroencephalographic (EEG) patterns discussed below [9], [11], [14], [47]. Three primary states dominate this cycle: Wakefulness, Non-REM (NREM) sleep, and Rapid Eye Movement (REM) sleep.

- **Wakefulness:** In this state, individuals experience heightened alertness and cognitive engagement. The EEG signature predominantly shows low-amplitude, mixed-frequency waves, particularly in the beta and alpha frequency bands. Cortical pyramidal neurons display more asynchronous firing patterns, leading to these faster EEG activities. Additionally, eye blinks, and muscle artifacts are characteristic of wakefulness. If a posterior dominant rhythm (PDR) is present, then to score as being awake within the AASM standard (30 second window), a minimum of 50% PDR must be present over the occipital region [9].
- **NREM Sleep:** Divided into three stages—N1, N2, and N3—each with unique EEG characteristics:
    - **N1:** This stage represents the transition from wakefulness to sleep. Often called the drowsy or pre-sleep stage, N1 features low-amplitude, mixed-frequency activity. Importantly, N1 does not display sleep-specific characteristics like spindles or K-complexes but shows the disappearance of PDR.

- **N2:** Characterized by sleep spindles and K-complexes, N2 shows a reduced overall neuronal firing compared to N1, with prevalent synchronous theta activity.
- **N3:** Also known as deep sleep or slow-wave sleep, N3 features high-amplitude (> 75 μV) and low-frequency (0.5 to 2Hz) delta activity. The cortical pyramidal neurons exhibit synchronized firing patterns, contributing to generating these slow waves.

Given the unique EEG characteristics and neuronal firing patterns associated with each NREM stage—N1's mixed-frequency activity, N2's sleep spindles and K-complexes, and N3's synchronized delta activity—it is conceivable that these stages could have distinct influences on the morphological characteristics of spikes observed in epileptic discharges [11], [14], [47]. In this context, N1 could offer a less stable baseline due to its transitional nature. In contrast, the reduced neuronal firing and prevalent synchronous theta activity in N2 might produce spikes with other specific attributes. N3, characterized by highly synchronized neuronal firing, could further modulate the characteristics of spikes in a different manner, potentially due to the involvement of cellular and subcellular processes like memory consolidation and cellular repair [11], [14], [47]. Thus, understanding the nuanced differences between these NREM stages is crucial for a comprehensive analysis of sleep-wake state-dependent spike morphological changes.

- **REM Sleep:** the electroencephalogram (EEG) displays desynchronized patterns featuring low-amplitude, mixed-frequency waves predominantly in the beta, theta, and gamma bands [48], [49]. This desynchronization suggests a state of heightened neural activity similar to wakefulness. The stage is also marked by unique characteristics such as rapid eye movements and almost complete paralysis of skeletal muscles, or muscle atonia. The high brain activity, evidenced by desynchronized EEG, occurs in stark contrast to this muscle inactivity. Importantly, REM sleep is crucial in neural plasticity, which refers to the brain's ability to reorganize itself by forming new neural connections [50], [51]. It is also significant for memory consolidation, where the brain stabilizes and stores information [52].

2.3.2 Ions, Neurotransmitters, Astrocytes, and Their Role in Modulating EEG

Understanding the complex interplay of biochemical factors is essential for decoding the EEG patterns in sleep-wake cycles, as well as in pathological states like epilepsy. Primary neurotransmitters such as glutamate and GABA maintain a balance of excitatory and inhibitory signals among cortical pyramidal neurons [32]. Ionic currents involving calcium (Ca^{2+}), sodium (Na^{+}), potassium (K^{+}), chloride (Cl^{-}), and magnesium (Mg^{2+}) are fundamental in mediating neuronal firing and synaptic communication [53].

Secondary neurotransmitters like acetylcholine (ACh), orexin, noradrenaline, and serotonin also play critical roles in modulating EEG patterns, particularly within sleep-wake cycles, which may affect paroxysmal depolarizing shifts (PDSs) characteristic of epileptic activity. ACh is crucial for REM sleep and wakefulness, influencing pyramidal neurons through muscarinic and nicotinic receptors [54]. Orexin, released from the lateral hypothalamus, is significant in maintaining wakefulness and stabilizing the transition between sleep states [55]. Noradrenaline, primarily released in the locus coeruleus, contributes to arousal and attention, and its reduced activity is associated with non-REM sleep [56]. Serotonin, originating from the dorsal raphe nuclei, has complex effects but generally promotes wakefulness and inhibits REM sleep [57]. These secondary neurotransmitters interact with primary neurotransmitters like glutamate and GABA, in conjunction with ion channels, to bring about a finely tuned balance of excitatory and inhibitory activity that manifests in the EEG as specific sleep-wake patterns or pathological states such as epilepsy.

Astrocytes are often overlooked but crucial players in this biochemical landscape. Their regulatory reach spans from ion homeostasis to neurotransmitter recycling and metabolic support to homeostatic sleep [58]. Through specialized gap junctions, astrocytes establish a robust network that facilitates the coordinated exchange of ions like Na^+, Ca^{2+}, and K^+, along with vital metabolites such as glucose and lactate [59]. These gap junctions are essential for ion balancing and metabolic trafficking, directly contributing to neuronal energy supply. In essence, astrocytes function as homeostatic regulators of ions, pH, and energy metabolites while contributing to network plasticity and synaptic modulation. They also have a hand in chemosensing, regulating the blood-brain barrier, lymphatic system, and glycogen synthesis, and even play a role in synaptic elimination and network stability [60], [61]. These multi-talented glial cells thus serve as versatile conductors orchestrating the symphony of neural activities captured in EEG patterns.

By setting this foundational stage, the following sections will offer a detailed exploration of these factors, explaining their specific roles and interactions in shaping the normal sleep-wake cycle and the unique neurophysiological patterns measured by scalp electrodes.

2.4 The Biochemical Landscape: Neurotransmitters, Ions, Astrocytes and More

2.4.1 Primary Neurotransmitters

Cortical neurons, the primary focus of electroencephalogram (EEG) measurements, are predominantly modulated by two neurotransmitters: Glutamate and GABA (Gamma-Aminobutyric Acid). Glutamate, the

primary excitatory neurotransmitter, and GABA, the main inhibitory neurotransmitter, work in tandem to regulate neural activity within the cortex [32]. Their effects are not limited to cortical neurons; they also influence deeper brain structures like the thalamus and hippocampus, which in turn modulate cortical activity [62]. These neurotransmitters interact through different types of receptors: ionotropic receptors directly influence ion channels for an immediate response, whereas metabotropic receptors work more slowly, using G-protein intermediaries to modulate other proteins, ion channels, or enzymes [32], [63]. This nuanced interplay between Glutamate and GABA is critical for understanding the events that occur and how they can be affected through the lens of EEG. While EEGs do not directly reveal these microscopic processes, the underlying dynamics can be inferred through rigorous supporting research, making the study of these neurotransmitters critical for understanding brain activity as observed through EEG [14].

2.4.1.1 Glutamatergic Activity:

Glutamate serves as the principal excitatory neurotransmitter in the central nervous system, modulating synaptic strength and neural excitability through its binding to receptors like AMPA, NMDA, kainate, and metabotropic glutamate receptors. During wakefulness and REM sleep, glutamate concentrations typically remain elevated to sustain cognitive functions, sensory processing, and memory consolidation [64], [65]. Dash [65] also emphasized as the brain transitions into non-REM sleep, glutamate levels generally decline, reaching their lowest during slow-wave sleep (N3). This fluctuation is not solely due to the amount of available glutamate but also involves complex mechanisms such as receptor trafficking, where binding sites may be internalized, and alterations in the rate of ion channel conductance. These mechanisms collectively modulate synaptic strength and neural excitability across different sleep-wake states.

Each receptor type brings unique properties to this modulation. AMPA receptors, known for their fast activation and inactivation kinetics, primarily permit the rapid influx of sodium and calcium ions [32], [41]. NMDA receptors, on the other hand, require not just glutamate binding but also membrane depolarization to remove magnesium (Mg^{2+}) blockage locally, thereby allowing a more controlled and sustained entry of calcium and sodium ions [32], [41], [66]. Kainate receptors contribute to this dynamic by almost exclusively gating sodium and possessing slower inactivation kinetics [41]. Their activation can thus sustain the paroxysmal depolarizing shift (PDS) changes over a more extended period, effectively modulating the event [67]. Finally, metabotropic glutamate receptors, another class of glutamate receptors, work through G-proteins to activate intracellular signalling pathways, thus having a more modulatory role in synaptic transmission and plasticity [32], [41]. They can fine-tune the excitatory input from ionotropic receptors like AMPA, NMDA, and kainate, particularly in

pathological conditions like epilepsy [68]. These combined mechanisms allow for complex regulation of synaptic plasticity and neural excitability across different sleep-wake states, influenced by receptor trafficking and ion channel conductance alterations [65], [69].

- **Ionotropic Glutamate Receptors**: These include AMPA (α-Amino-3-hydroxy-5-Methyl-4-isoxazole Propionic Acid), NMDA (N-Methyl-D-Aspartate), and kainate receptors. Activation of these receptors allows the influx of ions like Na^+ and Ca^{2+}, facilitating excitatory postsynaptic potentials.
    - **AMPA Receptors**: These are integral for fast excitatory synaptic transmission. They are predominantly permeable to sodium ions and, upon activation, lead to rapid depolarization of the postsynaptic membrane. This quick action allows AMPA receptors to mediate the fast component of excitatory postsynaptic potentials (EPSPs). During a PDS, the rapid and transient activation of AMPA receptors can initiate and contribute to the beginning of depolarization. Their swift kinetics allow them to respond effectively to high-frequency synaptic inputs, making them well-suited to start the early phases of a PDS where other processes, such as receptors or networks, play a role in their clustering synchronous firing [67], [70].
        1. **Wakefulness (Baseline)**: The brain is engaged in various activities that necessitate fast excitatory neurotransmission mediated by AMPA receptors. AMPA receptors are usually upregulated at the synapses due to higher sensory inputs and cognitive tasks, serving as the baseline AMPA receptor density and conductivity [71].
        2. **N1 (Drowsiness)**: As the brain transitions into light sleep (N1), cortical activity diminishes. AMPA receptor density and/or sensitivity may also likely decrease, although specific research data on AMPA receptors in the N1 stage is limited [65].
        3. **N2 (Sleep)**: Sleep spindles and K-complexes dominate the EEG readings during this stage. These might involve the downscaling of AMPA receptors, possibly reducing overall excitability and promoting energy conservation, consistent with the synaptic homeostasis hypothesis [64], [72], [73].
        4. **N3 (Deep Sleep)**: being that of the slowest-wave sleep, continues to decrease in overall AMPA density and activity. These conditions facilitate the brain's entry into a state of low excitability. This could either result from reduced glutamate release or an actual decrease in AMPA receptor density at synapses [74].

5. **REM (Rapid Eye Movement Sleep)**: the role of AMPA receptor trafficking and activity in cortical neurons is not yet fully understood. Given the complex interplay of cholinergic, GABAergic, and glutamatergic systems in regulating sleep-wake cycles and cortical function, the specific contributions of these neurotransmitter systems to AMPA receptor activity and overall cortical function during REM sleep remain an area for further research.

- **NMDA Receptors:** play a specialized role in excitatory synaptic transmission and are distinct from other ionotropic glutamate receptors like AMPA. Unlike AMPA receptors, which mediate rapid excitatory synaptic currents, NMDA receptors contribute to slower, more prolonged depolarization events [75], [76]. This characteristic makes them vital for the phenomena such as the paroxysmal depolarization shift (PDS). Activation of NMDA receptors requires the binding of two ligands: glutamate, released from the presynaptic neuron, and glycine, which is generally present in the synaptic cleft [77]. Notably, the NMDA receptor is both ligand-gated and voltage-gated; Mg2+ ions block it at resting membrane potentials. The removal of this Mg^{2+} block is not directly mediated by glycine but instead requires the depolarization of the postsynaptic membrane, often facilitated by the action of AMPA receptors or intrinsic membrane properties [77]. Once the Mg^{2+} block is relieved, the NMDA receptor allows Ca2+ and Na+ ions to pass, leading to longer-lasting depolarizations [77]. With further depolarizations, the trend of removing Mg^{2+} blockers enables the receptor to continue significantly contributing to sustaining a PDS [78]–[80].

    1. **Wakefulness (Baseline):** NMDA receptors play a critical role in sustaining heightened neural plasticity and supporting cognitive functions such as learning and memory. These receptors facilitate long-term potentiation, a process underlying memory formation. At this stage, NMDA receptors actively participate in synaptic transmission, fostering connectivity and information processing [81].

    2. **NREM sleep stages (N1, N2, & N3):** As one progresses deeper into the stages of NREM sleep, the behaviour of NMDA receptors begins to mirror that of AMPA receptors, aligning with a global downscaling of synaptic strength. This downscaling is theorized to serve as a mechanism to conserve energy and reset synaptic homeostasis. Despite this downscaling, NMDA receptors possibly retain a role in orchestrating the slow-wave oscillations typical of this phase, potentially aiding in synaptic pruning and the consolidation of memory [64], [82].

3. **REM (Rapid Eye Movement):** The REM sleep phase may witness a resurgence of NMDA receptor activity, fostering synaptic plasticity and aiding memory consolidation processes intrinsic to this sleep stage. Although the role of cortical NMDA receptors during this stage is not thoroughly understood, it is hypothesized that they mediate slow, prolonged depolarizations that could be linked to the heightened brain activity and vivid dreaming experiences characteristic of REM sleep. In contrast to the limited research on cortical NMDA receptors, NMDA receptors in the pedunculopontine tegmental nucleus (PPT) have been extensively studied. Research indicates when kainate receptors are activated, this results in REM sleep generation; however, when NMDA receptors also become activated on the PPT, it results in wakefulness, demonstrating intrinsic differences in characteristics throughout different receptor bindings [83], [84].

- **Kainate Receptors**: These have recently begun receiving attention, although literature concerning their role in sleep-wake states remains sparse, possibly due to a lack of appropriate pharmacological tools [85]. Most of the existing studies focus on REM sleep and epilepsy. In the realm of sleep, especially REM sleep, kainate receptors are mainly discussed in the context of deep brain structures. For instance, they have been implicated in the pedunculopontine tegmental nucleus (PPT) where they are hypothesized to regulate and perhaps extend the duration of REM sleep [86]–[88]. Activation of NMDA and kainate receptors in the PPT has been found to increase both the duration of REM sleep and wakefulness, with NMDA receptor activity more closely linked to wakefulness and kainate receptor activity potentially influencing REM sleep duration [86].

  In the epileptic context, the role of kainate receptors appears to be nuanced. For instance, the AMPA/kainate antagonist CNQX has been shown to abolish ictal spiking, although it does not entirely suppress interictal spikes [89]. This selective suppression suggests that kainate receptors could have a role in modulating the more subtle aspects of epileptiform activity. However, while these receptors are not essential for initiating a PDS, they can modulate the amplitude of the first action potential [67]. Furthermore, the most striking observation from Laryushkin's research [67] notes that blocking kainate receptors with an antagonist reduces the amplitude of this initial action potential and decreases the number of PDSs in a cluster. This clustering modulation could

affect the dipole measured by surface EEG, thereby changing the characteristics of epileptiform spikes.

- **Metabotropic Glutamate Receptors (mGluRs)**: These receptors function through G-proteins and can positively and negatively modulate neuronal excitability depending on the subtype [86].
    - mGluRs are central to cortical neuronal signalling and are theorized to undergo nuanced modulations throughout sleep-wake cycles, potentially echoing in the cortical activity detectable via scalp electrodes. In neurons, these receptors catalyze a cascade of signalling events mediated by secondary messengers such as cyclic AMP (cAMP), inositol trisphosphate (IP3), and diacylglycerol (DAG), fostering a complex intracellular dialogue vital for synaptic plasticity and memory consolidation [90]. This intricate cellular communication, initiated by the binding of glutamate to mGluRs, paints a dynamic canvas of cortical activity across various sleep phases, as reflected in the complex EEG patterns captured through scalp electrodes. It is possible that during different sleep states, alterations might occur in receptor density, G-protein coupling efficiency, or the dynamics of secondary messengers. However, concrete data delineating these changes remains elusive. Similarly, the role of mGluRs in astrocytes hints at a layered complexity, fostering rich neuron-astrocyte interactions integral to cerebral cortex function, which will be explored in the glial section [91].

2.4.1.2 GABAergic Activity:

GABA, or Gamma-Aminobutyric Acid, serves as the central nervous system's principal inhibitory neurotransmitter, counterbalancing glutamate's excitatory effects. During different sleep-wake phases, the GABAergic system undergoes various modulations to support cognitive processes like memory consolidation and facilitate transitions between sleep-wake cycles [92]. Central to the orchestration of sleep dynamics is the thalamocortical network, which drives most neural activities observed during different sleep phases, including the modulation of the GABAergic system to support cognitive processes like memory consolidation and transitions between sleep-wake cycles [93]. However, the thalamocortical network is not the sole entity governing these complex neural dynamics witnessed through the lens of EEG. Recent studies on neurogliaform interneurons reveal that a single depolarization of a glial cell triggers a flood of GABA, contributing to slow inhibitory activity in pyramidal neurons, and strongly activates $GABA_B$ receptors [94], [95]. It is not simply the pathways that create global brain activity throughout the sleep-wake states but a number of other cells and substances, adding a layer of complexity to our understanding of the neuronal processes captured by EEG.

GABA, the prominent inhibitory neurotransmitter in the brain, exhibits varied concentrations across different regions, thereby playing a pivotal role in modulating various neural processes. Specifically in the locus coeruleus (LC), a nucleus in the brainstem, the fluctuations in GABA levels are crucial in governing the dynamics of the REM sleep stage [28]. During REM sleep, heightened GABA activity in the LC curtails the release of norepinephrine, fostering the transition from deep NREM sleep to the lighter, dream-infused REM phase. Meanwhile, during wakefulness, the LC continues to have high GABA concentrations; therefore, the regulation of alertness and consciousness is more profoundly influenced by other brain regions, such as the thalamus, which collaborates with a spectrum of neural networks to modulate arousal levels, with less direct impact from the GABAergic system in the LC. This intricate interplay showcases GABA's nuanced role in different brain sectors in facilitating a balanced cycle of sleep and wakefulness [28], [96]. Yet, it is pertinent to note that while inhibitory influences are orchestrated from deeper brain structures and relayed to the cortex, the cortex itself actively modulates neural activities through GABAergic IPSPs. The exact dynamics of these cortical processes, including variations in GABA concentrations and receptor strengths during different sleep states, remain largely elusive [95].

Ionotropic GABA Receptors ($GABA_A$):

$GABA_A$ receptors are involved in mediating fast inhibitory synaptic transmission in the central nervous system by allowing the influx of chloride ions through ion channels [97]. Activating these receptors leads to hyperpolarization of the postsynaptic membrane, making neurons less likely to fire action potentials. Here, we will explore the potential role and modulation of $GABA_A$ receptors during different sleep stages:

1. **Wakefulness (Baseline)**: $GABA_A$ receptors are actively involved in maintaining a balance between neuronal excitation and inhibition, which can be reflected in EEG as stable and organized oscillatory activity. This state helps foster attention and cognitive function, potentially influencing EEG beta wave (13-30 Hz) activity, which is associated with alertness and focused attention [78].
2. **NREM Sleep (N1, N2, & N3)**: As the transition to deeper NREM sleep an increase in $GABA_A$ receptor activity can be observed, promoting deeper sleep stages. This slow wave activity (SWA) is reflected in the EEG as increased delta (0.5-4 Hz) and theta (4-8 Hz) wave activity, which are characteristic of NREM sleep, facilitating the generation of sleep spindles and K-complexes, hallmark EEG features of this sleep stage [46].
3. **REM (Rapid Eye Movement)**: Brown's [98] reviews of GABA activity within REM and how receptors throughout the brain influence cortical neurons either directly or indirectly reveal the EEG signals

indicative of REM. In understanding the impact of $GABA_A$ receptors on REM sleep, starting at the roots—deep within the brain's basal forebrain (BF) and ventral tegmental area (VTA) - is pivotal. GABAergic neurons are highly sensitive to neurotransmitters like acetylcholine, norepinephrine, histamines, and orexins in these areas. This sensitivity triggers a faster firing rate in these neurons, particularly during wakefulness and REM sleep. As these BF neurons project to the cortex, they exert a substantial influence over cortical excitability, laying the groundwork for the patterns observed on an EEG during REM sleep [97], [99], [100].

$GABA_A$ receptors have a multifaceted role in regulating REM sleep beyond just facilitating muscle atonia, which has been implied to play a minor role [101], [102]. Brown's [98] in-depth review of $GABA_A$ receptors discusses their involvement in complex neural networks determining when REM sleep is initiated, maintained, and terminated. For example, REM-off neurons in the brain's subcoeruleus (SubC), nucleus pontine reticular nucleus, and oral part (PnO) regions are primarily under inhibitory GABAergic control. When $GABA_A$ receptor antagonists like bicuculline are applied to these regions, a REM-like state is induced in cats and rats [103], [104]. This animal response is consistent with microdialysis measurements showing that GABA levels in the reticular formation vary across behavioural states, highest in wakefulness and lowest in REM sleep [105], [106].

Moreover, [98] highlights that GABAergic inputs to the SubC originate from regions like the PnO, ventrolateral periaqueductal grey matter (vlPAG), and the lateral pontine tegmentum (LPT). Inhibition of these areas using the $GABA_A$ receptor agonist muscimol is known to increase REM sleep substantially. Cell body-specific lesions in the vlPAG or LPT also cause an increase in REM sleep duration and frequency. However, it is worth mentioning that the role of $GABA_A$ receptors in this region is still under scrutiny. A contradicting study has indicated that the inactivation of GABAergic and glycinergic neurotransmission in these regions did not significantly alter REM sleep [107]. This contradiction suggests that the inhibition of REM-on neurons is influenced by alternative measures such as glutamatergic activity to other networks or even astrocytic regulation.

Metabotropic GABA Receptors ($GABA_B$):

$GABA_B$ receptors are G-protein coupled receptors that mediate prolonged inhibitory responses. These receptors function by modulating the activity of ion channels (potassium and calcium) and intracellular signalling pathways. Through the modulation of K^+ and Ca^{2+} ion channels, $GABA_B$ receptors contribute to the generation of

IPSPs, essentially providing inhibition by counteracting EPSPs when summated [108]. $GABA_B$ also has various indirect pathways for influencing cortical neurons; for example, modulating glutamate release [109].

1. **Wakefulness (Baseline)**: $GABA_B$ receptors stabilize neuronal networks during wakefulness by modulating synaptic transmission and preventing over-excitation, which can be reflected in the EEG as stable beta wave activity (13-30 Hz). While specific research directly linking $GABA_B$ receptor activity and EEG patterns during wakefulness is sparse, existing literature suggests a role of these receptors in maintaining the balance of excitation and inhibition, essential for alert cognitive states [109].
2. **NREM Sleep (N1, N2, & N3)**: $GABA_B$ receptors might play a role in generating slow-wave activity, characteristic of deep sleep stages, potentially reflected in the EEG as increased delta wave activity. These receptors might also contribute to synaptic downscaling, which could influence EEG patterns by modulating the amplitude and frequency of slow-wave activity [47].
3. **REM (Rapid Eye Movement)**: The functionality of cortical $GABA_B$ receptors during REM sleep is not thoroughly documented. Hypothesized roles include modulating the frequency and amplitude of theta waves (4-8 Hz), characteristic of REM sleep, possibly influencing vivid dreaming experiences and memory consolidation similar to $GABA_A$ [110], [111]. However, a study by Ulloor [112] reveals that $GABA_B$ is the sole GABA receptor within the PPT to influence REM sleep in rats.

2.4.2 Secondary Neurotransmitters

Secondary neurotransmitters and neuropeptides offer a more complex layer to the sleep-wake cycle than the classical neurotransmitters like glutamate and GABA. For instance, a handful of these transmitters that aid in regulating and modulating the sleep-wake states include, but are not limited to, acetylcholine (ACh), orexin, norepinephrine, and serotonin [98].

ACh is mainly concentrated in the basal forebrain and brainstem nuclei, such as the pedunculopontine tegmental (PPT) and laterodorsal tegmental (LDT) nuclei [47]. During wakefulness and REM sleep, levels of ACh are generally high, while REM sleep facilitates maximal concentration and activity, facilitating alertness and rapid eye movement respectively [113]. In contrast, during non-REM sleep, ACh levels are typically low. Its role is multifaceted, impacting sleep cycles, learning, and memory [114].

Orexin, also known as hypocretin, is produced in the lateral hypothalamus and is critical in regulating wakefulness and arousal [55], [115]. This neuropeptide influences various brain regions, including the ventrolateral preoptic area (VLPO), PPT, and LDT nuclei. Generally, orexinergic neurons promote wakefulness by

inhibiting sleep-promoting regions like the VLPO and activating wake-promoting areas. However, a lack of orexin can indirectly encourage sleep, as evidenced in conditions like narcolepsy [116]. In such cases, the absence of orexinergic activity allows sleep-promoting systems, such as the VLPO, to become more active [55], [115].

Norepinephrine (NE), primarily produced in the locus coeruleus, is a small nucleus in the pons found within the brainstem that plays a pivotal role in regulating wakefulness and attention [56], [117]. It has robust projections to several key brain areas, including the prefrontal cortex, amygdala, and thalamus [56], [117]. During wakefulness, the locus coeruleus is active, leading to heightened levels of norepinephrine that bolster attention and alertness [56], [117]. In contrast, during non-REM sleep, activity in the locus coeruleus—and therefore norepinephrine release—is reduced, contributing to a state of low arousal. Remarkably, norepinephrine levels drop to their lowest during REM sleep, with a complete cessation of neuronal firing within the LC [56], [117]. This neurotransmitter is essential for transitions between sleep and wakefulness, stabilizing wake periods and initiating sleep [56], [117]. Norepinephrine's role in sleep-wake regulation is complex, modulating the arousal systems and interacting with other neurotransmitters like serotonin and acetylcholine to fine-tune behavioural states [117]. Notably, the LC-norepinephrine system also significantly contributes to measured EEG arousals. Past research [117] further substantiates this by showing that measured EEG arousals decrease when serotonergic transmissions are inhibited and dopaminergic receptors are blocked. This evidence underscores the critical role of ascending neuromodulatory systems, including the LC-norepinephrine system, in shaping sleep-wake dynamics as visualized by scalp EEG.

Serotonin, predominantly produced in the raphe nuclei of the brainstem, serves as a critical neurotransmitter in the regulation of mood, anxiety, and, most notably, sleep-wake cycles [57], [118]–[120]. During waking hours, serotonin release is elevated, promoting alertness and wakefulness. However, serotonin release decreases during non-REM sleep and is reduced even more within REM sleep [118]. As previously discussed, serotonin works with other neurotransmitters to regulate sleep architecture and facilitate transitions between sleep and wakefulness within their respective inhibitions and excitations of arousal activity, be it with increased or decreased firing [98].

Moreover, reducing serotonin during REM sleep may play a primary role in the function of REM sleep muscle atonia [55]. This role is further substantiated when serotonergic activity is increased, leading to diminished REM atonia and heightened muscle activity [121]. Brook's [101] study additionally supports the hypothesis of serotonin's role in muscle atonia. Still, it proposes that the picture is more complex, involving additional factors such as decreased noradrenergic activity and increased $GABA_A$-mediated inhibition. Due to reduced muscle artifacts, these complex neurochemical mechanisms manifest particularly clearly in scalp EEG recordings.

These secondary neurotransmitters can indirectly influence cortical neurons and their measurements via scalp electrodes by modulating receptor sensitivities or participating in neuronal network changes, thus affecting the fundamentals of sleep and wake states. Their impact extends not only to direct modulation of neural firing rates but also to more nuanced regulatory roles, which include affecting the expression of primary neurotransmitters and their receptors, thus indirectly shaping sleep architecture and quality.

2.4.2.1 Acetylcholine:

Acetylcholine (ACh), an essential neurotransmitter, modulates cortical and subcortical neuronal activities. It acts both at the cortical level, influencing cortical neurons directly, and at the subcortical level, influencing the thalamus and brainstem nuclei such as the pedunculopontine tegmental nucleus (PPT), laterodorsal tegmental nucleus (LDT), and the nucleus basalis of Meynert [122]. This multifaceted influence of ACh is crucial in shaping cortical EEG rhythms, sleep-wake cycles, and cognitive functions. ACh achieves these roles through its action on nicotinic and muscarinic receptors, distributed across different neuronal populations [123]. Furthermore, ACh shares specific characteristics with glutamate, chiefly acting as an excitatory neurotransmitter; however, depending on the receptor and subunit, it can also act as an inhibitor. Particularly in cortical neurons, specific muscarinic receptors predominantly reduce potassium (K+) conductance, contributing to membrane depolarizations. This process restrains the efflux of K^+ ions from the cells, fostering a conducive environment for spontaneous cortical rhythms, particularly during brain activation [124]. Nicotinic receptors, on the other hand, allow an influx of small cations such as Na^+, Ca^{2+} and K^+ exceptionally quickly, resulting in an instantaneous depolarization [125], [126].

Direct Cortical Influence:

1. **Cortical Pyramidal Neurons**: These are directly modulated by ACh via muscarinic and nicotinic receptors, affecting their excitability and synaptic plasticity [127]. These processes influence EEG rhythms by altering the ionic milieu in these neurons, which can be dissected further as below:
    - **Wakeful State**: High ACh levels modulate pyramidal neurons to exhibit increased firing rates, facilitating alertness and attention. This modulation is often mirrored in the EEG as an increase in beta and gamma wave activity associated with alert and active brain states [29]. ACh also promotes synaptic plasticity in these neurons, enhancing learning and memory during wakeful states. This effect can be observed as changes in the power and coherence of specific EEG rhythms, which may manifest as a shift towards more desynchronous activity, indicative of enhanced cortical communication and processing [127].

- **NREM Sleep**: ACh levels decrease, leading to a reduction in the firing rates of pyramidal neurons [29]. This reduction is possibly due to the reduced restraining of K^+ ions and the reduced efflux of cations. Overall, the effect of the decrease in ACh level is reflected in the EEG as an increase in slow-wave (delta) activity, indicative of reduced cortical arousal.
- **REM Sleep**: Conversely, during REM sleep, there is a heightening of ACh levels on par or even greater than in wakefulness throughout different areas of the brain, facilitating increased neuronal activity, which can be reflected in the EEG as theta rhythms, a hallmark of REM sleep [29]. Like wakefulness, there may be increased ACh binding during REM, increasing influx of cations and decreasing K^+ efflux, promoting depolarizations and fostering increased theta activity in REM.

2. **Nucleus Basalis of Meynert (NBM)**:
    - **Cortical Projection**: The NBM is a significant source of cholinergic innervation to the cortex. It projects broadly to the cortex, including the thalamic reticular nucleus, modulating cortical arousal. This nucleus is primarily involved in attention and memory processes [128]. The effects during sleep are similar to those of cortical neurons; however, it should be noted that cholinergic neurons in the basal forebrain fire more quickly during wakefulness and REM, promoting increased excitation in cortical neurons [29].

Indirect Cortical Influence through Subcortical Pathways:

1. **Pedunculopontine Tegmental Nucleus (PPT) and Laterodorsal Tegmental Nucleus (LDT):** These cholinergic nuclei in the brainstem play a significant role in modulating thalamocortical rhythms, primarily by influencing the thalamic neurons and, subsequently the cortical activity and EEG patterns. They function as a bridge between the brainstem and the thalamus, modulating the oscillatory behaviour in various cortical areas [122].
    - **Wakefulness**: The PPT and LDT are active, facilitating cortical desynchronization through their projections to the thalamus. This interaction enhances alertness and fosters beta and gamma wave activities captured in the EEG as markers of attentiveness and active brain states [122].
    - **Transition to NREM Sleep**: The activity of the PPT and LDT reduces. This decrease allows for a shift towards slower oscillations, fostering the slow-wave patterns witnessed in EEG recordings during deep sleep stages [122].

- **REM Sleep**: In contrast, the REM phase sees a resurgence in the activity of these nuclei. This heightened activity promotes theta wave oscillations, evident in EEG readings, as markers of vivid dream experiences during this sleep phase [122].

2. **Reticular Activating System (RAS):** The RAS is a multifaceted network in the upper brainstem that critically regulates wakefulness and arousal. Precisely, the Ascending Reticular Activating System (ARAS), a vital component of the RAS, orchestrates a complex interplay of neurotransmitters to achieve this [129]. The ARAS encompasses critical brain regions, such as the locus coeruleus (LC), raphe nuclei, and reticular formation. Cholinergic neurons, primarily in the pedunculopontine and laterodorsal tegmental nuclei, are integral to the ARAS and modulate arousal and attention using ACh as a primary neurotransmitter [98], [130], [131]. Within this network, noradrenergic neurons from the LC promote wakefulness by sending excitatory signals to the cerebral cortex [132]. The serotonergic neurons from the raphe nuclei, also part of the ARAS, heighten arousal levels and sustain attention [57]. As previously discussed, many other systems, transmitters, and histamines all play a role in working together within the ARAS to facilitate the balance between sleep and wakefulness [98].

    - **Wakefulness**: The LC sends noradrenaline to depolarize thalamic neurons, making them more receptive to other incoming signals. Cholinergic neurons from the pedunculopontine and laterodorsal tegmental nuclei release ACh, facilitating excitatory signals reaching the cortex. This combined activity produces fast gamma and beta rhythms observable in the EEG [98], [130], [133].

    - **Transition to NREM Sleep**: The ARAS reduces its activity, specifically the release of excitatory neurotransmitters like noradrenaline and serotonin from the LC and raphe nuclei, respectively. These neurotransmitters lead to hyperpolarization of thalamic neurons, decreasing cortical excitability. The resultant EEG patterns manifest as theta rhythms and sleep spindles [98], [134].

    - **Deep Sleep (NREM Stage 3)**: Further reduced activity in the ARAS, allowing inhibitory GABAergic neurons from the hypothalamus to dominate. This results in slow-wave (delta) activity, as measured by EEG, indicative of a low level of cortical excitability [98], [134].

    - **REM Sleep**: The RAS becomes more active again, promoting depolarization in thalamic neurons that influence cortical activity. This interaction fosters desynchronous EEG patterns like wakefulness, marking the REM phase's unique characteristics of vivid dreams coupled with muscle atonia [135].

Thus, the ARAS is a complex, multifaceted system that employs various neurotransmitters like noradrenaline, acetylcholine, and serotonin to modulate the thalamic and cortical activity. These neurotransmitters and the brain regions from which they originate work together to regulate ionic states at the neuronal membranes and synaptic junctions. This regulation, in turn, dictates the EEG patterns associated with different sleep-wake states.

2.4.2.2 Orexin

The orexinergic system, located predominantly in the hypothalamus, plays a vital role in mediating the balance between sleep and wakefulness, emerging as a crucial focus in recent sleep research [55], [136]. It maintains wakefulness and prevents abrupt transitions between sleep stages through intricate interactions with neurotransmitter systems and astrocytes [137], [138]. Central to accommodating proper wakefulness and transitions begins within the basal forebrain, a region rich in cholinergic neurons, which integrates inputs from various brain areas, including orexinergic perifornical neurons, among others [137], [139]. These inputs facilitate the release of numerous neurotransmitters, such as histamine, dopamine, and noradrenaline, as well as acetylcholine (ACh), that influence the cortical neurons and, thus, play a pivotal role in sleep regulation [137], [138]. Studies in mice have shown that the absence of orexin neurons leads to an increase in REM sleep, characterized by more frequent and longer REM periods, reflecting a disruption in the usual orexin-mediated suppression of REM sleep bouts but maintains a consistent overall time spent in wake and NREM stages [140]. Therefore, the orexinergic system is fundamental in sustaining a stable circadian rhythm, characterized by smooth transitions between wakefulness, NREM, and REM sleep stages [141].

Exploring the detailed intricacies of the orexinergic system offers an enriched understanding of its pivotal role in regulating the sleep-wake cycle, with a particular focus on its function during REM sleep. This exploration has led to recent studies emphasizing the crucial role of orexin neurons in sustaining a stable sleep-wake cycle, noting that a deficiency in this system can significantly increase the duration of REM bouts [140]. Intriguingly, during REM sleep, a phase characterized by almost dormant orexinergic activity, there is a marked decrease in the occurrence of interictal epileptiform discharges (IEDs) and seizures, fostering a state of cortical desynchronization that inhibits the transition of aberrant epileptiform activities into seizures. A systematic review [142] highlighted that a negligible 1% of 1990 seizures in over 542 patients occurred during this sleep phase, and even holds in severe cases of pediatric epileptic encephalopathies.

Nevertheless, the role of the orexinergic system appears to have a variable impact on different forms of epilepsy, illustrating a nuanced interaction between orexinergic activity and epileptic manifestations [22]. For instance,

during wakefulness, a period of heightened orexinergic activity, there was an eightfold surge in seizures compared to REM sleep. This surge was accompanied by a threefold increase in generalized IEDs and a slightly smaller increase of 1.11 times in focal IEDs. The pronounced increase in seizures and generalized IEDs during periods of heightened orexinergic activity, contrasted with the relatively smaller increase in focal IEDs, could suggest that the orexinergic system has a more substantial impact on the broader cortical networks involved in generalized epilepsy than on the localized circuits in focal epilepsy. Adding another layer of complexity, slow wave sleep (SWS), characterized by cessation of orexinergic activity and increased cortical synchronization, exhibited a striking 60-fold increment in seizures and a sevenfold rise in generalized IEDs when compared to REM sleep, further highlighting the varying influences of different sleep states on seizure susceptibility.

Delving deeper, it becomes apparent that the orexin system's involvement influences cortical neuronal activity, notably intertwining with acetylcholine (ACh) release during REM sleep. This complex interplay between orexin and acetylcholine is central in modulating sleep-wake cycling and possibly the cortical desynchronization patterns. This synergy is primarily orchestrated through brain regions such as the laterodorsal tegmentum (LDT) and the pedunculopontine tegmentum (PPT), both of which are rich in cholinergic neurons. These regions foster desynchronized neuronal activity commonly observed during REM sleep, characterized by a surge in ACh release that promotes desynchronized activity in cortical EEG patterns, potentially influencing the dynamics underlying epileptogenesis [137], [138].

Wakefulness

During wakefulness, the orexinergic system is markedly active, particularly within the lateral hypothalamus [55], [137]. It significantly influences the basal forebrain and brainstem cholinergic systems, prominently involving the pedunculopontine tegmentum (PPT) and laterodorsal tegmentum (LDT) in the brainstem. Under the influence of orexin, these structures facilitate the widespread release of acetylcholine (ACh) across the cortex, fostering an enhanced state of alertness and vigilance. This enhanced alertness and vigilance is exhibited through a desynchronized EEG pattern, indicating active cortical engagement and information processing [55], [137].

NREM Sleep (Stages 1-3)

As one transitions from wakefulness to NREM sleep, there is a gradual decline in orexinergic activity [55], [137]. During the initial stages of NREM sleep (stages 1 and 2), orexin continues to modulate the sleep-wake cycle, albeit at a reduced capacity, fostering a blend of synchronized and desynchronized cortical activities that can be observed in the EEG readings. As one progresses to deeper stages of NREM sleep (stage 3 or slow-wave sleep), orexinergic activity diminishes to the extent the orexinergic activity ceases. This stage is characterized by highly

synchronized cortical activity, evident as high-amplitude slow waves on the EEG, indicative of deep sleep and reduced sensory responsiveness [55], [137].

REM Sleep

The REM sleep stage involves an intricate interaction between the orexinergic and cholinergic systems, involving crucial regions such as the PPT and LDT [55], [137]. These regions experience a surge in ACh release, engendering a state of desynchronized cortical activity, a hallmark of REM sleep observable in EEG patterns. This desynchronized activity, mediated through the dynamic interplay between orexin and ACh, forms the substrate for vivid dreams and rapid eye movements, characteristic features of this stage. This foundational process is intriguing as orexinergic activity was completely inactive and continues to be inactive with sudden bursts of activity during REM, specifically phasic REM [55].

Astrocytes and Feedback Mechanisms

In the lateral hypothalamus and perifornical area of the brain, astrocytes significantly influence the feedback mechanisms that modulate the activity of orexin neurons [137]. This positive feedback loop is primarily mediated by glutamate, instigating a sequence where orexin neurons depolarize and modulate glutamate release, activating and depolarizing astrocytes. In response, the astrocytes release lactate and protons into the surrounding environment. They serve dual roles: furnishing an energy source for orexin neurons via the astrocyte derived lactate and enhancing their activity through decreasing the extracellular pH via the astrocyte's monocarboxylate transporters activity [137]. Consequently, astrocytes play a crucial role in modulating orexin activity and, by extension, the circadian rhythm, demonstrating a complex interplay of cellular interactions vital for maintaining sleep homeostasis.

2.4.3 Astrocytes:

Cortical astrocytes play a vital role in modulating the activity of cortical pyramidal neurons, significantly influencing the EEG patterns observed during sleep-wake cycles [143]. These astrocytes maintain a symbiotic relationship with approximately two million synapses, affecting both EPSPs and IPSPs [60]. Their involvement extends to ensuring molecular homeostasis by regulating ions and neurotransmitter recycling, which are critical elements in synaptic plasticity and overall neuronal excitability [58]. Moreover, they participate in receptor trafficking and provide metabolic support, thus directly affecting neuronal energy provision [144].

While it is established that variations in astrocytes' intracellular pH impact glutamate uptake, especially under ischaemic conditions, the exact acidity levels required to initiate these protective mechanisms remain unclear

[145]. This pH-driven modulation, potentially acting as a critical last resort, may inhibit both regular and reversed glutamate uptake, thereby safeguarding neurons from excitotoxicity. This suggests that the astrocytes might employ this strategy only under extreme conditions, to halt excessive neuronal firing and prevent damage.

Astrocytes foster extensive network synchronization by communicating with each other through gap junctions, creating a cohesive network that can influence a vast array of synapses [59]. This complex communication network enables them to maintain and regulate the homeostatic properties crucial during different states of alertness or sleep, exerting a substantial influence on EEG dynamics.

In recent years, astrocytes, traditionally regarded as mere supporters within the central nervous system, have been repositioned at the core of sleep regulation, notably as possible instigators of REM sleep phases. Emerging research, such as that by [143], has highlighted these cells' crucial role in regulating and modulating sleep-wake cycles, neural plasticity, and circadian rhythms.

Astrocytes' roles are perpetual orchestrating fluctuations of extracellular potassium (K^+) and hydrogen (H^+) ions, integral to sleep transitions [146], [147]. This process, possibly mediated through pH-sensitive potassium channels or glial ion exchangers, suggests a dynamic involvement in maintaining brain homeostasis, with potential implications in modifying neural oscillations and fostering a cortical 'up state' within the neuronal network through K^+ spatial buffering. These cells may utilize channels like Kir5.1 and Kir4.1 to moderate pH sensitivity and regulate potassium levels during these transitions, facilitating an intricate dance of ion influx and efflux.

Astrocytes, beyond their established role in maintaining neural homeostasis, potentially spearhead novel pathways in memory consolidation and epilepsy management, acting as inhibitors against abnormal neuronal spikes [148]. These glial cells might function as central figures in the complex processes of sleep cycling, not just as facilitators, but as active participants safeguarding neural integrity and ensuring smooth transitions and optimal functionality during REM sleep. These glial cells can inhibit or foster various sleep states depending on their anatomical positioning. For instance, hypothalamus astrocytes are observed to enhance both REM and NREM sleep during the nocturnal phase, where astrocytes may be more active. In contrast, their counterparts in the cingulate cortex curtail NREM sleep in light periods where they may be less active, indicating a nuanced role in sleep regulation directly influenced by astrocytic activity [148]. This intricate relationship is further illustrated by their interaction with melanin-concentrating hormone neurons in the hypothalamus, which augments REM sleep, suggesting a direct regulatory role of astrocytes [141], [149]. The orchestration of these processes might either stem from a centralized clock mediating astrocytic activities or through extensive communication

networks involving gap junctions or gliotransmission of ATP through neurons, positioning them as the brain's chief regulators in sustaining sleep and homeostatic baselines. In this light, a plausible hypothesis could be derived from the orexinergic pathways, where the disruption of neuron functioning leads to a perturbance, rather than accentuating, REM. [140].

Astrocytes have a variety of additional roles, such as communication through neurons and gap junctions. They are the only cell in the brain that stores glycogen, allowing them to serve as metabolic buffers. Their function goes beyond mere support; they also act as buffers during periods of high metabolic and ionic demand, thus contributing to overall brain health [150]. These cells form intricate gap junction-mediated networks, mainly through the subunit connexin 43, which facilitates the trafficking of essential energy metabolites like glucose and lactate. Disrupting these networks, as evidenced by the knockout of connexin 43, leads to impaired functioning of orexin neurons in the lateral hypothalamic area, which is critical for promoting wakefulness. As a result, there is a manifestation of excessive sleepiness and fragmented wakefulness during typically active periods. These manifestations imply that astrocytes are integral for nutrient supply and modulating neural activity and behavioural states through their metabolic networks [151].

One pivotal study recently published by [152] demonstrated that calcium and pH-associated fluorescence changes in astrocytes can be imaged to possibly identify the onset of REM sleep. The study also depicts the increased intracellular acidity within astrocytes throughout REM, possibly due to their heightened metabolic processes generating more CO_2, which, when combined with water, forms carbonic acid, leading to a subsequent increase in H^+ ions and a decrease in pH. Paradoxically, this heightened metabolic state is accompanied by a reduction in astrocytic intracellular Ca^{+2} levels. This response might be a protective mechanism to avoid potential cell damage caused by high intracellular calcium levels. Furthermore, there is a surge in brain blood volume (BBV) during this phase, which may be a response to increased metabolic demands, facilitating nutrient and oxygen transport while aiding in waste product removal.

The study [152] further demonstrates that during epileptic kindling, the BBV does not increase further; however, the acidification of the astrocyte does increase with much more excess CO_2. Within this state, there is a lack of CO_2 regulation as the BBV did not further increase to sustain the amount of energy required for the astrocyte to maintain proper pH levels or manage the further accumulation of CO_2. One of the active processes astrocytes use to regulate their pH is the Na+/H+ exchanger, which restores normalcy during acidic phases [153].

Receptor Trafficking and Synaptic Modulation

Wakefulness

- **Ion Buffering:**
    - During the wakefulness state, astrocytes play a pivotal role in managing the extracellular ionic milieu within the brain. As one transitions from sleep to wakefulness, there is a significant shift in extracellular ion concentrations. A review by [154] illustrates that arousal from sleep instigated by a cocktail of neuromodulators (including norepinephrine, acetylcholine, dopamine, orexin, and histamine) led to a swift increase in extracellular potassium (K^+) levels, irrespective of the neural activity state. Furthermore, the same study highlighted that extracellular calcium (Ca^{2+}) and magnesium (Mg^{2+}) ion levels decreased, albeit five times slower than the alterations observed in potassium levels. This dynamic change in ion concentrations seems to be independent of synaptic activity. The involvement of astrocytes, particularly in the regulation of Ca^{2+} and Mg^{2+} levels, is crucial but not explicitly detailed in this context. Astrocytes, through mechanisms such as ion exchange and transport processes, can absorb excess Ca^{2+} and Mg^{2+} from the extracellular space and can release these ions back into the environment as needed. This is likely to contribute significantly to the slower modulation of these ions during the transition from sleep to wakefulness. However, the potassium changes potentially hint at the involvement of specific pH-sensitive glial potassium channels or ion exchangers that mediate hydrogen (H^+) influx and potassium (K^+) efflux during the transition from sleep to wakefulness, as hypothesized in the text. Moreover, recent findings [155] noted an increase in extracellular potassium levels across all analysed cortical regions when mice transitioned from stillness to locomotion, indicating a potential linkage between physical activity and ionic milieu during wakefulness.

- **Gliotransmitter Release and Uptake**:
    - Astrocytes actively release gliotransmitters such as glutamate, GABA, and ATP during wakefulness, significantly modulating synaptic transmission and enhancing plasticity [156]. This heightened release facilitates increased neuronal communication and activity. Furthermore, astrocytes play a pivotal role in the uptake of neurotransmitters, particularly glutamate, preventing excitotoxicity and fostering synaptic modulation. This function becomes pronounced during heightened synaptic activity in wakefulness [145], [157].

- **Receptor Trafficking**:
    - During wakefulness, astrocytes significantly influence receptor trafficking, including the dynamics of ionotropic and metabotropic receptors. They not only enhance the trafficking of receptors to synapses, facilitating heightened synaptic transmission and plasticity but also actively modulate the activity of specific receptors [58]. For instance, the release of D-serine from astrocytes can potentiate the activity of NMDA receptors, potentially increasing the ion flow through these receptors when activated, thereby influencing the synaptic strength and affecting the dynamics observed in EEG patterns [157].

NREM Sleep (N1-N3)

- **Ion buffering:**
    - During the NREM phase of sleep, a distinct shift in ion concentrations occurs, possibly facilitating the creation of slow oscillations, which have been documented to be in the range of 0.3-1 Hz in different studies [158], [159]. During this period, glial cells (mainly protoplasmic astrocytes) exhibit periodic depolarizing-repolarizing sequences closely mirroring the activities of adjacent neurons, thus potentially influencing the pace of slow oscillations through the modulation of extracellular K^+ concentrations [160], [161]. Additionally, spatial K^+ buffering by glia has been suggested to contribute to a stable distribution of K^+ around neurons, combined with changes in Ca^{2+} levels facilitating steady neuronal depolarization modulating excitability [162], [163].
- **Gliotransmitter Release and Uptake**:
    - In NREM sleep, astrocytes modulate the release and uptake of gliotransmitters to match the decreased neuronal activity typically observed during this phase [143], [164]. This modulation is evident in the altered synchronization between astrocytes and neuronal activity, influencing the patterns displayed in EEG recordings. Moreover, astrocytes actively participate in the synaptic homeostasis hypothesis of sleep by facilitating the global downscaling of synaptic strength through altered gliotransmitter release patterns.
- **Receptor Trafficking**:
    - During NREM sleep, astrocytes modulate receptor trafficking patterns to align with the observed global downscaling of synaptic strength. This modulation might involve diminishing the synaptic responsiveness, possibly by reducing the number of active excitatory receptors at the synapse,

thereby maintaining synaptic homeostasis. Importantly, these alterations in synaptic dynamics may play a significant role in shaping the characteristics of NREM phases as generally observed by scalp EEG [165].

REM Sleep

- **Ion Buffering:**
    - Scientific literature has not explored the role of astrocytes and ion buffering throughout REM sleep. Considering the review by Beckner [154], assumptions can be created where REM sleep would also involve a complex interaction of ionic changes, including modifications in K^+, Ca^{2+}, and Mg^{2+} concentrations, as well as potential pH-sensitive channel involvements, similar to those observed during transitions from sleep to wakefulness and NREM sleep. Exploration into this topic will be further discussed in future sections where pH levels have been identified within mice during REM, which could lead to alternative conclusions.
- **Gliotransmitter Release and Uptake**:
    - During REM sleep, astrocytes undergo dynamic changes, notably intracellular acidification, indicative of increased gliotransmitter release, specifically glutamate, an excitatory neurotransmitter [152]. This enhanced gliotransmission is pivotal in augmenting synaptic transmission dynamics, contributing to heightened synaptic and cortical activity in REM sleep.
- **Receptor Trafficking**:
    - Currently, scientific literature has not extensively explored the role of astrocyte receptor trafficking during REM sleep. Nevertheless, given the established active participation of astrocytes in the sleep-wake cycle, coupled with their known behaviour of releasing gliotransmitters like glutamate during REM sleep, it is plausible to hypothesize their potential influence on receptor trafficking during this phase.

      Considering the active, desynchronous state established during REM sleep, receptor trafficking could possibly influence the dynamics of excitatory and inhibitory receptors at the synapses. This influence might manifest as an upregulation in the production and synaptic incorporation of excitatory receptors, a reduction in inhibitory receptors, or a combination of both, mirroring the heightened neural activity characteristic of REM sleep. Furthermore, this dynamic in the synaptic

environment might also stimulate changes in the ion conductance properties of the receptors, potentially influenced by modulators such as D-serine, thereby contributing to the active modulation of synaptic transmission dynamics observed during this sleep phase.

2.4.4 Sleep-Wake Network Dynamics: An Overview

Sleep-wake network dynamics are foundational for understanding neurophysiological states, encompassing complexities beyond mere cycles of wakefulness and sleep [141], [166]. In each state—wakefulness, non-rapid eye movement (NREM) sleep, and rapid eye movement (REM) sleep—specific neural networks are either inhibited or excited using various processes, with profound effects on cortical signalling [98], [167]. The interplay of these regions is critical in the neuroanatomical regulation of sleep-wake states as discussed in their respective upcoming sections.

During wakefulness and REM sleep, the orexinergic pathway is notably active, contributing to a global increase in acetylcholine (ACh) release, which modulates various neural networks [47], [113], [137], [168]. This activation is part of the "flip-flop" switch mechanism, where the orexinergic neurons stabilize the state of wakefulness by inhibiting sleep-promoting regions such as the ventrolateral preoptic nucleus (VLPO) [169].

In contrast, during NREM sleep, and particularly its deepest stage known as slow-wave sleep (SWS), this pathway shows significantly reduced activity [55], [137]. The flip-flop switch here involves the activation of sleep-promoting neurons in the preoptic area, leading to the inhibition of the arousal system [169]. Neurotransmitter fluctuations, such as those of ACh and ion level changes, are critical in shaping EEG amplitudes and frequencies.

Additionally, synchronous and desynchronous neuronal activities have been identified as influential factors in the regulation of Paroxysmal Depolarizing Shifts (PDSs), although their specific roles vary between sleep-wake states [26]. The variation observed in these neural networks and physiological factors provides a foundation for the subsequent in-depth analysis of sleep-wake states, each characterized by the unique interplay among neural structures, neurotransmitter levels, and ion dynamics.

2.4.4.1 Wakefulness (Figure 3)

Ascending Reticular Activating System (ARAS) and Extended Network:

The ARAS constitutes a critical component of the neural circuitry responsible for wakefulness [129]. It encompasses a multitude of subcomponents, including but not limited to the raphe nuclei, locus coeruleus (LC), and ventral tegmental area (VTA). The VTA specifically contributes dopaminergic projections vital for attentional

processes [137], [138]. These components send glutamatergic projections to the thalamus and cortex, facilitating cortical arousal and attention.

Noradrenergic Locus Coeruleus (LC):

The LC, a nucleus in the pons, plays a prominent role in wakefulness through its widespread noradrenergic projections to the cortex, hippocampus, and thalamus [98], [130], [133]. It also inhibits the ventrolateral preoptic nucleus (VLPO) of the hypothalamus, a region pivotal in promoting sleep [168], [170].

Serotonergic System

The dorsal raphe nucleus releases serotonin, which acts on multiple brain regions, including the cortex and limbic system. This release promotes a wakeful state and modulates mood and alertness [57], [98], [171].

Cholinergic (acetylcholine-releasing) Projections from PPT/LDT:

The pedunculopontine tegmental and laterodorsal tegmental nuclei (PPT/LDT) are cholinergic centres that send excitatory projections to thalamic relay neurons and contribute to the regulation of cortical arousal [47], [122]–[124], [133]. The Basal Forebrain (BF) also plays a role, sending cholinergic projections to the cortex and hippocampus to support attention and memory processes.

Orexinergic System:

Orexinergic neurons in the lateral hypothalamus send projections to key wakefulness-promoting centres such as the LC, dorsal raphe, and BF [137]. These neurons are particularly active during periods of wakefulness and fostering cortical arousal.

Influence on Cortical Neurons and Scalp EEG:

The orchestrated interaction of these neurotransmitters and projections culminates in the specific activation patterns of cortical neurons. EEG readings during wakefulness typically display low-amplitude, high-frequency beta (13-30 Hz) and gamma (25-100 Hz) waves, indicative of an activated mixed frequency desynchronized cortical state [14]. Additionally, alpha waves (8-13 Hz), especially when a PDR, can be characteristic of relaxed wakefulness.

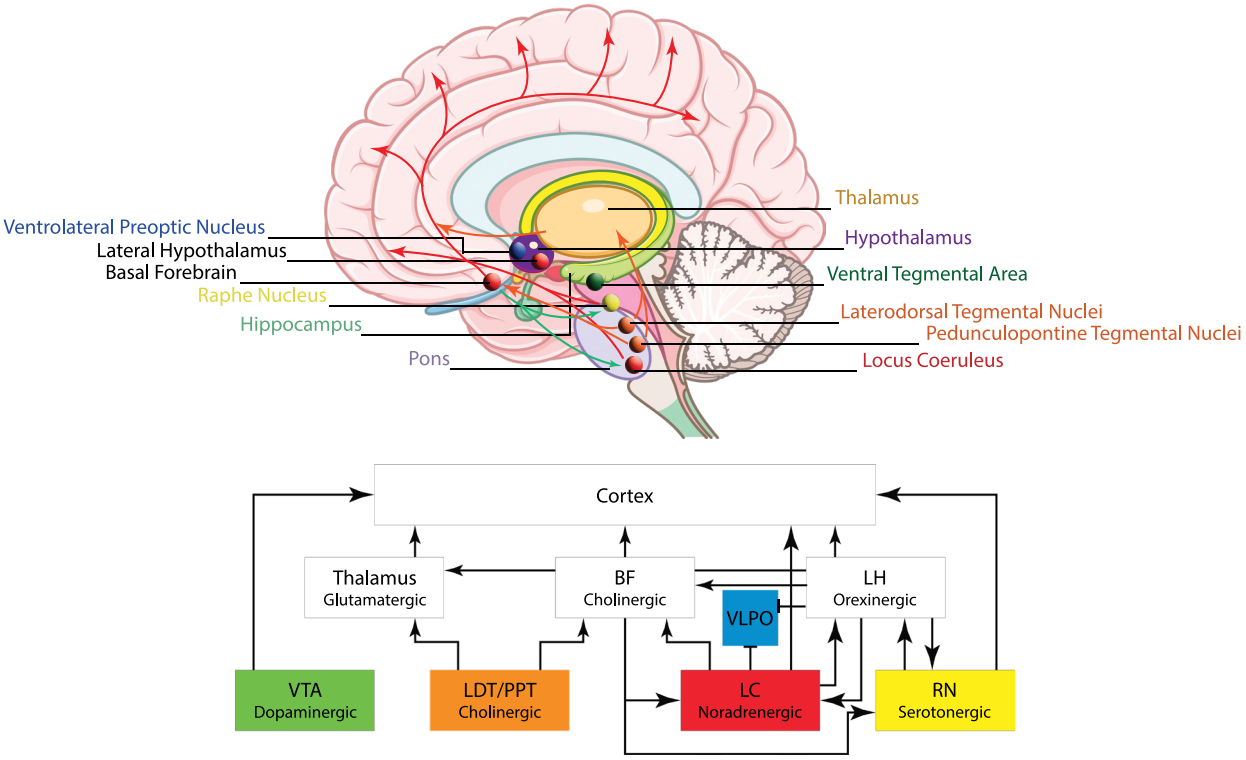


Figure 3: "Neural Circuitry of Wakefulness." Arousal-promoting centres, including the VTA, LDT/PPT, LC, and RN, exhibit heightened excitatory activity during wakefulness. The LC inhibits the sleep-promoting VLPO and excites the LH, cortex, and BF. The LDT/PPT further provides excitatory inputs to the BF and thalamus. In the BF, rich in various neuron types, there is a predominant amplification of its cholinergic activity, directly elevating cortical arousal. Feedback mechanisms exist wherein the BF sends regulatory signals to the LC and RN. This feedback, coupled with the LH's direct excitatory projections to the cortex and its inhibitory influence on the VLPO, jointly orchestrates wakefulness's alertness and cognitive function. The dominant neurotransmitter during wakefulness is displayed under each brain structure.
Source: Figure Reference [5]

2.4.4.2 NREM (Figure 4)

Ventrolateral Preoptic Nucleus (VLPO) and Extended Network:

''The VLPO serves as the sleep-promoting 'switch,' inhibiting arousal systems through its GABAergic and galaninergic neurons [168], [170]. The activity of VLPO neurons is especially high during NREM sleep, where it sends inhibitory signals to wake-promoting regions like the locus coeruleus (LC) and dorsal raphe, essentially quieting these regions to maintain sleep.

Thalamocortical Networks:

Thalamocortical neurons are central to NREM sleep dynamics. In the early stages, NREM1 and NREM2, these neurons generate theta rhythms and sleep spindles, regulated by the inhibitory feedback from GABAergic neurons in the thalamic reticular nucleus (TRN) [46], [128]. As sleep deepens into NREM3, the thalamocortical network, influenced by increased TRN inhibition, shifts to produce slow-wave activities marked by high-amplitude, low-frequency delta waves [46], [47]. These patterns, from spindles to delta waves, highlight the brain's synchronized activity during NREM, orchestrated by the balance between excitatory and inhibitory signals.

Modulatory Influences: VTA, Dorsal Raphe, and BF:

Dopaminergic neurons from the VTA show reduced activity during NREM sleep, complementing the inhibitory role of the VLPO [168], [170]. Additionally, the dorsal raphe, a serotonergic nucleus, downregulates its activity, contributing to the overall hypotonus of neurotransmitter release conducive to sleep [57].

During the transition to NREM sleep, the basal forebrain (BF) undergoes significant changes in its activity. While the BF has a prominent cholinergic component, its GABAergic neurons become particularly active during NREM [137], [172]. These GABAergic neurons project directly to the cortex, contributing to the characteristic slow-wave activity of NREM sleep. Moreover, GABAergic projections from the BF to the thalamic reticular nucleus (TRN) play a role in modulating thalamocortical rhythms, influencing synchronous activities such as sleep spindles [173]. Consequently, the combined reduction of cholinergic projections and the heightened GABAergic influence from the BF facilitate the shift from wakefulness to the deeper stages of NREM sleep.

Homeostatic and Neurotransmitter Factors:

During wakefulness, adenosine accumulates in the brain's extracellular space via the breakdown of ATP within neurons and glia, increasing sleep pressure [174]. This buildup signals a need for sleep by binding to adenosine receptors (e.g. A1 and A2A), predominantly in the basal forebrain effectively inhibiting wake-promoting neurons. Sleep reduces adenosine levels through decreased neuronal activity and increased clearance by astrocytes. Caffeine, an adenosine antagonist, blocks these receptors, preventing adenosine binding, which temporarily wards off sleepiness. The balance between adenosine production, receptor interaction, and clearance, influenced by factors like metabolism and external substances, helps orchestrate the sleep-wake cycle.

Concurrently, the BF is also described to have sleep-activating neurons where the inhibition of the wake-promoting neurons via adenosine could indirectly enhances the activity of GABAergic sleep-promoting neurons in the basal forebrain [175].

Influence on Cortical Neurons and Scalp EEG:

The orchestrated interaction of these neural networks and neurotransmitters culminates in distinct EEG characteristics across NREM stages. NREM1 is marked by theta waves (4-8 Hz), representing a transitional state from wakefulness to sleep [14]. NREM2 features sleep spindles (11-16 Hz) and K-complexes, which are believed to facilitate memory consolidation and offer a protective mechanism against arousal [14]. NREM3, or synchronous Slow-Wave Sleep, is characterized by high-amplitude, low-frequency delta waves (0.5–4 Hz), indicative of a deep restorative sleep state [14].

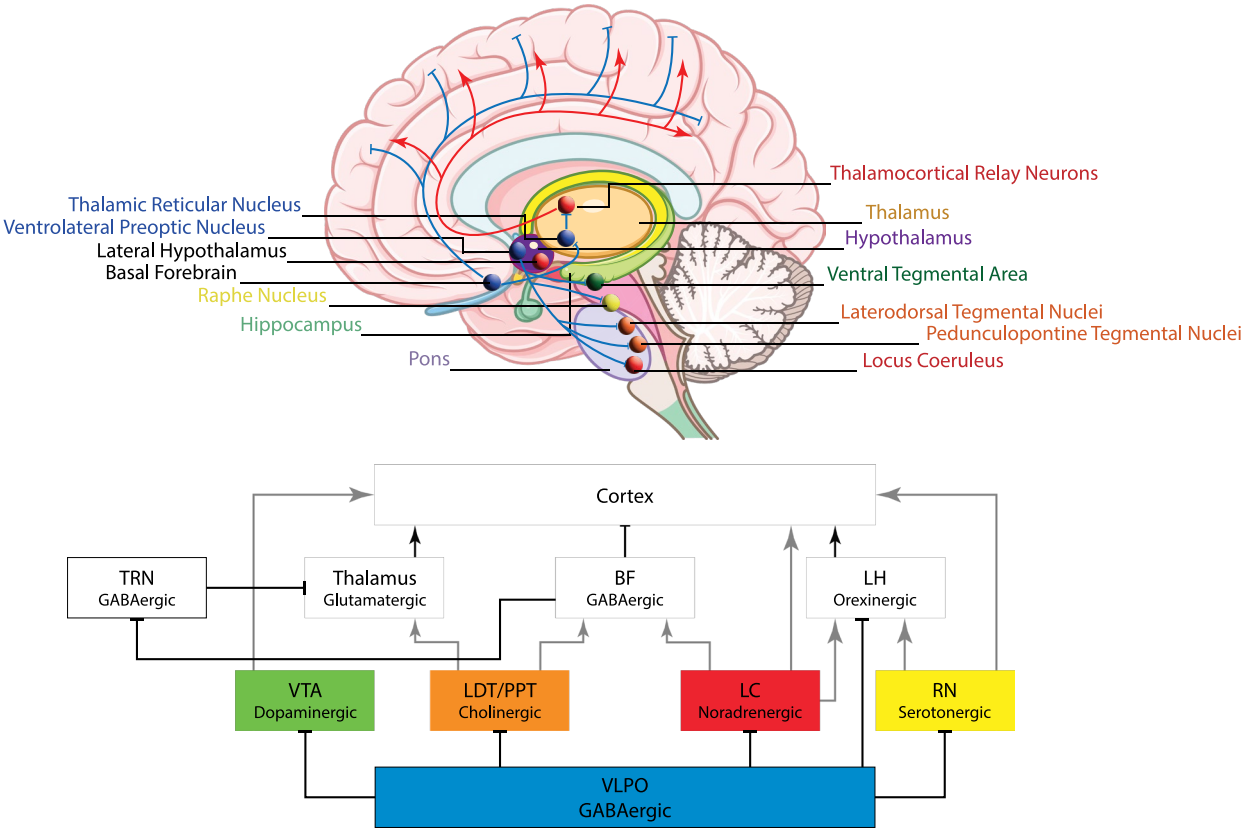


Figure 4: "Neural Circuitry of NREM Sleep Regulation." The transition from wakefulness to NREM is facilitated by the VLPO's inhibitory influence on arousal centres (VTA, LDT/PPT, LC, RN and LH), resulting in diminished excitatory activity from these regions. Concurrently, the BF's GABAergic neurons project to the cortex, inducing slow-wave activity, and to the TRN, modulating thalamocortical rhythms. The TRN's inhibitory action on thalamocortical relay neurons further contributes to the generation of sleep spindles and delta waves, hallmark features of NREM sleep. The dominant neurotransmitter during NREM sleep is displayed under each brain

structure.
Source: Figure Reference [5]

2.4.4.3 REM (Figure 5)

Sublaterodorsal Nucleus (SLD) and Extended Network:

The SLD in the brainstem serves as a linchpin for initiating REM sleep and its signature feature, muscle atonia. The SLD sends inhibitory GABAergic and glycinergic projections to deactivate motor neurons in the spinal cord, causing muscle paralysis [176], [177]. Simultaneously, it sends inhibitory signals to wake-promoting centres like the locus coeruleus (LC) and dorsal raphe, almost entirely silencing them to initiate and sustain REM sleep.

Thalamocortical and Thalamic Reticular Nucleus (TRN) Interactions:

During REM sleep, thalamic neurons show a general decrease in synchronization, especially in interactions with the cortex and TRN. This lack of synchronization partly contributes to the desynchronized EEG pattern observed during REM sleep [46], [128].

Modulatory Regions: LC, Basal Forebrain (BF), and Dorsal Raphe:

'The LC and dorsal raphe nuclei, usually essential for wake promotion, become nearly entirely inhibited, permitting REM sleep to occur [105], [119], [178]. The BF, predominantly cholinergic during wakefulness, adjusts its neuronal tone to be moderately active, significantly less so than during wakefulness [98].

Orexinergic System and Lateral Hypothalamus (LH):

Orexinergic neurons in the LH, generally promoting wakefulness, lower their activity during REM, complementing the overall decrease in arousal-promoting neurotransmitters and reinforcing muscle atonia [137], [141].

Cholinergic Activity:

In REM sleep, there is a surge of cholinergic activity from the pedunculopontine and laterodorsal tegmental nuclei (PPT/LDT), crucial for features like rapid eye movement and muscle atonia. These nuclei do not directly project to the cortex. Instead, their cholinergic projections often go through intermediary regions such as the thalamus and BF, which in turn influence cortical activity [47], [55], [113], [137], [142], [171].

The Laterodorsal and Pedunculopontine Tegmental nuclei (LDT/PPT) are known to supply acetylcholine (Ach) to cortical regions, potentially influencing cortical excitability and plasticity [47], [113], [142], [171]. Additionally, the Dorsal Raphe Nucleus (DRN) modulates the activity of LDT/PPT through serotonergic projections, potentially

altering the serotonergic tone in the cortex [171]. Both cholinergic and non-cholinergic cells also project to the medial geniculate (MG), which has thalamocortical projections that can modulate cortical activity during the sleep-wake cycle [179].

Influence on Cortical Neurons and Scalp EEG:

The orchestrated interactions among these neural networks and neurotransmitters result in a unique cortical state during REM sleep. The EEG patterns display a desynchronized, activated state featuring low-amplitude, mixed-frequency activity similar to wakefulness. These desynchronous patterns include theta, alpha, and even beta waves, representing the complex thalamic and cortico-cortical interactions that underlie the paradoxical nature of REM sleep [14]. The thalamus, acting as a relay and modulation centre, significantly influences the cortical EEG rhythms. In REM sleep, the thalamus exhibits a decrease in the typical synchronized activity seen in NREM sleep, leading to a more desynchronized, yet active, cortical state. This thalamic modulation, along with direct cortico-cortical communications, facilitates the complex and diverse EEG signatures of REM sleep. This state is crucial for various brain functions, such as memory consolidation, dreaming, and emotional processing.

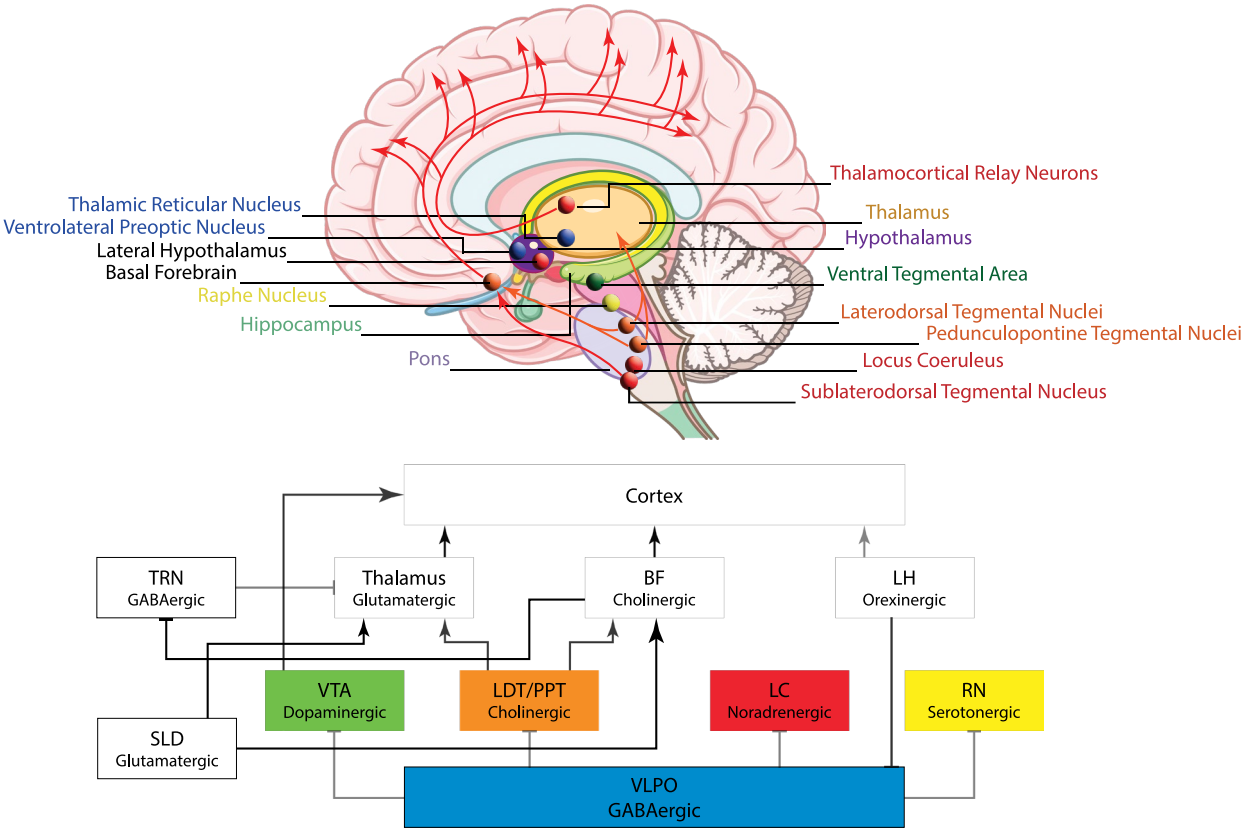


Figure 5: "Neural Circuitry of REM Sleep Regulation." A "REM-on" centre, the SLD, is central to REM initiation, which promotes muscle atonia via projections to the medulla and activates the cortex through pathways to the thalamus and BF. Concurrently, the LDT/PPT enhances cortical activity through cholinergic inputs to the thalamus. Decreased activity from wake-promoting centres like the LC and RN stabilizes REM. The LH's orexin neurons help consolidate REM episodes and inhibit the VLPO, allowing for increased firing within the VTA and LDT/PPT. The dominant neurotransmitter during REM sleep is displayed under each brain structure.
Source: Figure Reference [5]

2.5 Spike Morphology – Biological Mechanisms Derived from Scalp EEG Representation

In the preceding section, the intricate neurobiological landscapes governing brain function were examined, ranging from neurotransmitters' role to astrocytes' importance. While these mechanisms offer valuable insights in isolation, their relevance emerges when contextualized within observable phenomena. The subsequent discussions focus on interpreting these processes in relation to scalp EEG patterns, specifically epileptiform spikes, as depicted in Figure 6. By building on the foundational understanding of brain chemistry and cellular activity, the aim is to explore how these spikes are formed and how they could be modulated throughout the sleep-wake states, ultimately gathering information on possible ongoings that could govern their respective proliferation or suppression.

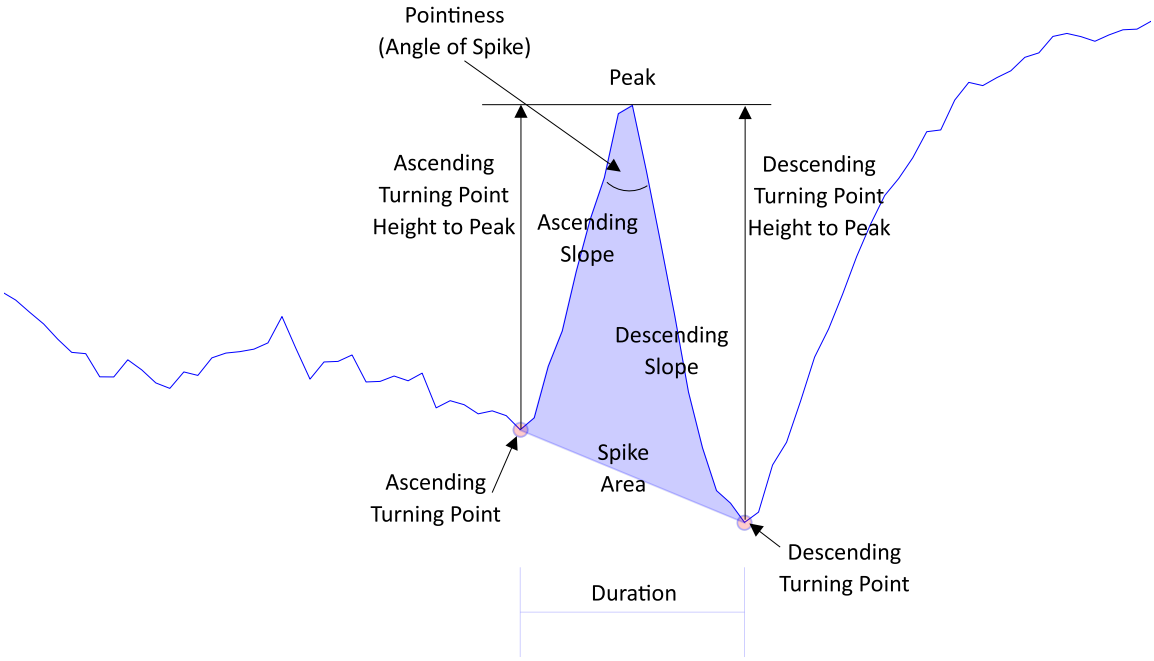


Figure 6: Detailed dissection of an epileptiform spike, annotated to spotlight the multifaceted processes governing its morphology. Commencing from the base, the 'ascending turning point' marks the onset of the spike, where a slew of excitatory mechanisms determines both the rapidity and height of the ascending slope. This trajectory culminates at the 'peak,' revealing the inhibitory processes' potency. These excitatory factors, in combination with the inhibitory effects, not only define the spike's 'spikiness' and 'asymmetry' but also dictate the speed at which neurons undergoing a Paroxysmal Depolarizing Shift (PDS) revert to baseline, thereby impeding their propensity to fire synchronously. The descent of the spike, characterized by the 'descending 'slope,' mirrors the efficacy of these inhibitory processes, converging finally at the 'descending turning 'point.' This point encapsulates the cumulative inhibitory impact on the neuronal zone, underlining the intricate balance between excitatory and inhibitory influences in shaping an epileptiform spike.

2.5.1 Ascending Slope

Biological identification: The ascending slope of an epileptic spike in scalp EEG recordings indicates the initiation of the Paroxysmal Depolarizing Shift (PDS). This initiation is a rapid membrane depolarization facilitated by Na^+ influx and a burst of action potentials maintained by calcium influx. The slope culminates at the peak, where the PDS has propagated to neighbouring neurons, resulting in maximal synchronized firing across an ensemble of neurons [32], [41].

Neuronal Dynamics Observed by Scalp EEG:

- Synchronous depolarizations occurring in the dendrites of pyramidal neurons lead to a distinct voltage difference across the cell that is detectable by EEG. This voltage difference enables the EEG to capture the continuous buildup of excitatory postsynaptic potentials (EPSPs) contributing to the Paroxysmal Depolarizing Shift (PDS) in a cluster of cortical neurons. This active capture underscores the role of dendritic activity in initiating and propagating epileptic events [14].
- A steeper ascending slope of an epileptic spike on the EEG indicates more rapid recruitment of neurons into the synchronized PDS firing.

Glutamatergic signalling (ionotropic): This is a neurotransmission pathway in the central nervous system primarily mediated by the excitatory neurotransmitter glutamate. This system is essential for various neural functions, including synaptic plasticity, learning, and memory. While it prominently involves ligand-gated ion channels like AMPA and NMDA receptors [180], it also encompasses metabotropic glutamate receptors (mGluRs). These mGluRs exist in multiple types and are found in pre- and postsynaptic locations. Specifically, Group 1 mGluRs signal via G protein-coupled receptors to activate intracellular signalling cascades (increase intracellular calcium) rather than directly controlling ion channels [181]. The PDS, however, is mainly dependent on only the ionotropic glutamic signalling due to:

- **AMPA receptors:** These receptors exhibit an immediate excitatory response by allowing an influx of Na^+ ions, resulting in rapid membrane depolarization. This response makes them crucial for initiating PDS [67].
- **NMDA receptors:** Unlike AMPA receptors, NMDA receptors are both ligand-gated and voltage-gated, making them unique in their activation requirements. They need both glutamate binding and postsynaptic depolarization for activation. The receptor has a magnesium (Mg^{2+}) block that must be removed by depolarization for the channel to open, subsequently allowing calcium (Ca^{2+}) and sodium (Na^+) ions to enter the cell. This characteristic makes NMDA receptors slower to activate but is critically important for enhancing neuronal excitability, a critical factor in the occurrence and maintenance of paroxysmal depolarizing shifts (PDS). The heightened excitability is due to the progressive removal of Mg^{2+} blocks with each depolarization, allowing for more Ca^{2+} and Na^+ influx and thus facilitating further depolarizations. Additionally, NMDA receptors have unique properties crucial for synaptic plasticity, which refers to the ability of synapses to change their strength over time, beyond just their level of excitability. In neurological conditions like epilepsy, aberrant NMDA receptor activity can contribute to

hyperexcitability, where neurons are more prone to fire inappropriately and sustain seizure activity [78]–[80].

2.5.2 Descending Slope

Biological Identification: The descending slope of an epileptic spike in EEG recordings signifies the termination phase of the PDS. This phase features the repolarization of the neuronal membrane, which is facilitated by the inactivation of Na^+ channels, ceasing further sodium influx and thus ending further depolarizations. Concurrently, voltage-gated K^+ channels open, allowing the efflux of potassium ions from the neuron into the extracellular space. This inhibition takes over, prompting reduced firing among the involved neurons. It is critical for returning the neurons to their baseline states, thereby terminating the bursts of action potentials that occur during a PDS [32], [41].

Neuronal Dynamics Observed by Scalp EEG:

- **Inhibitory Influence**: The EEG during the descending slope captures inhibitory postsynaptic potentials (IPSPs) as they take effect, suppressing further excitatory activity and bringing neurons back to their resting state. The inhibitory neurotransmitter GABA plays a central role in this process [14].
- **Rate of Descent**: A slower descending slope may indicate that inhibitory mechanisms are less efficient, possibly contributing to prolonged seizure activity or increased susceptibility to subsequent spikes. Conversely, a steeper slope indicates effective and rapid inhibitory action.

GABAergic Signalling: Gamma-Aminobutyric Acid (GABA) is a chief inhibitory neurotransmitter in the central nervous system that becomes particularly relevant during the descending slope. GABA receptors, primarily $GABA_A$ and $GABA_B$, mediate the effects of GABA.

- **Ionotropic GABA_A receptors**: These are ligand-gated ion channels that allow the influx of chloride ions (Cl^-) into the neuron [182]. This influx leads to hyperpolarization, essentially creating a “brake” on the neuron’s excitability. The immediate inhibitory response dampens the hyperactivity, which would otherwise contribute to the ascending slope of a PDS spike on the EEG.
- **Metabotropic $GABA_B$ receptors**: Unlike $GABA_A$ receptors, $GABA_B$ receptors function through G-protein coupled mechanisms that activate inwardly rectifying potassium (K^+) channels and inhibit voltage-gated calcium (Ca^{2+}) channels in neurons. This mechanism results in a more prolonged and sustained inhibitory effect than $GABA_A$ receptors [108]. Activation of these receptors contributes to a longer-lasting

hyperpolarization and a more sustained decrease in neurotransmitter release. This activation can modulate the descending slope of an epileptic spike during a PDS. Specifically, enhanced $GABA_B$ activity could facilitate a smoother, more gradual descending slope by effectively prolonging the period of reduced neural excitability.

2.5.3 Asymmetry (Ratio of Ascending Slope over Descending Slope)

Biological identification: The asymmetry feature in an epileptic spike focuses on the ratio between the rate of the Paroxysmal Depolarizing Shift (PDS) initiation and the rate of its suppression. This feature essentially captures the excitatory and inhibitory dynamics within a network of neurons. A higher ratio would suggest a quicker depolarization rate than repolarization, thereby highlighting the rates of EPSPs and IPSPs between excitatory and inhibitory systems.

’’’The rapid firing and the inherent delay in inhibitory feedback create a situation where the ascending slope can often be steeper than the descending slope, leading to the typical asymmetry observed in epileptiform spikes, which is possibly a consequence of multiple intertwined neurological factors and appears consistent across different age groups [183]. Rapid excitatory processes, driven by an imbalance in neurotransmission and ion channel abnormalities, make the initial surge of neuronal activity swift and steep, often outpacing the body’s inhibitory mechanisms [184], [185]. In contrast, inhibitory feedback processes tend to be more gradual and may be hampered by delays, which leads to a more subdued and less steep descending slope [185]. While it is theoretically possible for the descending slope to be steeper under certain atypical conditions, this is rare because of the inherent speed and ‘explosiveness’ of excitatory processes compared to inhibitory ones.

2.5.4 Pointiness/Spikiness

Biological Identification: While spikiness and asymmetry involve the ascending and descending slopes, they offer different perspectives on the dynamics between excitatory and inhibitory processes driving the PDS. The angle between the slopes, or spikiness, provides a nuanced representation of the balance between excitatory and inhibitory processes. A smaller angle between the slopes corresponds to a sharper, more pointed spike, reflecting rapid and potent excitatory and inhibitory activities. On the other hand, a larger angle suggests a more rounded or blunter spike, indicative of less efficient or slower excitatory and inhibitory mechanisms. This angle serves as an absolute measure of the instantaneous dynamic balance between these two opposing neural forces [32], [41].

In contrast, the asymmetry, calculated as the ratio of the ascending slope to the descending slope, provides a relative assessment of the steepness of each component of the spike. Therefore, while spikiness focuses on the aggregate outcome of excitatory and inhibitory processes, as evidenced by the angle between the slopes, asymmetry emphasizes the relative dominance of one process over the other. Both metrics are complementary and jointly contribute to a comprehensive understanding of the pathophysiology underlying epileptic activity.

- **Angle as a Combined Measure**: The angle between the ascending and descending slopes reflects a balance between the speed and effectiveness of excitatory uptake via glutamatergic signalling and inhibitory control via GABAergic signalling. A smaller angle is indicative of strong, rapid excitatory and inhibitory mechanisms, resulting in a sharp spike.
- **Synchronization and Speed**: A larger angle, indicating a blunter spike, could signify a slower uptake in synchronized neuronal firing via NMDA receptors during the PDS and a slower transition from excitatory to inhibitory states via $GABA_B$ receptors.

2.5.5 Peak height

Biological Identification: The peak height reflects the maximal synchronized dendritic depolarizations over the largest group of pyramidal cells during a PDS. It measures the largest area of neurons that are firing in synchrony, creating a unified dipole measured by the EEG. A higher peak indicates greater synchronized activity among the largest set of neurons involved in the PDS [32], [41]. It should be noted the peak amplitude is not normalized to any baseline and includes background neuronal activity. This feature serves as a gross indicator of the maximum extent of synchronized excitatory activity during a spike event in combination with surrounding activity.

- **Level of Synchrony:** A higher peak reflects greater synchronization among participating neurons during the PDS, thus serving as an indicator of the scale and intensity of the epileptiform activity.

2.5.6 Normalized Ascending Height

Biological Identification: In contrast to the peak, the height from the beginning of the ascending slope to the peak is a normalized measure of the pre-spike baseline that provides a more nuanced understanding of the neural dynamics specific to the epileptic spike. It reflects the magnitude of synchronized depolarization from the onset of the PDS to its peak, offering a more isolated representation of the spike's internal dynamics.

- **Normalized Measure**: Unlike the peak, this metric is normalized to the spike's own form, providing a more accurate representation of the excitatory and inhibitory mechanisms at play.

2.5.7 Normalized Descending Height

Like the Descending Slope metric, the Normalized Descending Height reflects inhibitory processes, particularly repolarization and hyperpolarization. Repolarization is mediated by the activation of voltage-gated K^+ channels, allowing K^+ ions to exit the neuron and drive the membrane potential towards its resting state. Hyperpolarization, in contrast, usually involves GABAergic signalling that permits the inward flow of Cl^- ions [32], [41]. While the Descending Slope metric assesses the rate of inhibitory regulation over time, this height measurement quantifies the total extent of inhibitory processes involved.

2.5.8 Duration/Length

Biological Identification: The duration of the spike captures the entire length of the PDS from the beginning of the ascending slope to the end of the descending slope. This metric fundamentally reflects the temporal summation of excitatory and inhibitory processes within the rapid synchronous neuronal activity. A longer duration might indicate a more prolonged interplay between excitatory and inhibitory mechanisms, while a shorter spike duration may point to a more rapid resolution of these processes [32], [41].

- **Relation to previous metrics**: While metrics like Ascending Slope, Descending Slope, and Heights from slope turning points to peak evaluate the qualities of individual aspects of the spike, duration provides an overarching view of how these components integrate over time.
- **Temporal Summation**: The duration of the spike could potentially indicate the summation of excitatory and inhibitory postsynaptic potentials (EPSPs and IPSPs) in a temporally coordinated manner.

2.5.9 Area of Spike

Biological Identification: The area is a cumulative metric that embodies the totality of both excitatory and inhibitory events during a PDS. Unlike individual metrics such as Peak Height, Duration, or Slopes, the area gives an integrated snapshot of the entire spike event, encapsulating the “total energy” or “intensity” committed during the spike. It is not a straightforward measure of how intense or prolonged the event is but rather an amalgamation of several previous metrics described.

- **Relation to other metrics**: The area synthesizes the various metrics previously discussed. It can be influenced by a range of factors, including the rate of depolarization and repolarization, the

peak's overall height, and the spike event's duration. It is a composite, holistic measure that summarizes a majority these contributing features.

- **Comprehensive Indicator**: As a cumulative measure, the area under the spike can offer unique insights. Different combinations of duration, peak height, and slopes can result in similar area measures, emphasizing the metric's role as a unified representation of the spike's overall biophysical characteristics.

2.6 Problem and Solution

In the preceding sections, an intricate exploration of the mechanisms governing the sleep-wake cycle has been undertaken, elucidating the roles of various neurotransmitters and processes, including glutamate, GABA, Ach, orexin, serotonin, norepinephrine and astrocytes, to create a proper understanding of possible morphological changes of epileptic spikes throughout the sleep-wake states. This analysis aims to formulate a generalized assumption regarding how epileptic spike morphology could alter within the context of normal sleep conditions based on the comprehensive processes explored thus far.

Considering the multifaceted nature of the exploratory study encompassing multiple dynamic systems, including the sleep-wake cycle, requires establishing a baseline understanding of "normal sleep" where differences can be derived. Changes within normal sleep are extensive, where a small portion has been discussed thus far. However, they are significant contributors to referencing ionic and neurotransmitter concentrations, synchronous activity, and general plasticity while also being critical players in epileptic activity. This analysis delineates the spikes observed during "normal sleep" conditions, grounding the study in a well-established baseline. This delineation avoids confounding the results with a myriad of potential variations that epileptic sleep might introduce,

Given the dynamic nature of epilepsy, patients often experience diverse disruptions in normal sleep patterns, initiating a cycle where epileptic events deteriorate sleep quality and subsequently influence the further manifestations of epileptic activity. This disruption presents a complex nexus of interactions potentially affecting the observed spike morphologies, necessitating a focused approach grounded in the baseline representation of normal sleep dynamics. This strategic approach aims to uncover any anomalies that might unexpectedly arise, thereby fostering a more detailed discussion in the forthcoming sections.

As discussed, glutamate and GABA serve as the building blocks of a Paroxysmal Depolarizing Shift (PDS) and play a vital role in overall brain function. On the other hand, Ach, though not essential for PDS, plays a significant role

in sleep regulation and possibly aids in the modulation of PDSs during REM sleep stages. Moreover, the investigation considers the implications of orexin, a principal regulator of sleep-wake cycling and REM sleep duration, and astrocytes, which exhibit multi-dimensional roles influencing every known process directly or indirectly.

In the ensuing section, the focus is shifted toward exploring the overview of spike features and their biological mechanisms derived from scalp EEG representation and understanding the roles played by different pathways, neurotransmitters, and ions in the genesis of a spike. Moreover, the following analysis postulates how these spikes might evolve throughout other sleep-wake states. This meticulous approach aims to elucidate the nuanced morphological changes witnessed in epileptic spikes, with guidance from the foundational insights gained through exploring the micro-neurological processes of sleep and the origins of PDS that manifest as spikes in scalp EEG recordings.

To summarize, the intricacies of sleep-wake states, coupled with the complexities of epilepsy, form a multi-dimensional landscape which is far from fully understood. While we have gained extensive insights into the role of various neurotransmitters, ions, and cellular components like astrocytes, a significant gap remains: we have yet to explore the morphological changes in spikes during these states, specifically within interictal conditions serving as a baseline.

This thesis seeks to fill this gap by investigating how the morphological features of spikes—such as their slopes, amplitudes, and durations—alter throughout different sleep-wake states. The aim is to study:

1. How morphological characteristics of spikes in “normal sleep” conditions differ from those in the context of epilepsy.
2. What roles are played by key neurotransmitters like glutamate, GABA, and orexin and cellular components, like astrocytes, in observed changes In spike morphology?
3. What are the translational challenges of applying animal studies findings to human neurophysiology?

By focusing on these aims, this thesis hopes to shed light on the underlying mechanisms that influence spike morphology, thereby contributing to our broader understanding of sleep and epilepsy. Ultimately, the goal is to explore the morphological changes of spikes throughout sleep-wake states, offering insights that could not only clarify why specific characteristics change but also potentially pave the way for future research into why spikes are more prevalent in NREM sleep and/or possible insights into REM sleep’s anti-epileptic function. The ensuing sections will present the methodologies used, followed by the findings and their implications.

In conclusion, section 2 has provided a detailed examination of the neurophysiological mechanisms potentially modulating the morphology of epileptiform spikes across sleep states. The section has methodically dissected the fundamental aspects of sleep architecture and the practical application of EEG in spike analysis, setting a precise context for our primary investigation. The critical mechanism changes explored throughout the sleep-wake states were glutamate, GABA, Ach, orexin, astrocytes, and sleep-wake network dynamics. The intricate descriptions of spike features, such as the spike slopes, heights and durations, have been grounded in these aforementioned biological processes. This work includes an in-depth analysis of the role of primary neurotransmitters like glutamate and GABA and their respective signalling pathways in shaping the characteristics of these spikes. The section thoroughly explored the initiation and termination phases of the Paroxysmal Depolarizing Shift (PDS), emphasizing the synchronous activity of neurons and the balance between excitatory and inhibitory forces as captured by scalp EEG.

As the thesis progresses, we delve into the empirical investigation of these spike features, examining how they vary across different sleep states. This investigation involves a detailed analysis of the EEG data collected, emphasizing the correlation of the theoretical insights presented in this section with the observed morphological variations in epileptiform spikes over the sleep-wake states.

3 Methodology

The third section of this thesis delves into the methodology underlying the investigation of epileptiform spike morphology across sleep-wake states. Central to the analysis is a Graphical User Interface (GUI), specifically designed for precisely identifying, marking and labelling epileptic spikes within EEG recordings. This section reveals the functionality of this interface, detailing its essential components and the rationale behind its design. Furthermore, the computational pipeline was developed to analyse these spikes, describing the rigorous data extraction process, pre-processing, and the computation of various spike criteria. These criteria, including slope characteristics, spike height, length, and other vital metrics, form the basis of the empirical investigation. This section also provides an in-depth overview of the statistical methods employed to analyse the data. Beginning with normality testing to determine the appropriate statistical techniques, then significance testing using the Kruskal-Wallis Test, and finally, post hoc analysis with the Dunn-Sidak Test and Bonferroni Correction. These statistical approaches are crucial for establishing whether significant differences exist in spike morphology across different sleep-wake states, primarily focusing on the unique characteristics of REM sleep.

The initial step involves meticulous data collection through expert visual identification of spikes to guarantee the quality of our dataset to the de facto gold standard. An experienced epileptologist utilized a specialized graphical user interface (Figure 7) to hand-mark these spikes, ensuring precise labelling. The process was designed to be streamlined for efficient data curation. Subsequent sections elaborate on the computational methods employed to transform this raw data into multiple features, which are then statistically analysed to identify variations across different sleep-wake states.

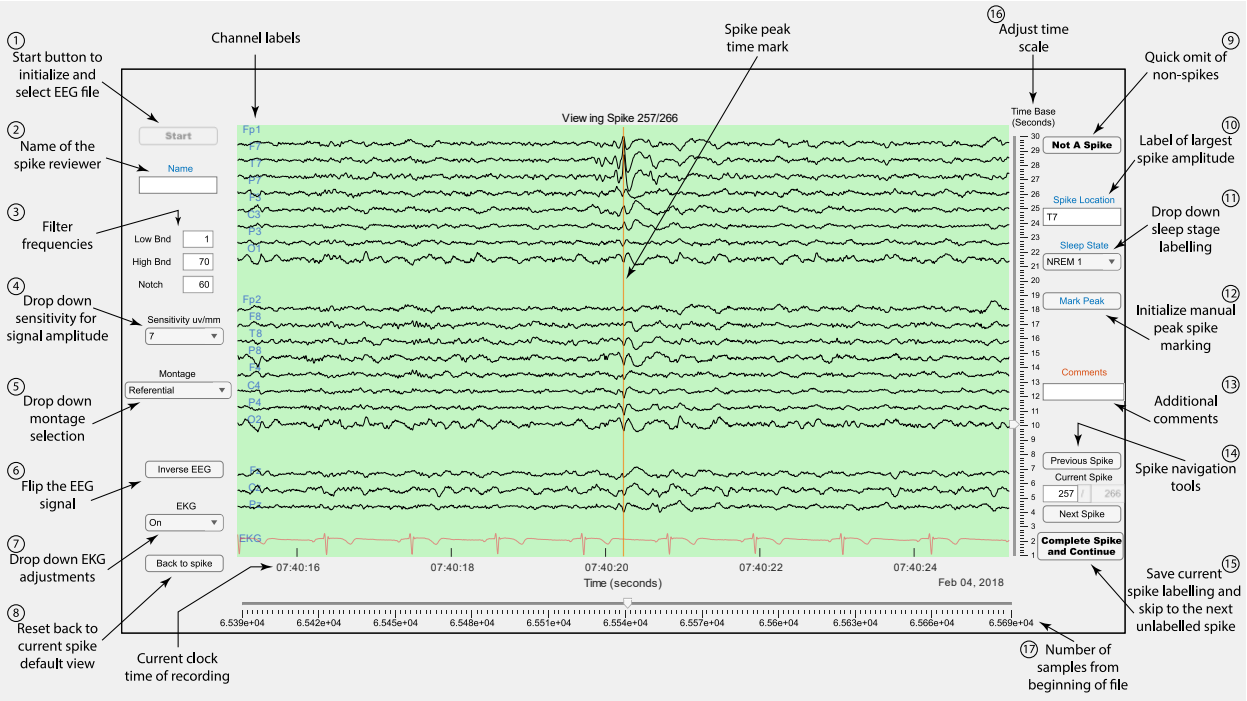


Figure 7: EEG Review Tool Interface. This GUI is designed for EEG professionals to review and label epileptiform spikes. (1) initializes the program and allows for EEG file upload; (2) records the reviewer's name; (3)-(7) are controls for filtering and displaying the EEG and EKG signals; (8) enables quick navigation back to the current spike's default view; (9)-(13) are tools for labelling and commenting on spikes; (14) are navigation tools for moving through spikes; (15) saves all labels and moves to the next unlabelled spike; (16) and (17) allow for adjustment of the time base and time scrolling, respectively.

3.1 Graphical User Interface

In epilepsy research, the accurate identification and characterization of epileptic spikes within electroencephalogram (EEG) recordings are paramount. However, researchers face a significant challenge in obtaining reliable and high-quality data sets, particularly in neurology, where creating a gold standard dataset relies on the expertise of neurologists who meticulously analyse vast EEG datasets to detect epileptiform discharges. A sophisticated graphical interface (GUI) has been painstakingly developed and tailored to meet the unique requirements of neurologists in this field.

This subsection introduces the spike scoring graphical interface, offering an overview of its crucial features and its potential to enhance the efficiency and accuracy of epileptic spike scoring. Special attention is given to the interface's intuitive design, its compatibility with existing spike-scored files, and its ability to organize essential information for comprehensive analysis. The following key points highlight the GUI's notable features and functionalities:

1. **Ease of Use:** The primary objective of the graphical interface is to streamline the process of scoring and labelling epileptic spikes. The interface has been meticulously designed to ensure user-friendly interaction, incorporating intuitive features and interactive tools that facilitate seamless navigation and manipulation of the EEG recordings. By providing neurologists with direct access to the spikes within the EEG, the graphical interface significantly reduces the information to assess, fostering an environment that enhances productivity and facilitates streamlined assessment.
2. **Integration of Existing Data:** The graphical interface eliminates the need for redundant work by seamlessly integrating with pre-scored files. Specifically, it allows neurologists to import previously scored files, including formats such as EDF+ (beta version) and those generated by proprietary software such as Persyst™. This integration empowers expert neurologists to focus exclusively on identified spikes without the need to review the entire EEG recording. Ultimately, the GUI creates a streamlined experience that increases the number of labelled spikes while minimizing the time required for analysis.
3. **Compatibility with Persyst:** Recognizing the widespread adoption of Persyst as a spike-scoring software, the graphical interface ensures seamless compatibility with Persyst-scored files. The files consist of a comprehensive list of potential spikes, where each entry is accompanied by its corresponding validation accuracy and precise date-time information. The interface empowers neurologists to effortlessly retrieve any spike at a specific time, significantly reducing the time required for spike validation and labelling.
4. **Organized Output for Further Analysis:** The graphical interface generates well-structured output files that incorporate essential information required for an in-depth analysis of the spikes. Alongside corrected spike occurrence timestamps, the output includes additional data, such as the spike date-time, sleep-wake state labelling, and relevant comments. The allocation of precise timestamps, sleep-wake labelling and validation of spikes within an organized output establishes the fundamentals for a gold standard dataset. This meticulous organization is pivotal as it serves as the cornerstone for conducting comprehensive spike analyses, enabling the application of various computational algorithms with heightened accuracy and unwavering reliability.

3.1.1 Functions of the Interface

3.1.1.1 Start

When the start button is pressed, it initiates the spike reviewing process. The GUI then displays only those spikes that have an accuracy equal to or greater than the value inputted, with the default set at 100%. The following subsections describe the different features and processes incorporated into the start button function:

1. **Inputting Accuracy threshold:** Before initiating the spike reviewing process, users can input a threshold for the accuracy of the spikes to be displayed. This threshold determines the minimum accuracy percentage required for a spike to be included for review. The interface only uses the information from the pre-scored algorithms (in this case, Persyst's spike scoring) whereby the default, the minimum threshold is 100%. Although the current implementation focuses on Persyst spikes, the algorithm can be adapted for different file formats and accuracy measures.
2. **File Selection:** Upon starting the program, by pressing the start button, users are prompted to choose a file for review through their respective operating systems file system. The operating system provides a file selection interface, allowing users to browse and select the desired file for review.
3. **File Compatibility Check:** If the selected file format is incompatible or unsuitable for review, the system prompts the user to choose another file. For example, if the Persyst dat file is chosen instead of a supported format, such as a Persyst lay file, the system requests the user choose an appropriate file format.
4. **Header Information Reading:** The system reads the header information of the selected file to extract essential details. In case the header information is unreadable, corrupted, or incomplete (e.g., missing the necessary *dat* and *lay* files for Persyst format), an error is flagged to the user.
5. **Spike Availability Check:** After reading the header information, the system verifies if there are any spikes present at and above the selected accuracy threshold in the selected file. If no spikes are found, the system displays a message indicating zero spikes where found, allowing the user to choose another file to review.
6. **Header Information Extraction:** After the file is verified to contain spikes, relevant information such as sampling rate, calibration, channel map, and date-time values are extracted from the header. The system reorganizes the channel names, discarding any entries that are not valid channel names. Additionally, the system can convert older EEG standards to the newer channel label standard. For instance, the T3 label is transformed to T7, T4 to T8, T5 to P7, and T6 to P8. This standardization

ensures consistency across different EEG datasets, particularly when dealing with a clinical Natus setup that may include additional annotations like "EEG" or ground reference denotations.

7. **Parallel Thread Initialization:** The system initializes parallel threads to enable concurrent processing, which leads to faster execution of tasks.
8. **Database / CSV File Handling:** After completing all error checks, the system looks for a CSV file within the same file directory and under the same name as the selected EEG. If no CSV file is found, the system creates one. The system identifies the last completed spike if a CSV file already exists. It begins the marking process from the next non-completed spike or, in the case of a completed file, offers the user the option to review the completed spikes. The CSV file is the database that holds all relevant information for each spike within the following columns:
    1. Spike time is determined by a spike detection algorithm such as Persyst in seconds from the beginning of the EEG recording.
    2. The marked spike time from the professional reviewer is recorded as seconds from the beginning of the EEG recording.
    3. Spike location from the spike detection software (if included).
    4. Reviewer's Inputted spike location of spike in time. The electrode location is determined by the channel with the highest spike amplitude, whereas in edge cases with multiple spikes having the same amplitude, an overall midpoint is chosen.
    5. Binary spike completion status is stored (1 for complete, 0 for not completed).
    6. Assigned sleep state
    7. Name of the reviewer marking the spike.
    8. Date-time of the reviewer's completion of the spike marking is recorded.
    9. Date-time of the marked spike is recorded. For example, instead of 4000 seconds after the beginning of recording, it would be displayed as 7:03 pm.
    10. And finally, any additional comments the reviewer would like to share, including transitional states or bad channels.
9. **Inefficiencies:** The system employs specific strategies to address inefficiencies in reading data from files to improve processing speed. Firstly, the entire database is held in memory and continuously updated as new spikes are completed. This approach compensates for the slow file-reading capabilities of Matlab. Additionally, the start function precomputes an entire date-time array for the entire loaded EEG dataset to optimize date-time computations. By storing this array in memory, the need for repeated computations during spike lookup is eliminated, resulting in faster generation of

the overall plot and allowing for near-instantaneous spike reviewing. These measures significantly enhance the system's overall performance and responsiveness.

10. **EEGread Function:** In the final stage, the start button initiates the EEGread function while incorporating a focus GUI call to enable the seamless utilization of shortcuts and associated commands within the program. This pivotal step enhances user experience and facilitates a streamlined review process.

The developed GUI amalgamates the functionality listed, providing reviewers with an efficient and streamlined data review and quick access to spike data to facilitate their analysis of the spikes.

3.1.1.2 Read EEG Segment

The reading EEG function begins with parsing the database for the current spike and extracts the spike time in seconds from the beginning of the recording.

The function aims to extract a 150-second duration before and after the spike to ensure proper assessment of the spike and any anomalies, including labelling of sleep state. If insufficient data exists (e.g. beginning or end of file), the interface extends from the recording's beginning to 165 seconds to allow for at least 15 seconds after the spike for sleep state labelling.

The data is extracted from the memory-mapped EEG file and calibrated to ensure the raw EEG signal corresponds to the correct physical units (microvolts [µV]). The calibration accounts for several factors, such as the amplifier gain and the digitation/compression of the signal.

In addition to calibrating the signal, filters are required to correctly display the EEG for standard viewing with parameters determined by the reviewer. The filtering function computes a notch, low and high pass filter with default parameters of 60Hz, 70Hz and 1Hz, respectively. The notch filter removes power line interference, a common noise source. The low-pass filter removes muscle artifacts, and the high-pass filter removes slow drifts and baseline shifts. These filters are typically applied to the EEG signal before it is displayed or analysed. By removing noise and artifacts, the filters can improve the signal-to-noise ratio and make it easier to see the underlying EEG signal.

The filters used in this application were designed using the fir1 function in MATLAB, which creates finite impulse response (FIR) filters with a linear phase response. The fir1 function offers flexibility in customizing the design of the filters with characteristics such as filter order and filter type. The choice of the filter order is a crucial trade-off between filter performance and complexity. A higher order was selected for the 1Hz high-pass filter to

achieve a steeper roll-off in the low-frequency range and effectively eliminate any signal components below 1Hz. A factor of 14 was chosen to balance the desired filter performance and computational complexity. Similarly, for the 60Hz stop band filter with a range of 59.5-60.5Hz, a higher order with a factor of 150 was employed to achieve high attenuation of the 60Hz power line interference. Lastly, for the 70Hz low-pass filter, a lower order with a factor of 20 was chosen to preserve more of the higher frequency components up to 70Hz. However, it's important to note that the actual order of the filter is based on the factor multiplied by the ratio of the sampling rate to the filter rate.

During filtering, the function may encounter a warning related to odd-order symmetric FIR filters and the gain at the Nyquist frequency. The function automatically increases the filter order by one to maintain a zero gain at the Nyquist frequency, ensuring proper filter design. Keeping track of these slight increases to the filter order is required for adjusting the time array to the time delay the filter creates.

In addition to the above steps, the function performs various chores. These tasks range from populating the time bar at the bottom of the interface to checking if a spike has already been professionally marked where it can be displayed on the plot. Furthermore, the zoom bar is reset to the default position for convenience.

Finally, the plot function is called to visualize the filtered signal. If the inverse button is activated, the function generates an alternative plot with the voltages inversed, providing data interpretation and analysis flexibility within the interface.

3.1.1.3 Plotting

For spikes to be correctly assessed, plotting the EEG onto the interface must be a quick and accurate process encompassing all the tools offered in professional EEG viewing software. These tools include various features such as filter ranges, montages, and sensitivity settings, enabling reviewers to evaluate spikes within the EEG data thoroughly.

When displaying the EEG, it is crucial to set the sensitivity correctly, which is expressed as microvolts per millimetre (μV/mm). For instance, a 7 μV/mm sensitivity signifies that a 7μV change in the electrical signal results in a 1 mm deflection on the EEG tracing. When determining the sensitivity, the code retrieves the pixel and centimetre (cm) height of the current plotting area for the current monitor. By dividing the pixel height by the cm height and then again by 10, we obtain the number of pixels per millimeter. Multiplying this value with the desired sensitivity specified by the reviewer allows us to establish the appropriate sensitivity for the EEG display.

Two primary montages are available for EEG display: bipolar longitudinal and referential montages, each serving specific purposes.

The bipolar longitudinal montage allows for an in-depth analysis of localized brain activity. Each montage requires various input parameters, such as the plot's axis handles, filtered data, date-time array, channel labels, spike position, sensitivity, EKG display preference, update behaviour, spike marking time (if applicable), and the time array in seconds. The channels expressed in the bipolar longitudinal montage are as follows:

- Left temporal: (FP1 - F7, F7 - T7, T7 - P7, P7 - O1)
- Right temporal: (FP2 - F8, F8 - T8, T8 - P8, P8 - O2)
- Left parasagittal (FP1 - F3, F3 - C3, C3 - P3, P3 - O1)
- Right parasagittal (FP2 - F4, F4 - C4, C4 - P4, P4 - O2)
- Midline: (Fz-Cz, Cz-Pz)
- And EKG, if specified to be displayed

The EEG is plotted within designated y-axis spacings, accounting for the inclusion or exclusion of an EKG. This montage is particularly useful for identifying spikes in specific brain regions, enhancing localization accuracy.

In contrast, the referential montage provides a broader perspective on overall brain activity. It shares many similarities with the bipolar longitudinal montage in terms of code structure. However, the channels in the referential montage are referenced to the average of the 19 displayed channels. The channels expressed in the bipolar longitudinal montage are as follows:

- Left hemisphere: (Fp1-Avg, F7-Avg, T7-Avg, P7-Avg, F3-Avg, C3-Avg, P3-Avg, O1-Avg)
- Right hemisphere: (Fp2-Avg, F8-Avg, T8-Avg, P8-Avg, F4-Avg, C4-Avg, P4-Avg, O2-Avg)
- Midline: (Fz-Avg, Cz-Avg, Pz-Avg)
- And EKG, if specified to be displayed

Spacing between channels and major brain regions is incorporated to facilitate ease of use for the reviewer and familiarity with standard montages. Spacing is automatically adjusted for whether there is an EKG signal, where the reviewer's ability to exclude the EKG signal ensures an unobstructed view of the EEG. In order to ensure an accurate assessment of spikes, it is crucial to confirm them in two different montages. While the bipolar montage is more localizing, the referential montage captures a comprehensive view of global brain activity, which proves advantageous in their different perspectives.

3.1.2 Tools Required for Assessing Spikes

In addition to the necessary features of the interface, several additional tools are implemented to optimize the user experience and facilitate efficient navigation and analysis of the spikes (Figure 7). These tools include:

1. Zoom Slider: This feature enables users to adjust the timeframe currently displayed in the plot from 1 second to 30 seconds of EEG. Users can conveniently drag the sliding bar or use a mouse scroll wheel when the mouse is hovered over or to the left of the time base bar. This flexibility allows for quick and intuitive zoom level adjustment, giving users a more detailed or broader view of the surrounding EEG.
2. Time Slider: This bar offers users a simple and efficient way to navigate the displayed EEG spike time. Like the zoom slider, users can drag the sliding bar or utilize the scroll wheel when the mouse hovers to the right of the time base bar. This feature enables users to swiftly traverse the timeline, facilitating seamless data exploration and analysis at different time points, which is integral for sleep staging.
3. Mark Peak button: This tool is vital for precise spike marking, automatically switching to the referential montage and zooming into the spike, displaying only 1 second of the EEG. The referential montage is exclusively used to ensure reproducibility, helps minimize background noise and ensures the spike's polarity is always in the same direction, allowing for a more accurate assessment of the spike's morphology. When the mark peak button is activated, *ginput*, a Matlab function, displays a pinpoint cursor that can collect the exact spike peak selected by the reviewer.
4. Complete Spike button: This button is crucial for a speedy and efficient transition between spikes and is an error-flagging tool for finalizing spikes without proper labelling. If a spike is being completed without being labelled with a sleep state and the electrode location, an error message will be presented to the user, and a red box will surround the area that needs attention. In addition, if the mark peak button was never used to mark the highest amplitude position precisely, then the original spike mark time is used, along with leaving a note that it was not marked. Furthermore, all relevant columns for the spike will be saved in memory and exported to an Excel sheet. This tool automatically progresses to the next unmarked spike, and if the file is complete, it notifies the user and prompts them to start a new file.
5. Not a Spike: The "Not a Spike" tool functions similarly to the complete spike tool but to fill the database with the "not a spike" classification for all unfilled fields. This tool ensures consistency and completeness in the recorded data, facilitating accurate analysis and interpretation.

In addition to the tools mentioned above, several keyboard shortcuts have been implemented to streamline the program's usability further and improve user efficiency:

- Left arrow and mouse wheel up (when hovered to the right of the time base bar): Scrolls forward through the EEG data.
- Right arrow and mouse wheel down (when hovered to the right of the time base bar): Scrolls backward through the EEG data.

- Mouse wheel scrolling (when hovered on top of or to the left of the time base bar): Scrolls through the time base bar.
- Up arrow and down arrow: Scrolls through sensitivity pre-sets.
- Control: Scrolls through montage pre-sets.
- Escape: Resets the plot view to default and centres the spike in the image.
- N: Quick key for the "Not a Spike" button.
- 1, 2, 3, 4, 5, 6: Selection of sleep state:
    1. NREM1
    2. NREM2
    3. NREM3
    4. Awake
    5. REM
    6. Inconclusive
- M: Quick key for marking the peak of the most prominent spike.
- Y: Quick key for the "Complete Spike" button.

By incorporating these additional tools and keyboard shortcuts, the program aims to provide users with a more efficient and user-friendly experience, enabling them to navigate, analyse, and interpret data easily.

3.2 Analysis results code:

3.2.1 Tasks Necessary for Code to Execute

The analysis section begins by collecting the completed marked spike sheets created by the spike marking interface. In brief, the steps involved in the data processing include an assortment of spike criteria derived from the definition of a spike in addition to relative powers and a variety of functional connectivity metrics. These metrics are all derived in three separate electrode computational combinations (montages), including the raw EEG (unaltered), an average referential (all electrodes referenced to average of all electrodes), and the Laplacian

reference (electrodes referenced only to neighbouring electrodes), enabling multiple spatial perspectives (Figure 8). The main focus of this study lies in the computation of the spike criteria, comprising essential metrics such as slope characteristics, heights and length. In the subsequent sections, we will investigate the detailed steps and code employed to derive these significant results.

To effectively complete the following tasks and analyses, a series of initial duties are implemented, beginning with initializing the parallel computing toolbox in MATLAB to optimize the time required to compute. Next, the file path for the folder that encompasses all subfolders that possess all the EEG data, including the GUI-generated spike databases, is inputted to be computed. Finally, output table headers are generated for computed data to reside within.

Once these fundamental preparatory actions are undertaken, we can construct the five comprehensive output tables for each type of analysis, beginning with the general spike criteria. These tables include identifiers such as patient number, spike number, sleep label, montage label and more, with result information such as descending slope value, asymmetry of the spike, spikiness, length and many more. Other result tables include relative power from before and after the spike within the prominent frequency bands, phase and power correlation, generalized eigendecomposition using the first and second components, and Granger causality. The output tables all retain similar identifying columns; however, they include only their respective multi-channel results.

3.2.2 Computational Pipeline for Analyzing Spikes, Including Spike Criteria

The computations begin by sequentially reading the marked spike databases, extracting the current path, and reading the spike Excel sheet to determine the number of spikes. Subsequently, real marked spikes, distinct from not a spike, are identified, and their indices in the Excel sheet are recorded. The EEG data is parsed for files containing marked spikes, outputting all header information, including an on-disk memory mapping of the EEG file for optimal memory usage. The memory-mapped file provides the ability to quickly move segments of the EEG file into memory to ensure low memory usage and overall speed. Using the indexed real spikes, data extraction of each spike ensues, including the spike's position in time per the reviewer's markings.

The *ExtractSpikeTime* function extracts the EEG segment, ensuring adequate temporal context around each spike. If sufficient time is available, this function extracts a raw EEG segment surrounding the spike for up to 20 seconds. Otherwise, depending on temporal constraints, it extracts the spike from the beginning to 20 seconds after the spike time or 20 seconds before the spike to the end of the file. The extracted spike is calibrated by transforming the raw digital values into corresponding physical units. This calibration involves using physical and

digital maximum and minimum values to approximate the original recorded physical signal as a floating-point number from the stored integer values.

Next, data filtering or pre-processing is performed using a notch filter to counter line noise at 60Hz, a low-pass filter to restrict frequencies above half the sampling rate (256Hz), and a high-pass filter to eliminate the DC component. The *lay_EEG_Filtering_V4* function, identical to the GUI pre-process filtering, applies the *fir1* MATLAB function to create a filter kernel and the *filter* function for high, low, and notch filters. Implementing the *filter* function in MATLAB is exponentially faster than the *filtfilt* function, making it a more efficient choice for computations, as it avoids the additional time required for filtfilt's double filtering process to achieve zero-phase filtering. Moreover, the phase correction in the *filter* function is updated using the length of the kernels, ensuring precise signal alignment without compromising on computational efficiency.

The time vector is constructed and re-adjusted to the computed delay, allowing perfect referencing to the spike according to the reviewer's markings. Subsequently, referential and Laplacian montages are computed using the *ComputeReferentialMontage* and *ComputeLaplacianMontage* functions, respectively. The referential montage involves averaging all channels over their time periods and subtracting them from individual channels (Figure 8), while the Laplacian montage averages surrounding electrodes and subtracts them from the target electrode (Figure 8). Currently, only three montages are computed (raw, referential, and Laplacian); however, more can easily be created and added to the *MontagesToCompute* array. Similarly, only the generic 19 electrodes within the 10-20 standard are employed, where additional channels can be added to the *CompChans* array for future analyses.

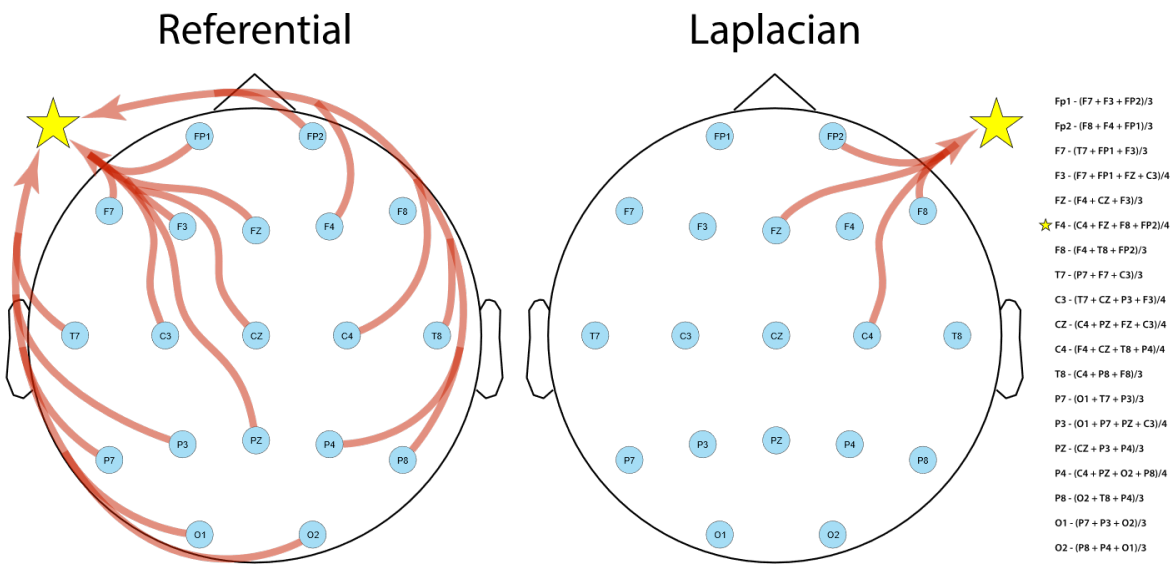


Figure 8: Representation of EEG montages in the 10-20 system. On the left, the 'Referential' montage highlights the practice of referencing each of the 19 electrodes to a global average, encapsulating the collective activity of all electrodes. Conversely, the right side depicts the 'Laplacian' montage, emphasizing the more localized referencing method. Here, individual electrodes, exemplified by the F4 electrode, are compared to a weighted average of their immediate neighbouring electrodes. An accompanying list details the specific neighbour groupings for each electrode in the Laplacian montage, with F4's configuration prominently indicated.

The following computation stage thoroughly analyses spike criteria within the various montages in a sequential loop. The calculations begin with the SpikeSlopes and SpikeSlopesResults functions, with the former focusing on the electrode selected by the reviewer with the highest amplitude and the latter computing metrics for all electrodes. The *SpikeSlopes* function efficiently processes the filtered data for a given montage (raw, referential, or Laplacian) with inputs of sampling rate, channel labels, time vector, marked spike location, and the exact time of the marked spike. During the computation, the function finds the index of the channel label corresponding to the marked channel label from the EEG file header and locates 100th of a second before and after that point, ensuring a 20ms window to accurately classify the exact spike peak while remaining within the minimum spike boundaries. This precaution ensures that the highest peak for a given electrode is adjusted if the reviewer's marking slightly deviates or occurs between multiple electrodes with the same highest amplitudes. The function continues by computing the ascending turning point, which signifies the start of the spike event, indicating the initial ascent towards the peak of the spike. The ascending turning point is determined by assessing each point from the peak backward until a subsequent amplitude becomes larger than the previous point, ending the downward trend. Similarly, the descending turning point marks the spike's end and is evaluated by travelling downwards until the next amplitude increases, ending the downward trend in the opposite direction. With the turning points evaluated, the ascending and descending slopes are obtained by fitting a first-degree linear line

from the turning point to the peak using the *polyfit* MATLAB function. Another slope-related parameter is the spike's asymmetry, calculated as the absolute value of the ascending slope divided by the absolute value of the descending slope. Using absolute values is essential since the slopes are permanently opposite each other. Therefore, we focus on the relative magnitude of the ratio, which signifies the difference between the ascending and descending slopes, rather than the direction of the ratio. Spikiness, represented by the angle Θ in degrees, is also derived from the slopes and portrays the angle between both slopes. The angle between two lines formula is as follows: $\Theta = \tan\text{^} - 1(|(\mathrm{m1} - \mathrm{m2}) / (1 + \mathrm{m1} * \mathrm{m2})|)$ where m1 is the ascending slope with m2 being the descending slope. The following two criteria, height ascending and height descending, are calculated by subtracting the peak amplitude value from the value at the respective turning points, providing results for a more in-depth understanding of the overall spike morphology. The length of the spike should not be overlooked and is derived by the seconds between the ascending and descending turning points. Finally, the spike's area is computed by creating the shortest line between the ascending and descending turning points, allowing integration of the complete spike shape and subtracting the area below the line to yield only the area within the spike.

These spike criteria metrics are the foundation for subsequent analyses, further enhancing the understanding of EEG spike patterns and facilitating additional computations reliant on these core calculations.

3.2.3 Statistical Approach:

This study aims to determine if significant differences exist among various sleep-wake states to grasp further possible insights into the mechanics that may stem from sleep and get insight into missed features that could help aid those with epilepsy. Therefore, to narrow this approach even further, specifically focusing on whether Rapid Eye Movement (REM) sleep significantly differs from other states due to the evident anti-epileptic properties this state possesses. Three statistical methods were used to approach these objectives: Normality testing, Significance testing, and Post hoc testing.

Hypothesis Testing

Hypothesis 1:

The primary hypothesis is to examine whether the sleep-wake states differ significantly from each other.

- Null Hypothesis (H0): No significant difference exists among any of the sleep-wake states.
- Alternative Hypothesis (H1): Significant differences exist among any of the sleep-wake states.

This hypothesis aims to understand if there is a distinction between any of the sleep-wake states in terms of their morphological characteristics. If the null hypothesis is rejected, it indicates that there is a significant distinction between any of these states.

Hypothesis 2:

The secondary hypothesis is sought to determine if REM sleep is significantly different from other sleep-wake states due to its unique electroencephalographic patterns and presumed anti-epileptic effects.

- Null Hypothesis (H0): There is no significant difference between REM sleep and any one of the other sleep-wake states.
- Alternative Hypothesis (H1): There is a significant difference between REM sleep and any one of the other sleep-wake states.

This hypothesis is driven by the peculiar nature of REM sleep, often associated with intense brain activity, vivid dreams, and rapid eye movement. Furthermore, REM sleep has been linked with anti-epileptic effects, with a noted decrease in epileptic events during this sleep stage [22], [142]. The unique electroencephalographic patterns during REM sleep, resembling wakefulness, differentiate this state from others. These distinctive morphological patterns could potentially be associated with the observed anti-epileptic effects of REM sleep which is the rationale for this secondary hypothesis. If the null hypothesis is rejected, it suggests that REM sleep has unique characteristics, which could be significant in understanding the functional role of different sleep stages, particularly their impact on conditions such as epilepsy.

3.2.4 Normality Testing

In this section, we will discuss the process of normality testing for the data obtained from the single channel spike criteria Excel sheet. The relevant information columns are as follows: ascending slope, descending slope, spike asymmetry, peak amplitude, spikiness, height ascending turning point to peak, height descending turning point to peak, spike length, and spike area.

Additionally, the montages are indexed, and all the information per feature is analysed within a single montage. The purpose of assessing the distribution of the data is to correctly choose the proper statistical analysis, which is determined by the following five normality tests: Jarque-Bera, Anderson-Darling, Shapiro-Wilk, Lilliefors, and Kolmogorov-Smirnov. Each test provides valuable insights into the data distribution and whether it follows a normal distribution.

3.2.4.1 Normality Tests

While the sample size is relatively large overall, it may still be deemed small when considering the complexity of the study, which involves multiple features, montages, and sleep states. Consequently, only a few instances are available for analysis within some groups. Due to the unbalanced dataset, the normality assumption required many statistical tests to determine normality or lack thereof.

1. Jarque-Bera test: Tests for normality based on skewness and kurtosis using the *jbtest* MATLAB function.
2. Anderson-Darling test: Tests for normality by comparing the empirical distribution function of the sample to the cumulative distribution using the *adtest* MATLAB function. Its strength is that it handles large sample sizes and has a higher power than other normality tests.
3. Shapiro-Wilk test: Tests for normality by comparing the distribution of the samples to the normal distribution using the *swtest* function [186]. It is potent for small to medium-sized samples and can efficiently detect deviations from normality in the distribution's tails.
4. Lilliefors test: Compares the sample distribution to a normal distribution with the same mean and variance using the *lillietest* MATLAB function.
5. Kolmogorov-Smirnov test: Tests for normality by comparing the empirical distribution function to the cumulative distribution function of the normal distribution using the *kstest* MATLAB function.

Results from these tests were compiled in the Excel sheet "SpikeCriteria" (Supplement 1). The sheet details statistical values for each montage and feature combination, including the h-value (the test outcome), p-value (the probability of observing the data given the null hypothesis), and the test statistic (measuring data deviation from the expected normal distribution).

Furthermore, the sheet also provides descriptive statistics that can aid in quickly analyzing any abnormalities in the data. There is a total of 15 metrics that were measured over every montage + feature, which help describe the normality of the data (Supplement 2):

1. Montage + Feature: Combination of montage and feature being evaluated.
2. Significance/Normality Test: The specific test used for normality assessment.
3. h-value: A binary value indicating the rejection (1) or failure to reject (0) of the null hypothesis.
4. p-value: The significance level where a p-value is deemed significant at $p<0.05$

5. Statistic Value: Measures the extent of data deviation from the expected normal distribution.
6. Critical Values: Thresholds at which the test rejects the null hypothesis of normality.
7. Mean: The mean of overall data within the montage + feature combination.
8. Median: The median of overall data within the montage + feature combination.
9. Standard Deviation: The standard deviation of the overall data within the montage + feature combination.
10. 25th Percentile: The 25th percentile of the overall data within the montage + feature combination.
11. 75th Percentile: The 75th percentile of the overall data within the montage + feature combination.
12. Inter-Quartile Range (IQR): This is the output from the subtraction between the 75^{th} percentile and 25^{th} percentile values of the overall data within the montage + feature combination.
13. Skewness: Represents the asymmetry of the probability distribution. A positive value indicates a longer right tail, while a negative value indicates a longer left tail, and 0 represents symmetry.
14. Kurtosis: Describes the shape of the distribution in terms of the degree of peakedness or flatness. Leptokurtic (>3) indicates peaked with fat tails, platykurtic (<3) indicates flat with thin tails, and mesokurtic (=3) indicates a normal distribution.
15. Outliers (2*std): The number of outliers found at 2 times the standard deviation.
16. Outliers (1.5*IQR): The number of outliers found at 1.5 times the interquartile range.

3.2.4.2 Visual Representations to Distinguish Normality

In the process of exploring the data and evaluating its normality, visual representations play an instrumental role. These graphical displays unveil underlying patterns, highlight potential outliers, and offer an intuitive understanding of the data's distribution. Each type of visual representation, be it a histogram, an Empirical Cumulative Distribution Function (ECDF) plot, a boxplot, a Quantile-Quantile (QQ) plot, or a kernel density plot, provides unique insights into the data's structure and can be utilized in concert to construct a holistic understanding of our data's distribution, particularly concerning the assumption of normality. The following sections delve into the specificities of these graphical tools and their respective roles in data examination and normality assessment (Figure 9).

- Histogram (*histogram* MATLAB function): A histogram is employed due to its invaluable graphical representation to elucidate the frequency distribution across various data bins. This graphical illustration offers an intuitive insight into the data's asymmetry, indicating the distribution's tail directions. As such, it allows for an initial assessment of potential deviations from normality, providing a foundation for subsequent statistical analyses.

- Empirical Cumulative Distribution Function (ECDF) plot (*ecdf* MATLAB function): An ECDF plot is integral to exploratory data analysis. This graphical display represents the cumulative distribution of the dataset along the y-axis, which spans between 0 and 1. It conveys the proportion of data lying within a specified percentile of the plot. In the case of a normal distribution, the ECDF plot manifests as a smooth, centred S-shaped curve, reflecting that half of the data points fall within the 50^{th} percentile of the cumulative distribution.

- Boxplot (*boxplot* MATLAB function): The boxplot is a compelling tool in data visualization, allowing for a robust comparison of distribution differences between various sleep states. Beyond comparison, the boxplot provides crucial insights into the data's central tendency, spread, and skewness, which are critical for assessing non-normality. Asymmetry in data distribution is flagged by a boxplot's elongated sides of the median, while the whiskers establish the range of typical data values. Outliers are identifiable as data points beyond the whiskers, serving as potential indicators of extreme observations.

- Quantile-Quantile (QQ) plot (*qqplot* MATLAB function): A QQ plot is a sophisticated graphical instrument designed to evaluate whether a given dataset aligns with a specific theoretical distribution, typically the normal distribution characterized by a straight line. This tool contrasts the quantiles of the dataset against the quantiles of the expected theoretical distribution. The degree of conformity to a straight line is a measure of alignment with the theoretical distribution, with deviations from this line indicating disparity from the expected distribution.

- Kernel Density Plot (*ksdensity* MATLAB function): A kernel density plot, although functionally similar to a histogram, substitutes discrete bars with a continuous, smooth curve representative of the data's underlying probability density function. This unique visualization presents an intuitive understanding of the data's distribution shape, where a bell-shaped curve signifies a normal distribution. Consequently, a kernel density plot allows for a refined sense of the data's distribution, and is essential for subsequent inferential statistical processes.

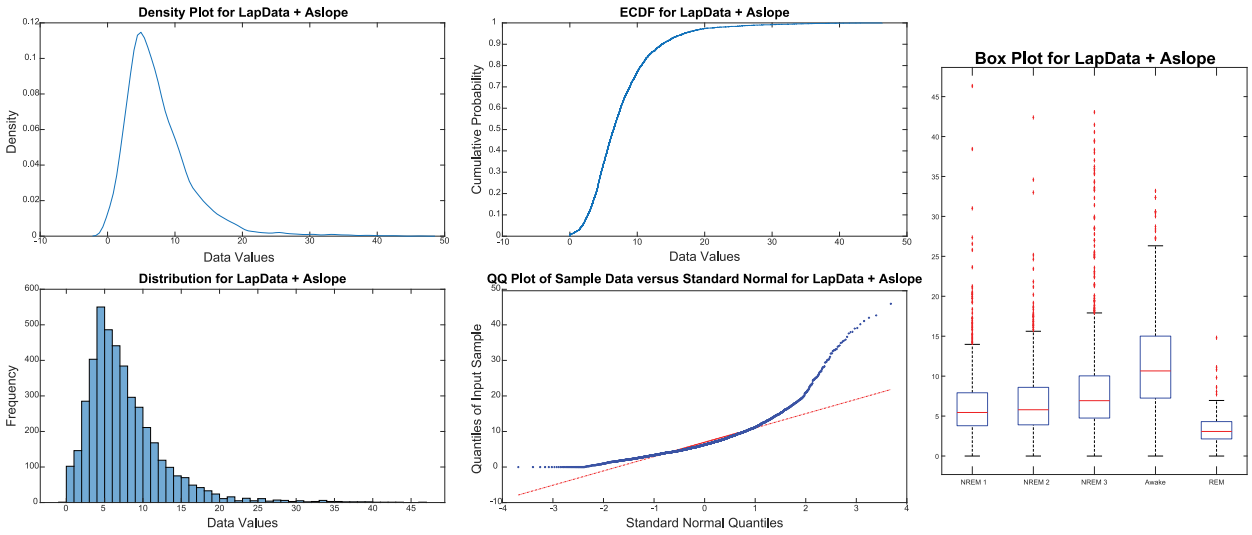


Figure 9: Comprehensive analysis of data non-normality for the ascending slope feature using the Laplacian montage. The Kernel Density Plot (top-left) and the Histogram (directly below) both reveal a left-skewed distribution, suggesting a higher frequency of lower values with a tail extending to the right, indicating deviations from a typical normal distribution. The ECDF Plot (middle-top) exhibits a sharp, almost immediate rise, deviating from the expected gradual S-curve of a normal distribution. This rapid ascent is further underscored in the QQ Plot (directly below), where data points significantly deviate from the standard normal line at both extremes. On the far right, the Boxplot delineates data spread across NREM stages and the awake state. Notably, several outliers are observed beyond the whiskers, and the median is positioned slightly lower than the IQR's centre, alluding to the data's pronounced left skewness and potential non-normal characteristics.

3.2.5 Significance Testing for Hypothesis 1: Kruskal-Wallis Test

Having established that our data does not follow a normal distribution, a non-parametric Kruskal-Wallis test was performed for each montage and morphological feature pairing. The Kruskal-Wallis test, which does not rely on the assumptions of normality or equal variance among groups, is optimal for this data analysis. This test aids in discerning significant differences among multiple groups (sleep states) by examining ranked data. The test results were subsequently compiled into an Excel sheet (Supplement 3), with each sheet corresponding to a unique combination of montage and morphological features.

In-depth scrutiny of the Kruskal-Wallis test results offers valuable insight into the data, mainly through analysing the mean ranks and standard error - two critical components of the test output. The mean ranks are significant as they illuminate the relative positions of the groups in terms of their ranked data. Notably, a group with a higher mean rank indicates that its data points generally possess values superior to those found in other groups.

The standard error, meanwhile, encapsulates the variability or uncertainty tied to the mean ranks. This measurement indicates how much the estimated mean ranks could vary should the Kruskal-Wallis test be

repeated with different samples from the same populations. A smaller standard error suggests a greater confidence in the estimated mean ranks, whereas a larger standard error connotes increased variability and, thus, less certainty in the results.

Establishing the threshold for the significance level below 0.05 facilitated the interpretation of the "Prob>Chi-sq" value present in the test's output as the p-value. This p-value corresponds to the likelihood of the observed results occurring purely by coincidence, under the premise that the null hypothesis is rejected. This comprehension and ensuing interpretation of the p-value prove pivotal in the endeavour to detect meaningful differences among the sleep-wake states.

3.2.6 Post Hoc Testing for Hypothesis 2: Dunn-Sidak Test and Bonferroni Correction

Upon completing the Kruskal-Wallis test, the key output is a comprehensive table featuring the computed results and group information. This output is the foundation of conducting multiple pairwise comparisons among the sleep state groups via the *multcompare* MATLAB function.

Dunn-Sidak test

The Dunn-Sidak test implemented following the Kruskal-Wallis analysis is crucial in investigating pairwise comparisons among sleep-state groups. The Dunn-Sidak method adjusts the significance level for each pairwise comparison to control the family-wise error rate, reducing the chances of Type I errors that may occur due to multiple comparisons. By computing the p-values for pairwise comparisons, the Dunn-Sidak test interprets the relative significance between each pair of sleep-state groups, contributing to a comprehensive understanding of the differences among these states.

The table resulting from Dunn-Sidak's test, contained in the "Comparisons" excel sheet, offers a systematic depiction of the test's findings (Supplement 3):

- The first column indicates the initial group involved in the comparison.
- The second column presents the second group partaking in the comparison.
- The third column delineates the lower bound limits of the 95% confidence intervals for the true mean difference.

- The fourth column describes the differential in median ranks between the two groups under comparison.
- The fifth column provides the upper bound limits of the 95% confidence intervals for the true mean difference.
- The sixth column presents the p-value for the hypothesis test that the corresponding difference in ranked means equals zero.

Bonferroni Correction

The Bonferroni correction is used to adjust the significance level for multiple comparisons. The correction is applied, as every analysis is computed over three separate montages (raw, referential, and Laplacian), ten pairwise sleep-wake state comparisons, and four groups of feature metrics:

- Group 1 (slope-related features) includes the ascending slope, descending slope, asymmetry, and spikiness with a correction factor of 0.05 / (4 * 3 * 10) = 4.166×10^{-4}.
- Group 2 (height/amplitude-related features) includes peak height, height at the ascending turning point to the peak, and height of the descending turning point to the peak with a correction factor of 0.05 / (3 * 3 * 10) = 5.55×10^{-4}.
- Group 3 (spike length): Correction factor of 0.05 / (3 * 10) = 1.66×10^{-3}.
- Group 4 (spike area): Correction factor of 0.05 / (3 * 10) = 1.66×10^{-3}.

This section has outlined a comprehensive methodological framework for analyzing epileptiform spikes. The GUI developed for this study is the foundation enabling such neuroscientific inquiry, allowing more precise and efficient data collection. The computational pipeline, which includes applying advanced statistical techniques, is a core component of the research strategy. This pipeline facilitates the extraction and processing of EEG data and enables the detailed analysis of spike morphology. The statistical methods employed, from normality testing to significance testing and post hoc analysis, have been carefully selected to suit the non-normal nature of our data. These methods allow us to rigorously test our hypotheses about the variations in spike morphology across sleep-wake states and provide a robust basis for the findings presented in the subsequent sections. As we move forward, the ensuing sections of this thesis builds upon this methodological groundwork. We describe the results of our analyses, discuss the potential factors of the spike's morphological features in their respective sleep-wake state, and discuss possible avenues for future research.

4 Results

Section 4 presents the empirical results of the extensive analysis of epileptiform spike features across various sleep-wake states and EEG montages (Laplacian, referential, and raw). This section is pivotal in demonstrating how the morphology of epileptiform spikes is influenced by the state of consciousness and the specific montage used in EEG analysis. The analysis is grounded in data from seven epilepsy patients, exploring nine distinct features of 4367 epileptiform spikes. These include the ascending and descending slopes, asymmetry, spikiness, peak height, normalized ascending and descending heights, duration, and spike area. The section meticulously details the variations in these features across NREM1, NREM2, NREM3, Awake, and REM states, as observed through different EEG montages. A key focus of this analysis is the differential characteristics of epileptic activity in REM sleep, which stands out in comparison to other states. Additionally, the section demonstrates how the choice of EEG montage influences the observed features of spikes, contributing to a more rounded understanding of epileptiform activity across sleep-wake states.

Seven epilepsy patients with various neurological conditions, underwent spike marking, including four females and three males, with an average age of 38.7 (SD = 18.1) over an average of 6.6 nights (SD = 2.4) (Table 1). Total number of spikes was NREM1 (n = 976 spikes), NREM2 (n = 1298 spikes), NREM3 (n = 1518 spikes), Awake (n = 511 spikes), and REM (n = 64 spikes), totalling 4367 spikes.

Table 1: Clinical characteristics of the participants. The table enumerates each patient, detailing the number of nights under EEG observation, total spikes recorded during various sleep stages (NREM1, NREM2, NREM3, Wake, and REM), age, and gender. Additionally, it provides information on the specific antiseizure drugs being administered (ltg: Lamotrigine, oxc: Oxcarbazepine, vpa: Valproic Acid (Valproate), lcm: Lacosamide, lev: Levetiracetam, cbz: Carbamazepine, per: Perampanel, clb: Clobazam, phb: Phenobarbital, pht: Phenytoin), including dosages (e.g. 200/200 signifies 200mg in the morning and another in the evening; 4qhs: 4 units quaque hora somni otherwise known as at bedtime), the classification of the epilepsy, the epileptic focus (BL-AQ, MF: Bilateral Anterior Quadrant, Mesial Frontal – Foci in both anterior quadrants and in the mesial (inner) frontal region, RPQ, MF: Right Posterior Quadrant, Mesial Frontal – Foci in the right posterior quadrant and also in the mesial frontal region, L TP: Left Temporal – Foci in the left temporal lobe, L Hemi: Left Hemisphere – Foci in left hemisphere of the brain, BL, Temp: Bilateral Temporal – Foci involving both temporal lobes), and the identified aetiology (Greig: Greig Cephalopolysyndactyly Syndrome - Genetic, NF1: Neurofibromatosis Type 1 - Genetic, Cavernoma: Cluster of abnormal blood vessels, Stroke: Loss of blood supply to brain leading to tissue damage, JME: Juvenile Myoclonic Epilepsy - Genetic), idiopathic or unknown for patient 5.

Patient	Nights	NREM1	NREM2	NREM3	Awake	REM	age	gender	antiseizure drug (asd)	Classification	Focus	Etiology
p1	7	104	472	982	94	7	19	f	ltg 200/200	Multifocal	BL-AQ, MF	Greig
p2	6	49	86	111	3	0	25	m	oxc 900/1200, vpa 500/750, lcm 150/150, lev 2000/2000	Multifocal	RPQ, MF	NF1
p3	5	2	10	2	0	0	54	m	ltg 150/150, CBZ 150/150/150/150	Focal	L TP	Cavernoma
p4	8	5	40	25	0	5	27	f	cbz 400/400, ltg 200/200, per 4qhs	Focal	L Hemi	Stroke
p5	7	773	601	369	39	52	62	f	ltg 75/75	Multifocal	BL Temp	
p6	7	27	25	20	373	0	27	f	clb 5/5, lev 750/750	Generalized		JME
p7	1	16	64	9	2	0	57	m	ltg 100/100/100, phb 45, pht 200, lev 1500/1500	Generalized		JME

The study applies Kruskal-Wallis tests, Dunn-Sidak multi-comparison analyses, and Bonferroni corrections to investigate differences in nine distinct features of epileptic spikes across sleep-wake states. These features, detailed in Figure 6, include ascending slope, descending slope, asymmetry, peak height, spikiness, height from the ascending turning point, height from the descending turning point, length, and area of the spike. The analyses cover three different montages—Laplacian, referential, and raw—with the overall median spikes represented in Figure 10. Tables 2-10 presents the Bonferroni-corrected p-values from multiple comparisons between each pair of sleep-wake states for each feature.

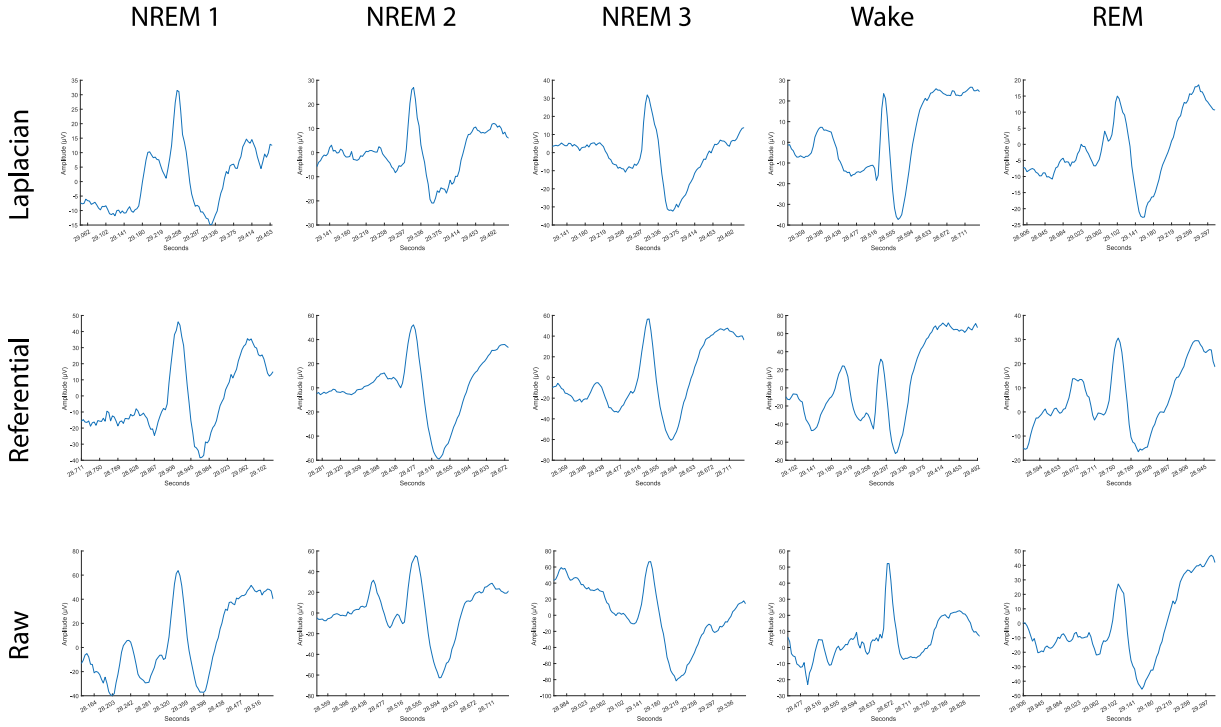


Figure 10: Illustration of the median epileptiform spikes identified through an aggregate analysis of nine morphological features. Initially, each feature was normalized to assess the percentage deviation from its median value across all spikes, effectively rendering a normalized difference. Subsequently, the sum of these normalized differences was computed for each spike across all nine features, facilitating the identification of the spike with the minimal cumulative distance from the median values of all features—hence, representing the most median spike relative to the medians of the nine features. The depicted median spikes are segregated by sleep-wake states—NREM1, NREM2, NREM3, Wake, and REM—and by montage types: Laplacian, Referential, and Raw

4.1 Ascending Slope (microvolts/sec)

The slope, characterized by positive values, signifies an upward trend towards the peak as time progresses. The magnitude of this slope serves as an indicator of steepness, where a larger value denotes a steeper incline, and a

smaller value corresponds to a more gradual, or shallower, ascent. Figure 11 highlights the largest differences in ascending slope medians, specifically between the two most divergent sleep-wake states.

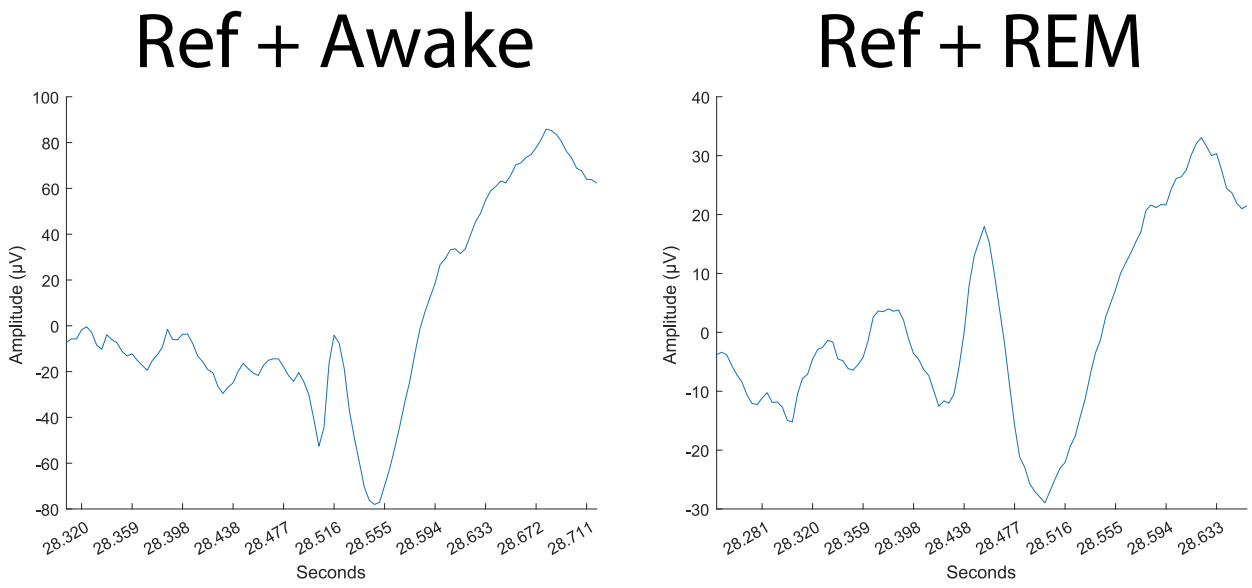


Figure 11: Visualization showcasing the substantial contrast in the ascending slope feature. The referential montage has the greatest depiction of this difference exhibiting the extremely steep ascending slope during wakefulness versus the much more gradual slope illustrated during REM.

- **Laplacian Montage:**
    - The Kruskal-Wallis test revealed a significant difference in the ascending slope values across the sleep-wake states (p = 4.63E-104). The median and standard deviations for the ascending slope values are as follows: NREM 1 (M = 5.45, SD = 4.20), NREM 2 (M = 5.80, SD = 4.02), NREM 3 (M = 6.93, SD = 5.63), Awake (M = 10.66, SD = 6.07), REM (M = 3.08, SD = 2.72) (Figure 12).
    - Correction for Multiple comparisons revealed that all comparisons were significant except for the comparison between NREM1 and NREM2 (Table 2).
- **Referential Montage:**
    - The Kruskal-Wallis test revealed a significant difference in the ascending slope values across the sleep-wake states (p = 1.83E-125). The median and standard deviations for the ascending slope values are as follows: NREM 1 (M = 8.17, SD = 5.45), NREM 2 (M = 8.74, SD = 5.67), NREM 3 (M = 10.52, SD = 8.75), Awake (M = 17.34, SD = 10.44), REM (M = 4.89, SD = 3.50) (Figure 12).

- Correction for Multiple comparisons revealed that all comparisons were significant; however, the comparison between NREM1 and NREM2 was no longer significant after Bonferroni correction (Table 2).

- **Raw Montage:**

  - The Kruskal-Wallis test revealed a significant difference in the ascending slope values across the sleep-wake states (p = 2.74E-63). The median and standard deviations for the ascending slope values are as follows: NREM 1 (M = 9.65, SD = 5.76), NREM 2 (M = 9.84, SD = 6.11), NREM 3 (M = 11.64, SD = 8.89), Awake (M = 14.74, SD = 9.10), REM (M = 5.65, SD = 2.92) (Figure 12).

  - Correction for Multiple comparisons revealed that all comparisons were significant except for the comparison between NREM1 and NREM2 (Table 2).

Table 2: Multiple comparisons across the Laplacian, Referential, and Raw montages are presented, with p-values for each grouping between all sleep-wake states. Colour-coding is employed to indicate the level of significance: green denotes significant, yellow signifies not significant after Bonferroni correction, and red indicates not significant.

Ascending Slpoe		*Laplacian*	*Referential*	*Raw*
Group1	**Group2**	**p-value**	**p-value**	**p-value**
NREM 1	*NREM 2*	0.35908784	0.00995276	0.54252082
NREM 1	*NREM 3*	<1.00E-05	<1.00E-05	<1.00E-05
NREM 1	*Awake*	<1.00E-05	<1.00E-05	<1.00E-05
NREM 1	*REM*	<1.00E-05	<1.00E-05	<1.00E-05
NREM 2	*NREM 3*	<1.00E-05	<1.00E-05	<1.00E-05
NREM 2	*Awake*	<1.00E-05	<1.00E-05	<1.00E-05
NREM 2	*REM*	<1.00E-05	<1.00E-05	<1.00E-05
NREM 3	*Awake*	<1.00E-05	<1.00E-05	<1.00E-05
NREM 3	*REM*	<1.00E-05	<1.00E-05	<1.00E-05
Awake	*REM*	<1.00E-05	<1.00E-05	<1.00E-05

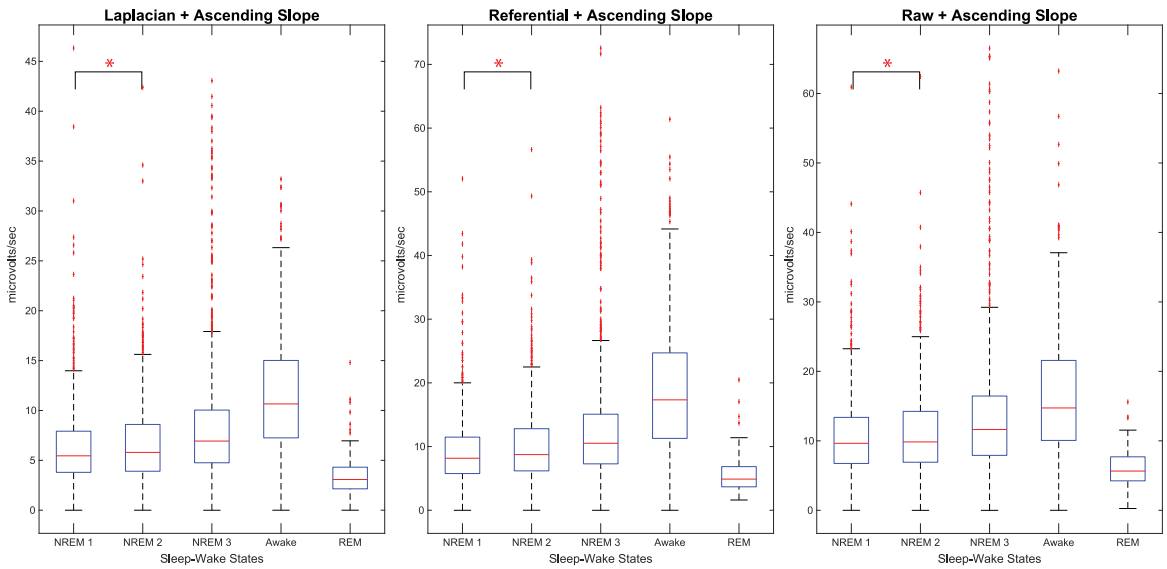


Figure 12: Box plots showing the distribution of ascending slopes between sleep-wake states over the three montages. Slopes are measured in microvolts. Outliers are indicated with red +s and non-significant pairs are represented by red asterisks.

4.2 Descending Slope (microvolts/sec)

The slope, characterized as negative, signifies a downward trend towards the turning point as time progresses. The magnitude of the slope further describes the steepness: a larger value corresponds to a steeper slope, and a smaller value represents a shallower slope. Figure 13 highlights the largest differences in descending slope medians, specifically between the two most divergent sleep-wake states.

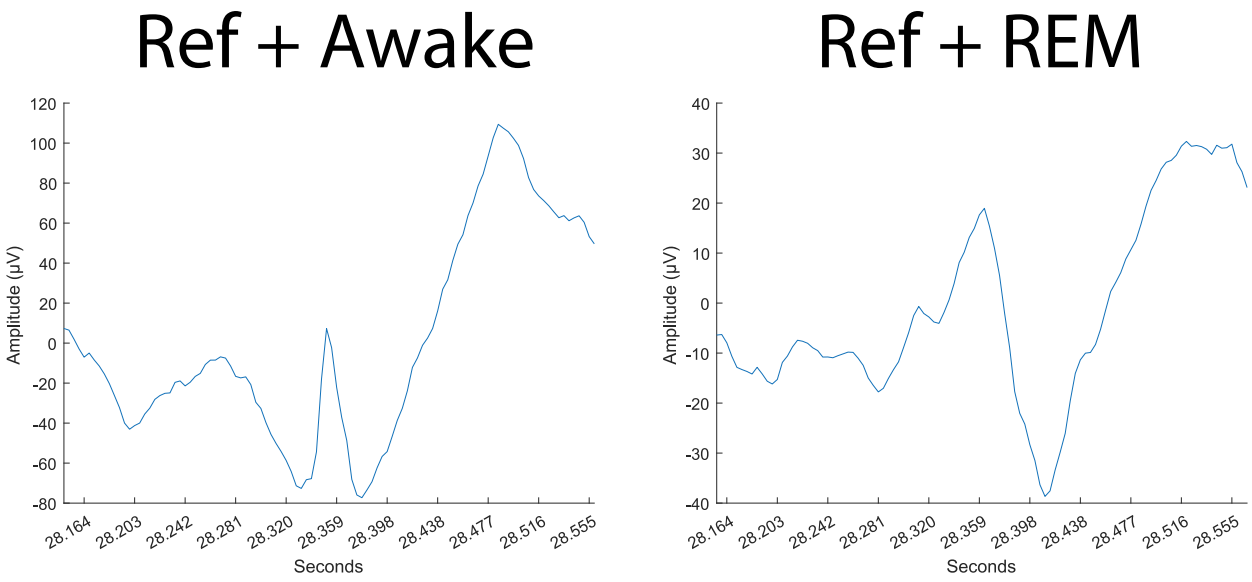


Figure 13: Visualization showcasing the substantial contrast in the descending slope feature. The referential montage has the greatest depiction of this difference exhibiting the extremely steep descending slope during wakefulness versus the much more gradual slope illustrated in REM.

- **Laplacian Montage:**
    - The Kruskal-Wallis test revealed a significant difference in the descending slope values across the sleep-wake states (p = 5.16E-116). The median and standard deviations for the descending slope values are as follows: NREM1 (M = -5.01, SD = 3.54), NREM2 (M = -4.97, SD = 2.83), NREM3 (M = -5.81, SD = 3.09), Awake (M = -8.45, SD = 3.64), REM (M = -3.00, SD = 1.32) (Figure 14).
    - Correction for Multiple comparisons revealed that all comparisons were significant except for the comparison between NREM1 and NREM2 (Table 3).
- **Referential Montage:**
    - The Kruskal-Wallis test revealed a significant difference in the descending slope values across the sleep-wake states (p = 4.29E-122). The median and standard deviations for the descending slope values are as follows: NREM1 (M = -7.88, SD = 3.73), NREM2 (M = -8.55, SD = 3.79), NREM3 (M = -9.93, SD = 4.54), Awake (M = -13.21, SD = 5.46), REM (M = -5.09, SD = 1.96) (Figure 14).
    - Correction for Multiple comparisons revealed that all comparisons were significant; however, the comparison between NREM1 and NREM2 was no longer significant after Bonferroni correction (Table 3).

- **Raw Montage:**
    - The Kruskal-Wallis test revealed a significant difference in the descending slope values across the sleep-wake states (p = 6.53E-36). The median and standard deviations for the descending slope values are as follows: NREM1 (M = -9.22, SD = 4.35), NREM2 (M = -9.64, SD = 4.46), NREM3 (M = -10.99, SD = 5.13), Awake (M = -9.73, SD = 7.69), REM (M = -6.43, SD = 2.31) (Figure 14).
    - Correction for Multiple comparisons revealed significant differences in most comparisons, with the exceptions of the comparisons between NREM1 and NREM2, NREM1 and Awake, and NREM2 and Awake (Table 3).

Table 3: Multiple comparisons across the Laplacian, Referential, and Raw montages are presented, with p-values for each grouping between all sleep-wake states. Colour-coding is employed to indicate the level of significance: green denotes significant, yellow signifies not significant after Bonferroni correction, and red indicates not significant.

Descending Slope		*Laplacian*	*Referential*	*Raw*
Group1	**Group2**	**p-value**	**p-value**	**p-value**
NREM 1	*NREM 2*	0.9955059	0.00183332	0.99843455
NREM 1	*NREM 3*	<1.00E-05	<1.00E-05	<1.00E-05
NREM 1	*Awake*	<1.00E-05	<1.00E-05	0.99738624
NREM 1	*REM*	<1.00E-05	<1.00E-05	<1.00E-05
NREM 2	*NREM 3*	<1.00E-05	<1.00E-05	<1.00E-05
NREM 2	*Awake*	<1.00E-05	<1.00E-05	0.99999998
NREM 2	*REM*	<1.00E-05	<1.00E-05	<1.00E-05
NREM 3	*Awake*	<1.00E-05	<1.00E-05	<1.00E-05
NREM 3	*REM*	<1.00E-05	<1.00E-05	<1.00E-05
Awake	*REM*	<1.00E-05	<1.00E-05	<1.00E-05

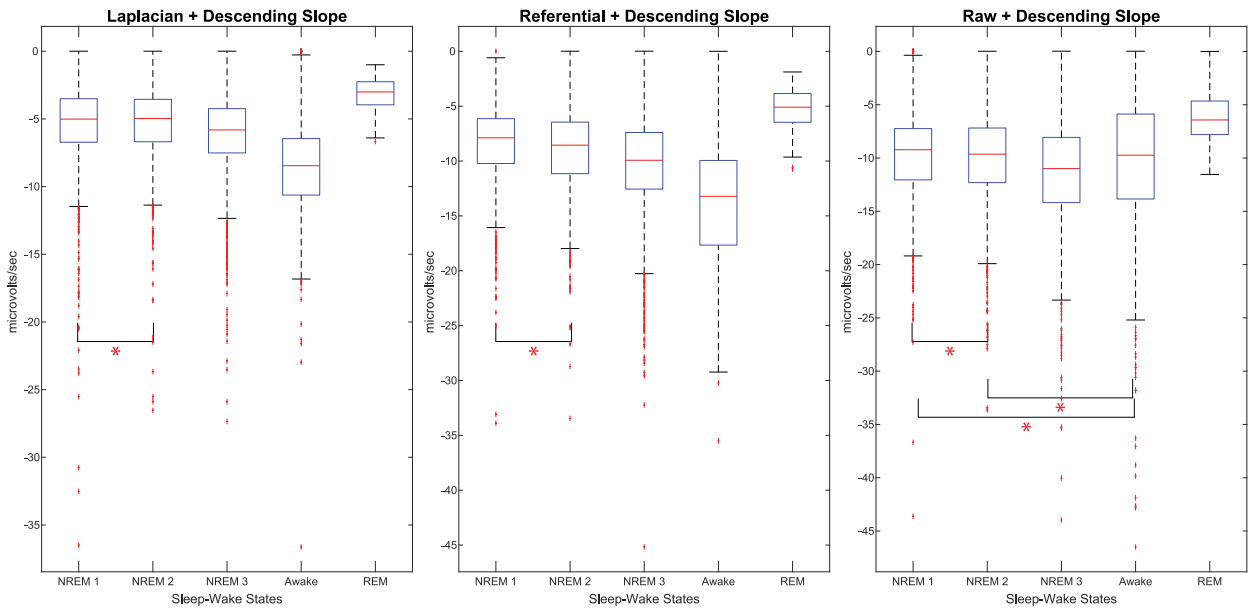


Figure 14: Box plots showing the distribution of descending slopes between sleep-wake states over the three montages. Slopes are measured in microvolts. Outliers are indicated with red +s and non-significant pairs are represented by red asterisks.

4.3 Asymmetry (unitless ratio of Ascending slope/Descending slope)

Asymmetry is defined by the ratio of the absolute values of the ascending over descending slopes. This ratio describes the difference in steepness between the two slopes: a value greater than 1 indicates that the ascending slope is steeper, and a value less than 1 denotes that the descending slope is steeper. Figure 15 highlights the largest differences in asymmetry medians, specifically between the two most divergent sleep-wake states.

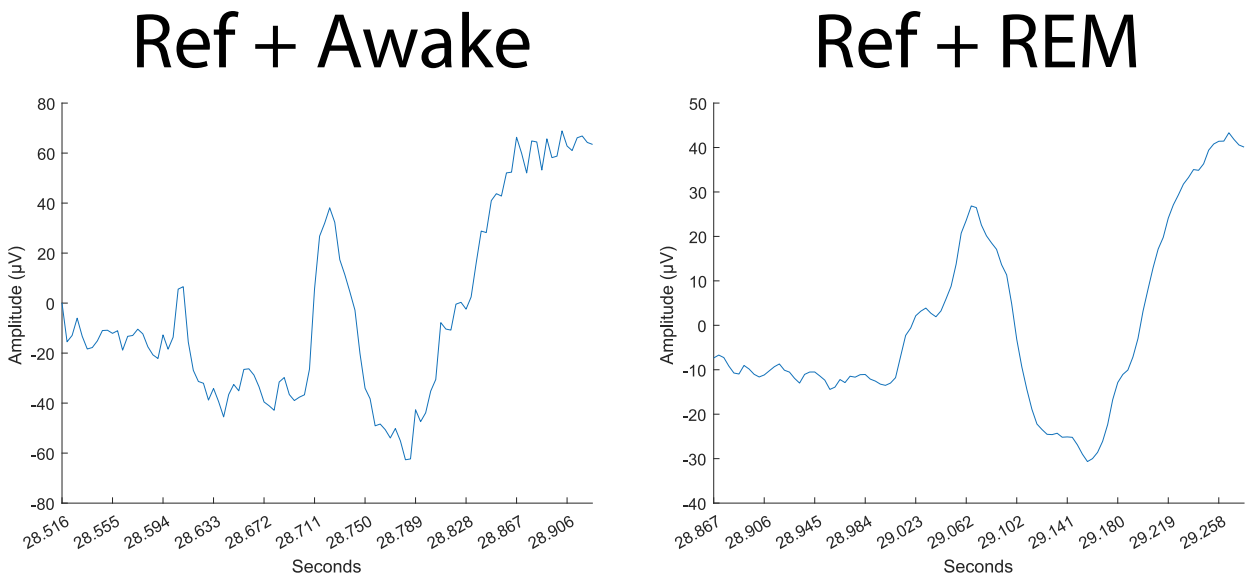


Figure 15: Visualization showcasing the substantial contrast in the asymmetry feature. The referential montage has the greatest depiction of this difference exhibiting the steeper ascending versus descending slope during wakefulness versus the more symmetric slopes illustrated in REM.

- **Laplacian Montage:**
    - The Kruskal-Wallis test revealed a significant difference in the asymmetry values across the sleep-wake states (p = 6.01E-9). The median and standard deviations for the asymmetry values are as follows: NREM1 (M = 1.15, SD = 667.39), NREM2 (M = 1.21, SD = 1504.47), NREM3 (M = 1.25, SD = 167.75), Awake (M = 1.28, SD = 1124.75), REM (M = 1.09, SD = 0.63) (Figure 16).
    - Correction for Multiple comparisons revealed significant differences only between NREM1 and NREM3 and NREM1 and Awake (Table 4).
- **Referential Montage:**
    - The Kruskal-Wallis test revealed a significant difference in the asymmetry values across the sleep-wake states (p = 9.17E-13). The median and standard deviations for the asymmetry values are as follows: NREM1 (M = 1.06, SD = 23.45), NREM2 (M = 1.08, SD = 358.28), NREM3 (M = 1.12, SD = 155.37), Awake (M = 1.33, SD = 1162.21), REM (M = 1.01, SD = 0.52) (Figure 16).
    - Correction for Multiple comparisons revealed significant differences in most comparisons between Awake and all other states except REM when corrected with Bonferroni (Table 4).

- **Raw Montage:**
    - The Kruskal-Wallis test revealed a significant difference in the asymmetry values across the sleep-wake states (p = 8.74E-36). The median and standard deviations for the asymmetry values are as follows: NREM1 (M = 1.03, SD = 334.09), NREM2 (M = 1.09, SD = 633.88), NREM3 (M = 1.10, SD = 633.88), Awake (M = 1.63, SD = 5950.02), REM (M = 0.96, SD = 75.93) (Figure 16).
    - Correction for Multiple comparisons revealed significance only between Awake to all other states (Table 4).

Table 4: Multiple comparisons across the Laplacian, Referential, and Raw montages are presented, with p-values for each grouping between all sleep-wake states. Colour-coding is employed to indicate the level of significance: green denotes significant, yellow signifies not significant after Bonferroni correction, and red indicates not significant.

Asymmetry		*Laplacian*	*Referential*	*Raw*
Group1	**Group2**	**p-value**	**p-value**	**p-value**
NREM 1	*NREM 2*	0.00393712	0.78085995	0.13113946
NREM 1	*NREM 3*	<1.00E-05	0.00996258	0.13839524
NREM 1	*Awake*	<1.00E-05	<1.00E-05	<1.00E-05
NREM 1	*REM*	0.99999567	0.999969	0.99995302
NREM 2	*NREM 3*	0.17180116	0.43078528	1
NREM 2	*Awake*	0.15541795	<1.00E-05	<1.00E-05
NREM 2	*REM*	0.7262511	0.98477644	0.88488481
NREM 3	*Awake*	0.99859121	<1.00E-05	<1.00E-05
NREM 3	*REM*	0.21899751	0.74545613	0.89815569
Awake	*REM*	0.13844243	0.00444988	<1.00E-05

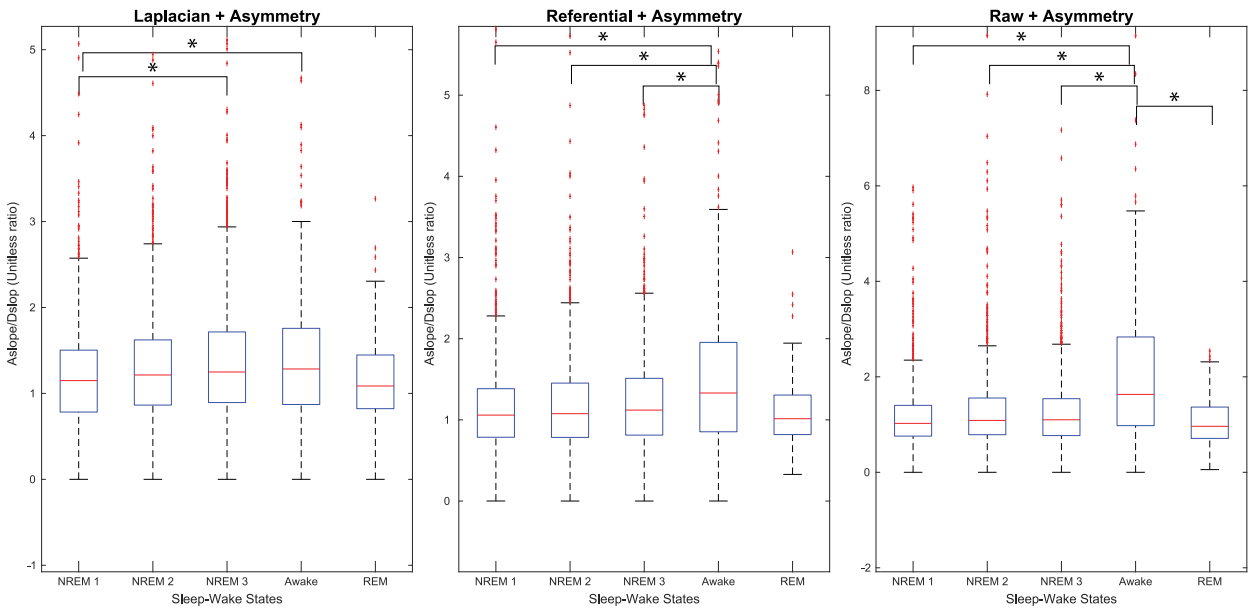


Figure 16: Box plots showing the distribution of asymmetry between sleep-wake states over the three montages. Asymmetry is a unitless ratio between the ascending slope versus the descending slope. Outliers are indicated with red +s and significant pairs are represented by black asterisks.

4.4 Spikiness/Pointiness (degrees)

The angle between the two slopes serves as a descriptive metric for the pointiness of the spike. Specifically, a higher angle corresponds to a blunter spike, while a smaller angle denotes a more pointed spike. Figure 17 highlights the largest differences in spikiness medians, specifically between the two most divergent sleep-wake states.

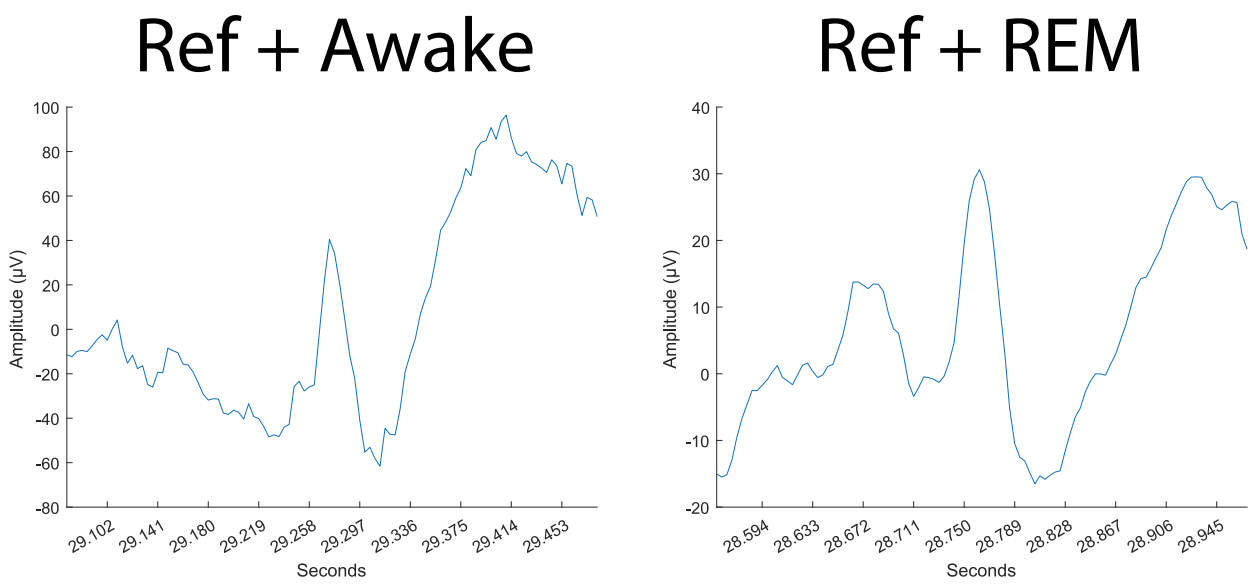


Figure 17: Visualization showcasing the substantial contrast in the spikiness feature. The referential montage has the greatest depiction of this difference exhibiting a much pointier spike during wakefulness versus the blunter more rounded spike during REM.

- **Laplacian Montage:**
    - The Kruskal-Wallis test revealed a significant difference in the spikiness values across the sleep-wake states (p = 2.55E-118). The median and standard deviations for the spikiness values are as follows: NREM1 (M = 22.32, SD = 14.63), NREM2 (M = 22.04, SD = 15.50), NREM3 (M = 18.47, SD = 13.22), Awake (M = 12.76, SD = 12.82), REM (M = 39.38, SD = 15.22) (Figure 18).
    - Correction for Multiple comparisons revealed that all comparisons were significant except for the comparison between NREM1 and NREM2 (Table 5).
- **Referential Montage:**
    - The Kruskal-Wallis test revealed a significant difference in the spikiness values across the sleep-wake states (p = 2.28E-134). The median and standard deviations for the spikiness values are as follows: NREM1 (M = 14.52, SD = 10.33), NREM2 (M = 13.47, SD = 10.89), NREM3 (M = 11.66, SD = 10.00), Awake (M = 7.97, SD = 11.43), REM (M = 24.12, SD = 8.31) (Figure 18).
    - Correction for Multiple comparisons revealed significant differences in all comparisons; however, after applying the Bonferroni correction, the significance between NREM1 and NREM2 was no longer observed (Table 5).

- **Raw Montage:**
    - The Kruskal-Wallis test revealed a significant difference in the spikiness values across the sleep-wake states (p = 7.71E-38). The median and standard deviations for the spikiness values are as follows: NREM1 (M = 12.37, SD = 10.68), NREM2 (M = 12.22, SD = 13.29), NREM3 (M = 10.49, SD = 12.19), Awake (M = 10.49, SD = 26.36), REM (M = 19.65, SD = 12.46) (Figure 18).
    - Correction for Multiple comparisons revealed significance in most comparisons, with the exceptions of NREM1 with NREM2, NREM2 with Awake as well between NREM3 and Awake (Table 5).

Table 5: Multiple comparisons across the Laplacian, Referential, and Raw montages are presented, with p-values for each grouping between all sleep-wake states. Colour-coding is employed to indicate the level of significance: green denotes significant, yellow signifies not significant after Bonferroni correction, and red indicates not significant.

Spikiness		*Laplacian*	*Referential*	*Raw*
Group1	**Group2**	**p-value**	**p-value**	**p-value**
NREM 1	*NREM 2*	0.99883271	0.00290642	0.96389826
NREM 1	*NREM 3*	<1.00E-05	<1.00E-05	<1.00E-05
NREM 1	*Awake*	<1.00E-05	<1.00E-05	<1.00E-05
NREM 1	*REM*	<1.00E-05	<1.00E-05	<1.00E-05
NREM 2	*NREM 3*	<1.00E-05	<1.00E-05	<1.00E-05
NREM 2	*Awake*	<1.00E-05	<1.00E-05	0.00045931
NREM 2	*REM*	<1.00E-05	<1.00E-05	<1.00E-05
NREM 3	*Awake*	<1.00E-05	<1.00E-05	0.32330504
NREM 3	*REM*	<1.00E-05	<1.00E-05	<1.00E-05
Awake	*REM*	<1.00E-05	<1.00E-05	<1.00E-05

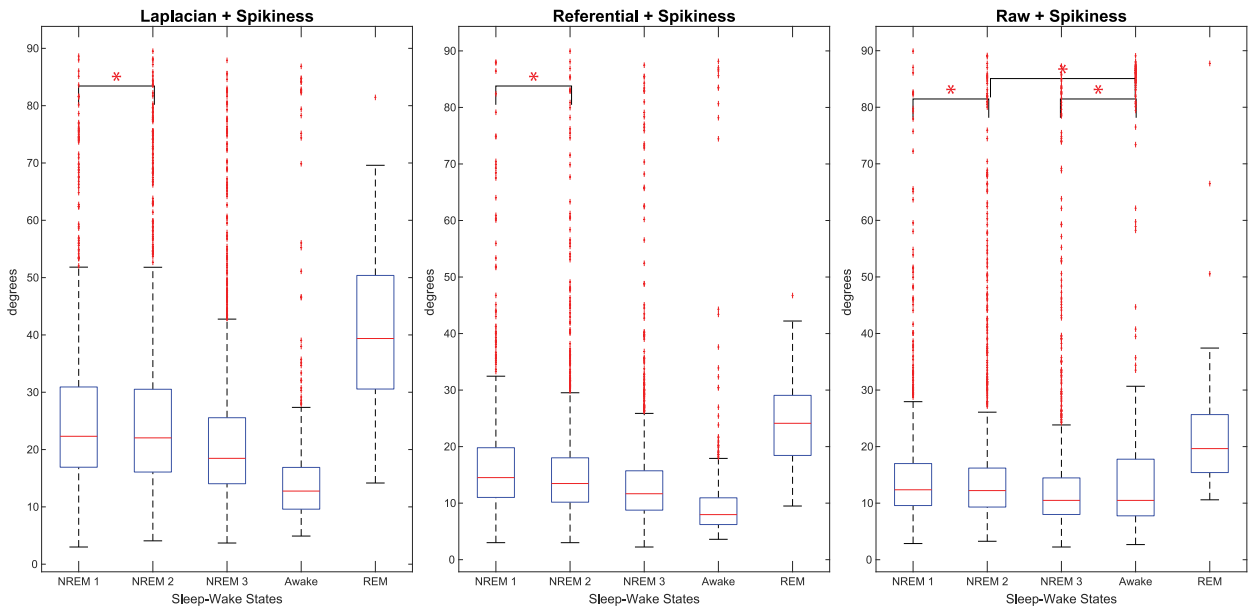


Figure 18: Box plots showing the distribution of spikiness between sleep-wake states over the three montages. Spikiness is measured in degrees. Outliers are indicated with red +s and non-significant pairs are represented by red asterisks.

4.5 Peak Height (microvolts)

The peak value, assessed without reference to a baseline, represents a specific but simple metric of the spike. While it may not be the most intrinsic feature, it still provides insight into the variability in neural excitability at the specific spike location. Figure 19 highlights the largest differences in peak height medians, specifically between the two most divergent sleep-wake states.

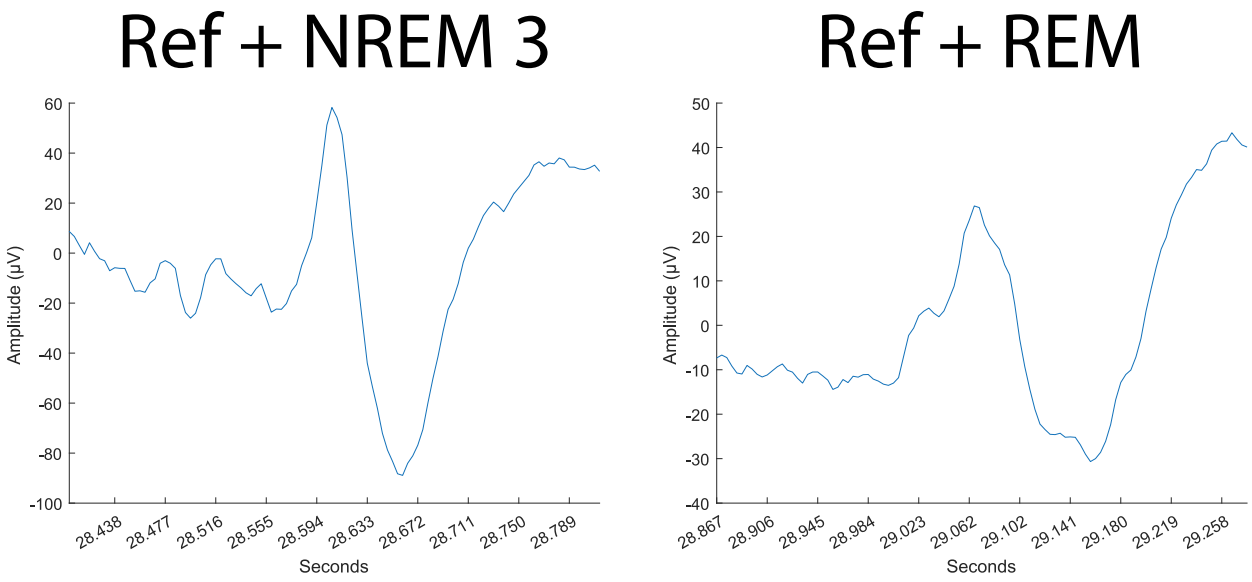


Figure 19: Visualization showcasing the substantial contrast in the peak height feature. The referential montage has the greatest depiction of this difference exhibiting the largest amplitude without baseline during NREM3 versus the lowest amplitude found during REM.

- **Laplacian Montage:**
    - The Kruskal-Wallis test revealed a significant difference in the peak height values across the sleep-wake states (p = 2.00E-55). The median and standard deviations for the peak height values are as follows: NREM1 (M = 30.66, SD = 16.91), NREM2 (M = 32.25, SD = 17.94), NREM3 (M = 35.27, SD = 19.40), Awake (M = 23.52, SD = 17.46), REM (M = 15.82, SD = 10.04).
    - Correction for Multiple comparisons revealed that all comparisons were significant except for the comparison between NREM1 and NREM2 (Table 6).
- **Referential Montage:**
    - The Kruskal-Wallis test revealed a significant difference in the peak height values across the sleep-wake states (p = 6.41E-87). The median and standard deviations for the peak height values are as follows: NREM1 (M = 50.89, SD = 27.48), NREM2 (M = 54.26, SD = 29.29), NREM3 (M = 58.26, SD = 33.99), Awake (M = 30.73, SD = 33.27), REM (M = 26.72, SD = 15.21).
    - Correction for Multiple comparisons revealed significant differences in most comparisons, with the exceptions of the comparisons between NREM1 and NREM2 and Awake and REM (Table 6).

- **Raw Montage:**
    - The Kruskal-Wallis test revealed a significant difference in the peak height values across the sleep-wake states (p = 1.81E-22). The median and standard deviations for the peak height values are as follows: NREM1 (M = 62.06, SD = 34.72), NREM2 (M = 63.51, SD = 35.64), NREM3 (M = 66.74, SD = 41.89), Awake (M = 52.18, SD = 45.53), REM (M = 34.46, SD = 20.39).
    - Correction for Multiple comparisons revealed significance in the majority of comparisons, with the exceptions of all NREM1 comparisons except with REM and between NREM2 and NREM3 (Table 6).

Table 6: Multiple comparisons across the Laplacian, Referential, and Raw montages are presented, with p-values for each grouping between all sleep-wake states. Colour-coding is employed to indicate the level of significance: green denotes significant, yellow signifies not significant after Bonferroni correction, and red indicates not significant.

Peak		*Laplacian*	*Referential*	*Raw*
Group1	**Group2**	**p-value**	**p-value**	**p-value**
NREM 1	*NREM 2*	0.98060664	0.36621822	0.99994829
NREM 1	*NREM 3*	<1.00E-05	<1.00E-05	0.02385795
NREM 1	*Awake*	<1.00E-05	<1.00E-05	0.00213186
NREM 1	*REM*	<1.00E-05	<1.00E-05	<1.00E-05
NREM 2	*NREM 3*	<1.00E-05	0.00017746	0.05822384
NREM 2	*Awake*	<1.00E-05	<1.00E-05	0.00019971
NREM 2	*REM*	<1.00E-05	<1.00E-05	<1.00E-05
NREM 3	*Awake*	<1.00E-05	<1.00E-05	<1.00E-05
NREM 3	*REM*	<1.00E-05	<1.00E-05	<1.00E-05
Awake	*REM*	<1.00E-05	0.06596909	<1.00E-05

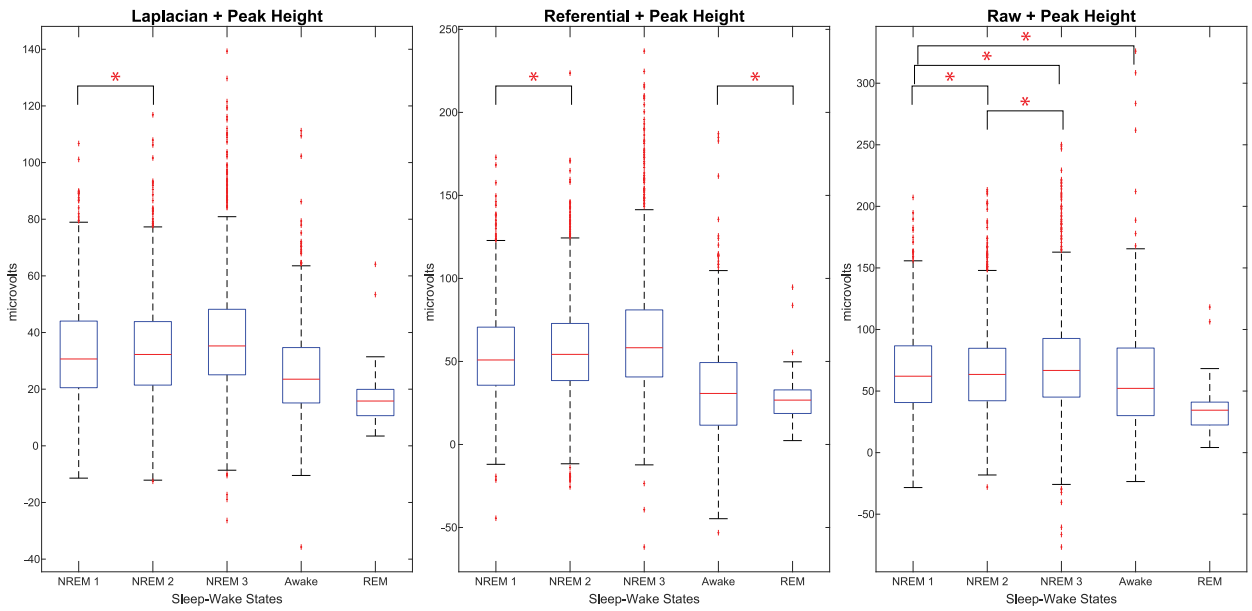


Figure 20: Box plots showing the distribution of peak height between sleep-wake states over the three montages. Peak height is measured in microvolts. Outliers are indicated with red +s and non-significant pairs are represented by red asterisks.

4.6 Normalized Ascending Height (microvolts)

This feature evaluates the height between the ascending turning point and the peak of the spike, specifically quantifying the vertical distance from where the slope begins its ascent to its zenith. By comparing this measurement to a baseline, it effectively normalizes all spikes, offering a standardized approach to assess the peak height. Figure 21 highlights the largest differences in normalized ascending height medians, specifically between the two most divergent sleep-wake states.

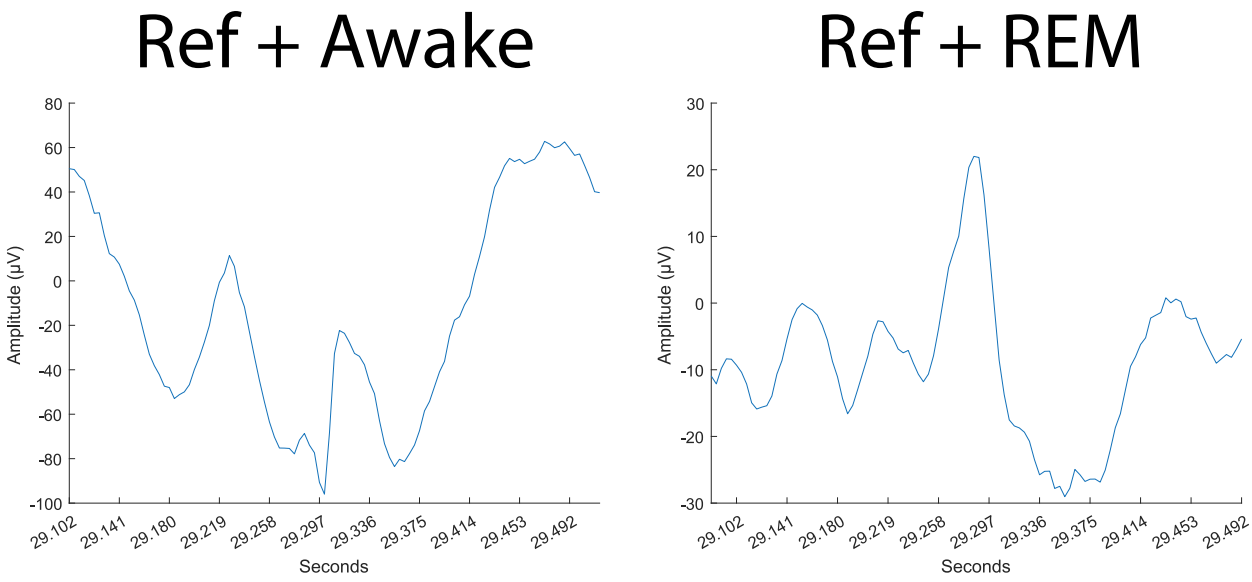


Figure 21: Visualization showcasing the substantial contrast in the normalized ascending height feature. The referential montage has the greatest depiction of this difference exhibiting the largest normalized amplitude during awake versus the lowest normalized amplitude observed during REM.

- **Laplacian Montage:**
    - The Kruskal-Wallis test revealed a significant difference in the normalized ascending height values across the sleep-wake states (p = 4.34E-39). The median and standard deviations for the normalized ascending height values are as follows: NREM1 (M = 33.56, SD = 21.50), NREM2 (M = 35.64, SD = 22.59), NREM3 (M = 42.00, SD = 27.50), Awake (M = 41.89, SD = 24.10), REM (M = 19.12, SD = 12.07) (Figure 22).
    - Correction for Multiple comparisons revealed significance in most comparisons, with the exceptions of NREM1 with NREM2 and NREM3 with Awake (Table 7).
- **Referential Montage:**
    - The Kruskal-Wallis test revealed a significant difference in the normalized ascending height values across the sleep-wake states (p = 3.41E-31). The median and standard deviations for the normalized ascending height values are as follows: NREM1 (M = 61.30, SD = 35.13), NREM2 (M = 61.98, SD = 36.43), NREM3 (M = 68.78, SD = 46.36), Awake (M = 73.64, SD = 40.49), REM (M = 33.60, SD = 18.01) (Figure 22).
    - Correction for Multiple comparisons revealed significance in most comparisons, with the exceptions of NREM1 with NREM2 and NREM3 with Awake (Table 7).

- **Raw Montage:**
    - The Kruskal-Wallis test revealed a significant difference in the normalized ascending height values across the sleep-wake states (p = 6.17E-31). The median and standard deviations for the normalized ascending height values are as follows: NREM1 (M = 71.54, SD = 43.07), NREM2 (M = 68.63, SD = 45.21), NREM3 (M = 80.54, SD = 54.27), Awake (M = 57.78, SD = 45.86), REM (M = 37.56, SD = 24.63) (Figure 22).
    - Correction for Multiple comparisons revealed significance in most comparisons, with the exception between NREM1 and NREM2 (Table 7).

Table 7: Multiple comparisons across the Laplacian, Referential, and Raw montages are presented, with p-values for each grouping between all sleep-wake states. Colour-coding is employed to indicate the level of significance: green denotes significant, yellow signifies not significant after Bonferroni correction, and red indicates not significant.

Ascending Height		*Laplacian*	*Referential*	*Raw*
Group1	**Group2**	**p-value**	**p-value**	**p-value**
NREM 1	*NREM 2*	0.60746409	0.9859867	1
NREM 1	*NREM 3*	<1.00E-05	<1.00E-05	<1.00E-05
NREM 1	*Awake*	<1.00E-05	<1.00E-05	0.00028422
NREM 1	*REM*	<1.00E-05	<1.00E-05	<1.00E-05
NREM 2	*NREM 3*	<1.00E-05	<1.00E-05	<1.00E-05
NREM 2	*Awake*	<1.00E-05	<1.00E-05	0.00022013
NREM 2	*REM*	<1.00E-05	<1.00E-05	<1.00E-05
NREM 3	*Awake*	0.97248672	0.75932842	<1.00E-05
NREM 3	*REM*	<1.00E-05	<1.00E-05	<1.00E-05
Awake	*REM*	<1.00E-05	<1.00E-05	<1.00E-05

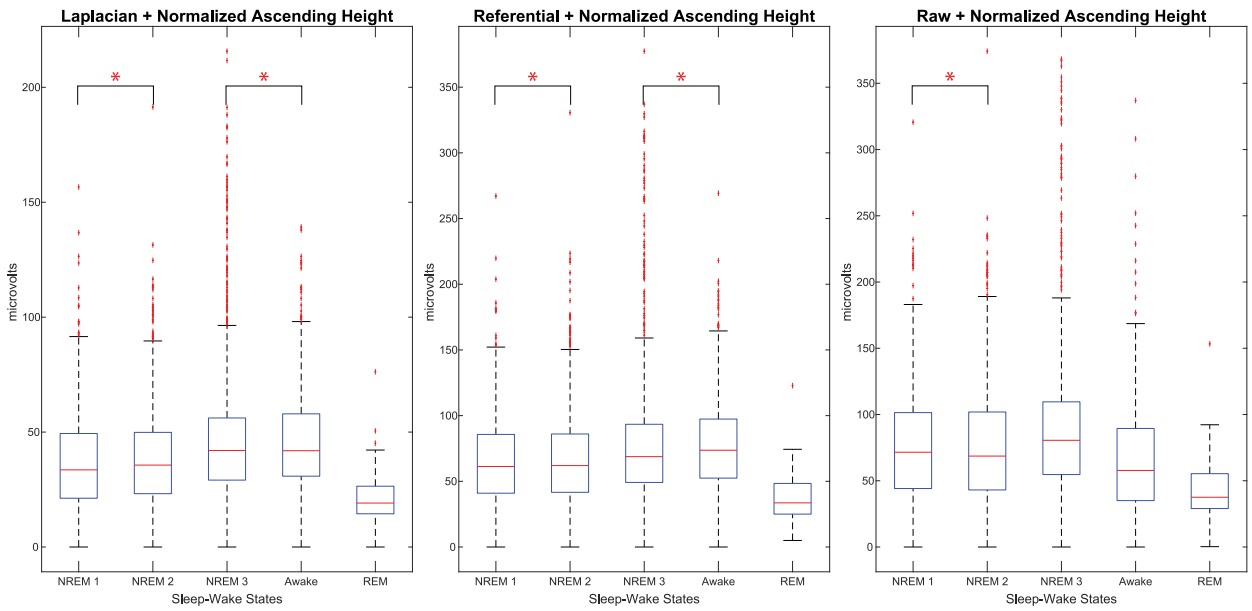


Figure 22: Box plots showing the distribution of normalized ascending heights between sleep-wake states over the three montages. The height is measured in microvolts. Outliers are indicated with red +s and non-significant pairs are represented by red asterisks.

4.7 Normalized Descending Height (microvolts)

This feature evaluates the height between the descending turning point and the peak of the spike, specifically quantifying the vertical distance from where the slope ends its descent to its peak. By comparing this measurement to a baseline, it effectively normalizes all spikes, offering another standardized approach to assess the peak height. Figure 23 highlights the largest differences in normalized descending height medians, specifically between the two most divergent sleep-wake states.

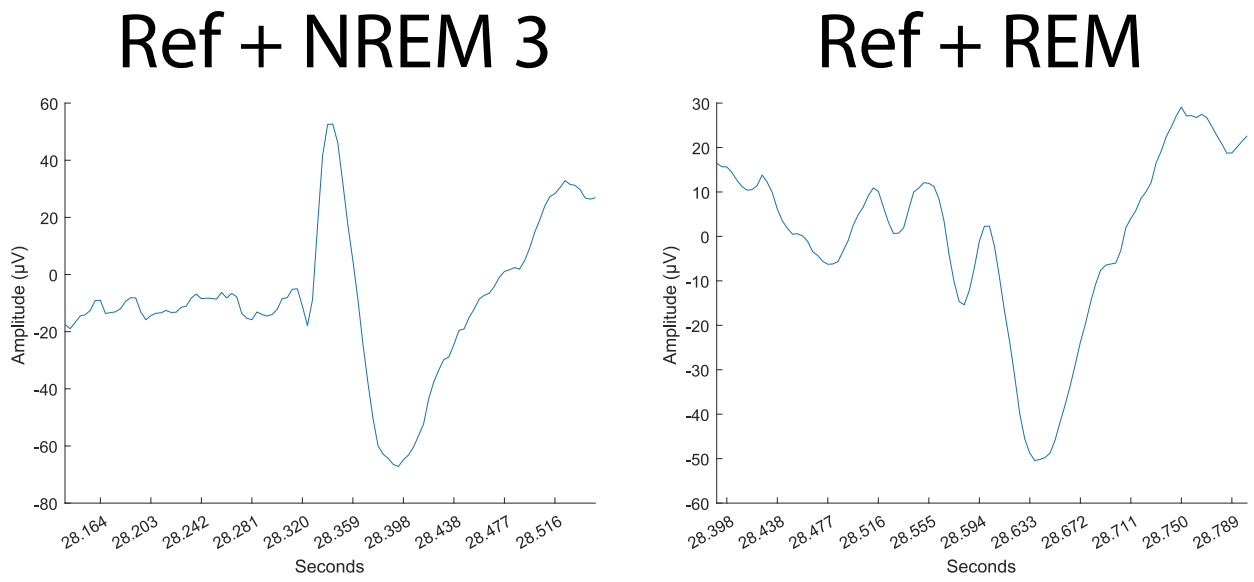


Figure 23: Visualization showcasing the substantial contrast in the normalized descending height feature. The referential montage has the greatest depiction of this difference exhibiting the largest normalized amplitude during NREM 3 versus the lowest normalized amplitude observed during REM.

- **Laplacian Montage:**
    - The Kruskal-Wallis test revealed a significant difference in the normalized descending height values across the sleep-wake states (p = 3.70E-94). The median and standard deviations for the normalized descending height values are as follows: NREM1 (M = 42.52, SD = 25.72), NREM2 (M = 52.53, SD = 28.18), NREM3 (M = 66.97, SD = 30.28), Awake (M = 60.36, SD = 23.89), REM (M = 28.79, SD = 14.03) (Figure 24).
    - Correction for Multiple comparisons revealed significant differences in all comparisons; however, after applying the Bonferroni correction, the significance between NREM3 and Awake was no longer observed (Table 8).
- **Referential Montage:**
    - The Kruskal-Wallis test revealed a significant difference in the normalized descending height values across the sleep-wake states (p = 5.12E-81). The median and standard deviations for the normalized descending height values are as follows: NREM1 (M = 84.87, SD = 44.24), NREM2 (M = 100.57, SD = 47.31), NREM3 (M = 119.85, SD = 49.86), Awake (M = 108.14, SD = 45.24), REM (M = 54.40, SD = 19.40) (Figure 24).

- Correction for Multiple comparisons revealed significance in most comparisons, with the exception between NREM2 and Awake (Table 8).

- **Raw Montage:**

  - The Kruskal-Wallis test revealed a significant difference in the normalized descending height values across the sleep-wake states (p = 7.52E-100). The median and standard deviations for the normalized descending height values are as follows: NREM1 (M = 99.28, SD = 55.63), NREM2 (M = 116.83, SD = 59.96), NREM3 (M = 140.84, SD = 65.75), Awake (M = 70.42, SD = 72.87), REM (M = 64.91, SD = 30.10) (Figure 24).

  - Correction for Multiple comparisons revealed significant differences in all comparisons; however, after applying the Bonferroni correction, the significance between Awake and REM was no longer observed (Table 8).

Table 8: Multiple comparisons across the Laplacian, Referential, and Raw montages are presented, with p-values for each grouping between all sleep-wake states. Colour-coding is employed to indicate the level of significance: green denotes significant, yellow signifies not significant after Bonferroni correction, and red indicates not significant.

Descending Height		*Laplacian*	*Referential*	*Raw*
Group1	**Group2**	**p-value**	**p-value**	**p-value**
NREM 1	*NREM 2*	<1.00E-05	<1.00E-05	<1.00E-05
NREM 1	*NREM 3*	<1.00E-05	<1.00E-05	<1.00E-05
NREM 1	*Awake*	<1.00E-05	<1.00E-05	<1.00E-05
NREM 1	*REM*	<1.00E-05	<1.00E-05	<1.00E-05
NREM 2	*NREM 3*	<1.00E-05	<1.00E-05	<1.00E-05
NREM 2	*Awake*	<1.00E-05	0.10366593	<1.00E-05
NREM 2	*REM*	<1.00E-05	<1.00E-05	<1.00E-05
NREM 3	*Awake*	0.00227896	<1.00E-05	<1.00E-05
NREM 3	*REM*	<1.00E-05	<1.00E-05	<1.00E-05
Awake	*REM*	<1.00E-05	<1.00E-05	0.01087816

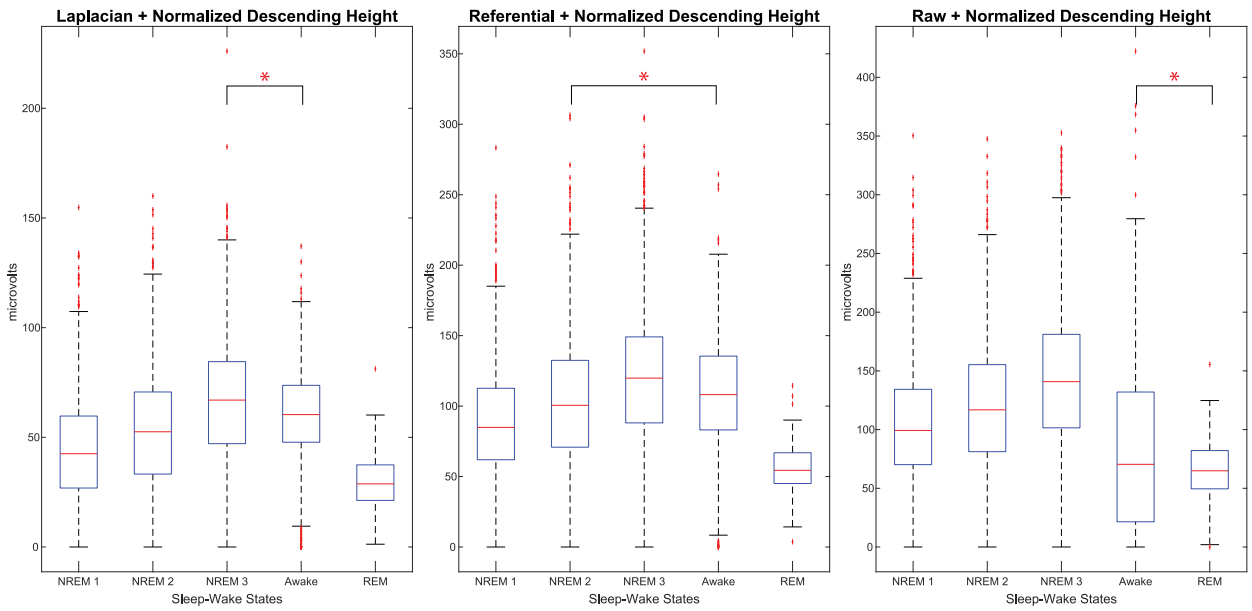


Figure 24: Box plots showing the distribution of normalized descending heights between sleep-wake states over the three montages. The height is measured in microvolts. Outliers are indicated with red +s and non-significant pairs are represented by red asterisks.

4.8 Spike Duration (milliseconds)

The spike length represents the time in milliseconds between the ascending and descending turning points of the spike. This measure provides insight into the duration of the spike, reflecting the time it takes for the spike to rise to its peak and then fall to its subsequent turning point. Figure 25 highlights the largest differences in spike duration, specifically between the two most divergent sleep-wake states.

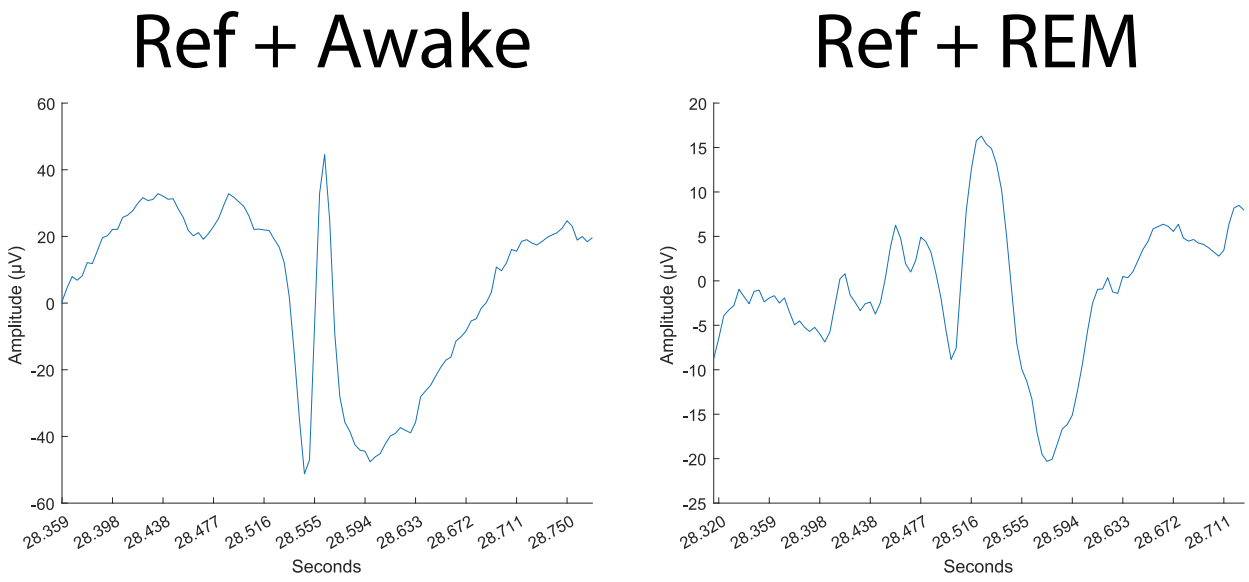


Figure 25: Visualization showcasing the substantial contrast in the spike duration feature. The referential montage has the greatest depiction of this difference exhibiting the shortest duration during wakefulness versus the significantly longer REM spikes.

- **Laplacian Montage:**
    - The Kruskal-Wallis test revealed a significant difference in the duration values across the sleep-wake states (p = 5.51E-111). The median and standard deviations for the duration values are as follows: NREM1 (M = 62.50, SD = 25.80), NREM2 (M = 66.41, SD = 24.54), NREM3 (M = 74.22, SD = 20.56), Awake (M = 46.88, SD = 16.37), REM (M = 70.31, SD = 16.99) (Figure 26).
    - Correction for multiple comparisons showed that most of the comparisons revealed significant differences, with the majority of comparisons involving REM being the exception. However, the comparison between REM and Awake was found to be significant (Table 9).
- **Referential Montage:**
    - The Kruskal-Wallis test revealed a significant difference in the duration values across the sleep-wake states (p = 4.80E-128). The median and standard deviations for the duration values are as follows: NREM1 (M = 78.13, SD = 28.54), NREM2 (M = 78.13, SD = 27.68), NREM3 (M = 78.13, SD = 23.00), Awake (M = 50.78, SD = 18.33), REM (M = 74.22, SD = 19.84) (Figure 26).
    - Correction for Multiple comparisons revealed that only Awake with every other state was significant (Table 9).

- **Raw Montage:**
    - The Kruskal-Wallis test revealed a significant difference in the duration values across the sleep-wake states (p = 2.54-101). The median and standard deviations for the duration values are as follows: NREM1 (M = 78.13, SD = 26.88), NREM2 (M = 78.13, SD = 28.60), NREM3 (M = 82.03, SD = 25.65), Awake (M = 46.88, SD = 29.27), REM (M = 70.31, SD = 21.02) (Figure 26).
    - Correction for Multiple comparisons revealed significance in most comparisons, with the exceptions between NREM1 with NREM2, NREM1 with REM, and NREM2 with REM (Table 9).

Table 9: Multiple comparisons across the Laplacian, Referential, and Raw montages are presented, with p-values for each grouping between all sleep-wake states. Colour-coding is employed to indicate the level of significance: green denotes significant, yellow signifies not significant after Bonferroni correction, and red indicates not significant.

Spike Duration		*Laplacian*	*Referential*	*Raw*
Group1	**Group2**	**p-value**	**p-value**	**p-value**
NREM 1	*NREM 2*	<1.00E-05	0.48407362	0.05599743
NREM 1	*NREM 3*	<1.00E-05	0.00444528	<1.00E-05
NREM 1	*Awake*	<1.00E-05	<1.00E-05	<1.00E-05
NREM 1	*REM*	0.71792051	0.99999461	0.37727217
NREM 2	*NREM 3*	<1.00E-05	0.57786186	0.00039678
NREM 2	*Awake*	<1.00E-05	<1.00E-05	<1.00E-05
NREM 2	*REM*	0.99999997	0.97841749	0.03421074
NREM 3	*Awake*	<1.00E-05	<1.00E-05	<1.00E-05
NREM 3	*REM*	0.62518647	0.75094788	0.0003329
Awake	*REM*	<1.00E-05	<1.00E-05	0.00022011

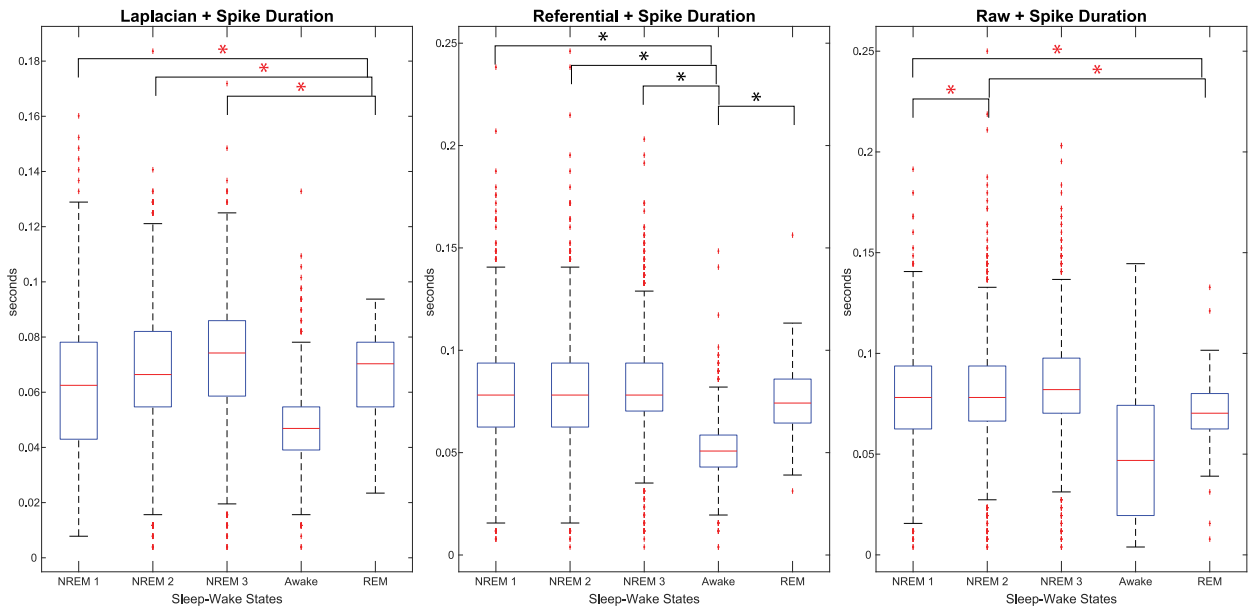


Figure 26: Box plots showing the distribution of spike durations between sleep-wake states over the three montages. The duration is measured in seconds. Outliers are indicated with red +s where significant pairs are represented by black asterisks and non-significant pairs are represented by red asterisks.

4.9 Spike Area (microvolts * seconds)

The spike area quantifies the enclosed region of a spike's shape. To compute this area, a straight line is drawn from the spike's ascending to descending turning point. The area is then determined by integrating the curve from the ascending to the descending turning point and subtracting the area beneath the traced line, focusing solely on the enclosed space within the spike. This calculation provides a specific measure of the overall form of the spike. Figure 27 highlights the largest differences in spike area, specifically between the two most divergent sleep-wake states.

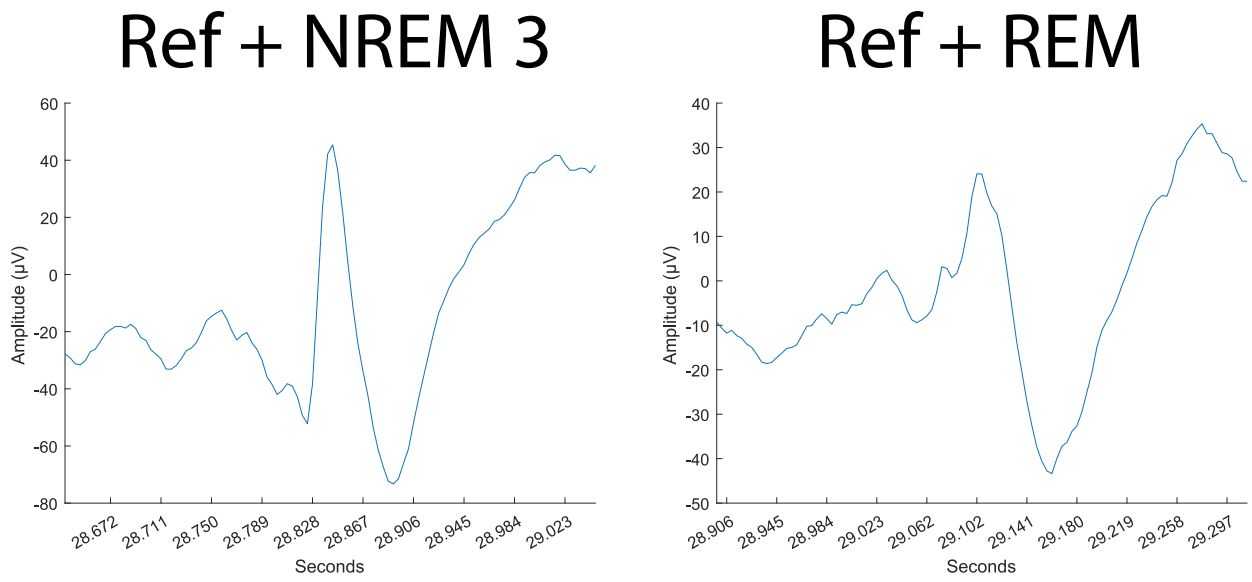


Figure 27: Visualization showcasing the substantial contrast in the spike area feature. The referential montage has the greatest depiction of this difference exhibiting the largest area during wakefulness versus the significantly smaller area of a REM spikes.

- **Laplacian Montage:**
    - The Kruskal-Wallis test revealed a significant difference in the spike area values across the sleep-wake states (p = 3.84E-57). The median and standard deviations for the spike area values are as follows: NREM1 (M = 261.67, SD = 233.83), NREM2 (M = 307.63, SD = 252.69), NREM3 (M = 393.32, SD = 258.14), Awake (M = 259.07, SD = 184.60), REM (M = 175.94, SD = 121.29) (Figure 28).
    - Correction for Multiple comparisons revealed significance in most pairs, with the exceptions between NREM1 with Awake and NREM2 with Awake after Bonferroni correction (Table 10).
- **Referential Montage:**
    - The Kruskal-Wallis test revealed a significant difference in the spike area values across the sleep-wake states (p = 9.43E-52). The median and standard deviations for the spike area values are as follows: NREM1 (M = 599.98, SD = 488.76), NREM2 (M = 659.38, SD = 555.94), NREM3 (M = 765.21, SD = 490.00), Awake (M = 481.97, SD = 369.00), REM (M = 335.57, SD = 202.92) (Figure 28).

- Correction for Multiple comparisons revealed significant differences in all pairs; however, after applying the Bonferroni correction, the significance between NREM1 with NREM2 and Awake with REM was no longer observed (Table 10).

- **Raw Montage:**

  - The Kruskal-Wallis test revealed a significant difference in the spike area values across the sleep-wake states (p = 2.62-83). The median and standard deviations for the spike area values are as follows: NREM1 (M = 698.13, SD = 585.71), NREM2 (M = 769.15, SD = 672.38), NREM3 (M = 915.80, SD = 683.04), Awake (M = 269.31, SD = 538.32), REM (M = 382.75, SD = 288.09) (Figure 28).

  - Correction for Multiple comparisons revealed significance in most pairs, with the exceptions between NREM1 with NREM2 and Awake with REM (Table 10).

Table 10: Multiple comparisons across the Laplacian, Referential, and Raw montages are presented, with p-values for each grouping between all sleep-wake states. Colour-coding is employed to indicate the level of significance: green denotes significant, yellow signifies not significant after Bonferroni correction, and red indicates not significant.

Spike Area		*Laplacian*	*Referential*	*Raw*
Group1	**Group2**	**p-value**	**p-value**	**p-value**
NREM 1	*NREM 2*	<1.00E-05	0.04282761	0.2143618
NREM 1	*NREM 3*	<1.00E-05	<1.00E-05	<1.00E-05
NREM 1	*Awake*	0.99999998	<1.00E-05	<1.00E-05
NREM 1	*REM*	0.0005412	<1.00E-05	<1.00E-05
NREM 2	*NREM 3*	<1.00E-05	<1.00E-05	<1.00E-05
NREM 2	*Awake*	0.00395717	<1.00E-05	<1.00E-05
NREM 2	*REM*	<1.00E-05	<1.00E-05	<1.00E-05
NREM 3	*Awake*	<1.00E-05	<1.00E-05	<1.00E-05
NREM 3	*REM*	<1.00E-05	<1.00E-05	<1.00E-05
Awake	*REM*	0.00059338	0.0038603	0.97314604

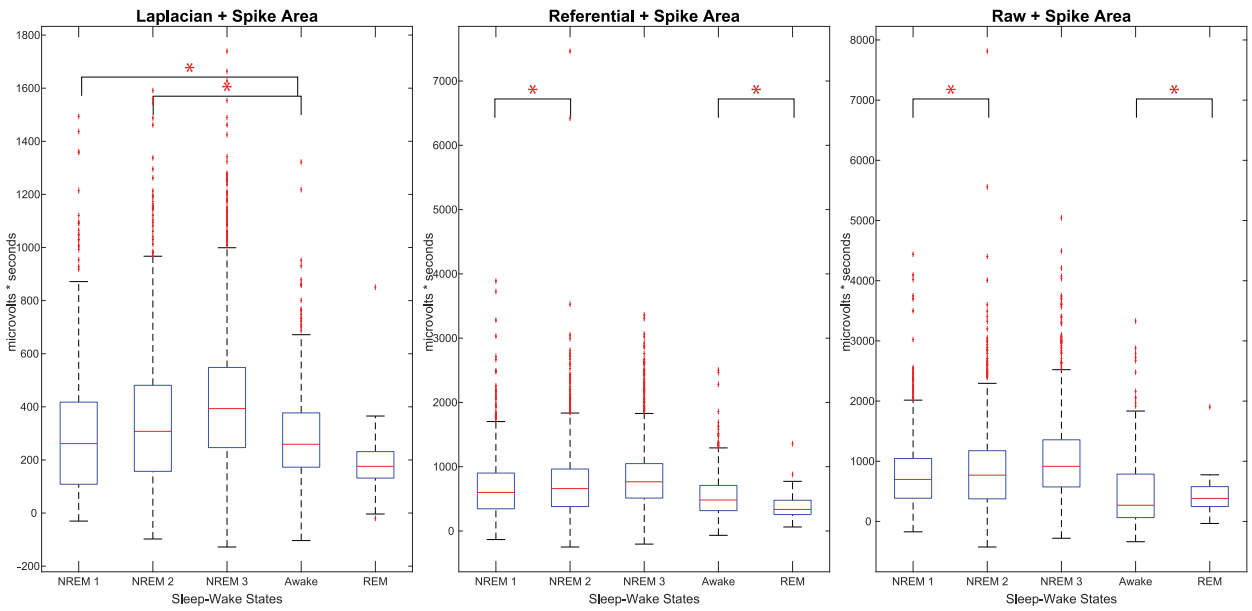


*Figure 28: Box plots showing the distribution of spike area between sleep-wake states over the three montages. The area is measured in microvolts*seconds. Outliers are indicated with red +s and non-significant pairs are represented by red asterisks.*

The results presented in Section 4 offer a nuanced perspective on the diversity of epileptiform spikes across sleep-wake states and different EEG montages. The findings illustrate that spike morphology is not a static entity but varies significantly depending on the state of consciousness and the montage used for EEG analysis. One of the pivotal observations is the distinct nature of spikes in REM sleep, which exhibit unique characteristics when compared with other sleep states. This finding is crucial in understanding the specific neurophysiological mechanisms that may be active during REM sleep, potentially influencing epileptic activity. Furthermore, the analysis reveals a general trend in spike features across the NREM stages, as progression into deeper sleep would result in gradually increasing or decreasing in magnitude, depending on the specific feature. The study also highlights the importance of EEG montages in the analysis of epileptiform spikes. The differences observed through Laplacian, referential, and raw montages indicate that the choice of montage can significantly influence the interpretation of spike morphology. As the thesis moves toward the discussion section, these observations will be integrated with existing literature, translating the methodological foundation laid in the previous section into processes capable of accentuating spike morphology, and offering insights into the neurophysiological underpinnings affecting said morphology across sleep-wake states.

5 Discussion – Spike Morphologies Throughout Sleep-Wake States

In section 5, we explore the nuanced alterations in epileptiform spike morphologies across various sleep-wake states, as observed through electroencephalogram (EEG) recordings. This section delves into the intricate interactions between neural processes and their manifestations in the characteristics of epileptic spikes. Each sub-section is dedicated to a specific spike feature, providing a comprehensive analysis of how these features vary with the brain's changing state during sleep and wakefulness. The discussion extends beyond mere observations, offering insights into the neurophysiological underpinnings of these variations. A special emphasis is placed on REM sleep due to its unique spike morphology, which potentially hints at anti-epileptic effects. Furthermore, the impact of different EEG montages on spike feature observation is explored, highlighting the complexity and multi-dimensional nature of EEG analysis in epilepsy research.

In the ensuing discussion, we aim to contextualize the findings presented in this study, specifically focusing on the observed alterations in spike morphologies across different sleep-wake states, as extensively evidenced in the results section and illustrated in Figure 10. Moreover, we will delve into the distinct differences between REM sleep and all other sleep-wake states to explore why REM sleep often exhibits drastically different characteristics, as depicted in the images provided in the results section. This specialized focus may shed light on its potential anti-epileptic effects.

The consensus on spike features across these states is synthesized in Table 3, encompassing nine key attributes that exhibit distinct behaviors during sleep and wakefulness. Furthermore, Table 4 offers a comprehensive framework for potential mechanisms that could be influencing these spike morphologies across sleep-wake states. For a more profound insight into these mechanisms, the nuances are thoroughly elaborated upon in the forthcoming discussion sub-sections. This discussion aims to reconcile our observations with existing literature, probe the implications of our findings, and suggest avenues for future research. It is also worth noting that the data suggest varying spike features when observed through different montages, highlighting the importance of taking multiple perspectives into account for a more robust understanding.

Table 11: Median values of nine spike features across five sleep-wake states in three different montages. Colours indicate ascending median values from orange (lowest) to blue (highest) for all features except descending slope, where colors are reversed to represent steepness. REM sleep consistently exhibits the lowest median values across most features, except for 'spikiness,' where it has a blunter peak. NREM stages show a consistent pattern of either increasing or decreasing values across montages. In contrast, the awake state displays notable variability, particularly in amplitude features.

Laplacian	NREM1	NREM 2	NREM 3	Awake	REM
Ascending Slope	5.45	5.8	6.93	10.66	3.08
Descending Slope	-5.01	-4.97	-5.81	-8.45	-3
Asymmetry	1.15	1.21	1.25	1.28	1.09
Spikiness	22.32	22.04	18.47	12.76	39.38
Peak Height	30.66	32.25	35.27	23.52	15.82
Normalized Ascending Height	33.56	35.64	42	41.89	19.12
Normalized Descending Height	42.52	52.53	66.97	60.36	28.79
Spike Duration	62.5	66.41	74.22	46.88	70.31
Spike Area	261.67	307.63	393.32	259.07	175.94

Referential	NREM1	NREM 2	NREM 3	Awake	REM
Ascending Slope	8.17	8.74	10.52	17.34	4.89
Descending Slope	-7.88	-8.55	-9.93	-13.21	-5.09
Asymmetry	1.06	1.08	1.12	1.33	1.01
Spikiness	14.52	13.47	11.66	7.97	24.12
Peak Height	50.89	54.26	58.26	30.73	26.72
Normalized Ascending Height	61.3	61.98	68.78	73.64	33.6
Normalized Descending Height	84.87	100.57	119.85	108.14	54.4
Spike Duration	78.13	78.13	78.13	50.78	74.22
Spike Area	599.98	659.38	765.21	481.97	335.57

Raw	NREM1	NREM 2	NREM 3	Awake	REM
Ascending Slope	9.65	9.84	11.64	14.74	5.65
Descending Slope	-9.22	-9.64	-10.99	-9.73	-6.43
Asymmetry	1.03	1.09	1.1	1.63	0.96
Spikiness	12.37	12.22	10.49	10.49	19.65
Peak Height	62.06	63.51	66.74	52.18	34.46
Normalized Ascending Height	71.54	68.63	80.54	57.78	37.56
Normalized Descending Height	99.28	116.83	140.84	70.42	64.91
Spike Duration	78.13	78.13	82.03	46.88	70.31
Spike Area	698.13	769.15	915.8	269.31	382.75

Highest 5
4
3
2
Lowest 1

Table 12: Overview of mechanisms and processes to be explored for identifying spike feature variations across sleep-wake states. The table serves as a guide for the subsequent discussion aimed at elucidating the overall morphological differences in spikes over these states. An asterisk (*) next to the overall trend of a feature denotes inconsistency across montages; for a more detailed account, refer to Table 11.

Spike Features / Sleep-Wake States	***Ascending slope*** *Shallow --> Steep* *REM<NREM1,2,3<Awake*	***Descending Slope*** *Shallow --> Steep* *REM<NREM1,2,3<Awake**	***Asymmetry*** *Ascending Slope Dominant --> Symmetrical* *REM<NREM1,2,3<Awake*	***Spikiness/Pointiness*** *Sharp --> Blunt* *Awake<NREM3,2,1<REM*	***Peak height*** *REM<Awake<NREM1,2,3*	***Normalized Ascending Height*** *REM<NREM1<NREM2<Awake<NREM3**	***Normalized Descending Height*** *REM<NREM1<NREM2<Awake<NREM3**	***Duration/Length*** *Awake<NREM=REM*	***Area of Spike*** *REM<Awake<NREM1,2,3**
Wakefulness	Increased metabolic state Increased glutamatergic signalling Astrocytic ion buffering and receptor trafficking - Increased extracellular (EC) potassium - Decreased EC calcium - Decreased EC magnesium - Upregulated NMDA receptors Desynchronous network dynamics	Fast potassium efflux Fast sodium channel inactivation Balanced GABAergic activity capable of responding to increased excitability Astrocytic potassium and glutamate buffering provide stability Desynchronous activity	Increased glutamatergic activity Increased extracellular potassium Balanced GABAergic Alert and responsive, allowing quick inhibition for changing focuses Overall desynchronous state	Rapid neuronal depolarizations Robust GABAergic activity Astrocytic stabilization Desynchronous activity	Active inhibitory biological failsafe mechanisms Lower overall amplitude state Desynchronous activity	Increased metabolic state Increased glutamatergic signalling Astrocytic ion buffering and receptor trafficking - Increased EC potassium - Decreased EC calcium - Decreased EC magnesium - Upregulated NMDA receptors Desynchronous activity	Increased excitatory signalling Robust Inhibitory countermeasures Desynchronous activity	Increased metabolic state Increased excitatory processes Robust inhibitory processes Desynchronous activity	Increased metabolic state Increased glutamatergic signalling Balanced GABAergic activity capable of responding to increased excitability Astrocytic regulation Stable ATP levels Desynchronous activity
NREM	Overall 15% decrease in metabolic state compared to wakefulness Regional increase of ATP Increased potassium efflux Increased EC calcium Increased EC magnesium Decreased excitatory signalling via AMPA and NMDA receptors Increased GABAergic activity Initiation of thalamocortical synchronous activity	Increased GABAergic activity Decreased glutamate and ACh Synchronous network activity	Increased GABAergic activity Decreased glutamate and ACh Synchronous activity Reduced cortical adenosine	Gradual Blunting of Peaks as Sleep lightens Sodium, potassium and calcium ion channel kinetics hasten as sleep deepens Greater synchronous activity	Synchronous activity Higher overall amplitude state as sleep deepens Density and kinetics of sodium and calcium voltage-gated channels	Synchronous activity Increased glutamate during state switching and slow wave activity	Increased GABAergic activity Decreasing cholinergic activity Decreasing excitatory neurotransmitters Overall higher peaks Decreased extracellular potassium Synchronous network activity	Homeostatic regulating processes - Neurotransmitter levels - Ion channel kinetics - Astrocytic activity - network dynamics Regulation through excitatory and inhibitory processes	Synchronous activity Interplay between neurotransmitters and ion kinetics Astrocytic mechanisms
REM	Increased ACh on par with wakefulness Decreased sensory and motor stimuli Desynchronous network dynamics	Increased ACh Reduced potassium efflux Decreased GABAergic inhibition Desynchronous activity	Increased ACh Decreased GABAergic activity Astrocytic stabilization of ions and neurotransmitters	Increased ACh Balanced slower excitatory and inhibitory mechanisms Desynchronous activity	Increased cholinergic activity Decreased GABAergic activity Active kainate receptors Astrocytic regulation and stabilization of extracellular space Desynchronous activity	Increased ACh Decreased GABAergic activity Increased orexinergic activity Increased kainate receptor activity Desynchronous activity	Increased ACh Decreased GABAergic activity Overall lower amplitude state	Increased ACh Decreased GABAergic activity Desynchronous activity	Increased ACh Increased Glutamate Decreased GABA BF excitatory and inhibitory effect on cortical neurons Astrocytic interactions with orexinergic systems within LH Further increased orexinergic activity within LH Desynchronous activity

Different montages - the Laplacian, average referential, and raw data - can accentuate disparate neural activity nuances, potentially elucidating the mechanisms behind the observed changes in the spike features during various sleep phases. For instance, the Laplacian montage calculates the potential at one electrode relative to the average potential of surrounding electrodes, facilitating a more localized insight into brain activity, aiding in a finer dissection of the synaptic dynamics during these states. Conversely, the average referential montage, which delineates a potential at a single electrode relative to the average potential of all electrodes, might be more adept at illustrating the widespread alterations in neural oscillations that occur across sleep stages, providing a macroscopic view of sleep's modulatory effects on brain activity. Moreover, the raw data montage offers insights by presenting neuronal activity in an unmanipulated state, thereby presenting a baseline to gauge the alterations brought about by sleep states. Utilizing a montage cognizant of the specific intricacies of sleep-wake neurochemistry and synaptic activity can thereby pave the way to a nuanced understanding of how sleep states can modulate epileptic spike features, aligning with the observed variations in ascending slope steepness across different sleep-wake stages.

5.1.1 Ascending slope

The ascending slope of the spike essentially captures the extent to which neurons are both participating in and propagating the Paroxysmal Depolarizing Shift (PDS), along with the degree of synchronous firing among them. The findings revealed that the median ascending slope during REM sleep was significantly lower than in other sleep-wake states across all montages, indicating a shallower ascent to the spike's peak (Figure 12). Moreover, the observed results show a systematic increase in median values as one progresses through the sleep-wake states: from REM to NREM1, NREM2, NREM3, and finally Awake. Notably, the statistical significance of these multiple comparisons held consistently across montages, with only the comparison between NREM1 and NREM2 being not significant.

Wakefulness

During wakefulness, the brain is in a state of desynchronized activity facilitated by various networks such as the LDT/PPT [122]. Yet, it is also a period of increased neural responsiveness and excitability, most likely due to the increased metabolic state and increased excitatory processes possibly underlying a more susceptible neuron which potentially leads to steeper slopes in epileptiform spikes [187]. The role of upregulated glutamatergic signalling in this context is crucial [71]. It contributes to the increased excitatory state, which is indicative of wakefulness, but does not necessarily imply a transition to synchronization. Instead, glutamatergic signaling may enhance the responsiveness and excitability of neurons within the inherently desynchronized state of

wakefulness. Despite this desynchronization, the steep ascending slope observed during wakefulness indicates a rapid proliferation of neuronal activity, particularly evident in neurons undergoing PDS firing. This suggests that while desynchronization characterizes the overall state, it may not significantly alter the rate of the slope, or the extent to which neurons fire synchronously during a PDS. Therefore, the steep slope, indicative of swift neuronal activation until maximal synchronous firing of surrounding neurons, appears to be primarily influenced by the overall excited state of wakefulness, rather than by desynchronization itself.

Additionally, wakefulness sees an increase in astrocytic activity, especially in ion buffering and potentially in NMDA receptor trafficking [154]–[157]. Ion buffering during wakefulness results in increased extracellular potassium with a decrease of calcium and magnesium at a fifth of the rate of potassium [154]. A higher extracellular potassium ion level can lead to an increased neuronal excitability while reduced magnesium could be indicative of a more susceptible NMDA receptor. Astrocyte trafficking on the other hand can modulate NMDA receptors to allow a larger influx of sodium and calcium ions which could support faster recruitment of neurons into the synchronized PDS firing by enhancing the functionality of NMDA receptors.

NREM Sleep

The steady increase in the steepness of the ascending slope of epileptiform spikes throughout the NREM stages from lightest to deepest sleep is indeed perplexing, particularly given the general decrease in neuronal excitability and activity during these stages. One might expect that as the brain becomes less excitable during deeper NREM stages, the ascending slope of these spikes would become more gradual rather than steepen. However, the data suggest the opposite, begging for an integrated interpretation across metabolic conditions, ions, neurotransmitters, and network activity, all of which impact cortical neurons as measured by scalp EEG.

Beginning with metabolic states, NREM sleep generally corresponds to a 15% reduction in brain energy usage compared to wakefulness [187]. This reduction is associated with a proportional decrease in overall neuronal firing rates, suggesting less capacity for rapid, synchronized activity. Yet, this metabolic downscaling does not appear to translate into more gradual slopes as the slopes become steeper while falling into deeper sleep, presenting a puzzling contradiction. Interestingly, the levels of ATP during sleep are increased compared to wakefulness, including large surges throughout different areas of the brain — one of which being the frontal cortex [188]. These increased levels of ATP may prove insightful when investigating specifically the potassium concentration within the extracellular space during NREM, and possibly aiding in the regulation of slow-wave activity.

Generally, the potassium concentration is high within a neuron and lower within the extracellular space; however, during NREM, the extracellular concentration is substantially lower than during wakefulness [189]. Specifically, the extracellular concentration of potassium is lower compared to wakefulness, creating a larger gradient between the inside and outside of the neuron. When a neuron fires an action potential, potassium ions naturally flow from the intracellular to the extracellular space [53], [63]. In the context of NREM sleep, this gradient difference is amplified, leading to a more significant efflux of potassium ions into the extracellular space than would occur during wakefulness. This increased efflux results in a hyperpolarized state for the neuron, making its overall resting membrane potential more negative. Because of this hyperpolarization, it becomes challenging for the neuron to fire subsequent action potentials. To compensate, the Na+/K+ ATPase pump must work harder to bring the neuron back to its normal homeostatic membrane potential [53], [63]. These processes all correlate with a lower firing rate and general increased difficulty of neuronal firing; however, the elevated levels of ATP during NREM may play a large role in ensuring the neurons are in a homeostatic state as quickly as possible, potentially validating the ability for successive neuronal firing albeit at a lower rate. In addition to K^+ ions, there is also a slight increase in extracellular Mg^{2+} and Ca^{2+} during NREM compared to wakefulness [187]. These changes serve as additional variables capable of manipulating neuronal excitability. Additional Mg^{2+} could potentially decrease excitability by ensuring the NMDA receptors have a block requiring co-activation from neurons that may have reduced firing capability. While elevated extracellular calcium levels during NREM sleep do not directly induce increased or decreased neuronal activity, they can potentiate the effectiveness of each individual depolarization event. In this way, the larger calcium gradient ensures a more robust neurotransmitter release upon depolarization, which could make even the reduced neuronal firing during NREM sleep more impactful in terms of post-synaptic responses [53], [63]. While a decrease in extracellular K^+ and an increase in Mg^{2+} may potentially lead to a more inhibitory state, the underlying dynamics of large groups of neuronal successive firing may be more engrained in neurotransmitter release and network systems.

In the neurotransmitter landscape during NREM sleep, excitatory signalling through AMPA and NMDA receptors is notably diminished, possibly attributable to decreased cortical glutamate levels furthering the notion of more gradual slopes within an inhibited brain [64], [65], [72]–[74]. Concurrently, the NREM stage is characterized by heightened GABAergic activity, exerting inhibitory control over various brain structures and networks implicated in wakefulness [28]. Specifically, elevated GABA levels target the locus coeruleus (LC), a principal source of norepinephrine (NE), thereby attenuating its activity. This leads to disinhibition of the ventrolateral preoptic nucleus (VLPO), culminating in increased GABAergic tone and further brain inhibition [28], [169]. The VLPO extends its inhibitory influence among various regions but also the lateral hypothalamus being the site of orexin

synthesis [170]. This sequence of events dampens the excitatory drive in arousal systems, including the pontine tegmentum regions (PPT and LDT), which consequently curtails cholinergic output. This pervasive downregulation of arousal systems during NREM sleep is instrumental in the manifestation of thalamocortical synchronous activities, such as sleep spindles and k-complexes [21], [26], [27], [47], [113], [122], [142], [171].

Despite the overwhelming evidence pointing toward a global downregulation of excitatory mechanisms and an upregulation of inhibitory processes during NREM sleep, the steepening of epileptiform spikes across NREM stages presents an intriguing paradox. One plausible explanation may lie in network dynamics: rather than rapid depolarizations in a localized area, the phenomena observed could be a product of large-scale, synchronized neuronal firing. Specifically, the high-amplitude slow-wave activity in conjunction with the thalamocortical rhythms characteristic of NREM could facilitate greater synchrony, allowing for the summation of dipoles even in an inhibited state, thereby contributing to the unexpected steepening of spike slopes.

REM Sleep

REM sleep presents an intriguing paradox: it is an excitatory state similar to wakefulness, yet it features the most gradual ascending slopes in epileptic spikes among all sleep-wake states. One contributing factor may be the neurotransmitter acetylcholine, which is released in high concentrations from the pedunculopontine and laterodorsal tegmental nuclei during REM sleep [47], [113], [142], [171]. Unlike wakefulness, where a mix of neurotransmitters such as norepinephrine and serotonin contribute to neuronal excitability, REM sleep relies predominantly on cholinergic mechanisms. This could provide a more controlled excitability that results in gradual ascending slopes in epileptic spikes, in contrast to the more abrupt changes in wakefulness [29], [56], [56], [57], [117].

The role of thalamocortical circuits further complicates this landscape. During REM sleep, the thalamus is more permeable to sensory signals compared to NREM sleep, where it filters sensory information and promotes slow-wave activity [47]. Despite this wake-like thalamic activity during REM, the presence of muscle atonia and the absence of external sensory input might limit rapid changes in cortical excitability and overall background artifacts that could influence the EEG. This could be another reason for the gradual ascending slopes in epileptic spikes observed during REM sleep.

Further, the unique architecture of REM sleep may contribute to these gradual slopes. Unlike the waking state where the cortex is awash in sensory stimuli and involved in motor planning, REM sleep occurs in a state of sensory isolation and motor inhibition. Regions specific to REM sleep, such as the subcoeruleus nucleus, may

regulate these unique aspects [47], [190]. These specific regions may contribute to a slower summation of synchronous firing, leading to a more gradual ascending slope.

5.1.2 Descending Slope

The descending slope of the spike primarily characterizes the rate at which inhibitory mechanisms suppress the PDS and return neurons to their baseline resting potential. Across the majority of montages, the data consistently revealed that the median descending slope during REM sleep was notably closer to zero compared to other sleep-wake states. This signifies a more gradual decline toward the inflection point of the spike (Figure 14). An anomaly was observed in the raw montage, where multiple non-significant pairs were found and the median value for the Awake state was interspersed between those of NREM2 and NREM3. Despite this irregularity in the raw montage, the prevailing trend in other montages indicated a systematic increase in median values, transitioning from REM through NREM1, NREM2, and NREM3, to the Awake state.

Wakefulness

The steep descending slope of epileptic spikes observed in cortical neurons during wakefulness can be attributed to a myriad of factors intricately intertwined. Key to this rapid decline is the robust activity of potassium channels during wakefulness, particularly Kv3.1 and Kv3.3 channels, which facilitate fast hyperpolarizations. Without these channels, neurons could engage in uncontrolled successive firing, thereby aggravating epileptic conditions [191]–[193]. This high activity is complemented by the faster inactivation of sodium channels, contributing to a rapid return to the baseline resting potential.

Neurotransmitter dynamics also play a pivotal role. During wakefulness, GABAergic interneurons are particularly active, releasing greater quantities of GABA that primarily act through α1-subunit-containing $GABA_A$ receptors in the cortex. These receptors are known for their fast kinetics and thus foster rapid IPSPs, serving as an efficient calming for excitatory spikes [28], [78], [194]. Concurrently, excitatory AMPA receptors may be downregulated or display faster desensitization, curtailing the excitatory drive [41], [195]. Notably, the role of acetylcholine (ACh) in promoting wakefulness and cortical arousal is well-established. However, recent studies suggest that specific subsets of basal forebrain (BF) GABAergic neurons may be even more influential in arousal regulation [196]. These GABAergic networks in the BF interact closely with the cortex and are thought to set the stage for a well-balanced excitatory-inhibitory cortical landscape. The greater activation of these GABAergic pathways during wakefulness ensures that there is a robust inhibitory backdrop against which excitatory activities like epileptic spikes can be quickly terminated [28], [194]. In this manner, the influence of GABAergic networks serves as an

additional layer of control that contributes to the steepness of the descending slope of epileptic spikes during wakefulness.

Cortical networks during wakefulness primarily exhibit desynchronized activity, a state often driven by higher cholinergic and noradrenergic modulation [29], [127]. This desynchronization makes the cortical neurons less susceptible to sustained, synchronous excitatory activity, which may facilitate not only the difficulty in the spreading of a PDS but also act to quickly terminate the epileptic spikes [46, 83].

Finally, astrocytic and metabolic dynamics are not just bystanders but active performers in shaping neuronal excitability. Astrocytes, known for their roles in ionic homeostasis and neurotransmitter buffering, exhibit heightened metabolic activity during wakefulness [29], [154]. Elevated glucose metabolism in these cells likely provides the energy required for enhanced astrocytic functions such as potassium buffering and glutamate uptake [197]. Effective potassium buffering by astrocytes stabilizes the extracellular ionic environment, aiding rapid repolarization of neurons and subsequently contributing to the steep descending slope of epileptic spikes. Additionally, astrocytes quickly clear extracellular glutamate, which otherwise would perpetuate excitatory signalling, thereby mitigating the duration and impact of epileptic spikes [198]. These metabolic and buffering capabilities of astrocytes work in concert to facilitate a rapid return of cortical neurons to their baseline activity, complementing other inhibitory mechanisms at play during wakefulness.

NREM Sleep

The observation that the steepness of the descending slopes of epileptiform spikes increases from NREM1 to NREM3 is at once intriguing and entirely fitting with the evolving inhibitory landscape of these sleep stages. Far from contradicting the general principles of neural inhibition, these findings may represent the quintessential expression of a brain in progressive downscaling. Multiple factors, from neurotransmitters to ions and network dynamics, coalesce to produce this phenomenon.

GABAergic signalling emerges as a cornerstone in understanding this trend. During deeper sleep stages, particularly NREM3, the increased GABAergic activity surges, working to not only inhibit neuronal firing but also to swiftly terminate any PDS activity that occurs [28], [29]. Concurrently, reduced levels of excitatory neurotransmitters like glutamate and acetylcholine further bolster the inhibitory environment. Glutamate levels are lowest during NREM3, which suggests a shortage of excitatory neurotransmitters to sustain PDS, allowing for quicker return to baseline [65]. Acetylcholine levels also dip during sleep to roughly 50% that exhibited during wake, further curbing the excitatory potential of cortical neurons [29].

Yet, neurotransmitters represent just one facet of the descending slope's steepness. The brain's ionic milieu is notably dynamic across NREM stages, particularly regarding astrocyte ion buffering of extracellular potassium, calcium, and magnesium concentrations. Lower levels of extracellular potassium could mean faster repolarization, and higher levels of calcium and magnesium may further catalyze this effect [154]–[157]. Specifically, in NREM3, the diminished activity of KCNQ channels further enables immediate repolarization, leading to more rapid attenuation of epileptiform spikes [199], [200].

Lastly, network dynamics offer the most nuanced layer of understanding, especially when discussing the seemingly contradictory effects of neural synchronization. Synchronous slow-wave activity, particularly salient during deeper NREM stages, is facilitated by thalamic and callosal projections engaging with local-circuit inhibitory neurons [24]. This synchronization produces a unique environment where neurons are not only primed for rapid and collective firing but are also set up for equally swift suppression. This is crucial to understand: while the same synchronous mechanisms that aid in the amplification of ascending slopes might seem counterintuitive in an inhibitory setting, they also play an integral role in steepening the descending slopes. During the down states of these synchronous oscillations, the local inhibitory neurons induce inhibitory postsynaptic potentials (IPSPs) across the network, leading to a swift, collective return to hyperpolarized states post-spike [24]. This synchronized termination mechanism effectively makes the descending slope of the epileptiform spikes steeper, serving as a large-scale affirmation of the inhibitory processes that characterize deeper sleep stages. Network dynamics not only facilitate synchronous activities but also have far-reaching implications in shaping the neurochemical landscape that aids in the steepening of the descending slopes during deep sleep stages. For example, elevated GABA levels lead to a reduction in locus coeruleus (LC) activity, subsequently lowering norepinephrine (NE) levels [28]. This cascade of events permits the ventrolateral preoptic nucleus (VLPO) to operate more efficiently in promoting sleep as it is no longer inhibited by NE. Moreover, research suggests that GABAergic mechanisms within the zona incerta offer another layer of inhibitory control by projecting to cortical neurons. This projection serves to modulate spontaneous spike-wave discharges, further contributing to the steeper descending slopes observed in epileptiform spikes [201], [202].

REM Sleep

The gradual descending slopes of epileptic spikes during REM sleep as observed through scalp EEG can be attributed to a confluence of factors including neurotransmitter activity, ion channel dynamics, astrocyte function, and network dynamics. REM sleep features elevated acetylcholine (ACh) levels, which not only promote excitability but also modulate potassium channel activity. Reduced potassium efflux due to ACh could

prolong the duration of neuronal depolarization, slowing down the return to baseline following periods of synchronous firing [29], [113].

This slower return to baseline is compounded by the lack of strong GABAergic inhibition that characterizes REM sleep [105], [106]. Without a quick termination to halt excitatory activity, the neuronal network takes longer to cease its activity, possibly contributing to a gradual descending slope.

The role of astrocytes may further contribute to this landscape. Their ability to modulate extracellular neurotransmitters and ion concentrations could influence the time course for the neuronal network's return to its baseline state, especially in the absence of strong GABAergic inhibition [137], [152], [154].

However, the most parsimonious explanation may lie in the network dynamics. In a globally desynchronized milieu typical of REM sleep, the Paroxysmal Depolarizing Shift (PDS) would not only take longer to initiate and propagate but also require an extended period to resolve and come to an end [46], [128].

Overall, the unique neurotransmitter profile and ion channel dynamics in REM sleep create an environment that can account for the more gradual descending slopes in epileptic spikes. This extends beyond the simplified understanding of REM sleep as merely an excitatory state, offering a more nuanced explanation for the observed EEG characteristics.

5.1.3 Asymmetry

The asymmetry metric offers a ratio that quantifies the relative prominence of a spike's ascending and descending slopes, effectively capturing the balance between excitatory and inhibitory phases. The intrinsic asymmetry of a spike from the IFCN depicts it having a steeper ascending slope than descending slope wherein the reverse is also possible [36]. A ratio greater than 1 underscores the relative dominance of the ascending slope, while a ratio under 1 indicates a more pronounced or steeper descending slope. Interestingly, although the asymmetry metric did not show significant differences across most sleep-wake states in multiple comparisons, the unique behaviour of each 'arm' of the asymmetry metric (i.e., the ascending and descending phases) varied between sleep-wake states, mirroring the trends observed in the median values of the slopes themselves, suggesting that the same underlying mechanisms within each state of the ascension and descension affect the asymmetry. Specifically, in the Laplacian montage, almost no significant differences were found. The raw montage, however, showed that the Awake state significantly differed from other sleep states, a pattern somewhat mirrored in the referential montage (Figure 16).

Notably, the REM state generally exhibited either a symmetric ratio between ascending and descending slopes or a bias towards a steeper descending slope, depending on the specific montage used. An exception to this trend was found in the Awake state, which occasionally showed significant deviations in asymmetry. It is important to note that the findings were affected by 4-5 outliers, depending on the montage, as indicated by a normality test (Supplemental 2), resulting in substantial variations in standard deviations.

In summary, despite these outliers, our data primarily showed unexpected uniformity in the asymmetry ratios across sleep-wake states, with particular distinctions appearing only in the Awake state. The overall trend displayed an increase in median asymmetry values progressing from REM through NREM1, NREM2, and NREM3, culminating in the Awake state, where the highest values signified a comparatively steeper ascending slope.

Wakefulness

As previously discussed, wakefulness is a state characterized by heightened excitability and responsiveness, with the contributions of neurotransmitter dynamics, ion channels, astrocytic activity, and cortical desynchronization each playing a part. In the context of wakefulness, the asymmetric feature with steeper ascending slopes can be explained through several key factors intrinsic to this state of consciousness.

The elevated median asymmetry values observed in wakefulness, characterized by steeper ascending slopes, can be understood as a nuanced interplay of the unique neurochemical, cellular, and network dynamics inherent to this state. Existing factors such as heightened extracellular potassium levels and upregulated glutamatergic signalling set the stage for quick neural depolarization, lending credence to the rapid engagement reflected in the steeper ascending slopes of the spikes [154]–[157]. In this context, the rapid depolarization can be viewed as a specialized neural function that prioritizes quick, localized engagement over prolonged, global activity. Moreover, the generally desynchronized state of neural activity during wakefulness may serve a dual role in shaping these steeper slopes [122]. By keeping neighbouring neurons in various states of activity, this desynchronization could effectively limit the spatial spread of the Paroxysmal Depolarization Shift (PDS), leading to a rapid peak in localized synchronous firing. Thus, the heightened asymmetry in wakefulness may represent an optimized neural strategy for achieving rapid, localized coordination against a backdrop of global desynchronization.

In summary, the dominant asymmetry during wakefulness can be seen as an optimized state, allowing for the rapid onset of PDS and synchronous firing when needed, while also being primed for quick inhibition. It encapsulates a brain optimized for alertness, responsiveness, and rapid information processing, underlining the intricate balance the brain maintains across various states of consciousness.

NREM Sleep

The intriguing trend of an increasing spike asymmetry ratio from NREM1 through NREM3 defies initial expectations, especially given the pronounced inhibitory environment in deeper NREM stages. Yet, a comprehensive understanding of the neural and chemical landscape across these stages offers nuanced insights into why this happens.

As previously discussed, when sleep progresses into its deeper stages, there is a notable decline in excitatory glutamatergic and cholinergic activities, alongside an increase in inhibitory GABAergic activity [28], [65]. One might hypothesize that, given these processes, the slopes would be more symmetric or even more prominently descending, due to the reduced excitatory activity and the progressive increase in GABAergic activity. However, this simplistic expectation does not fully explain the observed increase in the asymmetry towards a predominant ascending slope as sleep deepens. This anomaly may be attributed to synchronous neural events such as spindles, complexes, and slow-wave activity. Spindles are predominantly associated with N2 sleep, while slow-wave activity is characteristic of N3 sleep; K-complexes, on the other hand, can occur at any time in N2 or N3 sleep [9], [14]. Network dynamics appear to play a role in regulating these neural events, with N3 exhibiting the greatest degree of synchrony, likely contributing to more activation than deactivation, followed by N2, and with N1 being the least synchronous among the NREM sleep stages. These events potentially outweigh the inhibitory effects on the brain, enabling PDSs to return to baseline more quickly than anticipated. As sleep progresses into deeper stages, one would expect a decrease in neural energy and more dominant inhibitory processes [187]. Surprisingly, however, the spikes observed during these stages show a steeper and more dominant ascending slope, as opposed to a descending one. This indicates not only a potentially slower inhibitory response but also suggests a rapid summation of surrounding neurons firing. This pattern is intriguing as it seemingly contradicts the anticipated reduction in neural energy and activity typical of deeper sleep states.

Adenosine, another key neurotransmitter, offers insights into why spikes become increasingly asymmetric dominated by the ascending slope as one transitions into deeper sleep stages. Sleep pressure, a phenomenon governed by the accumulation of adenosine during wakefulness and its subsequent decrease during sleep, warrants investigation [174], [203]. It is important to note that during prolonged wakefulness, such as sleep deprivation, adenosine levels do not uniformly rise across all brain areas. Instead, an increase in adenosine is observed relatively selectively in the wake-promoting basal forebrain area [204]. To a lesser extent, the cortex also experiences a rise in adenosine, although levels in both regions generally decrease as sleep progresses. During slow-wave sleep, characterized by synchronous neuronal activity, the lower levels of adenosine in the brain are associated with reduced inhibition of cholinergic neurons in the basal forebrain, potentially

contributing to the maintenance of this synchronized state. As previously discussed, this synchronized state may influence the steeper ascending slopes as a product of large-scale synchronized neuronal firing that drives the PDS. It is important to clarify that adenosine primarily acts through A1 receptors, which are inhibitory [204]. Reduced adenosine levels, therefore, may create a less inhibited neural landscape. Activation of A1 receptors plays a protective role against neural hyperexcitability, particularly during sleep. A study by [205] found that mice lacking A1 receptors—or those treated with an A1 antagonist—showed faster spread of cortical hyperexcitability compared to their wild-type counterparts. This could suggest that lower levels of adenosine during NREM3 may contribute to the faster ascending slopes observed. The study also highlighted that the frequency and amplitude of local field potentials were largely consistent across different groups of mice, except for an increase in amplitude in mice lacking A1 receptors. This suggests that A1 receptor activation does not significantly alter spike morphology. Interestingly, the study negated cellular ATP as the source of adenosine, indicating that A1 receptor activation is not driven by ATP breakdown. Cellular ATP usually serves as an energy currency within the cell, and its role as a precursor for adenosine in other contexts had led to assumptions that it might be the source here as well. However, this finding leaves the door open for other cellular sources of adenosine, possibly specific types of neurons or glial cells like astrocytes. In summary, the decrease in adenosine during deeper sleep stages like NREM3 could modulate the speed of spike ascension, and perhaps even trigger a rapid release of adenosine to inhibit the activity, producing a steep descending slope.

REM Sleep

As previously discussed within the ascending and descending slope sections, during REM sleep, ACh levels are elevated, leading to an environment within sleep that possesses additional excitatory neural potential; indicative of the desynchronized brain activity commonly observed during this phase of sleep [29], [55]. Acetylcholine directly modulates ion channels, including potassium channels [113]. High ACh levels could stabilize membrane potentials by reducing potassium efflux, thus prolonging the depolarization phase of neurons. In essence, neurons are less likely to rapidly discharge and reset, leading to a more gradual and controlled spike on EEG, both in its rise and fall.

On the inhibitory side, GABAergic activity is less prominent in REM sleep compared to NREM sleep [105], [106]. Reduced GABAergic inhibition means that the descending phase of the spike, which is generally associated with inhibitory processes taking over, would occur more gradually. This reduced inhibitory drive could lead to a slower termination of the paroxysmal depolarization shifts (PDSs), thereby causing a more gradual descending slope.

Astrocytes could add another layer of control. They actively participate in neurotransmission by releasing gliotransmitters that modulate synaptic activity [152]. In an environment where excitatory and inhibitory activities are closely balanced, astrocytes could act as a stabilizing factor, further smoothing out abrupt changes in membrane potentials and neurotransmitter release. This could contribute to the observed symmetry between the ascending and descending slopes of spikes.

The raw montage demonstrates an interesting perspective identifying a noticeably steeper descending slope versus ascending. This could result from utilizing the raw information from the montage versus the more global/surrounding information of other montages. Alternatively, it may reflect the unique characteristics of REM sleep, one of which including a more steadily sustained ACh and GABAergic activity, leading to a faster descending slope compared to the ascending one [98].

In summary, REM sleep spikes display a unique symmetry, possibly reflecting a finely-tuned balance between excitatory and inhibitory neural processes. Elevated ACh levels may stabilize neuronal membrane potentials, while reduced GABAergic influence likely slows down the termination of paroxysmal depolarization shifts (PDSs). This balance could contribute to the spike symmetry observed across different EEG montages, albeit with slight variations in slope steepness depending on the specific conditions of REM sleep.

5.1.4 Spikiness/Pointiness

The spikiness metric, represented by the angle between the ascending and descending slopes of a spike, serves as an indicator of the rapidity and intensity of both excitatory and inhibitory neural processes during a PDS event. Larger, blunter angles suggest slower processes, whereas smaller angles indicate rapid, sharp transitions. Across montages, we observed general trends but also some variability (Figure 18). For instance, in both Laplacian and Referential montages, NREM1 and NREM2 did not significantly differ, while all other two state combinations did. In the Raw montage, the combination between NREM1 and NREM2 is also not significant in conjunction with the combinations of Awake states, except for its comparison with NREM1, which showed statistical significance.

The data revealed a gradation in spikiness, moving from sharper angles in the Awake state to increasingly blunt angles through NREM3-NREM2-NREM1 stages and culminating in the REM stage. Although the distinctions between Awake and NREM3, as well as between NREM2 and NREM1, were minor, a pronounced shift towards blunter angles was evident when transitioning to REM.

Wakefulness

The pronounced sharpness in spikiness observed during wakefulness—indicated by the smallest angles between ascending and descending slopes—can be interpreted as a hallmark of this state's unique metabolic, neurochemical, and network dynamics. This acute angular measure aligns well with the heightened metabolic and neurochemical activity previously discussed [71], [154]–[157]. In wakefulness, upregulated excitatory signalling and elevated extracellular potassium levels are conducive to rapid neuronal depolarization, while robust GABAergic activity and efficient ion channel kinetics support swift hyperpolarization [78], [191]–[193]. These inhibitory countermeasures are critical, especially considering the higher propensity for excitatory processes in wakefulness that could otherwise lead to runaway excitation in the case of epileptiform spikes. Additionally, heightened astrocytic activity during wakefulness plays an essential role in ionic buffering and neurotransmitter regulation, serving as a potential extra layer of inhibitory control [154]–[157]. The desynchronized neural activity prevalent during wakefulness may further contribute by localizing these rapid shifts in excitatory and inhibitory processes, resulting in smaller angles and sharper spikes. All these factors together suggest that the high degree of spikiness in wakefulness might represent an evolutionary optimization for the rapid, yet controlled processing demands inherent to this state.

NREM Sleep

One of the most captivating aspects of spikiness is the contradictory notion that NREM3 spikes show both a higher degree of asymmetry and a sharper peak, compared to the more symmetrical spikes in lighter stages of NREM sleep. One way to conceptualize the difference in PDS morphology between the various stages of NREM sleep, specifically regarding the sharpness and symmetry, could be through the temporal precision of the underlying ionic mechanisms. In the context of a Paroxysmal Depolarizing Shift (PDS), 'sharpness' characterizes the neuron's capacity for swift depolarization followed by rapid hyperpolarization. This reflects the neuron's proficiency in reaching a synchronized peak firing state and its subsequent prompt inhibition. 'Symmetry', on the other hand, denotes the equilibrium between the depolarizing and hyperpolarizing forces within the neuron. This balance is indicative of the neuron's coordinated excitatory and inhibitory responses during the PDS event. The sharper spikes can be characterized as a result of faster ion channel kinetics, specifically those of voltage-gated sodium and potassium channels. Other ions such as calcium can also contribute. In deeper stages of NREM sleep, there is a surge in low-frequency oscillations, often linked to elevated intracellular calcium levels [154]–[157]. In lighter stages of sleep (NREM1 and NREM2), ionic mechanisms and receptor-mediated processes might be less temporally precise than in deeper stages (NREM3). For instance, the opening and closing kinetics of voltage-gated calcium channels might be slightly delayed or desynchronized with respect to other channels

involved in the depolarization and subsequent hyperpolarization phases of a PDS. This could lead to a blunter and more symmetric spike, as neither the depolarizing nor hyperpolarizing phase dominates the other in terms of speed and amplitude. On the other hand, in deeper stages of sleep like NREM3, the precise temporal coordination of various ion channels and receptors may contribute to both the sharpness and asymmetry of the spikes. As mentioned earlier, elevated intracellular Ca^{2+} levels could facilitate a rapid and steep depolarizing phase. The rapid activation of inhibitory mechanisms, perhaps mediated by specialized receptor subtypes or downstream signalling pathways, could then quickly counter this depolarization, resulting in a sharp but asymmetric spike. The heightened temporal precision in deeper sleep might allow for a more rapid and coordinated interplay between these excitatory and inhibitory forces, facilitating both the steep ascent and sharp peak of the PDS.

Therefore, the key link between the different sleep stages and their corresponding PDS morphologies could be the temporal precision of the cellular and network dynamics surrounding the PDS peak. In lighter sleep stages, less precise coordination could lead to blunter, more symmetric spikes, whereas in deeper sleep, a heightened level of temporal precision could give rise to PDSs that are both sharper and more asymmetric.

REM Sleep

Similar to asymmetry, elevated levels of ACh from the pedunculopontine and laterodorsal tegmental nuclei could contribute to more prolonged excitatory mechanisms, leading to increased desynchronization and greater resistance to PDS formation and termination [47], [113], [142], [171]. Meanwhile, reduced GABAergic activity during REM could slow down the inhibitory processes [105], [106]. These more leisurely excitatory and inhibitory mechanisms could collectively lead to blunter spikes, corresponding to a larger angle between the ascending and descending slopes.

Astrocytes, too, may play a role in shaping this dynamic by modulating synaptic activity through gliotransmitter release [152]. They could serve as a stabilizing influence that further smooths out abrupt changes, leading to a more rounded or blunter spike appearance in EEG.

Additionally, REM sleep features muscle atonia and sensory isolation, which might further dampen artifactual rapid oscillations that may have contributed to a pointier spike. These unique conditions could contribute to the broader angle and thereby the blunter spikes observed in REM sleep.

5.1.5 Peak height

The peak amplitude serves as a direct measure of the maximum synchronized neuronal depolarization during a PDS, without any baseline referencing or normalization. Across different montages, the level of statistical significance varied between sleep-wake states, although the comparison between NREM1 and NREM2 remained consistently non-significant (Figure 20). In the Referential montage, no significant differences were observed between the Awake and REM states. Likewise, in the Raw montage, comparisons between NREM2 and NREM3, as well as between NREM1 and all states except REM, were not statistically significant. Overall, the general trend across all montages showed that REM had the lowest peak amplitude, which then increased progressively through Awake, NREM1, NREM2, and NREM3.

Wakefulness

The comparatively lower peak amplitude observed during wakefulness—higher only than REM but trailing all other sleep stages—may be informed by a confluence of unique neurochemical and network properties inherent to this state. As previously discussed, wakefulness is marked by desynchronized neural activity [29], [122], [127], which could naturally limit the potential for broad-scale neuronal synchronization, thereby capping the peak amplitude.

This amplitude restriction could also be considered an outcome of active inhibitory mechanisms, specifically, the role played by GABAergic interneurons and specialized ion channels [78]. These mechanisms serve as a biological failsafe against potentially dangerous runaway excitatory processes.

Moreover, the baseline oscillatory activity of the brain during wakefulness, characterized by low-amplitude mixed frequencies, may play a crucial role in influencing the height of the peak amplitude feature [9]. When the peaks are not normalized against this baseline activity, their relative size can be misleadingly perceived as smaller. This may be attributed to the inherent low-amplitude state of the brain's electrical activity during wakefulness, as opposed to other states with higher amplitude oscillations.

When normalized, these peaks actually rival or even exceed those observed in NREM3, revealing that the raw intensity of the excitatory and inhibitory processes may actually be quite similar across these states but masked by differing baseline activities. This phenomenon will be further reviewed in the normalized height sections to follow.

In summary, the specific characteristics of wakefulness, from active inhibitory processes to baseline neural oscillations, collectively contribute to the observed peak amplitude, painting a complex but coherent picture of neuronal behaviour in this state.

NREM Sleep

The observed increase in peak amplitude from NREM1 to NREM3 adds to the understanding of how sleep stages are differentiated at the neuronal level. As the transition moves from lighter to deeper sleep, there is a discernible uptick in the amplitude of these spikes. As previously discussed, increasing GABAergic and reduced excitatory responses might be paradoxical, considering that deeper stages of sleep are often considered less excitable than lighter ones or even the awake state. However, this amplitude escalation could be a manifestation of heightened neural synchrony, particularly driven by network processes such as thalamocortical interactions that are known to facilitate synchronous activities. The elevated synchrony enables a larger pool of neurons to fire almost simultaneously, resulting in larger amplitudes for each spike.

Substantiating this narrative are several physiological mechanisms. For example, while excitatory neurotransmitter activity like that of cholinergic and glutamatergic systems decreases as we enter deeper stages of sleep, inhibitory GABAergic activity rises [28], [55], [65], [137]. This shift in neurotransmitter dynamics is suggestive of a transitioning of brain activity from wakefulness-dominated regions to those governing sleep. which sets the stage for unique phenomena like sleep spindles and slow-wave activity to take place, predominantly in NREM2 [9]. Such synchronous neural events could be the driving force behind the observed higher peak amplitudes in PDSs at this stage as it may allow more neurons to fire in unison, creating a larger overall dipole, which is reflected as increased amplitude in EEG readings.

Additionally, ion channel activity plays a significant role. As sleep deepens, the density and kinetics of voltage-gated sodium and calcium channels may change [154]–[157]. The modulated activity of these channels could allow for a faster and more potent depolarization during a PDS event, thus contributing to the escalating peak amplitudes across NREM stages. The role of intracellular calcium levels is noteworthy, too, as they increase during slow-wave sleep and could serve as another facilitating factor for the heightened synchrony and thus larger peak amplitudes.

In essence, the augmented peak amplitudes in deeper NREM stages are likely a byproduct of heightened neural synchrony, shaped by intricate neurotransmitter dynamics and ionic processes.

REM Sleep

The finding that REM sleep has the lowest median peak height, signifying the least amount of synchronized firing among neurons, is paradoxical given that REM sleep is typically characterized by high levels of neural excitability similar to the awake state [64], [65]. Further complicating the picture is the role of kainate receptors, which are more active during REM and are known to modulate the first action potential in a PDS, as well as increase the number of synchronously firing neurons [67], [86]–[88]. This counterintuitive result may suggest that activities such as REM's desynchronous like activity, and of ACh and GABA, are more influential in determining synchronization levels, possibly reducing the impact of glutamate-mediated kainate receptor activity.

Cholinergic activity is heightened in REM sleep [47], [142], [171]. While ACh generally acts as an excitatory neurotransmitter, it also has modulatory effects on various ion channels, including potassium channels [113]. This modulation could potentially stabilize membrane potentials, leading to less extensive areas of synchronized dendritic depolarizations.

Additionally, GABAergic activity, which is generally inhibitory, is lessened in REM sleep [105], [106]. The reduced inhibitory activity could lead to a state where neuronal groups are less coordinated by inhibitory processes, potentially disrupting large-scale synchronized activity.

Astrocytes could also play a role in this context from regulating ions, neurotransmitter re-uptake, energy synthesis and more. In the perspective of regulating desynchronous like activity these glial cells can release gliotransmitters that modulate synaptic activity, and they are thought to play a role in regulating neural synchrony [152].

5.1.6 Normalized Ascending Height

The normalized ascending height, measured from the beginning of the ascending slope to the peak, offers a baseline-adjusted metric representing the number of synchronized neuronal firing by area from the onset of the PDS to its peak. Across montages, the results were largely consistent, showing significant differences between most states. Exceptions were found in the combinations of NREM1 and NREM2, and NREM3 and Awake in both the Laplacian and Referential montages (Figure 22). A similar trend was observed in the Raw montage, where the only non-significant pairing was between NREM1 and NREM2. The median normalized ascending height results revealed that REM had the lowest amplitude. It was followed by similar heights for NREM1 and NREM2, which were approximately 1.7 times taller than those in REM. NREM3 and Awake displayed comparable, but slightly taller heights than NREM1 and NREM2. However, the Raw montage deviated slightly, again indicating REM had

the smallest height; however, it is now followed by Awake, and then similar heights for NREM1 and NREM2, with NREM3 displaying the tallest height.

Wakefulness

The divergent findings for normalized ascending height in the awake state—showing comparable heights to NREM3 in the Laplacian and referential montages, but a more expected shorter height in the raw montage—demand a nuanced interpretation grounded in our earlier discussions. As previously outlined, the metabolic, neurochemical, and network dynamics during wakefulness promote rapid, desynchronized neuronal activity [29], [127], [154]–[157]. These characteristics might naturally lead one to expect shorter ascending heights, a notion supported by the raw montage which may possibly be due to desynchronous firing lowering the maximal number of neurons synchronously firing during a PDS.

While the raw montage has been noted for its direct unfiltered representation of brain activity, this advantage may be overshadowed by its susceptibility to noise, particularly in states of wakefulness where muscle artifacts and external interferences are prevalent. Unlike the Laplacian or referential montages, which employ spatial filtering and referencing techniques to mitigate noise, the raw montage can inadvertently amplify these unwanted signals. This amplification of noise can inadvertently amplify these disturbances due to its reliance on a potentially contaminated reference electrode. In this context, the apparent advantages of the raw montage in capturing unaltered neural signals could be misleading. Therefore, while the raw montage offers an unfiltered view of brain activity, its practical application is limited by its vulnerability to noise interference. In contrast, the Laplacian and average-reference montages, despite their potential for spatial distortion, could provide a more reliable and cleaner representation of neural activity, particularly in noise-rich environments such as wakefulness. The observed discrepancies in ascending height across different montages thus underscore the critical importance of montage selection in EEG studies.

NREM Sleep

The results demonstrate a clear variance in peak amplitude during different sleep stages: NREM 1 and NREM 2 stages have the shortest amplitude heights. On the other hand, the NREM 3 stage, being a deeper and more synchronous stage, facilitates the largest amplitude difference. This difference is notably larger than that of the REM stage, and this observation remains consistent, irrespective of the montage used.

As previously discussed, the synchronization particularly profound in NREM3, may be the primary contributor to the heightened ascending heights observed in NREM3, representing more neurons firing in sync from the onset

of the PDS to its peak. Additionally, the role of astrocytes could potentially aid in contributing to this crescendo in ascending height as they contradict the general trend of decreasing glutamate levels throughout sleep. In fact, [143] discusses that the surge in glutamate levels not only occurs during state switching, but it is also linked to the higher amplitudes observed during slow wave activity. Therefore, the results are indicative that perhaps the synchronous process governed by astrocytic glutamate release might contribute to the summation of EPSPs within the PDS, potentially resulting in larger peaks.

REM Sleep

The relatively low height within REM sleep is intriguing given the general excitatory nature of this sleep stage [64], [65]. While REM sleep shares similarities with wakefulness in its desynchronized EEG patterns, the underlying neural mechanisms appear distinct. For example, acetylcholine release from the PPT and LDT nuclei is known to be high during REM sleep, modulating the thalamocortical and possibly cortical-cortical networks reducing their synchronous effects [21], [26], [27], [47], [113], [122], [142], [171]. Elevated ACh levels might stabilize membrane potentials by affecting ion channels like potassium channels, thereby resulting in a lower magnitude of synchronous depolarization from the onset of paroxysmal depolarizing shifts (PDS) to their peak [29], [113].

Moreover, REM sleep's reduction in GABAergic—specifically from the ventrolateral preoptic area—and decrease in orexinergic activity could mean that inhibitory processes are less likely to shape a large-scale synchronous activity, leading to a lower height in the ascending slope [55], [115]. This could work in concert with the unique activity of kainate receptors, which are known to be more prominent in REM sleep. While these receptors encourage localized neuronal firing, they might not facilitate widespread synchronization as effectively as NMDA receptors, which are more active during wakefulness [67].

5.1.7 Normalized Descending Height

The Normalized Descending Height serves as a measure of the inhibitory processes that return the spike to baseline or further, depending on the intensity of inhibitory effects applied to quell synchronous firing during a PDS. Results shows that REM consistently exhibits the shortest normalized descending height across sleep-wake states (Figure 24). A distinct trend appears, with median heights gradually ascending from NREM1 through NREM2 to NREM3 across all montages. The Awake state presents a more complex profile: in the Laplacian montage, its median is similar to NREM3; in the Referential montage, it is around the NREM2 range; and in the Raw montage, it is as low as REM. This variability in the Awake state may point to unique dynamics that affect its

representation across montages. The discrepancy could possibly be attributed to the RAW montage having the worst signal-to-noise ratio compared to the referential and Laplacian montages.

Wakefulness

Given the varying results across montages for the normalized descending height during wakefulness, a nuanced interpretation is called for, consistent with the previous discussions on the dynamics of wakeful brain activity. As previously mentioned, the wakeful state is marked by rapid, desynchronized neural activity, characterized by upregulated excitatory signalling and robust inhibitory countermeasures [29], [127], [154]–[157]. These neural dynamics, including the coupled feature of an overall lower ascending height, suggest a rationale for expecting shorter descending heights in wakeful spikes. Firstly, the heightened excitatory activity during wakefulness suggests that neurons are firing more frequently, necessitating a quicker “reset,” which results in a possible shorter descending height. Secondly, the effective inhibitory countermeasures during wakefulness ensure that the spike is quickly dampened after reaching the peak, contributing to a possible reduced descending height. This pattern aligns with the brain's requirement for rapid, responsive processing in the wakeful state, where neurons must quickly recover post-firing to maintain an elevated level of cognitive functionality.

The varying results across montages underline the importance of carefully selecting the appropriate montage when investigating the complexities of inhibitory processes, particularly during wakefulness. The discrepancy could possibly be attributed to the RAW montage having the worst signal-to-noise ratio compared to the referential and Laplacian montages. These discrepancies serve as a cautionary note for electrophysiological studies and emphasize the need for more research to understand the interplay between montage selection and the reliable representation of neural dynamics.

NREM Sleep

The data clearly reveals an increasing trend in normalized descending heights from NREM1 through to NREM3. This phenomenon can be largely attributed to the sleep stage-specific neurotransmitter environment, particularly the higher GABA-to-ACh ratio prevalent in deeper NREM stages [28], [29]. Elevated GABA levels in deeper sleep phases, in conjunction with reduced levels of excitatory neurotransmitters like glutamate [65], lay the foundation for a stronger inhibitory state. This would naturally favour a faster and more robust descending slope, aligning with the observation of larger normalized descending heights in throughout deepening sleep.

Additional factors further amplify these descending heights. It is essential to consider that the measurements start from already elevated peaks within NREM. In combination with possible hyperpolarizing forces post-peak,

this could create an environment to solidify their larger amplitudes. Astrocytic ion buffering could be instrumental here; it modulates extracellular concentrations of ions like potassium, calcium, and magnesium [154]–[157]. Reduced extracellular potassium may reflect baseline hyperpolarization, thereby contributing to greater descending heights.

Lastly, synchronous neural activity, which plays a significant role in shaping the ascending characteristics of spikes in NREM sleep, could be equally crucial in determining the descending dynamics [23]. The high degree of synchrony might act as a powerful conductor, harmonizing the inhibitory mechanisms during the descending phase of the spike, further amplifying its height.

REM Sleep

Reduced GABAergic activity in REM sleep diminishes the efficacy of Cl^- influx via $GABA_A$ receptors, potentially lessening or even negating hyperpolarization [105], [106]. This finding is noteworthy, given that hyperpolarization usually serves to counterbalance the rapid sequences of action potentials seen in paroxysmal depolarizing shifts (PDS) [32], [41]. Therefore, the decreased Normalized Descending Height observed during REM may reflect weaker inhibitory post-synaptic potentials (IPSPs) rather than traditional hyperpolarization events. From the perspective of scalp EEG, this suggests that neurons are less likely to generate strong IPSPs during REM sleep, which means lower likelihood of baseline hyperpolarization, thereby leading to a shorter Normalized Descending Height. This is also consistent with the more gradual descent observed in the descending slope.

In parallel, the descending height of an epileptic spike is closely tied to the amplitude of the preceding excitatory peak. Given that REM sleep exhibits the lowest amplitude in ascending height, this influences the reduced need for repolarization, contributing to the lower Normalized Descending Height observed.

Furthermore, elevated levels of acetylcholine during REM sleep act on voltage-gated K^+ channels to expedite repolarization [29], [113]. This swift return to baseline could occur without a proportional increase in hyperpolarization, due to the aforementioned GABAergic inhibition reduction, ultimately lowering the Normalized Descending Height.

5.1.8 Duration/Length

The duration of a spike, measured from the onset of the ascending slope to the end of the descending slope, encapsulates the time required for a group of neurons to fire synchronously during a PDS and subsequently return to a less excitable state. Results across sleep-wake states indicated that while the sleep states (REM and

NREM stages) showed general similarities in spike duration, the Awake state stood apart, showing significant differences (Figure 26). Notably, in all montages, the median duration of spikes in the Awake state was almost half that in other states, underscoring the unique dynamics of wakefulness compared to sleep stages.

Wakefulness

The notably shorter duration of spikes during wakefulness in comparison to sleep states can be construed as another manifestation of the unique neurophysiological conditions prevalent in the awake state. As previously discussed, wakefulness is characterized by rapid, desynchronized neural activity and a high metabolic rate, along with efficient excitatory and inhibitory processes [29], [127], [154]–[157]. These factors contribute to the quick engagement and disengagement of neuronal populations, leading to shorter durations for each PDS event.

Given the swift dynamics of both excitatory and inhibitory processes during wakefulness, the shorter spike duration aligns well with the previously discussed features, such as heightened spikiness and rapid ascending slopes [78], [191]–[193]. These factors collectively suggest that the awake brain is optimized for rapid yet controlled neural processing, which is vital for the real-time cognitive and motor demands inherent to this state.

The shorter spike duration in wakefulness further corroborates the idea that this state prioritizes quick engagement and disengagement over sustained activity, offering another layer of insight into the unique neurophysiological behaviour of the awake brain [29], [127], [154]–[157]. This adds to the accumulating evidence that various neural features during wakefulness are interrelated and contribute to the state's specialized functional demands.

NREM Sleep

It is intriguing to note that despite the distinct peak heights, ascending slopes, and descending slopes across NREM stages, the duration of spikes appears to be constant between NREM stages. This consistency in duration suggests a fundamental characteristic of Paroxysmal Depolarization Shifts (PDS) that remains unaltered across different depths of NREM sleep. One could argue that the constant duration is a result of a finely-tuned orchestration of various processes in the brain from the neurotransmitter levels, ion channel kinetics, astrocytic activity, and network dynamics harmonizing to rectify the rapid successive firing. In this framework, the transient and rapid depolarization of neurons, characteristic of a PDS, is facilitated by excitatory neurotransmitters like glutamate and modulated by ions like sodium and calcium [41]. Following the peak, inhibitory processes, likely involving neurotransmitters such as GABA and regulated by ions like potassium, act swiftly to terminate the depolarization and lead to hyperpolarization [28], [65]. Astrocytic activity further adds a layer of regulation,

potentially through ion buffering, gliotransmission and various other homeostatic regulating features [154]–[157]. Network dynamics, including synchronous activity and slow-wave activity, may serve as the overarching framework that guides these cellular and molecular processes to occur within a stable time window across different NREM stages [24]. Thus, the consistent duration might represent an evolutionary optimized 'set point' that balances the need for synaptic activation and subsequent inhibition, all while accommodating a range of physiological changes associated with different sleep stages.

REM Sleep

In REM sleep, one intriguing finding is the consistently longer duration of spikes compared to wakefulness, and similar lengths across all other sleep states. Firstly, the longer spike durations in REM sleep, in contrast to awake, could be attributed to reduced GABAergic inhibition, as mentioned in the preceding sections. Weaker inhibition could slow down the resolution of neuronal activity, leading to longer-lasting synchronous events. Specifically, the diminished efficacy of Cl^- influx through $GABA_A$ receptors may prolong the interplay between excitatory and inhibitory mechanisms [105], [106].

Additionally, the already noted elevation of acetylcholine levels in REM sleep could play a role. High levels of acetylcholine primarily serve as an excitatory influence on neuronal activity, impacting the overall summation of excitatory versus inhibitory postsynaptic potentials (EPSPs and IPSPs). However, its role is more complex than simply creating a more excitable influence. According to the cholinergic desynchronization hypothesis, acetylcholine can disrupt the usual synchronized firing of neurons. This desynchronization inhibits the temporal and spatial summation of EPSPs and IPSPs, which may manifest as extended, or slower, spike durations in the overall neural activity [29], [113].

Furthermore, the intrinsic properties of neurons and network dynamics during REM sleep may also contribute to these longer durations. Again, as previously discussed, specific regions designated to REM may contribute to a slower summation of synchronous firing, leading to a more gradual ascending slope [47], [190].

In summary, the longer durations of spikes in REM sleep compared to wakefulness could arise from a confluence of factors that have been gone into depth, spanning from the ascending and descending slope mechanics, including their respective amplitudes designating the overall speed and number of neuronal firing summations and overall inhibitory soothing of the PDS.

Despite both wakefulness and REM sleep exhibiting desynchronous activity, they exhibit markedly different spike morphologies while sharing similarities with other sleep states. This lengthened duration is a complex interplay

of factors that have been discussed in detail throughout this section. These include the rate and extent of neuronal firing summations encapsulated within the ascending and descending slopes, as well as their respective amplitudes. These elements collectively shape the paroxysmal depolarizing shift, culminating in the unique spike durations observed in REM sleep.

5.1.9 Area of Spike (Summary of Features)

The area under the spike serves as an integrated metric that encapsulates various facets of the spike's profile, providing a composite snapshot of the biophysical dynamics at play. This metric essentially quantifies the total 'energy' or intensity invested throughout the PDS, from the onset of excitatory phases to the subsequent inhibitory termination. Notably, each of the preceding metrics—be it the ascending and descending slopes or the amplitude—contributes to shaping a specific 'energy landscape' for each spike. In REM sleep, for example, lower peak amplitudes coupled with more gradual slopes result in less intense but enduring PDS events, possibly reflecting a complex interplay of excitatory and inhibitory mechanisms governed by unique neurochemical settings.

Statistical analysis across sleep-wake states disclosed a clear hierarchy in spike areas (Figure 28). Across all montages, NREM3 consistently exhibited the largest spike area, followed in descending order by NREM2, NREM1, Awake, and finally REM. The spike areas for NREM1 and NREM2 were relatively similar, and in some montages, the Awake state occasionally did not significantly differ from these stages, although it generally registered lower values closer to those of REM.

Wakefulness

The area of spikes during wakefulness offers a compelling narrative that integrates various characteristics, such as spike duration, ascending and descending heights, and their slopes. Notably, across both Laplacian and referential montages, the spike area during wakefulness is smaller than during NREM sleep but larger than during REM sleep. In contrast, the raw montage indicates an even smaller spike area than that observed during REM sleep. These observations complement our understanding that wakefulness is a state characterized by high metabolic, neurochemical, and network activity, yet it is also marked by rapid and efficient neuronal engagement and disengagement [29], [127], [154]–[157].

An interesting feature is the steep slopes and potentially lower amplitudes (as observed in raw montages) during wakefulness, which are reminiscent of the medians seen in REM sleep. Despite REM sleep having fundamentally different underlying processes, it shares similar desynchronous dynamics with wakefulness. This similarity draws

attention to the role of astrocytes, which are known to regulate a broad range of brain functions and could serve as a potential layer of control for these seemingly disparate yet analogous features [154]–[157]. Astrocytes are vital for ionic buffering and neurotransmitter regulation, and they may significantly influence the “energy landscape” of individual spikes. Supporting these observations, the wakeful state is known to have a higher and more stable level of ATP compared to sleep, which provides the necessary energy not only for astrocytic regulation but also for rapid neuronal responses [188]. This likely contributes to the observed smaller spike area during wakefulness.

Our multi-faceted analysis of different spike features in distinct montages unearths a complex landscape that cannot be adequately explained by a single narrative. Importantly, our observations reiterate the critical role of montage configuration in the interpretation of electrophysiological data.

The raw montage, for example, provides an unaltered look at neuronal spikes, thus rendering it invaluable for observing phenomena such as spike duration, which remained consistent across montages. Conversely, the Laplacian and referential montages employ spatial filtering and referencing techniques that result in varying representations of spike characteristics like ascending and descending heights comparatively to the RAW montage. The discrepancy could possibly be attributed to the RAW montage having the worse signal-to-noise ratio compared to the referential and Laplacian montages.

NREM Sleep

Since spike durations between NREM stages remain relatively constant, it appears that the spike area is primarily determined by the ascending and descending heights of NREM spikes, where their area results mimic those from each states’ amplitude metrics where they decrease from NREM3 to NREM 1. As previously discussed, the larger area in NREM3 could be attributed to the higher degree of neuronal synchronization, which results in taller peaks and slopes during this stage [24]. These greater heights are mediated by complex interplay of neurotransmitters like glutamate and GABA, and regulated by ion kinetics involving sodium, calcium, and potassium [28], [41], [65]. Astrocytic activity further complements these molecular mechanisms by contributing to ion homeostasis and possibly the synchronous neural activities that characterize deeper stages of NREM sleep [154]–[157].

In summary, the variation in spike area across NREM stages serves as a compelling metric that encapsulates various biophysical and neurochemical processes. As one transitions from lighter to deeper sleep stages, there is an increase in the 'energy' invested in each PDS event, possibly reflecting a more rigorous synchronous network dynamic. Specifically, lighter sleep stages, often characterized by sleep spindles, contribute to lower ‘energy’ PDS

events. In contrast, deeper sleep stages, marked by K-complexes and slow-wave activity (SWA), are associated with higher 'energy' PDS events. Therefore, spike area may be directly linked to the network dynamics inherent to NREM sleep, with these synchronous events modulating their overall median values.

REM Sleep

The unique morphological characteristics of spikes during REM sleep—like their gradual ascending and descending slopes, near-symmetry, blunter peaks, lower amplitudes, and longer durations—contribute to their overall lower energy exhibited throughout a Paroxysmal Depolarizing Shift (PDS). Similar to the discussions on NREM, it is evident that in REM sleep, the amplitude levels notably influence the overall "energy" of the spikes as durations are again all similar. This contrasts with the wakefulness state, where the shorter duration of the spikes becomes a primary factor. In both NREM and REM, the lengths of the spikes are relatively similar, highlighting that the key distinguishing feature is the amplitude of both the ascending and descending heights. Therefore, the lower amplitude levels within REM spikes appear to be the driving factor that orchestrates their lower total energy; driven by the excitatory and inhibitory processes that partake in modulating the number of synchronous neuronal firings during a PDS. This leads to an overall lesser effect of neuronal synchrony and proliferation of synchronous neuronal firing, without expanding from the spike's area of origin. Concurrently, as discussed previously, inhibitory effects may provide a slower return to baseline within the excited area and possibly with a reduced hyperpolarization.

5.2 Synthesis: Potential Mechanisms Describing REM Sleep's Major Morphological Differences

In this section, we discuss the uniqueness of REM spike morphology comparatively to all other sleep-wake states. The sole quantitative experimental study [152] comparing normal and kindled REM in mice highlights that astrocytes in the lateral hypothalamus during normal REM display reduced intracellular calcium and pH (becoming more acidic) and an increased blood brain volume (BBV). In contrast, during kindled REM, these astrocytes become even more acidic without the other changes observed in normal REM.

5.2.1 Astrocytic Regulation of pH and Gliotransmitters (Figure 29)

Orexinergic neurons, while being responsive to a range of stimuli, may predominantly interact with glutamate [206]. This excitatory neurotransmitter has the potential to directly engage with orexin neuron receptors, via NMDA and other non-NMDA types, establishing a key regulatory mechanism [206].

The extracellular pH's role in directing orexinergic activity is crucial. Specifically, these neurons are remarkably pH-sensitive. For instance, at a pH of 6.9, they can achieve a firing rate of about 4Hz. However, even a slight pH alteration to 7.4 can entirely inhibit their activity [207]. Intriguingly, this pH-dependent firing mechanism is reversible, highlighting the critical nature of extracellular pH in directing orexinergic neuron function [207]. [207] denotes how even a minor extracellular CO2 fluctuation, from 5% to 10%, changes the extracellular pH from 7.25 to 7.02, respectively. This pH variation directly influences the firing rates of orexinergic neurons (0.8Hz and 3.7Hz respectively), underscoring the intricate CO2-pH-activity relationship.

Astrocytes play a central role in this extracellular pH modulation. During increased neuronal activity, particularly in the cortex and hippocampus, an increase in extracellular CO_2 and proton concentration is observed, leading to an acidic extracellular environment [208]. Astrocytes respond by activating various ionic exchangers, with the sodium-bicarbonate cotransporter (NBC) and the sodium-hydrogen exchanger (NHE) being particularly significant. In an acidic milieu, NBC can reverse its usual function, resulting in an efflux of bicarbonate (HCO_3^-), which accentuates the intracellular acidic condition [209]. Concurrently, the NHE, by exporting protons, works towards restoring the intracellular pH balance [209].

Astrocytic response to these changes is not just passive pH adjustments. Elevated intracellular calcium levels in astrocytes, often triggered by an acidic extracellular environment, instigate the release of gliotransmitters, such as glutamate, D-serine, and ATP [210]. This calcium-driven release mechanism, orchestrated by SNARE (Soluble N-ethylmaleimide-Sensitive Factor Attachment Proteins Receptors) proteins (key molecules involved in the transport and fusion of cellular vesicles), can have profound implications on nearby neurons [211]. Specifically, the released glutamate can engage with NMDA receptors on orexinergic neurons, potentially amplifying their activity. Furthermore, the synthesis and release of D-serine in astrocytes can be crucial for the activation of synaptic NMDA receptors, integrating with the understanding of glutamate's primary excitatory action via NMDA receptors [212].

Drawing insights from the intricate processes observed within cortical and hippocampal astrocytes, we can theorize a comparable mechanism at play in the hypothalamus, specifically influencing the activity of orexinergic neurons [208]. Given the pronounced pH sensitivity of orexinergic neurons, the acid-base homeostasis orchestrated by astrocytes could be a pivotal factor in modulating their firing dynamics [207].

Within the domains of the cortex and hippocampus, neuronal firing instigates a discernible acidification trend inside astrocytes, characteristic of their intrinsic role to stabilize the extracellular pH [208]. This internal acidic milieu propels a series of cellular responses: The sodium-bicarbonate cotransporter (NBC) springs into reverse

action, precipitating an outward flow of sodium (Na^+) and bicarbonate. The NHE supports the substantial inward flow of Na^+ to accommodate for the acidification of the astrocyte while also expelling H^+ acidifying the extracellular space. This sodium influx influences the reverse operation of the sodium/calcium exchanger, culminating in a surge of intracellular astrocytic calcium levels [208].

Astrocytes, through these multifaceted processes including the use of specialized membrane proteins like proton pumps and carbonic anhydrase, efficiently intake protons and CO_2 – metabolic remnants of neuronal activity – ensuring the extracellular milieu remains conducive for optimal brain function [208]. The pronounced expression patterns of NBC and intracellular carbonic anhydrase in astrocytes underscore their indispensable roles in the intricate regulation of extracellular CO_2/HCO_3^- buffering [208].

This buffering is integral to the equilibrium where $CO_2 + H_2O \rightleftharpoons HCO_3^- + H^+$ dictates extracellular pH [213]. Elevated CO_2 drives the reaction to produce more bicarbonate and protons, acidifying the environment. As astrocytes release bicarbonate, it can neutralize excess protons. Yet, in CO_2-rich conditions, a net extracellular acidification occurs. Importantly, this acidic milieu prompts calcium influx into astrocytes, crucial for the firing of orexin neurons [210].

5.2.2 How Astrocytic Acidification can Drive Orexinergic Neuronal Firing

Drawing from the detailed understanding of astrocytic processes, attention is now directed towards their potential role in the lateral hypothalamus, specifically around orexin neurons. It is proposed that astrocytes in this region could modulate orexin neuron firing by regulating the extracellular environment and potentially releasing excitatory gliotransmitters. According to [152], two distinct astrocytic states emerge within mice during REM sleep:

1. During normal REM sleep, astrocytes exhibit decreased internal calcium, a more acidic internal environment (acidification), and an increase in brain blood volume.
2. In contrast, during kindled REM (epileptic state), astrocytes no longer exhibit decreased calcium levels, demonstrate heightened acidification, and show no increase in brain blood volume.

In **Scenario 1 (Normal REM)**, the astrocytic environment leans acidic but might not be acidic enough to reverse the NBC's function. This means bicarbonate may not be expelled, and sodium would not be expelled. The NHE should be exporting protons to neutralize the internal environment, further importing sodium. However, the decrease in calcium contradicts the anticipated activity of the sodium-calcium exchanger, suggesting it might not be active. Without the influx of calcium and the subsequent release of excitatory gliotransmitters, orexinergic

neurons may receive minimal stimulatory input. Furthermore, without sufficient extracellular acidification, the environment might not be conducive for orexinergic neuron firing.

Scenario 2 (Kindled REM), in contrast, kindled REM showcases stable calcium levels within astrocytes, even more pronounced acidification, and unchanged brain blood volume. The enhanced astrocytic acidification could drive the NBC to reverse its function, facilitating the efflux of bicarbonate (HCO_3^-). The NHE's activity ensures a potential increase in intracellular sodium in combination with extracellular acidity, permitting the calcium influx dynamic, hinting at an active sodium-calcium exchanger directing calcium inwards. Elevated CO_2, because of the unchanged blood-brain volume, might drive the reaction between CO_2 and water to produce more bicarbonate and protons, thereby acidifying the extracellular environment. Such an acidic milieu is where orexinergic neurons have greatest propensity to fire. The stable calcium levels in this environment can trigger the release of gliotransmitters, potentially providing a strong excitatory stimulus to the orexinergic neurons, amplifying their firing propensity.

In summary, the contrasting astrocytic states during REM sleep, as influenced by pH regulation and calcium dynamics, might hold the key to understanding the excitatory or inhibitory influences on orexinergic neurons. The interplay of ions, particularly the balance of sodium, calcium, and bicarbonate, along with the CO_2-pH dynamic, emerges as a pivotal determinant of neuronal activity.

5.2.3 Why REM Spikes are Significantly Different

The distinct spike morphology in REM sleep may be primarily attributed to the irregular firing of orexinergic neurons, typically dormant in this phase [214], [215]. It is posited that this atypical orexinergic activity, facilitated by astrocytes, might enable the emergence of spikes in a phase where they are typically absent. Such activations could transiently push the neural dynamics towards those observed during wakefulness, potentially modifying spike morphologies to appear more "awake-like". However, the spike morphology during REM is opposite to that during awake which implies other factors such as increased ACh, reduced GABA, and desynchronous network dynamics as modulators of REM spikes where orexin is the initiator. While the precise role of orexin in the genesis of these spikes is still under scrutiny, the combined influence of these elements may offer a plausible explanation for the unique spike characteristics observed in REM [216].

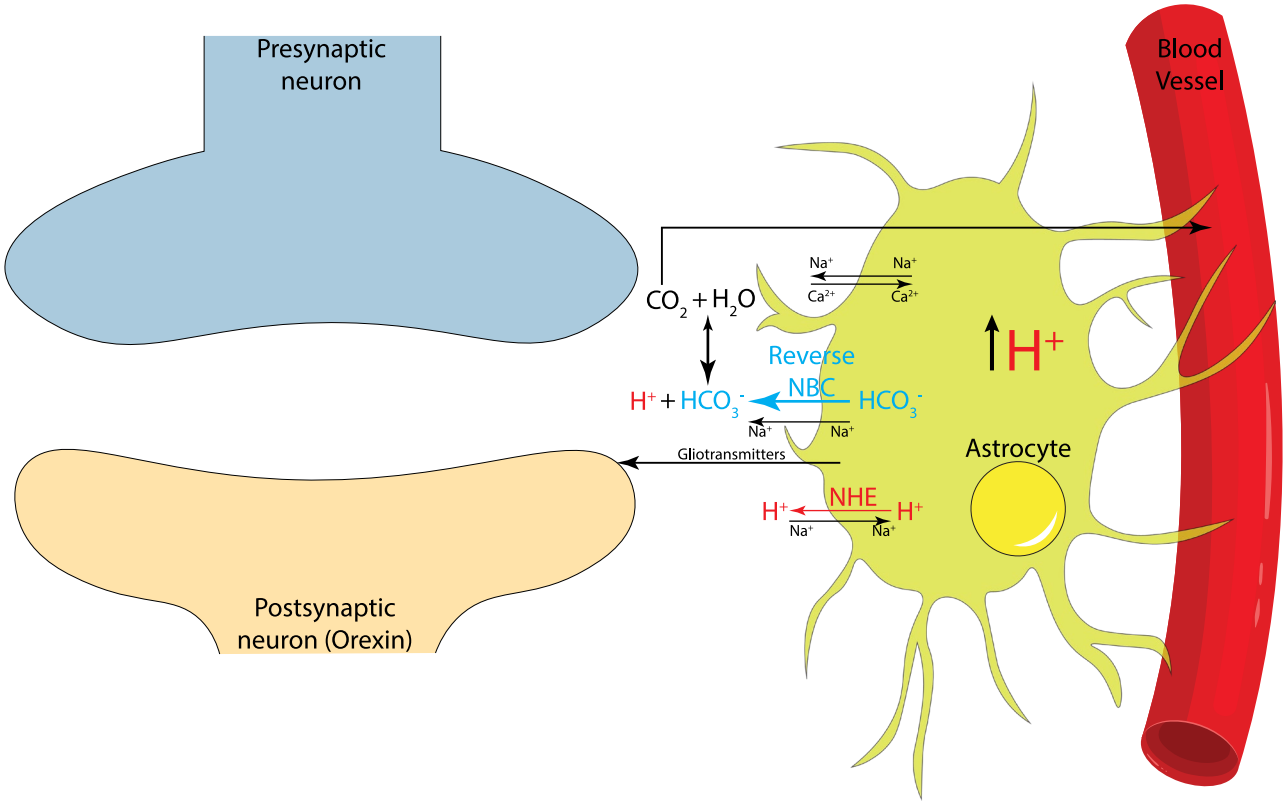


Figure 29: An illustration of astrocytic modulation in the lateral hypothalamus during Scenario 2 (kindled REM). In this context, astrocytes exhibit stable intracellular calcium levels, pronounced acidification, and unchanged brain blood volume. The acidic astrocyte is denoted by an increase of intracellular protons. The intensified intracellular acidification prompts the sodium-bicarbonate cotransporter (NBC) to reverse its function, leading to bicarbonate efflux. Alongside, the sodium-hydrogen exchanger (NHE) imports sodium and balances the intracellular pH. This dynamic, in conjunction with the extracellular acidity, facilitates calcium influx, suggesting an active sodium-calcium exchanger directing calcium inwards. Elevated CO_2, due to the non-increasing brain blood volume, promotes bicarbonate and proton production, acidifying the extracellular environment further. In this acidic milieu, stable influx of calcium into the astrocyte enables gliotransmitter release, notably glutamate, offering a potent excitatory stimulus to orexinergic neurons and potentially enhancing their firing rate.
Source: Figure References [6-7]

The exploration of epileptiform spike morphologies across different sleep-wake states in this thesis reveals a complex interplay of neurophysiological processes that govern these variations. The defining characteristics of spikes in each state—ranging from the steep ascending and descending slopes and dominant asymmetry in wakefulness to the blunter peaks and longer durations in REM sleep—are indicative of the underlying dynamic shifts in neuronal activity. In wakefulness, the desynchronous activity, driven by increased metabolic and excitatory signalling, shapes spikes with sharp features and high peaks, reflecting a state of heightened neural responsiveness. NREM sleep, characterized by synchronous neural activities and a higher overall amplitude state, showcases spikes with fairly steep ascending slopes and greater peak heights within deep sleep comparatively to

REM, influenced by the interplay of neurotransmitters and ion kinetics. REM sleep presents a contrasting scenario, where altered desynchrony, marked by increased acetylcholine and reduced GABAergic inhibition, leads to spikes with near-symmetry, blunter peaks, and lower amplitudes. This unique morphology in REM sleep, potentially driven by the novel interplay of orexinergic-astrocytic modulation and basal forebrain dynamics, underscores the intricacies of epileptiform activity in REM sleep. The comprehensive analysis demonstrates how variations in neurophysiological processes across sleep-wake states are intricately linked to the morphological characteristics of epileptiform spikes, offering insights into the complex mechanisms underlying epilepsy.

6 Limitations

Spatial Resolution and Biological Inferences

The most salient limitation of this study is the inherent constraint on spatial resolution when using scalp EEG. EEG primarily detects the summation of voltage changes from dendritic pyramidal cells, offering limited insights into more localized neural events [14]. This technological barrier hampers our ability to investigate nuanced biological processes, which often evolve rapidly in the dynamic field of neurology. Due to this limitation, our interpretations are reliant on current literature and may be subject to revision as the understanding of neurological processes deepens.

Participant Variables: Age, Epilepsy Syndrome, and Sleep Conditions

The morphological characteristics of EEG spikes can vary significantly with age. For instance, as individuals age, the slopes of spikes tend to become more gradual. Similarly, the spikes themselves become progressively blunter while decreasing in amplitude and their duration increases with age [183].

Likewise, the type of epilepsy syndrome plays a crucial role. Patients with juvenile myoclonic epilepsy (JME), for instance, generally exhibit polyspikes whereas patients with temporal lobe epilepsy classically manifest spikes or sharp waves [217]–[219].

Sleep conditions, including sleep disorders and deprivation, further contribute to these variations. For instance, sleep disorders such as primary insomnia are associated with altered EEG alpha activity potentially disrupting neural networks and manifesting changes in the sleep states such as reduction of duration within states, potentially confounding EEG results [220]. Such alterations can result in slow-wave activity deficiency and an increase in faster frequencies like the beta band, potentially confounding the interpretation of EEG spikes [221]. Furthermore, MRI studies show that sleep deprivation can lead to a decrease in the percent amplitude of fluctuations in the bilateral dorsolateral prefrontal cortex and reduced functional connectivity between the thalamus and various other brain regions [222], [223]. Such alterations could have implications for EEG readings, as sleep deprivation can modify brain activity and thus influence the characteristics of EEG spikes.

Human Error in Electrode Placement

The manual placement of electrodes introduces human error as an unavoidable limitation. Even small discrepancies in placement across different sessions or nights could lead to variations in the signal if the dipole always manifests in the same location. This overall variation would be influenced from by the effects of volume

conduction that could significantly reduce the overall amplitude or discernability if the electrode is not perpendicular to the dipole effect [224].

Location-Specific Spike Morphology

The morphological characteristics of interictal epileptiform discharges (IEDs) are intricately tied to the diverse physiological functions and baseline electrical synchronization levels of various brain regions. For example, the frontal lobe, known for complex cognitive functions, may show IEDs that are rhythmic or faster, reflecting its unique baseline activity patterns [14]. The likelihood of IEDs being associated with the ictal onset zone also varies based on their origin; discharges in the central, parietal, and occipital regions are generally less likely to correlate with clinical seizures compared to those in the frontal and temporal lobes, particularly in the absence of a structural lesion [225]. This complexity underscores the importance of considering the anatomical origin of IEDs, as their morphology can differ significantly depending on their location in the brain.

Influence of Anti-Seizure Drugs

Antiseizure medications can have nuanced effects on sleep architecture and EEG patterns, largely due to their diverse mechanisms of action. For instance, lamotrigine, which inhibits voltage-sensitive sodium channels and stabilizes neuronal membranes, appears to have a generally beneficial or neutral effect on sleep, without significant disturbances in EEG and possibly less arousals [226]–[229]. In contrast, carbamazepine and possibly oxcarbazepine, both sodium channel blockers, are known to reduce REM sleep and could cause alpha intrusion into delta sleep, potentially complicating EEG interpretations [226], [227], [230]–[232]. Lacosamide, another sodium channel modulator, has a mostly neutral impact on sleep but could induce drowsiness [233]. GABAergic agents like clobazam and phenobarbital tend to reduce REM sleep and sleep latency.[226], [227], [233]. Phenytoin, another sodium channel blocker, can cause sleep disruptions influencing an overall less effective sleep, while also reducing REM sleep, potentially adding additional disruptions into the EEG [227]. Levetiracetam has yet to undergo large-scale clinical trials for its effects on sleep; however with a range of smaller studies, with variable reported effects [226], [227], [233], [234]. Lastly, perampanel, an AMPA glutamate receptor antagonist, showed an improvement to sleep architecture while daytime sleepiness was not negatively affected [235]. It is crucial to recognize that these medications can simply influence cortical neurons regardless of sleep states by affecting various ion channels and neurotransmitter pathways, which not only impacts their respective fields of binding but also leads to significant alterations in sleep states and EEG patterns.

REM Sleep States and Spike Characteristics

One salient limitation of the study is the heterogeneity within REM sleep, which is not a monolithic state but consists of microstates; specifically, tonic and phasic REM [236].

While tonic REM and NREM sleep both involve reduced sensory input and motor output compared to wakefulness, and both contribute to memory consolidation, they differ significantly in brain wave activity and neurotransmitter release patterns. During phasic REM, bursts of acetylcholine from orexinergic systems occur [55]. This biochemical activity could have a pronounced influence on the morphological characteristics of epileptiform spikes captured in EEG data. The coexistence of these distinct microstates within REM sleep complicates the interpretation of the findings, possibly adding additional variability to REM morphological variability.

7 Future Work

In light of the complexities and limitations outlined in this study, future research should strive for a more rigorous and individualized methodology. One approach would be to limit the study to individuals with a single, specific epilepsy syndrome, thereby controlling for the numerous variables that epilepsy types introduce. In terms of data quality, focusing on a homogeneous population with similar medications, age groups, and even channel location of spikes may yield cleaner results by minimizing confounding variables. Furthermore, future analyses should categorize epileptiform discharges into their respective types—such as spikes, spike-and-slow-waves, sharp-waves, sharp-and-slow-waves, and polyspikes—prior to conducting morphological assessments. This categorization would allow for a more nuanced understanding of how these different forms of epileptiform activity vary across sleep-wake states. To delve deeper, the study could also account for patients with specific sleep disorders to examine how alterations in sleep architecture may drive paroxysmal depolarizing shift (PDS) functions. Additionally, as sleep-wake states are influenced by an array of factors—including homeostatic sleep pressure, circadian rhythms, and individual neuronal dynamics—future work could focus on how these elements modulate inhibitory processes and consequently affect the characteristics of epileptiform activity. By grounding the study in this highly specialized and rigorous methodology, we hope to shed clearer light on the morphological characteristics of epileptiform spikes across diverse sleep-wake states.

8 Conclusion

This study leveraged a meticulously human-scored spike-marking GUI to gather a gold-standard dataset, thereby facilitating a quick abundance of labelled epileptiform spikes across different sleep-wake states. The findings uncovered significant variations in spike morphology among these states, underscoring the importance of these sleep-wake stages in shaping epileptiform activity. While EEG methodologies are inherently limited in providing a direct biological explanation for these observations, this study's approach allowed for an inferential understanding based on existing literature regarding cortical neuronal activity.

One potentially groundbreaking avenue for future research lies in the complex interplay between the orexinergic system and astrocytes. Current literature suggests that astrocytes may play a pivotal role in shaping REM-specific spike morphology. A novel mechanism suggests that astrocytes, during epileptic REM, might modulate the orexinergic system, influencing neuronal firing. This modulation could lead to overstimulation of orexin directed at wakefulness regions, potentially enabling spike breakthroughs to occur in the first place. The intriguing uniformity in spike morphology during REM, a state known for its fluctuating levels of neuronal activity, underscores the possibility that astrocytes are a key determinant in this phenomenon. Our work implies that there is a pressing need for further research into how astrocytes regulate epileptiform activity, especially as a novel target for anti-seizure medications.

References

[1] World Health Organization, “Epilepsy.” Accessed: Oct. 01, 2023. [Online]. Available: https://www.who.int/news-room/fact-sheets/detail/epilepsy

[2] “Mission,” Epilepsy Canada. Accessed: Oct. 01, 2023. [Online]. Available: https://www.epilepsy.ca/mission

[3] W. Löscher, H. Potschka, S. M. Sisodiya, and A. Vezzani, “Drug Resistance in Epilepsy: Clinical Impact, Potential Mechanisms, and New Innovative Treatment Options,” *Pharmacol. Rev.*, vol. 72, no. 3, pp. 606–638, Jul. 2020, doi: 10.1124/pr.120.019539.

[4] D. J. Englot, D. Ouyang, P. A. Garcia, N. M. Barbaro, and E. F. Chang, “Epilepsy surgery trends in the United States, 1990 –2008,” 2012.

[5] I. D’Andrea Meira, T. T. Romão, H. J. Pires Do Prado, L. T. Krüger, M. E. P. Pires, and P. O. Da Conceição, “Ketogenic Diet and Epilepsy: What We Know So Far,” *Front. Neurosci.*, vol. 13, p. 5, Jan. 2019, doi: 10.3389/fnins.2019.00005.

[6] P. Wolf, “Non-medical treatment of first epileptic seizures in adolescence and adulthood,” *Seizure*, vol. 4, no. 2, pp. 87–94, Jun. 1995, doi: 10.1016/S1059-1311(95)80087-5.

[7] L. Nobili *et al.*, “Sleep and epilepsy: A snapshot of knowledge and future research lines,” *J. Sleep Res.*, vol. 31, no. 4, p. e13622, Aug. 2022, doi: 10.1111/jsr.13622.

[8] M. Kryger, T. Roth, and W. Dement, *Principles and Practice of Sleep Medicine*, 5th ed. Elsevier Health Sciences, 2011. doi: 10.1016/C2009-0-59875-3.

[9] R. Berry *et al.*, “The AASM Manual for the Scoring of Sleep and Associated Events: Rules, Terminology and Technical Specifications.”

[10] R. Stickgold, “Sleep-dependent memory consolidation,” *Nature*, vol. 437, no. 7063, pp. 1272–1278, Oct. 2005, doi: 10.1038/nature04286.

[11] M. H. Kryger, T. (Tom) Roth, C. A. Goldstein, and W. C. Dement, *Principles and practice of sleep medicine*, Seventh edition. Philadelphia, PA: Elsevier, 2022.

[12] G. Tononi and C. Cirelli, “Sleep function and synaptic homeostasis,” *Sleep Med. Rev.*, vol. 10, no. 1, pp. 49–62, Feb. 2006, doi: 10.1016/j.smrv.2005.05.002.

[13] J. H. Siegel, “The REM sleep-memory consolidation hypothesis. (Review)”.

[14] D. L. Schomer, F. H. Lopes da Silva, and E. Niedermeyer, *Niedermeyer’s electroencephalography : basic principles, clinical applications, and related fields*, 7 ed. in Electroencephalography. New York: Oxford University Press, 2017.

[15] B. A. Malow, “The interaction between sleep and epilepsy,” *Epilepsia Cph.*, vol. 48, no. s9, pp. 36–38, 2007, doi: 10.1111/j.1528-1167.2007.01400.x.

[16] H. Bonilla-Jaime, H. Zeleke, A. Rojas, and C. Espinosa-Garcia, “Sleep Disruption Worsens Seizures: Neuroinflammation as a Potential Mechanistic Link,” *Int. J. Mol. Sci.*, vol. 22, no. 22, p. 12531, Nov. 2021, doi: 10.3390/ijms222212531.

[17] M. M. Grigg-Damberger and N. Foldvary-Schaefer, “Sleep and Epilepsy,” *Neurol. Clin.*, vol. 40, no. 4, pp. 769–783, Nov. 2022, doi: 10.1016/j.ncl.2022.03.008.

[18] M. Grigg-Damberger and N. Foldvary-Schaefer, “Bidirectional relationships of sleep and epilepsy in adults with epilepsy,” *Epilepsy Behav.*, vol. 116, p. 107735, Mar. 2021, doi: 10.1016/j.yebeh.2020.107735.

[19] T. Wu, A. Y. Avidan, and J. Engel, “Sleep and Epilepsy, Clinical Spectrum and Updated Review,” *Sleep Med. Clin.*, vol. 16, no. 2, pp. 389–408, Jun. 2021, doi: 10.1016/j.jsmc.2021.02.011.

[20] P. Halász, “How Sleep Activates Epileptic Networks?,” *Epilepsy Res. Treat.*, vol. 2013, pp. 1–19, Sep. 2013, doi: 10.1155/2013/425697.

[21] P. Halász and A. Szűcs, “Sleep and Epilepsy Link by Plasticity,” *Front. Neurol.*, vol. 11, p. 911, Aug. 2020, doi: 10.3389/fneur.2020.00911.

[22] M. C. Ng, “Orexin and Epilepsy: Potential Role of REM Sleep,” *Sleep*, vol. 40, no. 3, Mar. 2017, doi: 10.1093/sleep/zsw061.

[23] A. Fouad *et al.*, “Interictal epileptiform discharges show distinct spatiotemporal and morphological patterns across wake and sleep,” *Brain Commun.*, vol. 4, no. 5, p. fcac183, Sep. 2022, doi: 10.1093/braincomms/fcac183.

[24] M. Steriade, D. Contreras, and F. Amzica, “Synchronized sleep oscillations and their paroxysmal developments,” *Trends Neurosci. Regul. Ed*, vol. 17, no. 5, pp. 201–207, 1994, doi: 10.1016/0166-2236(94)90105-8.

[25] R. Manni and M. Terzaghi, “Comorbidity between epilepsy and sleep disorders,” *Epilepsy Res.*, vol. 90, no. 3, pp. 171–177, Aug. 2010, doi: 10.1016/j.eplepsyres.2010.05.006.

[26] M. Steriade and F. Amzica, “Slow sleep oscillation, rhythmic K-complexes, and their paroxysmal developments,” *J. Sleep Res.*, vol. 7, no. S1, pp. 30–35, 1998, doi: 10.1046/j.1365-2869.7.s1.4.x.

[27] M. Steriade and F. Amzica, “Sleep Oscillations Developing into Seizures in Corticothalamic Systems,” *Epilepsia*, vol. 44, no. s12, pp. 9–20, Dec. 2003, doi: 10.1111/j.0013-9580.2003.12006.x.

[28] C. Gottesmann, “GABA mechanisms and sleep,” *Neuroscience*, vol. 111, no. 2, pp. 231–239, May 2002, doi: 10.1016/S0306-4522(02)00034-9.

[29] G. Vanini, R. Lydic, and H. A. Baghdoyan, “GABA-to-ACh Ratio in Basal Forebrain and Cerebral Cortex Varies Significantly During Sleep,” *Sleep*, vol. 35, no. 10, pp. 1325–1334, Oct. 2012, doi: 10.5665/sleep.2106.

[30] H. Berger, “Über das Elektrenkephalogramm des Menschen,” *Arch. Für Psychiatr. Nervenkrankh.*, vol. 87, no. 1, pp. 527–570, 1929, doi: 10.1007/BF01797193.

[31] G. Buzsáki, C. A. Anastassiou, and C. Koch, “The origin of extracellular fields and currents-EEG, ECoG, LFP and spikes,” *Nat. Rev. Neurosci.*, vol. 13, no. 6, pp. 407–420, 2012, doi: 10.1038/nrn3241.

[32] E. R. Kandel, J. Koester, S. Mack, and S. Siegelbaum, *Principles of neural science*, Sixth edition. New York: McGraw Hill, 2021.

[33] P. L. Nunez and R. Srinivasan, *Electric Fields of the Brain: The neurophysics of EEG*. Oxford University Press, 2006. doi: 10.1093/acprof:oso/9780195050387.001.0001.

[34] M. X. Cohen, *Analyzing neural time series data : theory and practice*. in Issues in clinical and cognitive neuropsychology. Cambridge, Massachusetts: The MIT Press, 2014.

[35] G. A. Light *et al.*, “Electroencephalography (EEG) and Event-Related Potentials (ERPs) with Human Participants,” *Curr. Protoc. Neurosci.*, vol. 52, no. 1, Jul. 2010, doi: 10.1002/0471142301.ns0625s52.

[36] N. Kane *et al.*, “A revised glossary of terms most commonly used by clinical electroencephalographers and updated proposal for the report format of the EEG findings. Revision 2017,” *Clin. Neurophysiol. Pract.*, vol. 2, pp. 170–185, 2017, doi: 10.1016/j.cnp.2017.07.002.

[37] S. Noachtar and J. Rémi, “The role of EEG in epilepsy: A critical review,” *Epilepsy Behav.*, vol. 15, no. 1, pp. 22–33, May 2009, doi: 10.1016/j.yebeh.2009.02.035.

[38] D. W. Klass and B. F. Westmoreland, “Nonepileptogenic epileptiform electroencephalographic activity,” *Ann. Neurol.*, vol. 18, no. 6, pp. 627–635, 1985, doi: 10.1002/ana.410180602.

[39] C. S. Nayak and A. C. Anilkumar, “EEG Normal Waveforms,” in *StatPearls*, Treasure Island (FL): StatPearls Publishing, 2023. Accessed: Oct. 19, 2023. [Online]. Available: http://www.ncbi.nlm.nih.gov/books/NBK539805/

[40] R. S. Fisher *et al.*, “Epileptic Seizures and Epilepsy: Definitions Proposed by the International League Against Epilepsy (ILAE) and the International Bureau for Epilepsy (IBE),” *Epilepsia*, vol. 46, no. 4, pp. 470–472, Apr. 2005, doi: 10.1111/j.0013-9580.2005.66104.x.

[41] R. A. B. Badawy, A. S. Harvey, and R. A. L. Macdonell, “Cortical hyperexcitability and epileptogenesis: Understanding the mechanisms of epilepsy – Part 1,” *J. Clin. Neurosci.*, vol. 16, no. 3, pp. 355–365, Mar. 2009, doi: 10.1016/j.jocn.2008.08.026.

[42] H. Kubista, S. Boehm, and M. Hotka, “The Paroxysmal Depolarization Shift: Reconsidering Its Role in Epilepsy, Epileptogenesis and Beyond,” *Int. J. Mol. Sci.*, vol. 20, no. 3, p. 577, Jan. 2019, doi: 10.3390/ijms20030577.

[43] M. Hotka and H. Kubista, “The paroxysmal depolarization shift in epilepsy research,” *Int. J. Biochem. Cell Biol.*, vol. 107, pp. 77–81, Feb. 2019, doi: 10.1016/j.biocel.2018.12.006.

[44] M. A. Kural *et al.*, “Accurate identification of EEG recordings with interictal epileptiform discharges using a hybrid approach: Artificial intelligence supervised by human experts,” *Epilepsia*, vol. 63, no. 5, pp. 1064–1073, May 2022, doi: 10.1111/epi.17206.

[45] D. A. McCormick and D. Contreras, “On The Cellular and Network Bases of Epileptic Seizures,” *Annu. Rev. Physiol.*, vol. 63, no. 1, pp. 815–846, Mar. 2001, doi: 10.1146/annurev.physiol.63.1.815.

[46] M. Steriade, D. A. McCormick, and T. J. Sejnowski, “Thalamocortical Oscillations in the Sleeping and Aroused Brain,” *Science*, vol. 262, no. 5134, pp. 679–685, Oct. 1993, doi: 10.1126/science.8235588.

[47] M. Steriade and R. W. McCarley, *Brain Control of Wakefulness and Sleep*, Second Edition. Boston, MA: Springer US. doi: 10.1007/b102230.

[48] B. Frauscher, N. Von Ellenrieder, F. Dubeau, and J. Gotman, “EEG desynchronization during phasic REM sleep suppresses interictal epileptic activity in humans,” *Epilepsia*, vol. 57, no. 6, pp. 879–888, Jun. 2016, doi: 10.1111/epi.13389.

[49] H. Merica and R. Blois, “Relationship between the time courses of power in the frequency bands of human sleep EEG,” *Neurophysiol. Clin.*, vol. 27, no. 2, pp. 116–128, 1997, doi: 10.1016/S0987-7053(97)85664-X.

[50] M. Aime *et al.*, “Paradoxical somatodendritic decoupling supports cortical plasticity during REM sleep,” 2022.

[51] W. Li, L. Ma, G. Yang, and W.-B. Gan, “REM sleep selectively prunes and maintains new synapses in development and learning,” *Nat. Neurosci.*, vol. 20, no. 3, pp. 427–437, Mar. 2017, doi: 10.1038/nn.4479.

[52] S. Scarpelli *et al.*, “Electrophysiological Correlates of Dream Recall During REM Sleep: Evidence from Multiple Awakenings and Within-Subjects Design,” *Nat. Sci. Sleep*, vol. Volume 12, pp. 1043–1052, Nov. 2020, doi: 10.2147/NSS.S279786.

[53] B. Hille, *Ion channels of excitable membranes*, 3rd ed. Sunderland, Mass: Sinauer, 2001.

[54] J. A. Hobson, E. F. Pace-Schott, and R. Stickgold, “Dreaming and the brain: Toward a cognitive neuroscience of conscious states,” *Behav. Brain Sci.*, vol. 23, no. 6, pp. 793–842, Dec. 2000, doi: 10.1017/S0140525X00003976.

[55] T. Sakurai, “The neural circuit of orexin (hypocretin): maintaining sleep and wakefulness,” *Nat. Rev. Neurosci.*, vol. 8, no. 3, pp. 171–181, Mar. 2007, doi: 10.1038/nrn2092.

[56] G. Aston-Jones and J. D. Cohen, “AN INTEGRATIVE THEORY OF LOCUS COERULEUS-NOREPINEPHRINE FUNCTION: Adaptive Gain and Optimal Performance,” *Annu. Rev. Neurosci.*, vol. 28, no. 1, pp. 403–450, Jul. 2005, doi: 10.1146/annurev.neuro.28.061604.135709.

[57] J. M. Monti, “Serotonin control of sleep-wake behavior,” *Sleep Med. Rev.*, vol. 15, no. 4, pp. 269–281, 2011, doi: 10.1016/j.smrv.2010.11.003.

[58] U. Pannasch and N. Rouach, “Emerging role for astroglial networks in information processing: from synapse to behavior,” *Trends Neurosci.*, vol. 36, no. 7, pp. 405–417, Jul. 2013, doi: 10.1016/j.tins.2013.04.004.

[59] C. Giaume, A. Koulakoff, L. Roux, D. Holcman, and N. Rouach, “Astroglial networks: a step further in neuroglial and gliovascular interactions,” *Nat. Rev. Neurosci.*, vol. 11, no. 2, pp. 87–99, 2010, doi: 10.1038/nrn2757.

[60] N. J. Allen and C. Eroglu, “Cell Biology of Astrocyte-Synapse Interactions,” *Neuron*, vol. 96, no. 3, pp. 697–708, Nov. 2017, doi: 10.1016/j.neuron.2017.09.056.

[61] B. A. Barres, “The Mystery and Magic of Glia: A Perspective on Their Roles in Health and Disease,” *Neuron*, vol. 60, no. 3, pp. 430–440, Nov. 2008, doi: 10.1016/j.neuron.2008.10.013.

[62] G. L. Sarlo and K. F. Holton, “Brain concentrations of glutamate and GABA in human epilepsy: A review,” *Seizure*, vol. 91, pp. 213–227, Oct. 2021, doi: 10.1016/j.seizure.2021.06.028.

[63] Dale. Purves, *Neuroscience*, 5th ed. Sunderland, Mass: Sinauer Associates, 2012.

[64] G. Tononi and C. Cirelli, “Sleep and the Price of Plasticity: From Synaptic and Cellular Homeostasis to Memory Consolidation and Integration,” *Neuron*, vol. 81, no. 1, pp. 12–34, Jan. 2014, doi: 10.1016/j.neuron.2013.12.025.

[65] M. B. Dash, C. L. Douglas, V. V. Vyazovskiy, C. Cirelli, and G. Tononi, “Long-Term Homeostasis of Extracellular Glutamate in the Rat Cerebral Cortex across Sleep and Waking States,” *J. Neurosci.*, vol. 29, no. 3, pp. 620–629, Jan. 2009, doi: 10.1523/JNEUROSCI.5486-08.2009.

[66] G. L. Collingridge *et al.*, “The NMDA receptor as a target for cognitive enhancement,” *Neuropharmacology*, vol. 64, pp. 13–26, Jan. 2013, doi: 10.1016/j.neuropharm.2012.06.051.

[67] D. P. Laryushkin, S. A. Maiorov, V. P. Zinchenko, V. N. Mal’tseva, S. G. Gaidin, and A. M. Kosenkov, “Of the Mechanisms of Paroxysmal Depolarization Shifts: Generation and Maintenance of Bicuculline-Induced Paroxysmal Activity in Rat Hippocampal Cell Cultures,” *Int. J. Mol. Sci.*, vol. 24, no. 13, p. 10991, Jul. 2023, doi: 10.3390/ijms241310991.

[68] T.-S. Chen, T.-H. Huang, M.-C. Lai, and C.-W. Huang, “The Role of Glutamate Receptors in Epilepsy,” *Biomedicines*, vol. 11, no. 3, p. 783, Mar. 2023, doi: 10.3390/biomedicines11030783.

[69] A. Reiner and J. Levitz, “Glutamatergic Signaling in the Central Nervous System: Ionotropic and Metabotropic Receptors in Concert,” *Neuron*, vol. 98, no. 6, pp. 1080–1098, Jun. 2018, doi: 10.1016/j.neuron.2018.05.018.

[70] J. M. Henley and K. A. Wilkinson, “Synaptic AMPA receptor composition in development, plasticity and disease,” *Nat. Rev. Neurosci.*, vol. 17, no. 6, pp. 337–350, 2016, doi: 10.1038/nrn.2016.37.

[71] M. Pfister-Genskow, V. V. Vyazovskiy, U. Faraguna, C. Cirelli, and G. Tononi, “Molecular and electrophysiological evidence for net synaptic potentiation in wake and depression in sleep,” *Nat. Neurosci.*, vol. 11, no. 2, pp. 200–208, 2008, doi: 10.1038/nn2035.

[72] C. Volk, V. Jaramillo, R. Merki, R. O’Gorman Tuura, and R. Huber, “Diurnal changes in glutamate + glutamine levels of healthy young adults assessed by proton magnetic resonance spectroscopy,” *Hum. Brain Mapp.*, vol. 39, no. 10, pp. 3984–3992, Oct. 2018, doi: 10.1002/hbm.24225.

[73] G. H. Diering, R. S. Nirujogi, R. H. Roth, P. F. Worley, A. Pandey, and R. L. Huganir, “Homer1a drives homeostatic scaling-down of excitatory synapses during sleep,” *Science*, vol. 355, no. 6324, pp. 511–515, Feb. 2017, doi: 10.1126/science.aai8355.

[74] F. Lanté, J.-C. Toledo-Salas, T. Ondrejcak, M. J. Rowan, and D. Ulrich, “Removal of Synaptic Ca $^{2+}$ -Permeable AMPA Receptors during Sleep,” *J. Neurosci.*, vol. 31, no. 11, pp. 3953–3961, Mar. 2011, doi: 10.1523/JNEUROSCI.3210-10.2011.

[75] J. D. Rothstein *et al.*, “Localization of neuronal and glial glutamate transporters,” *Neuron Camb. Mass*, vol. 13, no. 3, pp. 713–725, 1994, doi: 10.1016/0896-6273(94)90038-8.

[76] Y. H. Huang and D. E. Bergles, “Glutamate transporters bring competition to the synapse,” *Curr. Opin. Neurobiol.*, vol. 14, no. 3, pp. 346–352, Jun. 2004, doi: 10.1016/j.conb.2004.05.007.

[77] A. M. VanDongen, *Biology of the NMDA Receptor*, 1st ed. in Frontiers in neuroscience. Baton Rouge: CRC Press, 2008. doi: 10.1201/9781420044157.

[78] J. L. Noebels and H. H. (Herbert H. Jasper, *Jasper’s basic mechanisms of the epilepsies*, 4th ed. / edited by Jeffrey L. Noebels ... [et al.]. in Contemporary neurology series ; 80. New York: Oxford University Press, 2012.

[79] P. Paoletti, C. Bellone, and Q. Zhou, “NMDA receptor subunit diversity: Impact on receptor properties, synaptic plasticity and disease,” *Nat. Rev. Neurosci.*, vol. 14, no. 6, pp. 383–400, 2013, doi: 10.1038/nrn3504.

[80] S. F. Traynelis *et al.*, “Glutamate Receptor Ion Channels: Structure, Regulation, and Function,” *Pharmacol. Rev.*, vol. 62, no. 3, pp. 405–496, Sep. 2010, doi: 10.1124/pr.109.002451.

[81] J. Lisman and S. Raghavachari, “A unified model of the presynaptic and postsynaptic changes during LTP at CA1 synapses,” *Sci. Signal Transduct. Knowl. Environ. STKE*, vol. 2006, no. 356, p. re11, 2006, doi: 10.1126/stke.3562006re11.

[82] S. Chauvette, J. Seigneur, and I. Timofeev, “Sleep Oscillations in the Thalamocortical System Induce Long-Term Neuronal Plasticity,” *Neuron*, vol. 75, no. 6, pp. 1105–1113, Sep. 2012, doi: 10.1016/j.neuron.2012.08.034.

[83] S. Datta, “Cellular and chemical neuroscience of mammalian sleep,” *Sleep Med.*, vol. 11, no. 5, pp. 431–440, May 2010, doi: 10.1016/j.sleep.2010.02.002.

[84] S. Datta and R. R. MacLean, “Neurobiological mechanisms for the regulation of mammalian sleep–wake behavior: Reinterpretation of historical evidence and inclusion of contemporary cellular and molecular evidence,” *Neurosci. Biobehav. Rev.*, vol. 31, no. 5, pp. 775–824, Jan. 2007, doi: 10.1016/j.neubiorev.2007.02.004.

[85] D. E. Jane, D. Lodge, and G. L. Collingridge, “Kainate receptors: Pharmacology, function and therapeutic potential,” *Neuropharmacology*, vol. 56, no. 1, pp. 90–113, Jan. 2009, doi: 10.1016/j.neuropharm.2008.08.023.

[86] E. Garcia-Rill, A. Charlesworth, D. Heister, M. Ye, and A. Hayar, “The Developmental Decrease in REM Sleep: The Role of Transmitters and Electrical Coupling,” *Sleep*, vol. 31, no. 5, pp. 673–690, May 2008, doi: 10.1093/sleep/31.5.673.

[87] T. Kobayashi, R. D. Skinner, and E. Garcia-Rill, “Developmental decrease in REM sleep: the shift to kainate receptor regulation,” *Thalamus Relat. Syst.*, vol. 2, no. 4, pp. 315–324, 2004, doi: 10.1017/S1472928804010027.

[88] S. Datta, “Evidence That REM Sleep Is Controlled by the Activation of Brain Stem Pedunculopontine Tegmental Kainate Receptor,” *J. Neurophysiol.*, vol. 87, no. 4, pp. 1790–1798, Apr. 2002, doi: 10.1152/jn.00763.2001.

[89] G. Panuccio, G. Curia, A. Colosimo, G. Cruccu, and M. Avoli, “Epileptiform synchronization in the cingulate cortex,” *Epilepsia*, vol. 50, no. 3, pp. 521–536, Mar. 2009, doi: 10.1111/j.1528-1167.2008.01779.x.

[90] F. M. Ribeiro, L. B. Vieira, R. G. W. Pires, R. P. Olmo, and S. S. G. Ferguson, “Metabotropic glutamate receptors and neurodegenerative diseases,” *Pharmacol. Res.*, vol. 115, pp. 179–191, Jan. 2017, doi: 10.1016/j.phrs.2016.11.013.

[91] L. L. Haak, H. C. Heller, and A. N. Van Den Pol, “Metabotropic Glutamate Receptor Activation Modulates Kainate and Serotonin Calcium Response in Astrocytes,” *J. Neurosci.*, vol. 17, no. 5, pp. 1825–1837, Mar. 1997, doi: 10.1523/JNEUROSCI.17-05-01825.1997.

[92] M. R. Zielinski, J. T. McKenna, R. W. McCarley, and 1 Veterans Affairs Boston Healthcare System, West Roxbury, MA 02132, USA and Harvard Medical School, Department of Psychiatry, “Functions and Mechanisms of Sleep,” *AIMS Neurosci.*, vol. 3, no. 1, pp. 67–104, 2016, doi: 10.3934/Neuroscience.2016.1.67.

[93] M. Steriade, *Neuronal substrates of sleep and epilepsy*. in Neuronal Substrates of Sleep & Epilepsy. Cambridge: Cambridge University Press, 2003.

[94] M. V. Sanchez-Vives, A. Barbero-Castillo, M. Perez-Zabalza, and R. Reig, “GABAB receptors: modulation of thalamocortical dynamics and synaptic plasticity,” *Neuroscience*, vol. 456, pp. 131–142, Feb. 2021, doi: 10.1016/j.neuroscience.2020.03.011.

[95] J. S. Isaacson and M. Scanziani, “How Inhibition Shapes Cortical Activity,” *Neuron*, vol. 72, no. 2, pp. 231–243, Oct. 2011, doi: 10.1016/j.neuron.2011.09.027.

[96] B. N. Mallick, S. Majumdar, M. Faisal, V. Yadav, V. Madan, and D. Pal, “Role of norepinephrine in the regulation of rapid eye movement sleep,” *J. Biosci.*, vol. 27, no. 5, pp. 539–551, Sep. 2002, doi: 10.1007/BF02705052.

[97] O. K. Hassani, M. G. Lee, P. Henny, and B. E. Jones, “Discharge Profiles of Identified GABAergic in Comparison to Cholinergic and Putative Glutamatergic Basal Forebrain Neurons across the Sleep–Wake Cycle,” *J. Neurosci.*, vol. 29, no. 38, pp. 11828–11840, Sep. 2009, doi: 10.1523/JNEUROSCI.1259-09.2009.

[98] R. E. Brown, R. Basheer, J. T. McKenna, R. E. Strecker, and R. W. McCarley, “Control of Sleep and Wakefulness,” *Physiol. Rev.*, vol. 92, no. 3, pp. 1087–1187, Jul. 2012, doi: 10.1152/physrev.00032.2011.

[99] S. J. Mihic and R. A. Harris, “GABA and the GABAA receptor,” *Alcohol Health Res. World*, vol. 21, no. 2, pp. 127–131, 1997.

[100] R.-S. Lee, S. C. Steffensen, and S. J. Henriksen, “Discharge Profiles of Ventral Tegmental Area GABA Neurons during Movement, Anesthesia, and the Sleep–Wake Cycle,” *J. Neurosci.*, vol. 21, no. 5, pp. 1757–1766, Mar. 2001, doi: 10.1523/JNEUROSCI.21-05-01757.2001.

[101] P. L. Brooks and J. H. Peever, “Unraveling the Mechanisms of REM Sleep Atonia,” *Sleep*, vol. 31, no. 11, pp. 1492–1497, Nov. 2008, doi: 10.1093/sleep/31.11.1492.

[102] A. J. Berger, “What Causes Muscle Atonia in REM?,” *Sleep*, vol. 31, no. 11, pp. 1477–1478, Nov. 2008, doi: 10.1093/sleep/31.11.1477.

[103] M.-C. Xi, F. R. Morales, and M. H. Chase, “Evidence That Wakefulness and REM Sleep Are Controlled by a GABAergic Pontine Mechanism,” *J. Neurophysiol.*, vol. 82, no. 4, pp. 2015–2019, Oct. 1999, doi: 10.1152/jn.1999.82.4.2015.

[104] M.-C. Xi, F. R. Morales, and M. H. Chase, “Interactions between GABAergic and Cholinergic Processes in the Nucleus Pontis Oralis: Neuronal Mechanisms Controlling Active (Rapid Eye Movement) Sleep and Wakefulness,” *J. Neurosci.*, vol. 24, no. 47, pp. 10670–10678, Nov. 2004, doi: 10.1523/JNEUROSCI.1987-04.2004.

[105] D. Nitz and J. Siegel, “GABA release in the dorsal raphe nucleus: role in the control of REM sleep,” *Am. J. Physiol.-Regul. Integr. Comp. Physiol.*, vol. 273, no. 1, pp. R451–R455, Jul. 1997, doi: 10.1152/ajpregu.1997.273.1.R451.

[106] D. Nitz and J. M. Siegel, “GABA release in the locus coeruleus as a function of sleep/wake state,” *Neuroscience*, vol. 78, no. 3, pp. 795–801, Mar. 1997, doi: 10.1016/S0306-4522(96)00549-0.

[107] M. Krenzer *et al.*, “Brainstem and Spinal Cord Circuitry Regulating REM Sleep and Muscle Atonia,” *PLoS ONE*, vol. 6, no. 10, p. e24998, Oct. 2011, doi: 10.1371/journal.pone.0024998.

[108] B. Bettler, K. Kaupmann, J. Mosbacher, and M. Gassmann, “Molecular Structure and Physiological Functions of $GABA_B$ Receptors,” *Physiol. Rev.*, vol. 84, no. 3, pp. 835–867, Jul. 2004, doi: 10.1152/physrev.00036.2003.

[109] N. G. Bowery *et al.*, “International Union of Pharmacology. XXXIII. Mammalian γ-aminobutyric acidb receptors: Structure and function,” *Pharmacol. Rev.*, vol. 54, no. 2, pp. 247–264, 2002, doi: 10.1124/pr.54.2.247.

[110] E. F. Pace-Schott and J. A. Hobson, “The Neurobiology of Sleep: Genetics, cellular physiology and subcortical networks,” *Nat. Rev. Neurosci.*, vol. 3, no. 8, pp. 591–605, Aug. 2002, doi: 10.1038/nrn895.

[111] V. Varga, A. Sik, T. F. Freund, and B. Kocsis, “GABAB receptors in the median raphe nucleus: distribution and role in the serotonergic control of hippocampal activity,” *Neuroscience*, vol. 109, no. 1, pp. 119–132, Jan. 2002, doi: 10.1016/S0306-4522(01)00448-1.

[112] J. Ulloor, V. Mavanji, S. Saha, D. F. Siwek, and S. Datta, “Spontaneous REM Sleep Is Modulated By the Activation of the Pedunculopontine Tegmental $GABA_B$ Receptors in the Freely Moving Rat,” *J. Neurophysiol.*, vol. 91, no. 4, pp. 1822–1831, Apr. 2004, doi: 10.1152/jn.01104.2003.

[113] B. E. Jones, "*Modulation of Cortical Activation and Behavioral Arousal by Cholinergic and Orexinergic Systems*," *Ann. N. Y. Acad. Sci.*, vol. 1129, no. 1, pp. 26–34, May 2008, doi: 10.1196/annals.1417.026.

[114] M. E. Hasselmo and M. Sarter, "Modes and Models of Forebrain Cholinergic Neuromodulation of Cognition," *Neuropsychopharmacology*, vol. 36, no. 1, pp. 52–73, Jan. 2011, doi: 10.1038/npp.2010.104.

[115] L. De Lecea *et al.*, "The hypocretins: Hypothalamus-specific peptides with neuroexcitatory activity," *Proc. Natl. Acad. Sci.*, vol. 95, no. 1, pp. 322–327, Jan. 1998, doi: 10.1073/pnas.95.1.322.

[116] C. E. Mahoney, A. Cogswell, I. J. Koralnik, and T. E. Scammell, "The neurobiological basis of narcolepsy," *Nat. Rev. Neurosci.*, vol. 20, no. 2, pp. 83–93, Feb. 2019, doi: 10.1038/s41583-018-0097-x.

[117] C. W. Berridge and B. D. Waterhouse, "The locus coeruleus–noradrenergic system: modulation of behavioral state and state-dependent cognitive processes," *Brain Res. Rev.*, vol. 42, no. 1, pp. 33–84, Apr. 2003, doi: 10.1016/S0165-0173(03)00143-7.

[118] R. Ursin, "Serotonin and sleep," *Sleep Med. Rev.*, vol. 6, no. 1, pp. 55–67, Feb. 2002, doi: 10.1053/smrv.2001.0174.

[119] J. M. Monti, "The role of dorsal raphe nucleus serotonergic and non-serotonergic neurons, and of their receptors, in regulating waking and rapid eye movement (REM) sleep," *Sleep Med. Rev.*, vol. 14, no. 5, pp. 319–327, Oct. 2010, doi: 10.1016/j.smrv.2009.10.003.

[120] T. Jenkins, J. Nguyen, K. Polglaze, and P. Bertrand, "Influence of Tryptophan and Serotonin on Mood and Cognition with a Possible Role of the Gut-Brain Axis," *Nutrients*, vol. 8, no. 1, p. 56, Jan. 2016, doi: 10.3390/nu8010056.

[121] J. W. Winkelman and L. James, "Serotonergic Antidepressants are Associated with REM Sleep Without Atonia," *Sleep*, vol. 27, no. 2, pp. 317–321, Mar. 2004, doi: 10.1093/sleep/27.2.317.

[122] M. Steriade, "Acetylcholine systems and rhythmic activities during the waking–sleep cycle," in *Progress in Brain Research*, vol. 145, Elsevier, 2004, pp. 179–196. doi: 10.1016/S0079-6123(03)45013-9.

[123] D. A. McCormick, "Neurotransmitter actions in the thalamus and cerebral cortex and their role in neuromodulation of thalamocortical activity," *Prog. Neurobiol.*, vol. 39, no. 4, pp. 337–388, Oct. 1992, doi: 10.1016/0301-0082(92)90012-4.

[124] M. Steriade, F. Amzica, and D. Contreras, “Synchronization of fast (30-40 Hz) spontaneous cortical rhythms during brain activation,” *J. Neurosci.*, vol. 16, no. 1, pp. 392–417, Jan. 1996, doi: 10.1523/JNEUROSCI.16-01-00392.1996.

[125] N. Unwin, “Nicotinic acetylcholine receptor and the structural basis of neuromuscular transmission: insights from *Torpedo* postsynaptic membranes,” *Q. Rev. Biophys.*, vol. 46, no. 4, pp. 283–322, Nov. 2013, doi: 10.1017/S0033583513000061.

[126] J.-P. Changeux and Y. Paas, *Nicotinic Acetylcholine Receptors*. 2009.

[127] M. Sarter, M. E. Hasselmo, J. P. Bruno, and B. Givens, “Unraveling the attentional functions of cortical cholinergic inputs: interactions between signal-driven and cognitive modulation of signal detection,” *Brain Res. Rev.*, vol. 48, no. 1, pp. 98–111, Feb. 2005, doi: 10.1016/j.brainresrev.2004.08.006.

[128] M.-M. Mesulam, E. J. Mufson, A. I. Levey, and B. H. Wainer, “Cholinergic innervation of cortex by the basal forebrain: Cytochemistry and cortical connections of the septal area, diagonal band nuclei, nucleus basalis (Substantia innominata), and hypothalamus in the rhesus monkey,” *J. Comp. Neurol.*, vol. 214, no. 2, pp. 170–197, Feb. 1983, doi: 10.1002/cne.902140206.

[129] E. F. M. Wijdicks, “The Ascending Reticular Activating System,” *Neurocrit. Care*, vol. 31, no. 2, pp. 419–422, Oct. 2019, doi: 10.1007/s12028-019-00687-7.

[130] B. E. Jones, “Neurobiology of waking and sleeping,” in *Handbook of Clinical Neurology*, vol. 98, Elsevier, 2011, pp. 131–149. doi: 10.1016/B978-0-444-52006-7.00009-5.

[131] J. A. Hobson and E. F. Pace-Schott, “The cognitive neuroscience of sleep: neuronal systems, consciousness and learning,” *Nat. Rev. Neurosci.*, vol. 3, no. 9, pp. 679–693, Sep. 2002, doi: 10.1038/nrn915.

[132] G. Aston-Jones and J. D. Cohen, “Adaptive gain and the role of the locus coeruleus-norepinephrine system in optimal performance,” *J. Comp. Neurol. 1911*, vol. 493, no. 1, pp. 99–110, 2005, doi: 10.1002/cne.20723.

[133] E. Garcia-Rill, “Neuroepigenetics of arousal: Gamma oscillations in the pedunculopontine nucleus,” *J. Neurosci. Res.*, vol. 97, no. 12, pp. 1515–1520, 2019, doi: 10.1002/jnr.24417.

[134] S. Garbarino, L. Nobili, and G. Costa, *Sleepiness and Human Impact Assessment*, 1st ed. Milano: Springer Milan, 2014. doi: 10.1007/978-88-470-5388-5.

[135] M. Steriade, “Arousal--Revisiting the Reticular Activating System,” *Science*, vol. 272, no. 5259, pp. 225–225, Apr. 1996, doi: 10.1126/science.272.5259.225.

[136] T. Tsunematsu and A. Yamanaka, “The Role of Orexin/Hypocretin in the Central Nervous System and Peripheral Tissues,” in *Vitamins & Hormones*, vol. 89, Elsevier, 2012, pp. 19–33. doi: 10.1016/B978-0-12-394623-2.00002-0.

[137] I. Villano *et al.*, “Basal Forebrain Cholinergic System and Orexin Neurons: Effects on Attention,” *Front. Behav. Neurosci.*, vol. 11, Jan. 2017, doi: 10.3389/fnbeh.2017.00010.

[138] J. P. Kukkonen, “Physiology of the orexinergic/hypocretinergic system: a revisit in 2012,” *Am. J. Physiol.-Cell Physiol.*, vol. 304, no. 1, pp. C2–C32, Jan. 2013, doi: 10.1152/ajpcell.00227.2012.

[139] P. Fuller, D. Sherman, N. P. Pedersen, C. B. Saper, and J. Lu, “Reassessment of the structural basis of the ascending arousal system,” *J. Comp. Neurol.*, vol. 519, no. 5, pp. 933–956, Apr. 2011, doi: 10.1002/cne.22559.

[140] S. Kantor, T. Mochizuki, A. M. Janisiewicz, E. Clark, S. Nishino, and T. E. Scammell, “Orexin Neurons Are Necessary for the Circadian Control of REM Sleep,” *Sleep*, vol. 32, no. 9, pp. 1127–1134, Sep. 2009, doi: 10.1093/sleep/32.9.1127.

[141] T. E. Scammell, E. Arrigoni, and J. O. Lipton, “Neural Circuitry of Wakefulness and Sleep,” *Neuron*, vol. 93, no. 4, pp. 747–765, Feb. 2017, doi: 10.1016/j.neuron.2017.01.014.

[142] M. Ng and M. Pavlova, “Why Are Seizures Rare in Rapid Eye Movement Sleep? Review of the Frequency of Seizures in Different Sleep Stages,” *Epilepsy Res. Treat.*, vol. 2013, pp. 1–10, Jun. 2013, doi: 10.1155/2013/932790.

[143] K. E. Poskanzer and R. Yuste, “Astrocytes regulate cortical state switching in vivo,” *Proc. Natl. Acad. Sci.*, vol. 113, no. 19, May 2016, doi: 10.1073/pnas.1520759113.

[144] A. Verkhratsky and M. Nedergaard, “Physiology of Astroglia,” *Physiol Rev*, vol. 98, 2018.

[145] A. Sinning and C. A. Hübner, “Minireview: pH and synaptic transmission,” *FEBS Lett.*, vol. 587, no. 13, pp. 1923–1928, Jun. 2013, doi: 10.1016/j.febslet.2013.04.045.

[146] A. Bellot-Saez, O. Kékesi, J. W. Morley, and Y. Buskila, “Astrocytic modulation of neuronal excitability through K+ spatial buffering,” *Neurosci. Biobehav. Rev.*, vol. 77, pp. 87–97, 2017, doi: 10.1016/j.neubiorev.2017.03.002.

[147] A. Bellot-Saez, G. Cohen, A. van Schaik, L. Ooi, J. W Morley, and Y. Buskila, “Astrocytic modulation of cortical oscillations,” *Sci. Rep.*, vol. 8, no. 1, pp. 11565–13, 2018, doi: 10.1038/s41598-018-30003-w.

[148] Y. Li *et al.*, “Exploring Astrocyte-Mediated Mechanisms in Sleep Disorders and Comorbidity,” *Biomedicines*, vol. 11, no. 9, p. 2476, 2023, doi: 10.3390/biomedicines11092476.

[149] K. A. Lyon and N. J. Allen, “From Synapses to Circuits, Astrocytes Regulate Behavior,” *Front. Neural Circuits*, vol. 15, pp. 786293–786293, 2022, doi: 10.3389/fncir.2021.786293.

[150] J. O’Donnell, F. Ding, and M. Nedergaard, “Distinct Functional States of Astrocytes During Sleep and Wakefulness: Is Norepinephrine the Master Regulator?,” *Curr. Sleep Med. Rep.*, vol. 1, no. 1, pp. 1–8, Mar. 2015, doi: 10.1007/s40675-014-0004-6.

[151] J. Clasadonte, E. Scemes, Z. Wang, D. Boison, and P. G. Haydon, “Connexin 43-Mediated Astroglial Metabolic Networks Contribute to the Regulation of the Sleep-Wake Cycle,” *Neuron*, vol. 95, no. 6, pp. 1365-1380.e5, Sep. 2017, doi: 10.1016/j.neuron.2017.08.022.

[152] Y. Ikoma, Y. Takahashi, D. Sasaki, and K. Matsui, “Properties of REM sleep alterations with epilepsy,” *Brain*, p. awac499, Mar. 2023, doi: 10.1093/brain/awac499.

[153] E. R. Slepkov, J. K. Rainey, B. D. Sykes, and L. Fliegel, “Structural and functional analysis of the Na+/H+ exchanger,” *Biochem. J.*, vol. 401, no. 3, pp. 623–633, 2007, doi: 10.1042/BJ20061062.

[154] M. E. Beckner, “A roadmap for potassium buffering/dispersion via the glial network of the CNS,” *Neurochem. Int.*, vol. 136, p. 104727, Jun. 2020, doi: 10.1016/j.neuint.2020.104727.

[155] R. Rasmussen *et al.*, “Cortex-wide Changes in Extracellular Potassium Ions Parallel Brain State Transitions in Awake Behaving Mice,” *Cell Rep.*, vol. 28, no. 5, pp. 1182-1194.e4, Jul. 2019, doi: 10.1016/j.celrep.2019.06.082.

[156] M. M. Halassa, T. Fellin, and P. G. Haydon, “The tripartite synapse: roles for gliotransmission in health and disease,” *Trends Mol. Med.*, vol. 13, no. 2, pp. 54–63, Feb. 2007, doi: 10.1016/j.molmed.2006.12.005.

[157] A. Araque, G. Carmignoto, P. G. Haydon, S. H. R. Oliet, R. Robitaille, and A. Volterra, “Gliotransmitters Travel in Time and Space,” *Neuron*, vol. 81, no. 4, pp. 728–739, Feb. 2014, doi: 10.1016/j.neuron.2014.02.007.

[158] M. Steriade, A. Nuiiez, and F. Amzica, “A Novel Slow (<I Hz) Oscillation of Neocortical Neurons in viva: Depolarizing and Hyperpolarizing Components”.

[159] F. Amzica and M. Steriade, “Electrophysiological correlates of sleep delta waves,” *Electroencephalogr. Clin. Neurophysiol.*, vol. 107, no. 2, pp. 69–83, Apr. 1998, doi: 10.1016/S0013-4694(98)00051-0.

[160] F. Amzica and D. Neckelmann, “Membrane Capacitance of Cortical Neurons and Glia During Sleep Oscillations and Spike-Wave Seizures,” *J. Neurophysiol.*, vol. 82, no. 5, pp. 2731–2746, Nov. 1999, doi: 10.1152/jn.1999.82.5.2731.

[161] F. Amzica and M. Steriade, “Neuronal and Glial Membrane Potentials during Sleep and Paroxysmal Oscillations in the Neocortex,” *J. Neurosci.*, vol. 20, no. 17, pp. 6648–6665, Sep. 2000, doi: 10.1523/JNEUROSCI.20-17-06648.2000.

[162] F. Amzica, M. Massimini, and A. Manfridi, “Spatial Buffering during Slow and Paroxysmal Sleep Oscillations in Cortical Networks of Glial Cells *In Vivo*,” *J. Neurosci.*, vol. 22, no. 3, pp. 1042–1053, Feb. 2002, doi: 10.1523/JNEUROSCI.22-03-01042.2002.

[163] F. Amzica, “In vivo electrophysiological evidences for cortical neuron–glia interactions during slow (<1 Hz) and paroxysmal sleep oscillations,” *J. Physiol.-Paris*, vol. 96, no. 3–4, pp. 209–219, May 2002, doi: 10.1016/S0928-4257(02)00008-6.

[164] M. M. Halassa *et al.*, “Astrocytic Modulation of Sleep Homeostasis and Cognitive Consequences of Sleep Loss,” *Neuron*, vol. 61, no. 2, pp. 213–219, Jan. 2009, doi: 10.1016/j.neuron.2008.11.024.

[165] S. Jia *et al.*, “Chronic intermittent hypoxia enhances glycinergic inhibition in nucleus tractus solitarius,” *J. Neurophysiol.*, vol. 128, no. 6, pp. 1383–1394, Dec. 2022, doi: 10.1152/jn.00241.2022.

[166] D. W. Carley and S. S. Farabi, “Physiology of Sleep,” *Diabetes Spectr.*, vol. 29, no. 1, pp. 5–9, Feb. 2016, doi: 10.2337/diaspect.29.1.5.

[167] C. J. Watson PhD, H. A. Baghdoyan PhD, and R. Lydic PhD, “Neuropharmacology of Sleep and Wakefulness,” *Sleep Med. Clin.*, vol. 5, no. 4, pp. 513–528, 2010, doi: 10.1016/j.jsmc.2010.08.003.

[168] C. B. Saper, T. E. Scammell, and J. Lu, “Hypothalamic regulation of sleep and circadian rhythms,” *Nature*, vol. 437, no. 7063, pp. 1257–1263, 2005, doi: 10.1038/nature04284.

[169] C. B. Saper, P. M. Fuller, N. P. Pedersen, J. Lu, and T. E. Scammell, “Sleep State Switching,” *Neuron Camb. Mass*, vol. 68, no. 6, pp. 1023–1042, 2010, doi: 10.1016/j.neuron.2010.11.032.

[170] E. Arrigoni and P. M. Fuller, “The Sleep-Promoting Ventrolateral Preoptic Nucleus: What Have We Learned over the Past 25 Years?,” *Int. J. Mol. Sci.*, vol. 23, no. 6, p. 2905, 2022, doi: 10.3390/ijms23062905.

[171] J. M. Monti, H. Jantos, V. Catenaccio, and S. Xavier, “Blockade of the NMDA and AMPA/kainate receptors in the dorsal raphe nucleus prevents the 5-HT3 receptor agonist m-chlorophenylbiguanide-induced suppression of REM sleep in the rat,” *Prog. Neuropsychopharmacol. Biol. Psychiatry*, vol. 35, no. 5, pp. 1341–1348, Jul. 2011, doi: 10.1016/j.pnpbp.2011.04.001.

[172] C. B. Saper and P. M. Fuller, “Wake–sleep circuitry: an overview,” *Curr. Opin. Neurobiol.*, vol. 44, pp. 186–192, 2017, doi: 10.1016/j.conb.2017.03.021.

[173] S. Thankachan *et al.*, “Thalamic Reticular Nucleus Parvalbumin Neurons Regulate Sleep Spindles and Electrophysiological Aspects of Schizophrenia in Mice,” *Sci. Rep.*, vol. 9, no. 1, pp. 3607–3607, 2019, doi: 10.1038/s41598-019-40398-9.

[174] A. Jagannath *et al.*, “Adenosine integrates light and sleep signalling for the regulation of circadian timing in mice,” *Nat. Commun.*, vol. 12, no. 1, pp. 2113–11, 2021, doi: 10.1038/s41467-021-22179-z.

[175] M. D. Schwartz PhD and T. S. Kilduff PhD, “The Neurobiology of Sleep and Wakefulness,” *Psychiatr. Clin. North Am.*, vol. 38, no. 4, pp. 615–644, 2015, doi: 10.1016/j.psc.2015.07.002.

[176] J. Peever and P. M. Fuller, “The Biology of REM Sleep,” *Curr. Biol.*, vol. 27, no. 22, pp. R1237–R1248, 2017, doi: 10.1016/j.cub.2017.10.026.

[177] H. Feng *et al.*, “Orexin signaling modulates synchronized excitation in the sublaterodorsal tegmental nucleus to stabilize REM sleep,” *Nat. Commun.*, vol. 11, no. 1, pp. 3661–3661, 2020, doi: 10.1038/s41467-020-17401-3.

[178] F. A. Mir and S. K. Jha, “Locus Coeruleus Acid-Sensing Ion Channels Modulate Sleep–Wakefulness and State Transition from NREM to REM Sleep in the Rat,” *Neurosci. Bull.*, vol. 37, no. 5, pp. 684–700, 2021, doi: 10.1007/s12264-020-00625-0.

[179] S. D. Motts, “Cholinergic and non-cholinergic projections from the pedunculopontine and laterodorsal tegmental nuclei to the medial geniculate body in guinea pigs,” *Front. Neuroanat.*, vol. 4, 2010, doi: 10.3389/fnana.2010.00137.

[180] G. L. Collingridge, R. W. Olsen, J. Peters, and M. Spedding, “A nomenclature for ligand-gated ion channels,” *Neuropharmacology*, vol. 56, no. 1, pp. 2–5, Jan. 2009, doi: 10.1016/j.neuropharm.2008.06.063.

[181] C. M. Niswender and P. J. Conn, “Metabotropic Glutamate Receptors: Physiology, Pharmacology, and Disease,” *Annu. Rev. Pharmacol. Toxicol.*, vol. 50, no. 1, pp. 295–322, Feb. 2010, doi: 10.1146/annurev.pharmtox.011008.145533.

[182] R. W. Olsen and W. Sieghart, “International Union of Pharmacology. LXX. Subtypes of γ-Aminobutyric Acid $_A$ Receptors: Classification on the Basis of Subunit Composition, Pharmacology, and Function. Update,” *Pharmacol. Rev.*, vol. 60, no. 3, pp. 243–260, Sep. 2008, doi: 10.1124/pr.108.00505.

[183] E. Aanestad, N. E. Gilhus, and J. Brogger, “Interictal epileptiform discharges vary across age groups,” *Clin. Neurophysiol.*, vol. 131, no. 1, pp. 25–33, Jan. 2020, doi: 10.1016/j.clinph.2019.09.017.

[184] W. A. Catterall, “Sodium Channels, Inherited Epilepsy, and Antiepileptic Drugs,” *Annu. Rev. Pharmacol. Toxicol.*, vol. 54, no. 1, pp. 317–338, Jan. 2014, doi: 10.1146/annurev-pharmtox-011112-140232.

[185] D. M. Treiman, “GABAergic Mechanisms in Epilepsy,” *Epilepsia*, vol. 42, no. s3, pp. 8–12, Jul. 2001, doi: 10.1046/j.1528-1157.2001.042suppl.3008.x.

[186] A. BenSaïda, “Shapiro-Wilk and Shapiro-Francia normality tests.” [MATLAB Central File Exchange]. Available: https://www.mathworks.com/matlabcentral/fileexchange/13964-shapiro-wilk-and-shapiro-francia-normality-tests

[187] M. DiNuzzo and M. Nedergaard, “Brain energetics during the sleep–wake cycle,” *Curr. Opin. Neurobiol.*, vol. 47, pp. 65–72, 2017, doi: 10.1016/j.conb.2017.09.010.

[188] M. Dworak, R. W. McCarley, T. Kim, A. V. Kalinchuk, and R. Basheer, “Sleep and brain energy levels: ATP changes during sleep,” *J. Neurosci.*, vol. 30, no. 26, pp. 9007–9016, 2010, doi: 10.1523/JNEUROSCI.1423-10.2010.

[189] F. Ding, J. O’Donnell, Q. Xu, N. Kang, N. Goldman, and M. Nedergaard, “Changes in the composition of brain interstitial ions control the sleep-wake cycle,” *Sci. Am. Assoc. Adv. Sci.*, vol. 352, no. 6285, pp. 550–555, 2016, doi: 10.1126/science.aad4821.

[190] J. J. Fraigne, Z. A. Torontali, M. B. Snow, and J. H. Peever, “REM Sleep at its Core - Circuits, Neurotransmitters, and Pathophysiology,” *Front. Neurol.*, vol. 6, pp. 123–123, 2015, doi: 10.3389/fneur.2015.00123.

[191] H.-S. Wang *et al.*, “KCNQ2 and KCNQ3 Potassium Channel Subunits: Molecular Correlates of the M-Channel,” *Sci. Am. Assoc. Adv. Sci.*, vol. 282, no. 5395, pp. 1890–1893, 1998, doi: 10.1126/science.282.5395.1890.

[192] S.-B. Li *et al.*, “Hyperexcitable arousal circuits drive sleep instability during aging,” *Sci. Am. Assoc. Adv. Sci.*, vol. 375, no. 6583, pp. eabh3021–eabh3021, 2022, doi: 10.1126/science.abh3021.

[193] R. H. Joho, G. A. Marks, and F. Espinosa, “Kv3 potassium channels control the duration of different arousal states by distinct stochastic and clock-like mechanisms,” *Eur. J. Neurosci.*, vol. 23, no. 6, pp. 1567–1574, 2006, doi: 10.1111/j.1460-9568.2006.04672.x.

[194] X. Yu *et al.*, “Wakefulness Is Governed by GABA and Histamine Cotransmission,” *Neuron Camb. Mass*, vol. 87, no. 1, pp. 164–178, 2015, doi: 10.1016/j.neuron.2015.06.003.

[195] J. T. R. Isaac, M. C. Ashby, and C. J. McBain, “The Role of the GluR2 Subunit in AMPA Receptor Function and Synaptic Plasticity,” *Neuron Camb. Mass*, vol. 54, no. 6, pp. 859–871, 2007, doi: 10.1016/j.neuron.2007.06.001.

[196] S. C. Holst and H.-P. Landolt, “Sleep-Wake Neurochemistry,” *Sleep Med. Clin.*, vol. 17, no. 2, pp. 151–160, 2022, doi: 10.1016/j.jsmc.2022.03.002.

[197] G. A. Dienel, “Brain Glucose Metabolism: Integration of Energetics with Function,” *Physiol. Rev.*, vol. 99, no. 1, pp. 949–1045, 2019, doi: 10.1152/physrev.00062.2017.

[198] J. D. Rothstein *et al.*, “Knockout of Glutamate Transporters Reveals a Major Role for Astroglial Transport in Excitotoxicity and Clearance of Glutamate,” *Neuron Camb. Mass*, vol. 16, no. 3, pp. 675–686, 1996, doi: 10.1016/S0896-6273(00)80086-0.

[199] D. A. Brown and P. R. Adams, “Muscarinic suppression of a novel voltage-sensitive K + current in a vertebrate neurone,” *Nat. Lond.*, vol. 283, no. 5748, pp. 673–676, 1980, doi: 10.1038/283673a0.

[200] B. Suh and B. Hille, “Regulation of KCNQ channels by manipulation of phosphoinositides,” *J. Physiol.*, vol. 582, no. 3, pp. 911–916, 2007, doi: 10.1113/jphysiol.2007.132647.

[201] F.-Z. Shaw, Y.-F. Liao, R.-F. Chen, Y.-H. Huang, and R. C. S. Lin, “The zona incerta modulates spontaneous spike-wave discharges in the rat,” *J. Neurophysiol.*, vol. 109, no. 10, pp. 2505–2516, 2013, doi: 10.1152/jn.00750.2011.

[202] R. Cossart and S. Garel, “Step by step: cells with multiple functions in cortical circuit assembly,” *Nat. Rev. Neurosci.*, vol. 23, no. 7, pp. 395–410, 2022, doi: 10.1038/s41583-022-00585-6.

[203] E. MURILLO-RODRIGUEZ, C. BLANCO-CENTURION, C. SANCHEZ, D. PIOMELLI, and P. J. SHIROMANI, “Anandamide enhances extracellular levels of adenosine and induces sleep: An in vivo microdialysis study,” *Sleep N. Y. N*, vol. 26, no. 8, pp. 943–947, 2003, doi: 10.1093/sleep/26.8.943.

[204] J. Monti, S. R. Pandi-Perumal, and C. M. Sinton, *Neurochemistry of Sleep and Wakefulness*. Cambridge: Cambridge University Press, 2008. doi: 10.1017/CBO9780511541674.

[205] D. Lovatt *et al.*, “Neuronal adenosine release, and not astrocytic ATP release, mediates feedback inhibition of excitatory activity,” *Proc. Natl. Acad. Sci. - PNAS*, vol. 109, no. 16, pp. 6265–6270, 2012, doi: 10.1073/pnas.1120997109.

[206] O. Eyigor, Z. Minbay, and I. M. Kafa, “Glutamate and Orexin Neurons,” *Vitam. Horm.*, vol. 89, pp. 209–222, 2012, doi: 10.1016/B978-0-12-394623-2.00011-1.

[207] R. H. Williams, L. T. Jensen, A. Verkhratsky, L. Fugger, and D. Burdakov, “Control of hypothalamic orexin neurons by acid and CO2,” *Proc. Natl. Acad. Sci. - PNAS*, vol. 104, no. 25, pp. 10685–10690, 2007, doi: 10.1073/pnas.0702676104.

[208] S. M. Theparambil *et al.*, “Astrocytes regulate brain extracellular pH via a neuronal activity-dependent bicarbonate shuttle,” *Nat. Commun.*, vol. 11, no. 1, pp. 5073–5073, 2020, doi: 10.1038/s41467-020-18756-3.

[209] J. W. Deitmer and C. R. Rose, “Ion changes and signalling in perisynaptic glia,” *Brain Res. Rev.*, vol. 63, no. 1, pp. 113–129, 2010, doi: 10.1016/j.brainresrev.2009.10.006.

[210] F. Yang *et al.*, “Astrocytic Acid-Sensing Ion Channel 1a Contributes to the Development of Chronic Epileptogenesis,” *Sci. Rep.*, vol. 6, no. 1, pp. 31581–31581, 2016, doi: 10.1038/srep31581.

[211] A. Mielnicka and P. Michaluk, “Exocytosis in Astrocytes,” *Biomol. Basel Switz.*, vol. 11, no. 9, p. 1367, 2021, doi: 10.3390/biom11091367.

[212] D. Attwell and N. B. Hamilton, “Do astrocytes really exocytose neurotransmitters?,” *Nat. Rev. Neurosci.*, vol. 11, no. 4, pp. 227–238, 2010, doi: 10.1038/nrn2803.

[213] E. N. Marieb and Katja. Hoehn, *Human anatomy & physiology*, Tenth edition. in Human anatomy and physiology. Boston: Pearson, 2016.

[214] L. I. Kiyashchenko *et al.*, “Release of Hypocretin (Orexin) during Waking and Sleep States,” *J. Neurosci.*, vol. 22, no. 13, pp. 5282–5286, 2002, doi: 10.1523/jneurosci.22-13-05282.2002.

[215] B. Y. Mileykovskiy, L. I. Kiyashchenko, and J. M. Siegel, “Behavioral Correlates of Activity in Identified Hypocretin/Orexin Neurons,” *Neuron Camb. Mass*, vol. 46, no. 5, pp. 787–798, 2005, doi: 10.1016/j.neuron.2005.04.035.

[216] M. Sheibani, M. Shayan, M. Khalilzadeh, M. Ghasemi, and A. R. Dehpour, “Orexin receptor antagonists in the pathophysiology and treatment of sleep disorders and epilepsy,” *Neuropeptides*, vol. 99, p. 102335, Jun. 2023, doi: 10.1016/j.npep.2023.102335.

[217] L. G. Sadleir, I. E. Scheffer, S. Smith, B. Carstensen, K. Farrell, and M. B. Connolly, “EEG features of absence seizures in idiopathic generalized epilepsy: Impact of syndrome, age, and state,” *Epilepsia Cph.*, vol. 50, no. 6, pp. 1572–1578, 2009, doi: 10.1111/j.1528-1167.2008.02001.x.

[218] M. Domin *et al.*, “Juvenile Myoclonic Epilepsy Shows Potential Structural White Matter Abnormalities: A TBSS Study,” *Front. Neurol.*, vol. 9, pp. 509–509, 2018, doi: 10.3389/fneur.2018.00509.

[219] C. S. Nayak and S. Bandyopadhyay, “Mesial Temporal Lobe Epilepsy,” in *StatPearls*, Treasure Island (FL): StatPearls Publishing, 2023. Accessed: Oct. 21, 2023. [Online]. Available: http://www.ncbi.nlm.nih.gov/books/NBK554432/

[220] A. Runnova, A. Selskii, A. Kiselev, R. Shamionov, R. Parsamyan, and M. Zhuravlev, “Changes in EEG Alpha Activity during Attention Control in Patients: Association with Sleep Disorders,” *J. Pers. Med.*, vol. 11, no. 7, p. 601, 2021, doi: 10.3390/jpm11070601.

[221] H. Merica, R. Blois, and J.-M. Gaillard, “Spectral characteristics of sleep EEG in chronic insomnia,” *Eur. J. Neurosci.*, vol. 10, no. 5, pp. 1826–1834, 1998, doi: 10.1046/j.1460-9568.1998.00189.x.

[222] B. Zeng, J. Zhou, Z. Li, H. Zhang, Z. Li, and P. Yu, “Altered Percent Amplitude of Fluctuation in Healthy Subjects After 36 h Sleep Deprivation,” *Front. Neurol.*, vol. 11, pp. 565025–565025, 2021, doi: 10.3389/fneur.2020.565025.

[223] B.-Z. Li *et al.*, “Relation of Decreased Functional Connectivity Between Left Thalamus and Left Inferior Frontal Gyrus to Emotion Changes Following Acute Sleep Deprivation,” *Front. Neurol.*, vol. 12, pp. 642411–642411, 2021, doi: 10.3389/fneur.2021.642411.

[224] P. Gloor, “Neuronal Generators and the Problem of Localization in Electroencephalography: Application of Volume Conductor Theory to Electroencephalography,” *J. Clin. Neurophysiol.*, vol. 2, no. 4, pp. 327–354, 1985, doi: 10.1097/00004691-198510000-00002.

[225] W. Tatum and W. Tatum IV, *Handbook of EEG Interpretation*, 2nd ed. New York: Springer Publishing Company, Incorporated, 2014.

[226] B. M. S. Carvalho, J. Chaves, and A. M. da Silva, “Effects of antiepileptic drugs on sleep architecture parameters in adults,” *Sleep Sci. São Paulo SP*, vol. 15, no. 2, pp. 224–244, 2022, doi: 10.5935/1984-0063.20220045.

[227] C. W. BAZIL, “Effects of Antiepileptic Drugs on Sleep Structure: Are All Drugs Equal?,” *CNS Drugs*, vol. 17, no. 10, pp. 719–728, 2003, doi: 10.2165/00023210-200317100-00003.

[228] F. Matsuo, “Lamotrigine,” *Epilepsia Cph.*, vol. 40, no. s5, pp. s30–s36, 1999, doi: 10.1111/j.1528-1157.1999.tb00917.x.

[229] “Lamotrigine,” *Psychopharmacol. Update*, vol. 33, no. 5, 2022.

[230] C. S. Nayak, S. Sinha, M. Nagappa, T. Kandavel, and A. B. Taly, “Effect of carbamazepine on the sleep microstructure of temporal lobe epilepsy patients: A cyclic alternating pattern−based study,” *Sleep Med.*, vol. 27–28, pp. 80–85, 2016, doi: 10.1016/j.sleep.2016.08.017.

[231] F. Ayala-Guerrero, G. Mexicano, V. González, and M. Hernandez, “Effect of oxcarbazepine on sleep architecture,” *Epilepsy Behav.*, vol. 15, no. 3, pp. 287–290, 2009, doi: 10.1016/j.yebeh.2009.04.013.

[232] M. J. Brodie, “Sodium Channel Blockers in the Treatment of Epilepsy,” *CNS Drugs*, vol. 31, no. 7, pp. 527–534, 2017, doi: 10.1007/s40263-017-0441-0.

[233] C. Liguori, M. Toledo, and S. Kothare, “Effects of anti-seizure medications on sleep architecture and daytime sleepiness in patients with epilepsy: A literature review,” *Sleep Med. Rev.*, vol. 60, pp. 101559–101559, 2021, doi: 10.1016/j.smrv.2021.101559.

[234] O. Chaneva, “Effects of Levetiracetam on Sleep Architecture and Daytime Sleepiness,” *Folia Medica Plovdiv*, vol. 63, no. 5, pp. 631–636, 2021, doi: 10.3897/folmed.63.e57985.

[235] R. Rocamora, I. Álvarez, B. Chavarría, and A. Principe, “Perampanel effect on sleep architecture in patients with epilepsy,” *Seizure*, vol. 76, pp. 137–142, Mar. 2020, doi: 10.1016/j.seizure.2020.01.021.

[236] P. Simor, G. van der Wijk, L. Nobili, and P. Peigneux, “The microstructure of REM sleep: Why phasic and tonic?,” *Sleep Med. Rev.*, vol. 52, pp. 101305–101305, 2020, doi: 10.1016/j.smrv.2020.101305.

Figure References

[1] VectorMine, "Meninges as central brain part structure or under skin layers outline diagram labeled educational and anatomical parts location scheme with healthy medical skull elements example. Vector illustration", Adobe Stock, Image 464056744, Licensed Image, [Online]. Available: https://stock.adobe.com/ca/images/meninges-as-central-brain-part-structure-or-under-skin-layers-outline-diagram-labeled-educational-and-anatomical-parts-location-scheme-with-healthy-medical-skull-elements-example-vector-illustration/464056744

[2] designua, "Types Of a multipolar Neurons", Adobe Stock, Image 80758932, Licensed Image, [Online]. Available: https://stock.adobe.com/ca/images/types-of-a-multipolar-neurons/80758932

[3] Peter Hermes Furian, "Electric field lines of two opposing charges separated by a finite distance. Physical dipole, two poles, made by electric equal charged balls. Red plus and blue minus points. Illustration over white.", Adobe Stock, Image 119260880, Licensed Image, [Online]. Available: https://stock.adobe.com/ca/images/electric-field-lines-of-two-opposing-charges-separated-by-a-finite-distance-physical-dipole-two-poles-made-by-electric-equal-charged-balls-red-plus-and-blue-minus-points-illustration-over-white/119260880

[4] vasilisatsoy, "Selected Cell and Fiber Groups. structures of the forebrain. Collectively, these structures are called the basal ganglia and are an important part of the brain systems that control movement", Adobe Stock, Image 252806212, Licensed Image, [Online]. Available: https://stock.adobe.com/ca/images/selected-cell-and-fiber-groups-structures-of-the-forebrain-collectively-these-structures-are-called-the-basal-ganglia-and-are-an-important-part-of-the-brain-systems-that-control-movement/252806212

[5] Taleseedum, "Parts of human brain anatomy side view", Adobe Stock, Image 226607208, Licensed Image, [Online]. Available: https://stock.adobe.com/ca/images/parts-of-human-brain-anatomy-side-view/226607208

[6] Fernando, "GABA-Glutamate-glutamine cycle [Astrocytes and neurons]", Adobe Stock, Image 561689390, Licensed Image, [Online]. Available: https://stock.adobe.com/ca/images/gaba-glutamate-glutamine-cycle-astrocytes-and-neurons/561689390

[7] L.Darin, "Vector infographic of Neuron and glial cells (Neuroglia). Astrocyte, microglia and oligodendrocyte, ependymal cells (ependymocytes and tanycytes)", Adobe Stock, Image 269896857, Licensed

Image, [Online]. Available: https://stock.adobe.com/ca/images/vector-infographic-of-neuron-and-glial-cells-neuroglia-astrocyte-microglia-and-oligodendrocyte-ependymal-cells-ependymocytes-and-tanycytes/269896857